EVALUATION OF USE OF HIGH PERFORMANCE MATERIALS IN RC BEAM-COLUMN JOINTS SUBJECTED TO CYCLIC LOADS

Ph.D Thesis

by

R. SIVA CHIDAMBARAM

DEPARTMENT OF EARTHQUAKE ENGINEERING
INDIAN INSTITUTE OF TECHNOLOGY ROORKEE
ROORKEE – 247667 (INDIA)
FEBRUARY, 2016

EVALUATION OF USE OF HIGH PERFORMANCE MATERIALS IN RC BEAM-COLUMN JOINTS SUBJECTED TO CYCLIC LOADS

A THESIS

Submitted in partial fulfilment of the requirements for the award of the degree of

DOCTOR OF PHILOSOPHY

in

EARTHQUAKE ENGINEERING

by

R. SIVA CHIDAMBARAM

DEPARTMENT OF EARTHQUAKE ENGINEERING
INDIAN INSTITUTE OF TECHNOLOGY ROORKEE
ROORKEE – 247667 (INDIA)
FEBRUARY, 2016

INDIAN INSTITUTE OF TECHNOLOGY ROORKEE
ROORKEE

CANDIDATE'S DECLARATION

I hereby certify that the work which is being presented in the thesis entitled **"EVALUATION OF USE OF HIGH PERFORMANCE MATERIALS IN RC BEAM-COLUMN JOINTS SUBJECTED TO CYCLIC LOADS"** in partial fulfilment of the requirements for the award of the Degree of Doctor of Philosophy and submitted in the Department of Earthquake Engineering, Indian Institute of Technology Roorkee, Roorkee is an authentic record of my own work carried out during a period from July,2011 to February,2016 under the supervision of Prof. Pankaj Agarwal, Professor, Department of Earthquake Engineering, Indian Institute of Technology Roorkee, Roorkee.

The matter presented in the thesis has not been submitted by me for the award of any other degree of this or any other Institute.

(R.SIVA CHIDAMBARAM)

This is to certify that the above statement made by the candidate is correct to the best of my knowledge.

(PANKAJ AGARWAL)
Supervisor

The Ph. D. Viva-Voce Examination of ....., Research Scholar, has been held on .....

Chairman, SRC **Signature of External Examiner**

This is to certify that the student has made all the corrections in the thesis.

Signature of Supervisor **Head of the Department**

Dated: _____

Abstract

There is a continuous research on the behaviour of joints particularly to increase shear strength. The conventional way to enhance the joint's shear strength is to provide increased dimension with closely spaced transverse/shear reinforcement in the hinge region. The recommendations on the basis of confinement of joints are incorporated in national and international codes. This critical confinement in the joint region leads to steel congestion and also poses difficulty in construction. The provision of confinement at the joint region helps only upto a certain extent to increase the shear capacity of the joint due to the poor tensile property of concrete. The confined joints still behave inelastically under severe seismic loading in spite of acting as rigid panel zone for the development of desirable failure mechanism.

In the recent years, the use of different high performance materials is being explored to improve the in-elastic behavior of joint without using special confinement reinforcement. These high performance materials are available in different forms namely (1) Fibers such as in discrete forms and as fabric, fiber reinforced polymer, (2) mineral admixtures in micro and nano size particles, (3) solid form material like plates/sheets/rods, carbon grids, geo-grids, shape memory alloys. Different chemical admixtures and adhesives are also widely used in reinforced concrete structural members to enhance the required strength at the concentrated regions. The research programme is focussed on different types of high performance materials used in the joint region of the external beam-column joints tested under cyclic loading.

The feasibility of geo-grid as a reinforcing and confining material in reinforced concrete structural components is examined under monotonic and cyclic loading. The pre and post yield behavior of specimens with the derived parameters shows that the geo-grid can be effectively used as a confinement material in structural engineering. The geo-grid may become more effective with steel fiber to improve the damage tolerance capacity.

The influence of different fibers with concrete is also investigated under compression and flexure. The possible use of different fibers and hybrid fibers (to reduce the higher volume of fibers) to improve the shear resistance capacity of beam-column joint without critical confinement is examined under cyclic loading. The enlarged hysteretic loop of FRC composite specimens establishes enhancement of shear strength and post

yield stiffness retention of the joint. The energy dissipation and damping characteristics of FRC composite show that the discrete fiber reinforced concrete can be used in critical joint region without confinement.

Influence of High Performance Fiber Reinforced Cement Composite (HPFRCC) in improving the post yield performance of reinforced concrete structural components is investigated under static and cyclic loading. The moment carrying capacity, post yield stiffness and energy dissipation behavior of RC specimen show that the HPFRCC can be effectively used in the RC components at hinge region without critical reinforcement. The use of fiber hybridization may become more effective in improving the ductile performance and damage tolerance capacity without increasing the fiber volume.

The influence of precast SIFCON core enabled beam-column joint region is examined under cyclic loading. The hysteretic behaviour, energy dissipation and damage index of the specimens show a significant improvement of the post-yield behaviour of the joint with SIFCON core as compared to other conventionally confined joint specimens.

An analytical model for predicting the shear strength of the beam-column joint is proposed under the unconfined and confined conditions based on existing experimental data base. A comparison is also made to predict shear strength with the shear strength of the model proposed in American Concrete Institute (ACI), New Zealand (NZ) and Architecture Institute of Japan (AIJ) codes. The proposed equations are closer to experimental test results of the joint with reasonable co-variance. The proposed model is further upgraded for SIFCON Core and the SFRC. The modified equation is able to predict the shear strength of specimen with reasonable accuracy.

The performance evaluation of epoxy filled mechanical couplers connecting the two cut ends of a reinforcing bar is carried out by conducting the monotonic and cyclic testing of beam and beam-column joint specimens. The moment-curvature, hysteretic behavior, stiffness degradation, energy dissipation and damage tolerance capacity of this coupler enabled specimens are quantified and compared with the conventional specimens. The pre and post yield behaviour of specimens with couplers at different locations authenticates its usage in retrofitting work where the buckling of longitudinal reinforcement is possible. An experimental case study is also carried out on the use of mechanical couplers in plastic hinge region of columns and the results are compared with conventional techniques of retrofitting.

Acknowledgement

This research is carried out in the Department of Earthquake Engineering, Indian Institute of Technology Roorkee, India. I would like to thank the following people. Without their advice, encouragement and support, this thesis would not have been completed.

I wish to express my heartfelt emotion to my supervisor, Prof. Pankaj Agarwal for his inspiration, benevolent guidance with constant enthusiasm and support. I thank for his moral support and invaluable guidance in crafting my work and my knowledge.

I do acknowledge the help that I have received from the head of the department Prof. M.L. Sharma and former head Prof. H.R Wason along with the faculty members of the Department of Earthquake Engineering, IIT Roorkee.

I am thankful to Prof. Yogendra Singh, Prof. D. K. Paul, Dr. R. N. Dubey and Dr. R.S. Jakka for their valuable advice and suggestions.

I extend my gratitude to all the technical and non technical staff members of Department of Earthquake Engineering for their kind cooperation. Thanks are due to Mr. Dharamveer and my lab supporters Mr. Rishi Chand, Mr. Jinda Hasan, Mr. Prem Chand for their help in my experimental work.

I am thankful to Prof. G. S. Thirugnanam, Institute of Road and Transport Technology Erode, for his interest and advice.

I extend my thanks to Prof. Naveen Kwatra, Head, Department of Civil Engineering, Thapar University, for kind support.

Thanks are extended to my friends Dr. A. B. Danie Roy; Mrs. Shermi Roy; Franklin F. R. Frederick; Dr. N. Siva Kumar; Dr. Gowardan; Raja Singh; Dr. Narayan Roy; Dr. Ranjay Hazra; Dr. Sathish Kumar; Dr. John Robert Prince; Dr. Mrs. A. Manju; Dr. P. Purushothaman; Dr. Senthil; J. Venkatesan; Ganesan; Dr. Siva Sakthivel; Amit Goyal; K.V. Naveen Kumar; Kasi Viswanathan and Imtiyaz Ansari for their help in the experimental program.

The material support provided by Strata India, Reliance Industries, Kasthuri Metals, Bakert, Fosroc Chemicals, Sika Chemicals and Dr. Fixit chemicals is also gratefully

acknowledged. I would like to extend my thanks to Department of Earthquake Engineering, Indian Institute of Technology – Heritage fund, Ministry of Human Resource and Development for their financial support.

Last but foremost, I owe my sincere thanks to my father K. Rajendran, my mother Late Mrs. Prema Rajendran, my sister Mrs. R. Yamuna Devi, my wife Mrs. Poornima Chidambaram and my other family members, for their unwavering support in spirit and livelihood.

CONTENTS

CHAPTER 8

CYCLIC TESTING OF RETROFITTED COLUMNS WITH BUCKLED REINFORCEMENT - AN EXPERIMENTAL CASE STUDY

CHAPTER 9

SUMMARY AND CONCLUSIONS

List of Figures

List of Tables

Nomenclature

Symbols	Description	Units
P/F	applied load	kN
l	span length	mm
b	breadth of the specimen	mm
d	depth of the specimen	mm
f_t	flexural tensile strength	MPa
V_f	volume of fiber	%
P_y/F_y	yield load	kN
P_m	maximum load	kN
P_u	ultimate load	kN
Δ_y	yield deflection	mm
Δ_m/δ_m	maximum deflection	mm
Δ_u/δ_u	ultimate deflection	mm
δ_f	failure deflection	mm
μ	ductility index	
δ	deflection	mm
K	stiffness	kN/mm
K_y	yield stiffness	kN/mm
dE	dissipated energy	kN-mm
β	is the strength degradation parameter	0.1
$M_x/\emptyset_x$	minimum secant stiffness	
$M_y/\emptyset_y$	initial elastic stiffness	
f_y	yield strength	MPa or N/mm^2
λ	0.75 for light weight concrete and 1 for normal weight concrete	0.75 and 1
γ	6 for unconfined joint and 12 for confined joint	6 and 12
A_j	the effective horizontal joint area	mm^2
f_c'	cylindrical compressive strength	MPa or N/mm^2
f_t	Flexural strength	MPa or N/mm^2
N	axial load	kN
b_j	effective joint width	mm
A_g	gross area of column	mm^2

k	0.7 for “T” shape joints	0.7
α	joint index constant	
ρ_t	percentage of reinforcement	%
r	compressive strength constant	
n_b	number of bar	
n_{sl}	number of leg	
f_{sy}	yield strength of stirrups	MPa
d	diameter of bar	mm
H_b	depth of beam	mm
B_b	width of beam	mm
B_c	width of column	mm
h_c	depth of column	mm

Abbreviations

MRF	Moment Resisting Frame
RC	Reinforced Concrete
MD	Machine Direction
CMD	Cross Machine Direction
UD	Uni-directional
BD	Bi Directional
GGC	Geo-grid Confined
RED	Relative Energy Dissipation
CED	Cumulative Energy Dissipation
DI	Damage Index
MFDR	Modified Flexural Damage Ratio
PP	Polypropylene Fiber
HSF	Hooked End Steel fiber
CSF	Crimpled Steel Fiber
BSF	Brass Coated Steel Fiber
FRC	Fiber Reinforced Concrete
SFRC	Steel Fiber Reinforced Concrete
MFRC	Macro Synthetic Fiber Reinforced Concrete
HyFRC	Hybrid Fiber Reinforced Concrete
FRCC	Fiber Reinforced Cementitious Composites
HPFRCC	High Performance Fiber Reinforced Cementitious Composites
SIFCON	Slurry Infiltrated Fibrous Concrete
ECC	Engineered Cementitious Composites
HECC	Hooked End Steel Fiber Enabled Cementitious Composites
CECC	Crimpled Steel Fiber Enabled Cementitious Composites
BECC	Brass Coated Steel Fiber Enabled Cementitious Composites
FRP	Fiber Reinforced Polymers
GFRP	Glass Fiber Reinforced Polymers
CFRP	Carbon Fiber Reinforced Polymers
BFRP	Basalt Fiber Reinforced Polymers

ACI	American Concrete Institute
AIJ	Architecture Institute of Japan
NZ	New Zealand
ASCE	American Society of Civil Engineers
IS	Indian Standards

Chapter 1

Introduction

1.1 General

The consideration of seismic loads in design of high-rise moment resisting framed (MRF) building has now attained more attention due to catastrophic failure in past earthquakes. The past damage reports also underline the importance of beam-column joints on the earthquake resistance of a building. In MRF, beam-column sub-joint is the most important part in dissipating the seismic energy and in transferring the forces from beam to column and finally to the foundation. These joints are expected to carry significant load without loss during inelastic deformation under severe loading and are capable to resist large shear forces by developing the desirable failure mechanism for the ductile performance. The forces transferred to a joint by the adjacent beam and column elements are resisted through the diagonal strut and truss mechanism. Post earthquake examination reveals that the formation of negative and positive plastic hinges at joint face, lesser shear reinforcement ratio, brittle nature of concrete and inadequate anchorage of flexural reinforcement into the joint are the prime factors to make the joints vulnerable. Also the inadequate confinement in the plastic hinge region during higher rotation causes concrete crushing and spalling which lead the reinforcement to buckle. It is extremely difficult to perform realistic repair or reinforcement work on badly damaged beam-column joints because of large deformations and severe damages. Thus, a building suffering from joint damages is usually considered economically unfit for reuse or requires advanced techniques to rehabilitate instead of demolition.

The ductile performance of an MRF building depends on the post elastic strength and stiffness retention with energy dissipation during higher deformation. The conventional way to enhance the ductile behavior of a structure is by improving the shear capacity of the joint at possible plastic hinge regions. The shear capacity of a joint can be increased either by use of high strength concrete or by increasing the percentage of shear reinforcement at the joint as well as at plastic hinge regions. The increased flexural reinforcement anchorage length inside the joint is also important to avoid early

reinforcement slip and to transfer the tensile forces from the beam to column without interruption during higher deformation. The contribution of shear reinforcement and concrete is vital in resisting the diagonal tension and compression respectively. The confinement largely helps to confine the concrete in the joint region and to increase the shear resistance capacity of the joint. The confining shear reinforcement requirement and its detailing in the joint region build up congestion of reinforcement and create practical difficulty in concreting work. Moreover, the provision of shear reinforcement in the joint region only helps upto a certain extent to increase its shear capacity of the joint due to the poor tensile property of concrete.

The use of different high performance materials in reinforced concrete structure addresses the above mentioned problems and may be an alternative to increase the shear resistance capacity of beam-column joints. These materials are available in different forms and their application depends on the structural requirement. High performance materials are available in different forms namely (1) Fibers (steel fiber, polypropylene fiber, polyethylene fiber, poly vinyl alcohol fiber, poly acryl nitrate fiber etc.,) such as in discrete forms and fabric form, (2) mineral admixtures fly ash, micro silica, ground granulated blast furnace slag etc., in micro and nano size particles, (3) solid form material like plates/sheets/rods, carbon grids, geo-grids, shape memory alloys. Different chemical admixtures and adhesives are also widely used in reinforced concrete structural members to enhance the required strength at the concentrated regions.The foremost important point in improving the joint performance is to increase the joint shear strength without critical confinement. The past few decades' research paves the clear path to utilize discontinuous steel fibers in concrete in lesser volume to enhance the shear strength without higher stirrups ratio. This randomly distributed discontinuous steel fiber increases the tensile strength and strain capacity by arresting the early crack formation and decreases the rate of crack formation by bridging the cracks after initiation (Ganesan et al. (2007); Holschemacher et al. (2010); Adel et al. (2014)). The bridging property of fiber not only bridges the cracks but also restricts the concrete spalling and crushing that leads to enhance the strength as well as ductility of concrete. In addition to that, the anchorage behavior of different fibers such as crimpled, hooked end steel fiber improves the effectiveness of the fiber bridging ability. Therefore Steel Fiber Reinforced Concrete (SFRC) is an effective and alternative way to improve the shear strength and inelastic response of the structural member without special confinement in the joint region. However, the entire performance of SFRC depends on the uniform dispersion and % volume of fiber in concrete.

To avoid the problems associated with the SFRC, High Performance Fiber Reinforced Cementitious Composites (HPFRCC) are developed where coarse aggregate is replaced with fibers and mineral admixtures. Considerable amount of work has already been carried out to develop different types of HPFRCC, such as Slurry Infiltrated Concrete (SIFCON), Engineered Cementitious Composites (ECC) etc. In SIFCON, higher volume of steel fibers are pre-packed layer by layer in mould and after that slurry is poured with a little pressure. In ECC, minimum of 2% Poly-Vinyl Alcohol (PVA) and Poly-Ethylene (PE) fibers are used with cementitious materials to prepare the composites. The absence of coarse aggregates and presence of fine materials like fly ash and silica fume fill the voids that effectively improves the strength. Many studies have already been carried out on the mechanical properties such as compressive, tensile and shear behavior of SIFCON and ECC and the results have shown enhanced shear and ductility response over conventional FRC. In spite of a better strength and energy dissipation capacity of SIFCON, the effective and practical application of SIFCON is limited due to construction difficulty. The strain-hardening behavior of ECC with more than 1% strain capacity in tension enhances the ductile behavior and damage tolerance capacity of reinforced concrete members without construction difficulty. The tensile property of ECC has remarkable effect on crack resistance and ductility of structural components (Victor et al. (1993), (1994) and (1998)). The effective application of HPFRCC on structural components may eliminate the required special transverse reinforcement with higher energy dissipation and slower stiffness degradation capability (Gregor, et al. (2002) and (2003); Shannag et al. (2002) and (2005)). The proposed study mainly focuses on the possibility of wider application and use of composite concrete with different types of fiber.

In general, high performance materials significantly improve the tensile property of concrete due to bridging effect that may be more effective under the confinement. The conventional confinement in reinforced concrete structural member is provided by the steel reinforcement that may be sometimes difficult to provide particularly at the joint region due to heavy congestion of reinforcement. Confinement by the flexible type of reinforcement may be more effective at the congested region. In the present study, geo-grid which is a flexible material can be transformed into any shape, as confinement reinforcement. Earlier, geo-grids are widely used in confining and reinforcing the soil to add tensile strength and deformation properties. It is also used to confine and increase the stiffness, bearing capacity of the base course materials and to prevent its lateral movement in asphalt paved roads. Recently few works have focused on the use of geo-grids in

concrete pavement. The feasibility of geo-grid in plain concrete beam used as tensile reinforcement and suggestion for grid reinforced concrete in thin layer concrete work is suggested (Tang et al. 2010). Recently, the flexural behavior of geo-grid reinforced beams and its deflection and energy absorption is studied and observed to enhance energy dissipation (Meski et al. 2014).

Another class of high performance materials used for strengthening and retrofitting work in reinforced concrete structural member is the application of Fiber Reinforced Polymers (FRP) and the epoxy bonding agent. There is a peculiar problem in the retrofitting of structural member that is the buckling of main longitudinal reinforcement due to inadequate confinement at the plastic hinge regions. The practical solution for the peculiar problem is to connect the two ends of the buckled reinforcement by the mechanical coupler. In the proposed study, new epoxy filled couplers with a series of external bolts are used to connect the two ends of the main reinforcement and finally the retrofitted members are wrapped with different types of FRP layers. The proposed work addresses the above mentioned concerns particularly related to confinement at the beam-column joint with the objectives as given in the next section.

1.2 Objectives of the Research

The primary aim of this research is to investigate the inelastic cyclic behavior of exterior beam-column joints with the use of different high performance materials with the following objectives:

(1) To investigate the inelastic cyclic behavior of geo-grid confined beam-column joints with and without steel fiber to improve the shear performance

(2) To investigate the possibility of using steel fibers and fiber hybridization with minimum shear reinforcement in beam- column joints

(3) To evaluate the effectiveness of high performance fiber reinforced cementitious composites using different fibers to increase the inelastic response and damage tolerance capacity of beam-column joints

(4) To study the cyclic behavior of beam-column joints with the use of precast SIFCON core for the improvement of the joint shear strength capacity

(5) To develop a regression based analytical model to predict the shear strength of conventional joints, precast SIFCON core enabled joints and SFRC beam-column joints.

(6) To study the use of epoxy filled mechanical rebar couplers for the retrofit work of beam-column joint and to retrofit the buckled/yielded reinforcement in structural members.

1.3 Scope and Methodology

To achieve the aforementioned objectives; a detailed literature review is made to explore the ongoing research work on the use of high performance materials. An extensive experimental program is proposed to develop the shear resistance analytic empirical model of the beam-column joints. The experimental program consists of preparation and testing of exterior beam-column joint specimens and reinforced concrete (RC) beam specimens along with companion specimens. The materials used, testing method adopted and instrumentation used for this study are described below;

The possibility of geo-grid confinement in improving the shear resistance and post yield behavior of reinforced concrete components is explored by conducting an extensive experimental program. The geo-grid confined concrete specimens under compression and flexure are studied to examine its mechanical properties. The efficacy of geo-grid as an alternative confining material in plastic hinge region or in different structural component such as reinforced concrete beams and beam-column joints is examined under monotonic and cyclic testing. The load-deformation test results are interpreted in the form of post yield response, stiffness retention and energy dissipation.

The influence of fiber reinforced concrete along with hybrid fibers at beam-column joint region is explored under cyclic loading. The aim of the investigation is to improve the shear resistance capacity of joint without critical confinement. The test results are compared with the conventionally confined beam-column joint specimens in terms of hysteretic curve, strength and stiffness degradation curves, energy dissipation and damage tolerance capacity.

The use of HPFRCC with different fibers in improving the shear resistance and post yield behavior of reinforced concrete components without critical confinement is investigated by conducting an experimental program. The HPFRCC with different fiber mix ratio specimens under compression and indirect tension is studied to examine its physical properties. The influence of fiber reinforced cementitious composites with different fibers and fiber hybridization in plastic hinge region or of different structural component such as reinforced concrete beams and beam-column joints is examined under

static and reverse cyclic testing. The moment-curvature and hysteretic curve test results are interpreted in the form of post yield response, stiffness retention and energy dissipation.

SIFCON is a high strength and ductile cementitious composite that may improve the shear resistance capacity of a structural member. There are a number of constraints and construction difficulties associated with SIFCON which restrict its application in the construction work. Precast SIFCON inner core may be an efficient way to be used in cast-in-place concrete structure at the critical region such as beam-column joint region and may also eliminate the execution problem. In present study, an extensive experimental program is made on precast SIFCON core enabled beam-column joint specimens. These specimens are tested under cyclic loading and the test results are interpreted in the form of hysteretic curve, strength and stiffness retention, energy dissipation and damage tolerance capacity. The test results of the specimens show a significant improvement in the post-yield behaviour of the joint with SIFCON core.

An analytical model for predicting the shear strength of the beam-column joints is proposed under unconfined and confined conditions based on existing experimental data obtained from past studies. A comparison is made to predict shear strength with the shear strength model proposed in American concrete institute (ACI), New Zealand (NZ) and Architecture institute of Japan (AIJ) codes. The proposed model is further upgraded for SIFCON Core and the SFRC.

The post failure analysis of different RC structures shows reinforcement buckling and yielding failure in the damaged region. The conventional way of retrofitting is the removal of damaged concrete replacing it with fresh concrete but the reinforcement will be replaced with lap splice or welding. But this conventional practice is not suitable everywhere and also requires welding in sufficient length to connect the new bars. In order to address this, in-house made mechanical rebar coupler is proposed to connect the broken rebars. The efficacy of this coupler in connecting to various diameter bars and at various locations is examined using RC beams and beam-column joint specimens. This coupler is used in the RC structural components and tested under static and cyclic loading to understand its ability to resist the different types of loading with active connection. The detailed result analysis in the form of moment-rotation curve, hysteretic curve, strength and stuffiness retention, energy dissipation and damage tolerance capacity is done to manifest the use of rebar coupler in broken rebar connection.

1.4 Organization of Thesis

The complete investigation work under this thesis is organised in nine chapters namely;

Chapter 1 provides a brief introduction about the seismic importance of beam- column joints and the problems associated with the joints. An overview is presented on past studies and the present work focuses on the shear strength enhancement of exterior beam-column joint using high performance materials.

Chapter 2 presents the experimental investigations carried out on the use of geo-grid confinement in plastic hinge region of RC beam and beam-column joint specimens. The construction procedure, specimen details, testing methods are described in detail. The test results on the mechanical properties of concrete with and without geo-grid under compression, split tension and bending are explained. The application of geo-grid confinement on beam-column joint and the cyclic test result with the interpretation are also explained in detail.

Chapter 3 reports an experimental study on inelastic cyclic behavior of beam-column joints using different fibers in concrete. The complete details of casting procedure, details of specimens and the adopted testing methods are explained. The mechanical properties of concrete with different fibers under compression and flexure are determined and explained. The application of different fiber reinforced concrete on beam-column joints and result analysis with discussion of the test results are also explained in detail.

C**hapter 4** presents the construction and testing sequence of reinforced concrete beams and beam-column joint specimens using High Performance Fiber Reinforced Cementitious Composites (HPFRCC) in plastic hinge region. The physical properties of different composites and its application in beams and beam-column joints with test analysis and result are discussed.

Chapter 5 addresses the cyclic behavior of beam-column joints with precast SIFCON core. The experimental testing and results of beam-column joint with precast SIFCON core are presented. The experimental findings including the physical properties and cyclic behavior of joints are also presented

Chapter 6 covers an analytical shear strength model proposed for exterior beam-column joints under confined and un-confined conditions, SIFCON core enabled condition with different fiber composites at the joint region. The shear strength model equations are based on the present experimental work.

C**hapter 7** addresses the issues related to retrofitted work at the region of beam-column joints whereas the possibilities of formation of plastic hinges may exist. The study is based on using the epoxy filled couplers to connect the two ends of cut/buckled longitudinal reinforcing bars in the plastic hinge region. The construction and testing details of mechanical couplers enabled reinforced concrete beams and beam-column joints are presented. The experimental results from the tests are also presented.

C**hapter 8** presents an experimental case study on retrofitting of columns with foundation using mechanical rebar couplers and testing sequence of reinforced concrete columns with foundation. This study compares the performance of coupler enabled specimens with conventionally welded specimens with and without external strengthening. The retrofitting procedure, connection details and testing details of mechanical couplers enabled reinforced concrete column are presented. The experimental results from the tests are also presented.

Chapter 9 provides a complete summary and the findings of comprehensive experimental work carried out under this study. These findings may be directly applicable in the field for enhancing the seismic performance of structural elements of the buildings as well as for retrofitting. The recommendations proposed in the thesis may be used to update the codal provisions.

References

Adel, K., Djamel, A., Francois, D., and Lidia, R., (2014), "Effect of mineral admixtures and steel fiber volume contents on the behavior of high performance fiber reinforced concrete," *Materials and Design*, 63,493–499.

Ganesan, N., Indira,P. V. and Ruby, A., (2007), "Steel fibre reinforced high performance concrete beam-column joints subjected to cyclic loading," *ISET Journal of Earthquake Technology,* 44, 445-456.

Gregor, F., Hiroshi, F., and Victor, C. L., (2002), "Effect of matrix ductility on the performance of reinforced ECC column under reverse cyclic loading condition," *Proceedings of JCI International. Workshop on Ductile Fiber Reinforced Cementitious Composites—Application and Evaluation*, pp. 269–278.

Gregor, F., and Victor, C. L., (2003), "Intrinsic response conventional of moment-resisting frames utilizing advanced composite materials and structural elements," *ACI Structural Journal*, 100(2),166–176.

Holschemacher, K., Mueller, T., and Ribakov, Y., (2010), "Effect of steel fibres on mechanical properties of high-strength concrete," *Materials and Design*, 31, 2604-2615.

Meski, El. F., and Chehab, G., (2014), "Flexural behavior of concrete beams reinforced with different types of geogrids," *Journal of Materials in Civil Engineering*, 26, (8), pp.04014038.

Shannag, M. J., Barakat, S., and Abdul, K. M., (2002), "Cyclic behavior of HPFRC repaired interior beam-column joints," *Materials and Structures*, 35,348–356.

Shannag, M. J., Nabeela, A. D., and Ghazi, A. F., (2005), "Lateral load response of high performance fiber reinforced concrete beam–column joints," *Construction and Building Materials*,19,500–508.

Tang, X., Chehab, G. R., and Kim, S., (2008), "Laboratory study of geo-grid reinforcement in Portland cement concrete," *RILEM International Conference on Cracking in Pavements*.pp.769-778.

Victor, C. L., (1993), "From micromechanics to structural engineering the design of cementitious composites for civil engineering applications," *JSCE Journal of Structural Mechanics and Earthquake Engineering,*10,37-48.

Victor, C. L., Mishra, D. K., Naaman, A. E., Wight, J. K., LaFave, J. M., Wu, H. C., and Inada, Y., (1994), "On the shear behavior of engineered cementitious composites," *Journal of Advanced Cementitious Based Materials,*1 (3),142–149.

Victor, C. L., Tetsushi, K., (1998), "Engineered cementitious composites for structural applications," *ASCE Journal of Materials in Civil Engineering*,10, 66-69.

Chapter 2

Inelastic Behavior of Geo-Grid Confined R.C Components under Static and Cyclic Loading

2.1 Introduction

Geo-grid is one of the constituent materials classified under geo-synthetics, manufactured by using knitted polyester yarns having high molecular weight and tenacity with a proprietary coating in different strengths that can be transformed into any shape. Geo-grids are available in various forms such as poly-propylene based, polyester based, poly-ethylene based and generally having two ribs i.e. Machine Direction (MD) ribs and Cross Machine Direction (CMD) ribs. Geo-grid having both the ribs is classified as bi-directional (BD) or uni-directional (UD). The strength of both the ribs is the same in BD grids but differs in UD grids. The strength of CMD ribs is lesser than MD ribs which provides lateral resistance to the MD ribs in UD geo-grids. Geo-grids are widely used in confining and reinforcing of soil, to add tensile strength and to increase the stiffness and bearing capacity of the base course materials. Geo-grid confinement may be an alternative solution for the confinement of reinforced concrete section because of its flexibility, less labor and efficacy in corrosive environment. A few studies are conducted in the past to examine the feasibility of geo-grid as flexural reinforcement in concrete beams. However, an extensive research work is required to prove its worth in construction industry. This study intends to investigate the feasibility of geo-grid application in structural components by conducting an extensive experimental program on simply supported beams and exterior beam-column joints confined with geo-grid. The use of Steel Fiber Reinforced Concrete (SFRC) is also explored as an alternative to achieve higher shear capacity and to improve the ductile behavior with minimum amount of transverse reinforcement.

2.2 Early Studies

Numerous experimental studies have been conducted in the past on inelastic behaviour of beam-column joints using different reinforcement details that suggest the transverse reinforcement in the joint region, to resist the shear forces other than confining

concrete (Shyh et al. 2004, Hwang et al. 2005, Jung et al. 1991). The transverse confinement enhances joint performance and shear strength (Fadel et al. 1991, Surya et al. 2013) It may also enhance the bond behavior, resist the longitudinal reinforcement slippage (Murthy et al. 2003, Nicholas et al. 2006) and help to enhance the plastic rotation capacity (Surya et al. 2013). The recommended codal provisions based on ductile detailing improve the shear resistance but also lead to reinforcement congestion in the joint zone leading to construction difficulty in practice (Hwang et al. 2004, Shyh et al. 2004, Gregoria et al. 2012, and Siva et al. 2012). The joint shear behavior can also be improved without special ductile detailing by using SFRC (Jiru et al. 1992, Giuseppina et al. 2011, Ganesan et al. 2007, Somma et al. 2008).

SFRC enables to dissipate energy significantly after cracking because of its fiber bridging property. These unique properties of SFRC may be an alternative for the enhancement of flexural and shear resistant capacity by eliminating the need of closely spaced transverse detailing in the plastic hinge region of a structural member (Narayan et al. 1987, Ei-Niema 1987, Li et al. 1992, Giuseppe 2008, Dinh et al. 2011). The test results indicate that an optimum quantity of steel fibers in a reinforced concrete element may change the failure mechanism from brittle shear failure to ductile behavior (Adebar et al. 1997 and Yoon et al. 2002). However, the excessive use of SFRC as per volume fraction may sometimes lead to fiber segregation and excessive air entrainment (Naaman 1992) and may reduce its effectiveness. Uneven dispersion of fibers, orientation, aspect ratio and its anchorage behavior may also affect its behavior (Li et al. 1992, ACI 544-1997, Faith et al. 2007, Bensaid et al. 2010). Therefore, complete replacement of transverse reinforcement may not be possible by using SFRC in a structural member and its estimation to increase of shear strength is also difficult (Dinh et al. 2010).

A number of experimental studies based on geo-synthetic materials have been carried out in the past to improve the behaviour of pavement design although the application of geo-grid in concrete is limited. Hoe et al. (2001) and Ali et al. (2009) have studied the use of geo-synthetic materials for the reduction of reflection cracking in asphalt overlays. Shin et al. (2000) has studied improvement in the bearing capacity of a strip foundation on geo-grid reinforced sand. Gerald et al. (2003) has conducted experimental study on the effect of geo-grid reinforcement on unbound aggregates. Xiaochao et al. (2008) has studied the effect of geo-grids for stabilizing weak pavement sub-grade. Tang et al. (2008) and Meski et al. (2013) have conducted experimental tests to study the flexural behaviour of geo-grid reinforced plain cement concrete beam under monotonic loading.

2.3 Compression and Flexural Behavior of Geo-grid Confined / Reinforced Concrete Specimens

Standard cylindrical specimens are tested under compression to examine the confinement effect of geo-grid and its synergetic effect on plain concrete as well as concrete with steel fibers. Geo-grid reinforced concrete prism specimens are also tested under flexure to determine the flexure tensile strength.

2.3.1 Compression Behavior of Geo-grid Confined Concrete Specimens

Cylindrical specimens confined with geo-grid of size 150 mm × 300 mm were cast and tested under uni-axial compression. In order to prepare the geo-grid confined specimens, a geo-grid cage with nominal steel wires was inserted first in the cylindrical mould as shown in Figure 2.1 and the concrete was laid afterwards.

Table 2.1 shows the different configuration of compression specimens confined with geo-grid.

Table 2.1: Details of geo-grid confined compression specimens

Specimen	Volume of Steel Fiber (%)	Remarks
C1	-	Conventional
C2	2	Steel fiber reinforced
C3	-	Geo-grid confinement(GC)
C4	1	GC with Steel fibers

The cylindrical specimens were tested under 3000kN capacity compression testing machine. The concrete used in the specimens was prepared using a mix proportion of 1:1.45:2.25 in Ordinary Portland Cement (OPC) of Grade 43, locally available river sand as fine aggregate, and well graded crushed coarse aggregate having 20 mm maximum size. Water-cement (W/C) ratio was kept 0.45 with 0.5% super-plasticizer for better workability. The hooked end steel fiber (Figure 2.2a) of 35mm length, 0.60 mm diameter with an aspect ratio of 60 having the nominal tensile strength of 1100 MPa was used to prepare SFRC in different volumes (V_f = 0.5%, 1% and 2%). In order to equate the density of conventional concrete a slightly modified concrete mix proportion 1:1.40:2.20 was used to prepare concrete with 1% steel fiber. Uni-axial geo-grids (Figure 2.2b) were employed with three variable strengths (100 kN/m, 200 kN/m and 300 kN/m).

The strength of geo-grid is represented by its tensile strength in machine/main direction and expressed in terms of kilo Newton per meter (kN/m). The above mentioned geo-grid strengths are average tensile strengths in machine direction and the strength of cross machine direction (CMD) rib is 30kN/m. Figure 2.2 shows the details of steel fiber and geo-grid in MD and CMD and the typical details are shown in Figure 2.2c.

(a) Tubular form (b) Placing the grid

Figure 2.1: Preparation of cylindrical specimens confined with geo-grid

(a) Hooked end steel fiber

(b) Uni-axial geo- grid

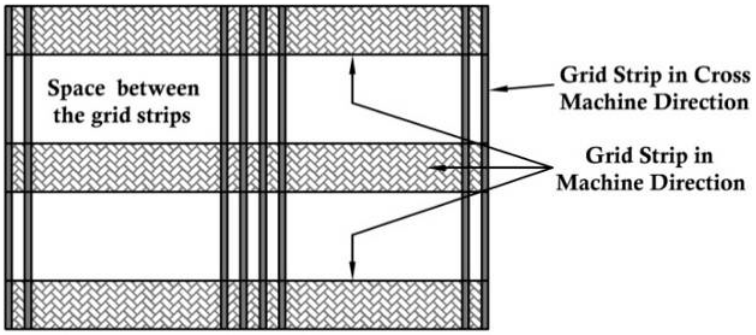

(c) Geo-grid details

Figure 2.2: Typical details of geo-grid and steel fiber

Typical stress-strain curve of compression specimens is shown in Figure 2.3. Initially, a linear behavior is observed, followed by a gradual nonlinear behavior upto the maximum load. The average compressive strength of conventional specimen (C1) is 27 MPa without any considerable post peak behavior. The average compressive strength of steel fiber reinforced specimen (C2) is 35 MPa and corresponding strain at failure is 0.025 which is approximately ten times higher than the conventional specimen (C1). The steel

fibers restrain the spalling and crushing of concrete with enhanced energy dissipation capacity as shown in Figure 2.4. There is no significant increase in strength of geo-grid confined specimen (C3) but the failure strain is higher as compared to conventional specimen (C1). The post peak behavior of geo-grid confined specimen (C3) is considerably improved as compared to specimens C1 and C2. The stress-strain behavior of the specimens (C4) i.e. confined with geo-grid and steel fiber is significantly improved. The combined effect of steel fibers with geo-grid confinement increases the compressive strength upto 42MPa which is approximately 40-50% higher than other specimens of higher strain. The post peak behavior of specimen C4 clearly shows more ductile failure pattern of the specimen as compared to other specimens. The post peak degradation is also gradual with more energy dissipation.

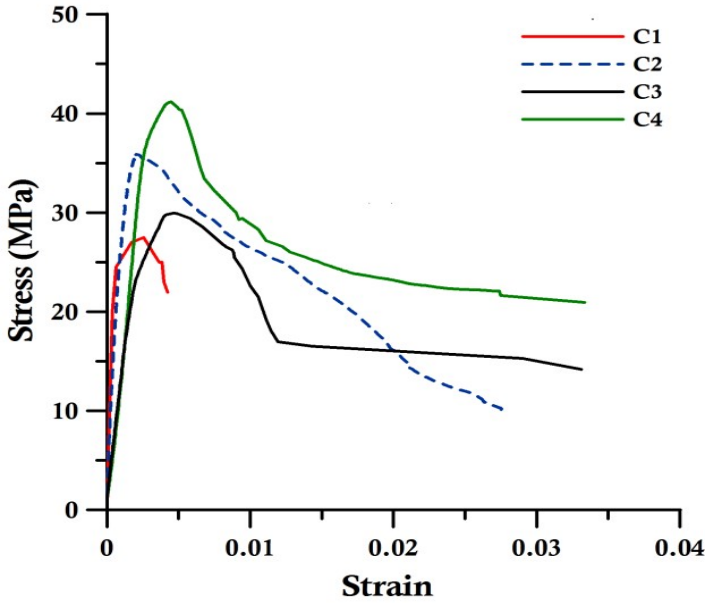

Figure 2.3: Axial stress–strain behavior of geo-grid confined compression specimens

C1-Conventional C2-Steel fibers C3-Geo-grid confined (GC) C4-GC + Steel fibers

Figure 2.4: Failure pattern of geo-grid confined compression specimens

2.3.2 *Flexural Behavior of Geo-grid Confined Reinforced Concrete Prisms with Steel Fiber*

Twelve sets of prism specimens of size 100×100×500 mm as shown in Figure 2.5 were cast with different configuration to examine the effect of geo-grid on the flexural strength and its bond characteristics as summarized in Table 2.2. In the preparation of prism specimens with geo-grid, firstly the concrete cover was laid in the mould before placing the layer(s) of geo-grid on the concrete cover as shown in Figure 2.6.

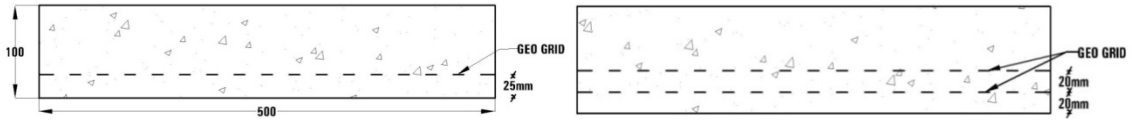

(a) (b)

Figure 2.5: Prism specimens reinforced with (a) single layer (b) double layer geo-grid

Table 2.2: Details of prism specimens with geo-grid and steel fibers under flexure

Specimens	Details of Prism Specimens	Volume of Steel Fiber (%)	Number of Geo-grid layers
S1	Conventional	-	-
S2	Steel fibers Mixed specimen	0.5	-
S3	Steel fibers Mixed specimen	1	-
S4	100kN/m geo-grid at the distance of 2.5cm from the bottom.	-	Single layer
S5	200kN/m geo-grid at the distance of 2.5cm from the bottom.	-	Single layer
S6	300kN/m geo-grid at the distance of 2.5cm from the bottom.	-	Single layer
S7	100kN/m geo-grid at the distance of 2cm interval from the bottom.	-	Double layer
S8	200kN/m geo-grid at the distance of 2cm interval from the bottom.	-	Double layer
S9	300kN/m geo-grid at the distance of 2cm interval from the bottom.	-	Double layer
S10	100kN/m geo-grid at the distance of 2.5cm from the bottom.	0.5	Single layer
S11	200kN/m geo-grid at the distance of 2.5cm from the bottom.	0.5	Single layer
S12	300kN/m geo-grid at the distance of 2.5cm from the bottom.	0.5	Single layer

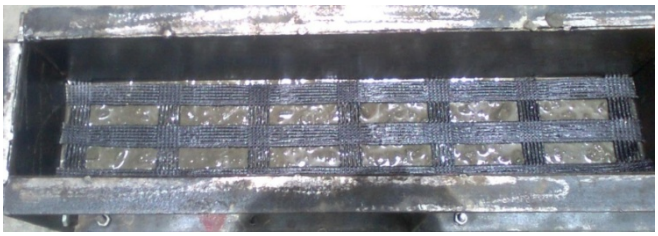

Figure 2.6: Placing of geo-grid layer during casting of specimen

Prism specimens supported on two rollers with a span length of 400 mm were tested under two point loading. Linear Variable Differential Transducer (LVDT) was used to measure the mid span deflection of specimens and flexural tensile strength, f_t, is calculated from the maximum applied load using Equation 2.1.

$$f_t = \frac{Pl}{bd^2} \qquad \textbf{2.1}$$

Note: *where ''P'' is the applied load; ''l'' is the span length; ''b'' is the breadth of the specimen; and ''d'' is depth of the specimen.*

Figure 2.7 shows the load-deflection behavior of all prism specimens. The measured average flexural strength and dissipated flexural energy of prism specimens are presented in Table 2.3.

Table 2.3: Test results of geo-grid and steel fiber reinforced flexure specimens

Specimen ID	**Flexural Stress**	**Flexural Energy**
	MPa	kN-mm
S1	4.0	33.8
S2	5.0	43.9
S3	5.5	60.4
S4	4.8	226.8
S5	5.3	219.9
S6	4.9	294.1
S7	7.2	425.0
S8	6.0	475.0
S9	9.2	500.3
S10	5.5	363.5
S11	6.1	468.8
S12	6.6	503.8

The load–deflection behavior of the first three specimens S1, S2 and S3 is shown in Figure 2.7a. After initial crack, there is sudden decrease in load carrying capacity of specimens that clearly indicates brittle type behavior. The conventional plain concrete beam specimen fails completely in brittle mode with a maximum strength of 4.0 MPa. Gradual post peak load deformation is observed due to the bridging effect of steel fibers (V_f = 0.5%) in specimen S2 with maximum strength of 5.0MPa with 8 mm deformation at failure. As the volume of steel fiber (V_f = 1%) increases in specimen S3, a remarkable improvement in post peak performance and energy dissipation capacity of specimen is noticed as compared to specimen S2.

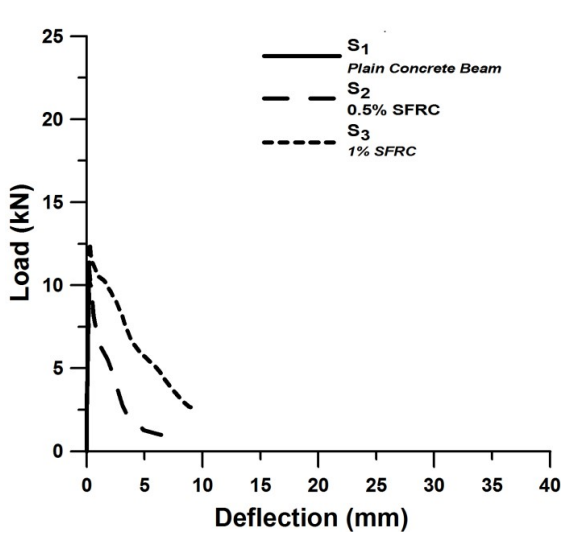

(a) Conventional and SFRC

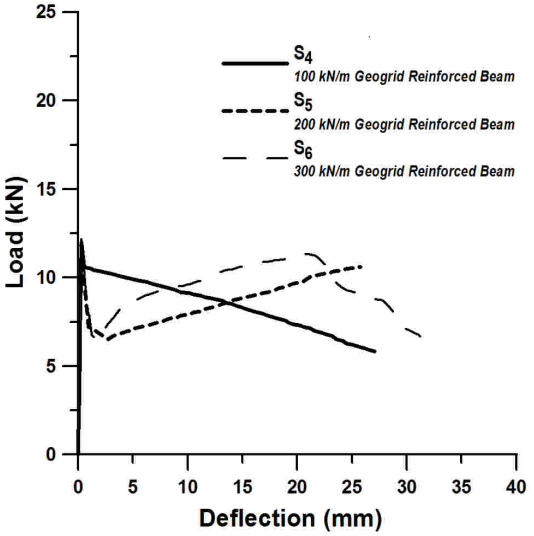

(b) Single layer geo-grid reinforced

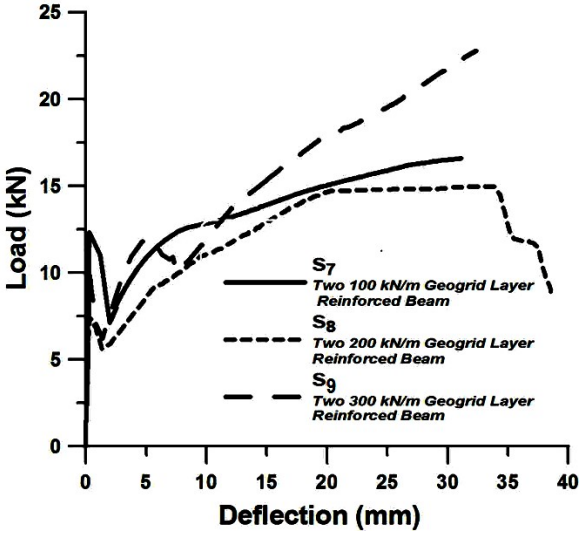

(c) Double layer geo-grid reinforced

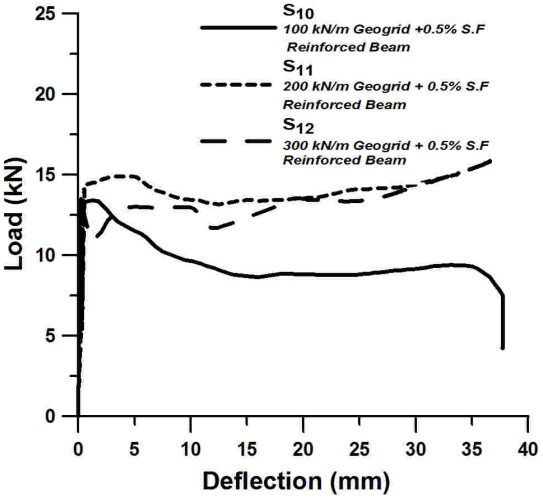

(d) Geo-grid and steel fiber reinforced

Figure 2.7: Load-deflection behavior of geo-grid and steel fiber prism specimens under flexure

The load deformation behavior of specimens S4–S6 with single layer of geo-grid as well as specimens S7–S9 with two layers of geo-grid is shown in Figure 2.7 b and 2.7c. In these specimens, a different type of load–deflection behavior is observed because of the embedded grid. The embedded geo-grid in specimens remains inactive until it gets stressed. After the initial cracking, the tensile forces are gradually transferred to the embedded geo-grid. As the concrete cracks the entire load will directly be transferred to the geo-grid and specimens still resist further load.

This load resisting mechanism of geo-grid specimens is categorized into three different stages as shown in Figure 2.8. The load-deformation behavior of the first stage is similar to the conventional specimen S1 but the crack propagation is restricted in tension zone due to embedded geo-grid. In 2nd stage, the applied load is resisted by the geo-grid with a gradual increase in load capacity. In 3rd stage, load starts to degrade after the yielding of geo-grid and the specimens fail in two halfs. Among the three stages, concrete contribution is predominant in first stage; later geo-grid contribution is predominant in the next two stages. Especially higher flexural strength is observed with high strength geo-grid reinforced prism specimens. A significant increase in flexural strength and deformation capacity of specimen with geo-grid is observed as compared to specimen without geo-grid.

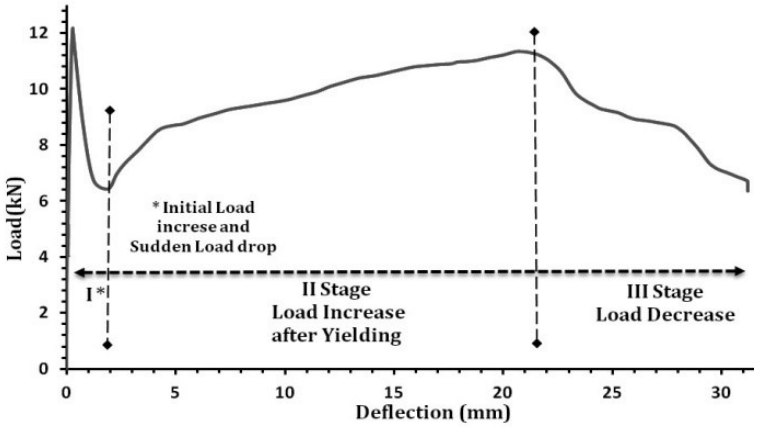

Figure 2.8: Three stages of geo-grid reinforced specimens load-deflection behaviour

The effect of resisting the flexure tension by the geo-grid increases as the layer of geo-grid increases (doubled) which can be clearly observed in the specimens S7–S9 with limited crack width but with secondary cracks in the mid portion of the specimens as shown in Figure 2.9. However, the load–deformation behavior is again similar to previous 3-stages pattern. The peak flexure strength of the specimens with two layers of geo-grid increases from 1.5 to 2.25 times depending on the strength of geo-grid as compared to specimens with single layer. In these specimens concrete spalling at the mid central portion

of the specimen is observed at large deflection. This shows the significance of double layer geo-grid reinforcement under bending.

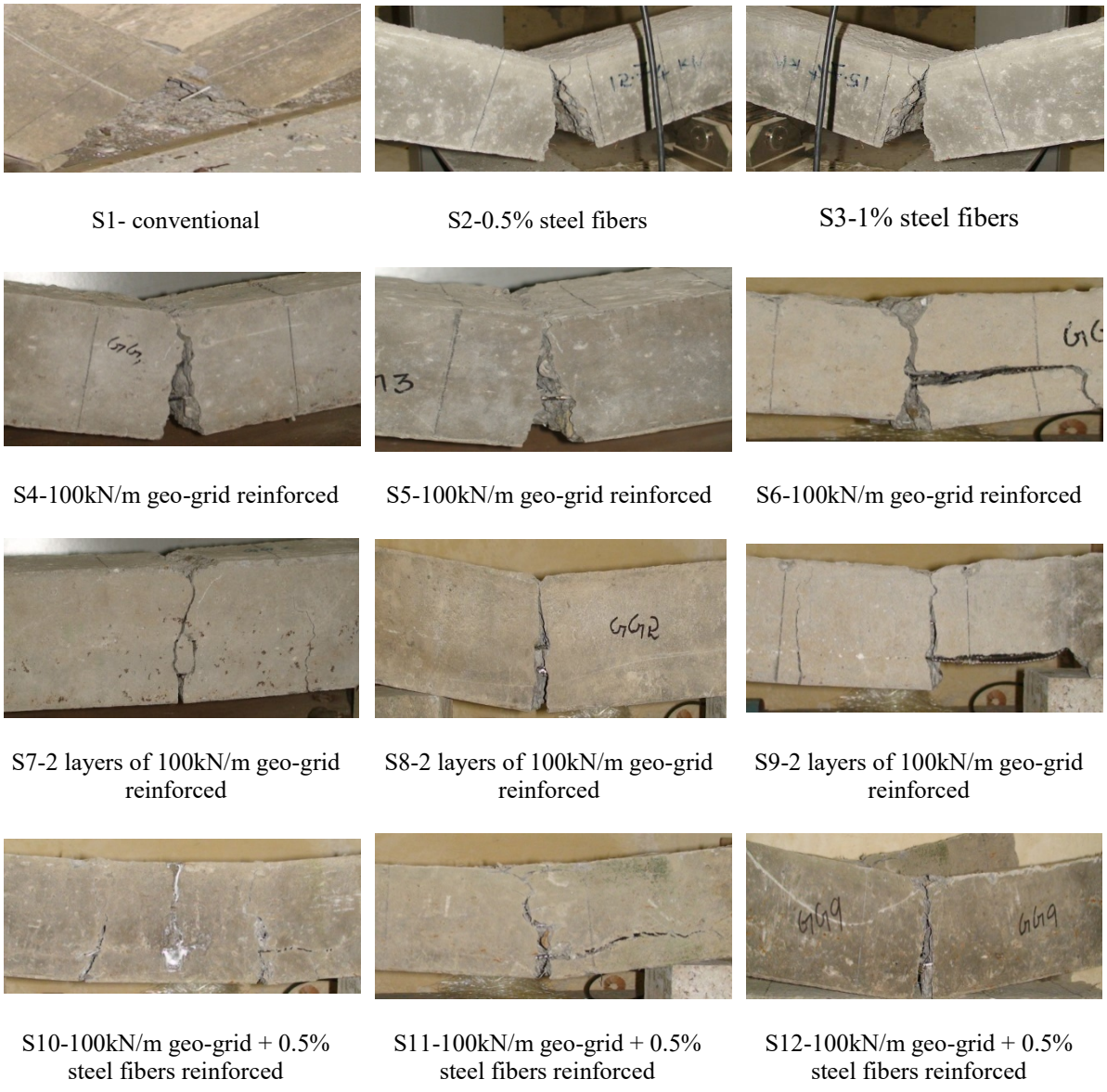

Figure 2.9: Failure pattern of flexure specimens

A significant change in the load deformation behavior and pattern of failure is observed in specimens S10–S12 reinforced with single layer of geo-grid and steel fibers of 0.5%. A complete ductile behavior can be clearly observed from the load–deformation behavior of geo-grid specimens as shown in Figure 2.7d. These specimens have also undergone the lesser cracking with no sudden spalling of concrete cover as compared to other specimens reinforced with single layer geo-grid. Even with the horizontal cracks the specimen exhibits flexure failure against the brittle failure as observed in previous tested specimens. The presence of steel fibers supports the geo-grid not only at the initial stage of

cracking but also supports to resist the applied load and limiting the crack widening as shown in Figure 2.9.

The load-deformation behavior of specimens S11 and S12 shows that the specimens after reaching its peak capacity of 15 kN at the deflection of 2 mm, resist the same load up to the deflection of 35 mm. The presence of steel fibers in concrete increases the aggregate interlock property and restricts the embedded geo-grid to slip that improves the post yield deflection. The failure of these specimens is also not sudden as observed in the previous specimens with geo-grid alone. This shows the effective composite action of steel fiber and geo-grid under flexure. This combined failure mechanism is clearly depicted in Figure 2.10. It is clear from the load-deformation behavior as well as failure pattern of the specimens S10–S12 that synergic effect of geo-grid and steel fibers change the failure pattern from brittle to ductile but also sustain the peak load to a higher deflection without significant loss in load carrying capacity. The effectiveness of composite mechanism completely depends on the strength, type and position of geo-grid in specimens. Hence the geo-grid can be efficacious in transferring tensile stress across the crack and can act like continuous fibers in bridging the cracks.

(a) Composite effect of geo-grid (100kN/m) and steel fiber

(b) Composite effect of geo-grid (200kN/m) and steel fiber

Figure 2.10: Enlarge failure pattern view of geo-grid reinforced specimens with steel fibers

Performance of the prism specimens under flexure is also compared in the form of energy dissipation which is calculated on the basis of area under the load–deformation curves. Figure 2.11 shows the energy dissipation of the specimens with and without geo-grid. It is clearly observed from the energy dissipation that the geo-grid with steel fiber specimens is effective for resisting the flexure tension. The dissipation of energy under different types of specimen varies from 1 to 10 times in comparison to conventional specimen (S1). Steel fibers reinforced specimens (S3) exhibit brittle mode of failure but provide gradual load degradation till the failure occurs. It enhances the specimen to dissipate 100% higher energy than S1. However, the only use of geo-grid in specimens S4–

S6 increases the flexure resisting capacity significantly. These performances of specimens increase to a greater extent by the use of multiple geo-grid layers in specimens S7–S9. There is a steady absorption in energy with the use of steel fibers with single layer geo-grid in prism specimens S10–S12. However, the presence of steel fiber restricts the sudden degradation in load after initial cracks and supports the grid reinforcement enhancing the inelastic behavior with improved energy absorption capacity as compared to geo-grid reinforced specimens without steel fibers. The observed energy absorption equals the measured value of two layer geo-grid specimens. It can be concluded that the use of steel fibers with single layer geo-grid reinforcement can provide enhanced inelastic behavior and damage tolerance capacity.

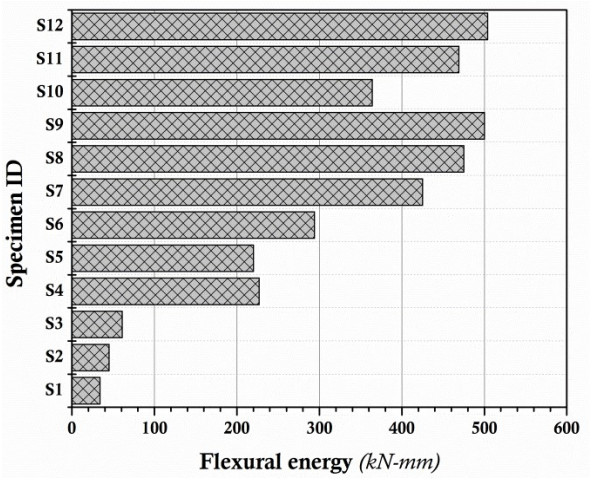

Figure 2.11: Cumulative energy dissipation of geo-grid reinforced flexural prism specimens

2.4 Flexural Behavior of Geo-Grid Confined RC Beam Specimens with Steel Fibers

Eighteen RC beams with different configurations were prepared and tested under static loading. The foremost objective of testing RC beam specimens under flexure and shear was to evaluate the confining effect of geo-grid with different stirrups spacing. The synergetic effect of steel fibers was also studied with and without geo-grid confinement to improve the inelastic behavior. The primary testing element of this experimental program consisted of four types of RC beams with different reinforcement detailing and configurations.

The detailed configuration of RC beam specimens of type A, B, C and D is summarized in Table 2.4.

Table 2.4: Detailed configuration of geo-grid confined RC beam specimens

Specimen ID	Longitudinal reinforcement		Transverse reinforcement		Steel fiber	Description
	top (mm)	**bottom** (mm)	**size** (mm)	**spacing** (mm)	%	
Type A	**Confined**					
B 1	2 Nos. 8 Ø	2 Nos. 10 Ø	6Ø	150	-	Conventional beam I
B 2	2 Nos. 8 Ø	2 Nos. 10 Ø	6Ø	150	1.0	Steel fiber reinforced beam-I
B 3	2 Nos. 8 Ø	2 Nos. 10 Ø	6Ø	150	0.5	Geo-grid confinement in hinge region with steel fiber.
Type B	**Moderately confined**					
B 4	2 Nos.8 Ø	2 Nos. 10 Ø	6Ø	250	-	Conventional beam II
B 5	2 Nos.8 Ø	2 Nos. 10 Ø	6Ø	250	1.0	Steel fiber reinforced beam- II
B 6	2 Nos.8 Ø	2 Nos. 10 Ø	6Ø	250	1.0	Geo-grid confinement in hinge region with SFRC
Type C	**Lightly confined**					
B 7	2 Nos.8 Ø	3 Nos. 10 Ø	6Ø	450	-	Conventional beam III
B 8	2 Nos.8 Ø	3 Nos. 10 Ø	6Ø	450	1.0	Steel fiber reinforced beam- III
B 9	2 Nos.8 Ø	3 Nos. 10 Ø	6Ø	450	0.5	Confined using 100 kN/m geo-grid with steel fiber.
B 10	2 Nos.8 Ø	3 Nos. 10 Ø	6Ø	450	0.5	Confined using 200 kN/m geo-grid with steel fiber.
B 11	2 Nos.8 Ø	3 Nos. 10 Ø	6Ø	450	1.0	Confined using 100 kN/m geo-grid with steel fiber.
B12	2 Nos.8 Ø	3 Nos. 10 Ø	6Ø	450	1.0	Confined using 200 kN/m geo-grid with steel fiber.
Type D	**Confined to Moderately Confined**					
B 13	2 Nos.12 Ø	2 Nos. 20 Ø	8Ø	150	-	Conventional Beam IV
B 14	2 Nos.12 Ø	2 Nos. 20 Ø	8Ø	200	-	Geo-grid (250 kN/m) confinement along with 200 mm stirrups spacing
B 15	2 Nos.12 Ø	2 Nos. 20 Ø	8Ø	200	0.5	Geo-grid (250 kN/m) confinement along with 200 mm stirrups spacing
B 16	2 Nos.12 Ø	2 Nos. 20 Ø	8Ø	250	-	Geo-grid (250 kN/m) confinement along with 250 mm stirrups spacing
B 17	2 Nos.12 Ø	2 Nos. 20 Ø	8Ø	250	0.5	Geo-grid (250 kN/m) confinement along with 250 mm stirrups spacing
B 18	2 Nos.12 Ø	2 Nos. 20 Ø	8Ø	200	1.0	Steel fiber 1% with 150mm stirrups spacing

Fe 500 grade steel was used for longitudinal reinforcement and Fe 250 grade steel reinforcement was used for transverse reinforcement in first three types A, B, C (Figure 2.12). The cross sectional sizes of these specimens remained the same but the percentage of flexural and shear reinforcement differed. In type D specimens Fe 500 grade steel was used for both longitudinal and transverse reinforcement.

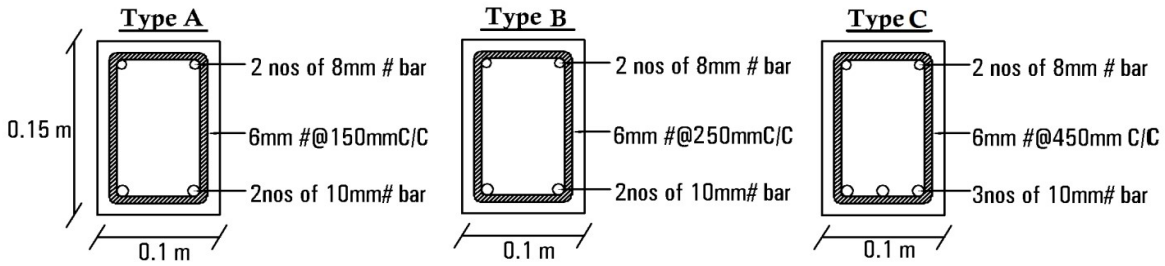

Figure 2.12: Reinforcement and cross section details of RC beams specimens (Type A, B, C)

In the first two types, geo-grid confinement was used only in plastic hinge region. Geo-grid was wrapped around the longitudinal reinforcement of beam specimens with 100mm over lap length as shown in Figure 2.13. The two ends of the grid were tied with the help of binding wire in the compression zone, since the CMD ribs in bottom and other two sides will restrict the lateral movement of geo-grid. In the third type of specimen, geo-grids were completely wrapped between the provided stirrups to avoid practical difficulties during concreting. Alternative grid strips were removed in compression zone of the beam specimens as shown in Figure 2.14. In the fourth type, three different spacing of stirrups were used with and without geo-grid confinement and steel fibers as shown in Figure 2.15.

(a) Reinforcement (b) Geo-grid positioning (c) Geo-grid cofinement (d) Grid confinement

Figure 2.13: Construction technique of geo-grid confinement in RC beams

Figure 2.14: Typical geo-grid confinement details in Type-C beam

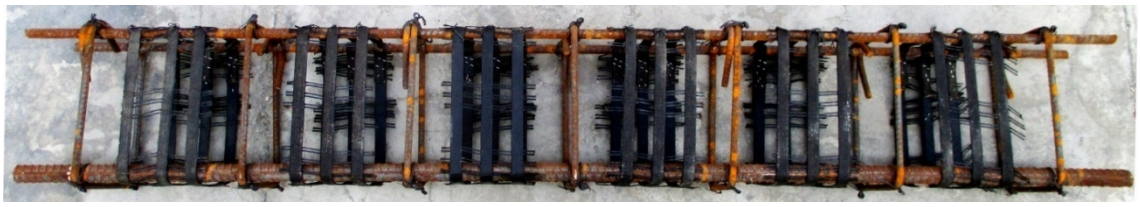

Figure 2.15: Partial geo-grid confinement in Type-D specimen

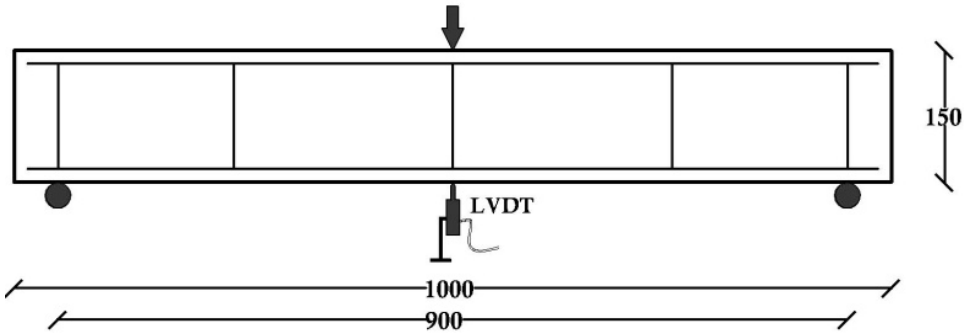

Figure 2.16: Typical experimental test setup of Type-A, B and C RC beam specimens

The first three types of beam specimens were tested under single point static loading as shown in (Figure 2.16) and the fourth type (Figure 2.17) beam specimens were tested under two point loading in a computerized 3000kN capacity flexural testing machine under load control with the rate of 50N/s. The corresponding mid-span deflection was measured using LVDT as shown in Figure 2.16.

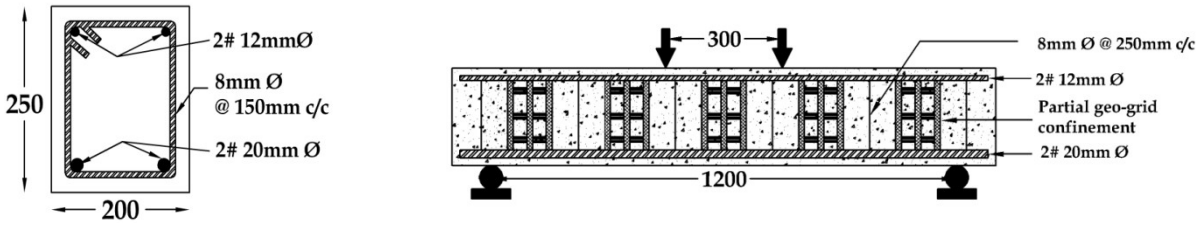

(a) Cross section (b) Test setup

Figure 2.17: Typical details of Type-D RC beam specimens

2.4.1 Load–Deflection Behavior of RC Beams

The load-deflection responses of each tested beam specimens as given in Table 2.5 are presented in Figure 2.18 and the test results are summarized in Table 2.5. The beam with steel fibers shows different load-deflection behavior with respect to the provided confinement. The specimens B2 and B5 show remarkable increase in post yield deflection as compared to conventional beam specimens B1 and B4 respectively. In the specimen B 8, shear strength increases but is unable to manifest the post peak behavior as a result of

inadequate stirrups. It clearly demonstrates the significance of closer confinement in ductility of beams with steel fibers

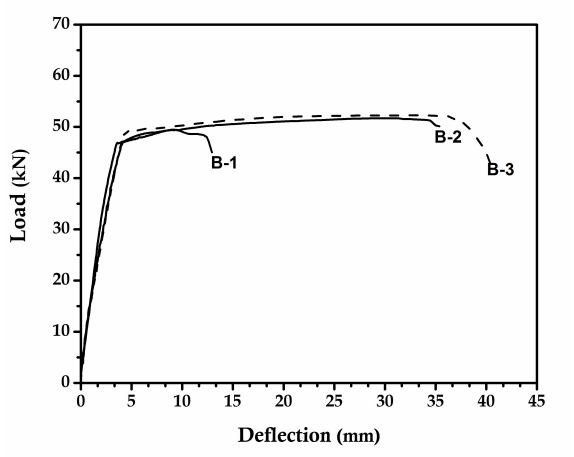

(a) Type-A-confined

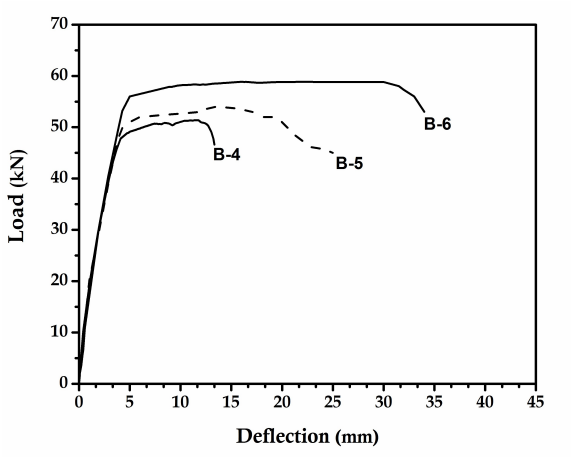

(b) Type-B-moderately confined

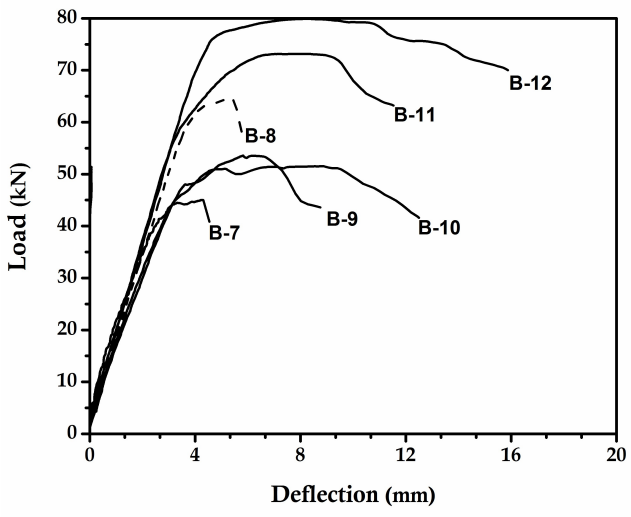

Type-C-lightly confined

Figure 2.18: Load deflection curve of all types of RC beams

. Beam specimens with closely spaced transverse reinforcement and the fiber stress transferring mechanism across the crack help to hold the peak load upto a large deflection after yield and allow the tension reinforcement to yield. In beam specimen B5, the higher spacing of transverse reinforcement restricts the steel fiber composite action as compared to beam specimen B2. This test result emphasises the importance of transverse reinforcement ratio with steel fibers since the distribution of steel fiber during concrete mixing may not be even as expected and not be placed in the expected region of a section where energy is dissipated. Thus adequate amount of transverse reinforcement is recommended to make proper and reliable use of fibers to effectively enhance the strength and deformation capacity of RC member.

Table 2.5: Summarized average test results of RC beam specimens

Specimen ID	Yield stage		Maximum stage		Ultimate stage		Ductility factor (μ)	Energy dissipation (kN)-mm
	P_y(kN)	Δ_y (mm)	P_m(kN)	Δ_m(mm)	P_u(kN)	Δ_u(mm)		
Type A								
B 1	48.0	3.4	49.5	09.1	45.03	12.9	3.8	540
B 2	49.0	3.2	52.2	30.1	48.32	36.0	11.3	1704
B 3	51.0	4.0	52.3	32.9	42.31	45.0	11.3	1976
Type B								
B4	50.0	3.2	51.4	11.7	46.61	13.3	4.0	584
B5	51.0	3.5	54.0	13.0	45.00	25.0	7.1	1191
B6	58.0	4.0	58.9	16.4	53.00	34.0	8.5	1856
Type C								
B7	44.1	3.1	45.0	4.3	40.86	4.5	1.4	150
B8	63.8	5.0	64.6	5.3	57.85	5.8	1.2	230
B9	47.8	3.6	53.5	6.3	43.61	8.8	2.5	354
B10	45.3	3.4	51.5	8.4	41.85	12.4	3.8	538
B11	70.0	4.9	73.2	7.3	63.21	11.5	2.4	649
B12	74.1	4.4	79.9	8.1	70.25	15.8	3.6	1056
Type D								
B13	261.4	6.6	261	6.6	200	7.2	1.1	1090
B14	235.9	6.2	235	6.2	165	10	1.6	1587
B15	269.2	5.8	270	6.0	230	10.4	1.8	2040
B16	270.2	6.3	273	6.7	230	8.2	1.3	1440
B17	250.1	6.1	254	6.5	220	9.8	1.6	1757
B18	280.5	6.1	281	6.5	220	9.6	1.6	1880

The test results also point out the synergetic effect of geo-grid confinement and fibers on the flexure and shear behavior of RC beams. There is significant improvement in

load carrying capacity of beam specimen B3 as compared to specimens B1 and B2, with a stable and improved post yield behavior, as shown in Figure 2.18. In specimen B3 the geo-grid confinement allows crack formation but restricts its rate of growth and enhances the efficiency of steel fiber in concrete even with lesser volume as compared to specimen B2. This can be clearly seen from the failure pattern of specimen B2 and B3. In Type-B, the geo-grid confinement works more effectively than with closely spaced conventional transverse reinforcement (Type-A). This is possibly due to the adequate spacing between the stirrup and the grid confinement. In the Type-A the contribution of stirrup in resisting the force is predominant because of closer spacing, while in Type-B the confining action of grid confinement and fibers with stirrups cause synergetic effect and significantly enhances the post yield behavior. In specimen B6, the measured average ultimate load is 20% higher than specimens B4 and B5 respectively. It also contributes higher energy dissipation by sustaining the peak load upto 30mm deflection, whereas steel fiber specimen does not hold the peak load after 20mm deflection as shown in Figure 2.18.

The test results of Type-C beam specimens evidently prove the influence of geo-grid confinement on the shear behavior of RC beams. As expected, conventional specimen B7 fails in brittle shear due to large spacing of stirrups. The use of steel fiber (V_f -1%) in beam specimen B8 contributes to an average of 50% increase in shear strength over the control beam specimen B7, but the specimen again fails in shear. This increase in strength is due to the increased tensile strain property of fiber reinforced concrete over plain concrete. The beam specimen B9 shows 20% higher shear strength with prominent post yield response over conventional and steel fiber specimen. The observed load at failure is 43kN with 9 mm deflection which clearly reveals the synergetic effect of steel fiber and geo-grid confinement in shear resistance behavior after yield. It is also observed that with the high strength geo-grid and same % of steel fiber (V_f -0.5%) as in case of beam specimen B10, the extent of deflection after shear cracking is much larger as compared to lower strength geo-grid. In beam specimens B11, an average of 75% to 100% higher shear strength is observed as compared to control specimen B7. This increase in shear strength becomes 10% to 30% higher as compared to fiber reinforced beam specimen B8. It is also observed that the higher volume of steel fiber works better with geo-grid confinement than lower volume, particularly in case of shear deficient beam as shown in Figure 2.18. It also shows constant peak load after yielding upto a certain deflection with a stable post-yield behavior with gradual post yield degradation. The improved load - deformation characteristics of beam specimens B11 and 12 confined with high strength geo-grid and

higher volume of steel fiber (V_f= 1.0 %), are compared to other specimens including geo-grid confined specimens with lesser volume steel fibers.

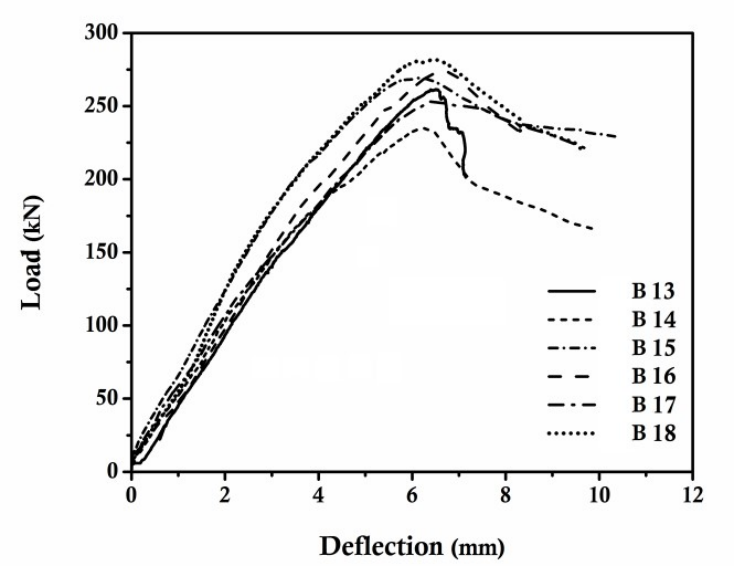

Figure 2.19: Load deflection curve of Type D beam specimens

In Type-D the lesser span to depth ratio with increased percentage of longitudinal reinforcement leads the specimens to fail in shear. Figure 2.19 shows the load deflection behavior of Type D specimens. The conventional specimen (B 13) exhibits sudden drop in load after peak as a result of shear crack widening. As discussed earlier the specimen B 16 with geo-grid confinement having higher stirrups spacing shows better load carrying capacity over B 14. The addition of steel fiber in partial geo-grid confined specimen improves the load carrying capacity and post peak deflection. In particular the specimen B 18 shows 10% increase in maximum load and shows enhanced post peak behavior over conventional (B 13) specimen. But the rate of post peak degradation is high as compared to geo-grid confined specimen.

2.4.2 Cumulative Energy Absorption

In order to examine the ductile behavior, energy absorption is calculated by estimating the area under the load-deflection curve. The energy absorption capacity of a component is also a significant parameter for the measurement of its post yield response and the calculated energy absorption is presented in Table 2.5. In type-A beam specimens (B2 and B3), the contribution of steel fiber and grid confinement can be clearly understood as the energy absorption capacity increases 3 to 4 times as compared to conventional beam specimen (B1). In Type-B beam specimens, the strength enhancement along with higher inelastic deformation is exhibited by grid confinement with steel fiber. The beam

Specimens B6 and B5 show 3 times and 1.5 times higher energy absorption than conventional specimen (B4). The lightly confined shear deficient beam specimens B7 - B12 show a meager energy absorption performance. However, the absorption of energy depends on the strength of geo-grid and % volume of steel fiber. The beam specimens with higher volume of steel fiber with geo-grid confinement show much higher energy dissipation than conventional (B7) and steel fiber beam specimen (B8). In type-D specimens, a marginal enhancement in energy absorption is observed over conventional beam specimen (B13). The geo-grid confined specimens with and without fibers show improved energy absorption. The combined effect of geo-grid with steel fiber absorbs higher energy as compared to merely geo-grid confinement.

2.4.3 Strength and Stiffness Degradation

Stiffness (k) property of a structural element is a measure of the resistance to deformation, given in Equation 2.2

$$k = \left[\frac{P}{\delta}\right] \qquad \textbf{2.2}$$

Where; P– load, kN; δ- deflection, mm

In load-deflection curve the initial slope (tangent) represents the initial stiffness whereas the slope of line joining the point of origin to the failure point represents the secant stiffness of the specimens. Normally, the difference between these two stiffness shows the post yield behavior of a structural component. In this study, the degradation in stiffness and strength are calculated in terms of post elastic strength degradation over yield strength [$F_{Deg\%}$] and post elastic stiffness degradation over yield stiffness [$K_{Deg\%}$] using the following Equation 2.3 and Equation 2.4 to estimate the inelastic behavior of all tested beam specimens

$$F_{deg}\% = \left[1 - \frac{(F - F_y)}{F_y}\right] * 100 \qquad \textbf{2.3}$$

$$K_{deg}\% = \left[1 - \frac{(K - K_y)}{K_y}\right] * 100 \qquad \textbf{2.4}$$

Where; $\boldsymbol{F}$ – Maximum load of each cycle, kN; $\boldsymbol{F_y}$- Yield load kN; $\boldsymbol{K}$ – Stiffness of each cycle, kN/mm; $\boldsymbol{K_y}$ – Yield stiffness, kN/mm

The inelastic performances of structural components are measured using the rate of change in strength and stiffness degradation over the post elastic rotation. Low rate of

change in degradation shows ductile performance of structural component and vice-versa. Figure 2.20 shows the stiffness and strength degradation plot over post elastic rotation of all the four types of RC beam specimens. The degradation plot of conventional specimens B1 and B4 shows 70% of stiffness degradation before rotation reaches 0.02 radian. The absence of stirrups in (Type-C) beam specimen B7, the degradation is 60% over the post yield rotation of 0.005. The effect of reinforcement yielding can easily be understood by comparing the degradation plot of all the four conventional specimens B1, B4, B7 and B13. The degradation plot of B7 is nearly a straight line i.e. no yielding behavior whereas the plot of conventional specimens B1 and B4 is linear upto a certain extent and becomes non-linear due to yielding of longitudinal reinforcement. The effect of steel fiber can also be evident from the degradation plot, beam specimen B2 shows more than 80% stiffness degradation at 0.06 rad., whereas the same degradation occurs in specimen B5 at 0.04 rad.

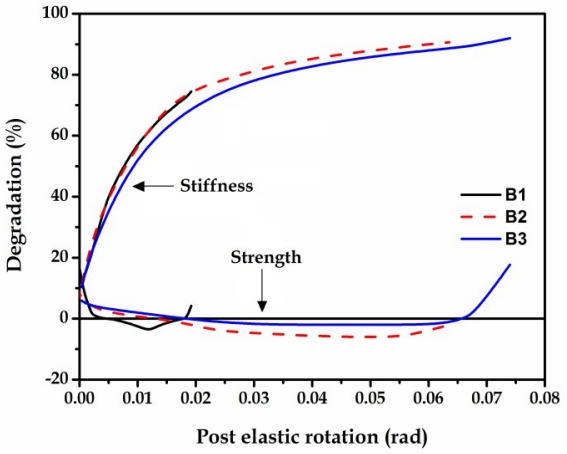

(a) Type-A (confined)

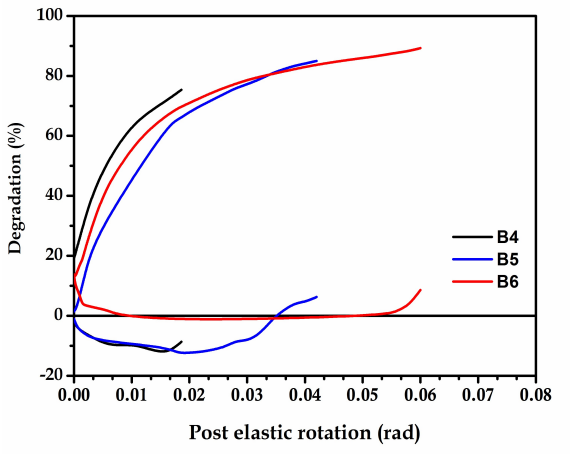

(b) Type-B (moderately confined)

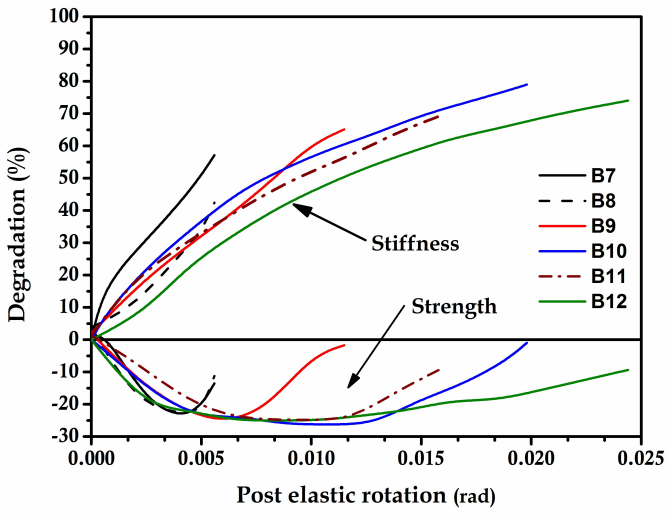

Type-C (lightly confined)

Figure 2.20 Strength and stiffness degradation of geo-grid confined RC beams

The degradation plot of specimen B8 is nearly straight due to the absence of stirrups i.e. approximately 60% degradation occurs at 0.01 rad. The degradation plot of the geo-grid confinement specimens shows better post elastic behavior over conventional and SFRC beam specimens. The specimen B3 shows 90% degradation at 0.07 radian and specimen B6 at 0.06 radian. In particular, beam specimen B6 shows 1.5 to 3 times higher post elastic rotation over steel fiber (B5) and conventional (B4) specimens. Two to three times increase in post elastic rotation of specimens B9 to B12 is observed as compared to beam specimen B7 and B8. The employed high strength geo-grid with higher volume steel fiber specimen shows significantly higher post elastic rotation over other specimens.

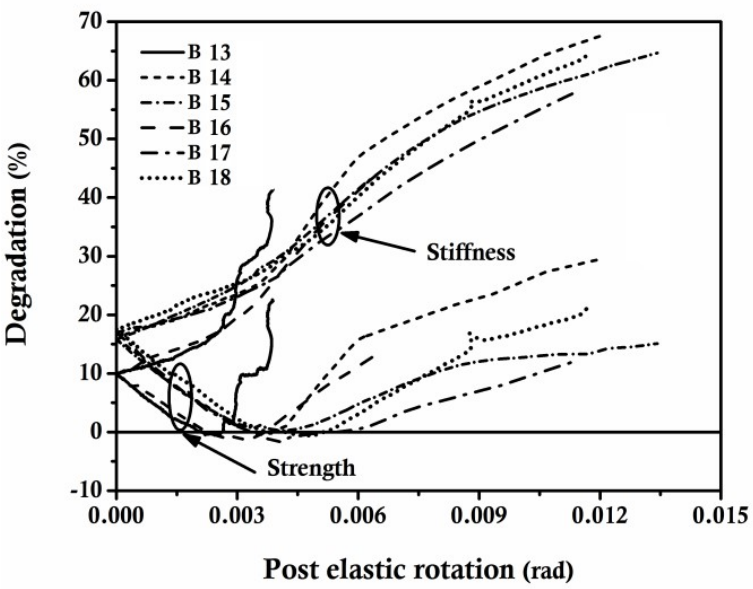

Figure 2.21: Stiffness degradation of Type D (moderate to lightly confined) RC beams

Figure 2.21 shows the stiffness degradation of Type D specimens. The early shear crack formation and brittle failure in specimen B 13 in Type-D show least performance in strength and stiffness degradation. The degradation plot of beam specimen B 13 is nearly vertical with high rate of degradation and finally the specimen fails at 0.004 radian. The other specimens in type D sustain the post yield rotation up to 0.012 radian that reflects the influence of geo-grid confinement. The rate of strength and stiffness degradation is less in beam specimen B 15 and B 17 as compared to specimen B 14 and B 16 because of the presence of steel fiber. It is clearly indicated that the contribution of geo-grid confinement even with higher spacing stirrups possesses better post yield stiffness retention. The synergetic effect of steel fibers further enhances the performance of beam specimens.

2.4.4 *Cracking Behavior and Failure Pattern*

The formation of cracks and their patterns are monitored in beam specimens during testing and are marked on the surface of the specimens as shown in Figure 2.22-2.24.

(a) B1-Conventional specimen(confined)

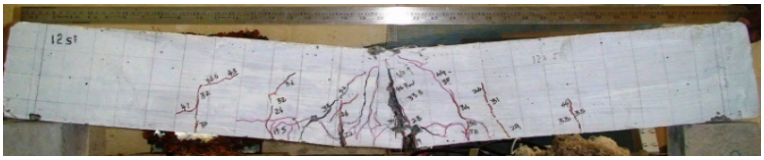

(b) B2-Steel fiber reinforced concrete

(c) B3-Geo-grid confinement with steel fibers

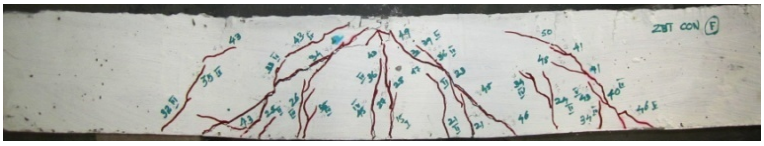

(d) B4-Conventional specimen(moderately confined)

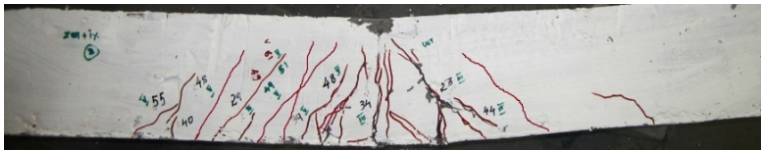

(e) B5-Steel fiber reinforced concrete

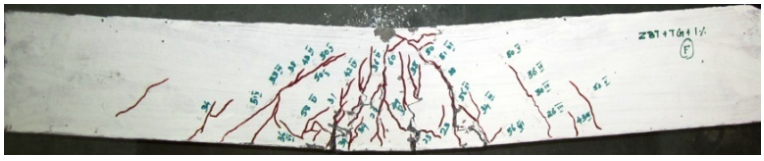

(f) B6-Geo-grid confinement with steel fibers

Figure 2.22: Crack pattern and failure mode of Type-A and Type-B beams

In case of conventional beam specimens; the amount of shear reinforcement governs the crack formation. The formation of cracks in beam specimens confined with geo-grid and steel fibers differs with respect to geo-grid confinement, strength of geo-grid along with volume of steel fiber. Generally, in beam specimens, the first crack is initiated at mid span region and as the load increases, vertical cracks are formed throughout the depth of beam specimen till the failure occurs. In beam specimens B2 and B5 with steel fiber, initially flexural cracks develop and as the load further increases a few more inclined

cracks are observed. At final stage, multiple micro vertical cracks are also noticed with a few flexural cracks at the mid span region. As the load further increases, the cracks become intense and allow the tensile reinforcement to yield and the specimen exhibits ductile mode of failure. In specimen B3, initial cracks are noticed in the region between geo-grid confinement and stirrups along with the flexural cracks. In specimen B6, numerous micro cracks are developed initially in the mid region. At failure, three to four primary cracks with an average width of 3 mm to 10 mm are measured. It is noteworthy to mention here that in beam specimen B6, the dominance of dense flexural cracks is noticed till failure without the development of any inclined crack.

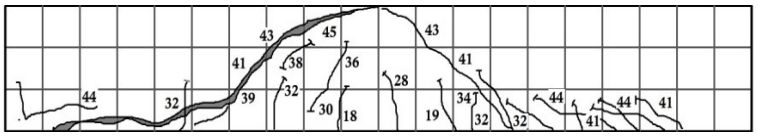

(a) B7-Conventional specimen (lightly confined)

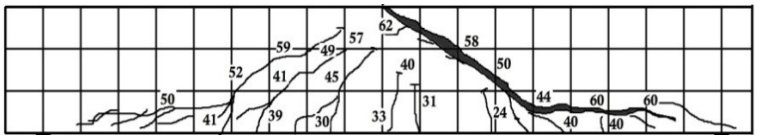

(b) B8-Steel fiber reinforced concrete

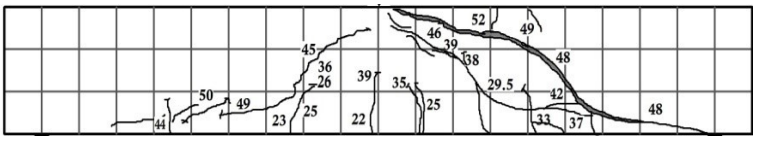

(c) B9-Geo-grid confinement with steel fibers

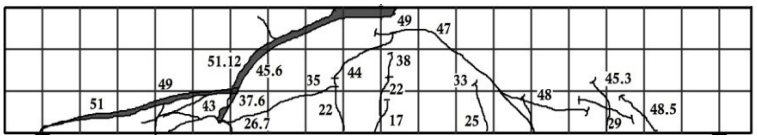

(d) B10-Geo-grid confinement with steel fibers

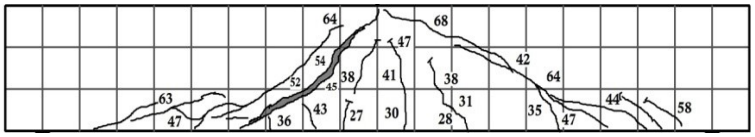

(e) B11-Geo-grid confinement with steel fibers

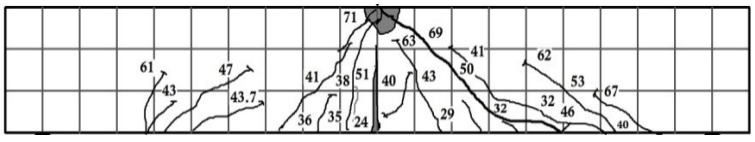

(f) B12-Geo-grid confinement with steel fibers

Figure 2.23: Crack pattern and failure mode of Type-C specimens

The relationship between the stirrups and geo-grid confinement under flexure can be clearly observed from the failure pattern of beam specimens B9 to B12. The geo-grid confinement increases the post yield behavior along with the existing stirrups and steel

fibers that are effective in increasing the shear strength of beam specimens. Numerous inclined cracks are noticed but failure takes place with the widening of single shear crack as shown in Figure 2.23. The sudden shear failure demonstrates the ineffectiveness of steel fibers with inadequate shear reinforcement. Specimens with geo-grid confinement and 1% steel fiber (B11 and B12), show different crack patterns over 0.5% steel fiber specimens (B9 and B10). The contribution of higher volume steel fiber restricts the formation of shear cracks at early stage of loading. It is noticed that the contribution of high strength geo-grid with 1% steel fiber in specimen B12 increases the post yield deflection behavior by the formation of mid span vertical crack.

B 13-Type- D conventional specimen

B 14-Geo-grid confinement with 200mm stirrups

B 15-Geo-grid confinement with steel fibers

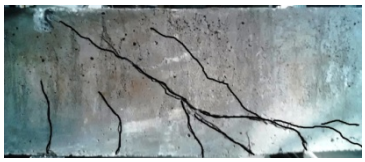

B 16-Geo-grid confinement with 250mm stirrups

B 17-Geo-grid confinement with steel fibers

B 18-Steel fiber reinforced concrete

Figure 2.24: Crack pattern and failure mode of Type-D specimens

Beam specimens of type-D, encounter shear failure as a result of low span to depth ratio. In conventional specimen, flexural cracks are noticed in the mid region during intial stage of loading, as the load increases, the inclined cracks occur in the shear span and finally specimen fails in shear as shown in Figure 2.24. The geo-grid confined beam specimen B 14 and specimen B15 with steel fibers show inclined cracks in the shear span region and specimens fail in shear with one primary crack as shown in Figure 2.24. In specimen B 16 and B 17 flexural cracks occur in mid span region and later inclined cracks develop in the shear span region as shown in Figure 2.24. The crack pattern of beam specimens B 14 and B 16 shows that the higher stirrups spacing allows the geo-grid to perform better than the closer spacing. The addition of steel fiber improves the failure behavior and damage tolerance capacity of beam specimens.

2.5 Cyclic Behavior of Geo-grid Confined Beam-column Joint Specimens

Two types of exterior beam-column joint specimens with different stirrups ratio were tested under reverse cyclic loading. Fe 500 grade steel was used as longitudinal reinforcement and Fe 250 grade steel was used as transverse reinforcement.

The complete details of these specimens are given in Table 2.6 in which five specimens are shear deficient and named as (EJ) and remaining four are retrofitted (REJ) to explore the efficacy of geo-grid confinement under different applications.

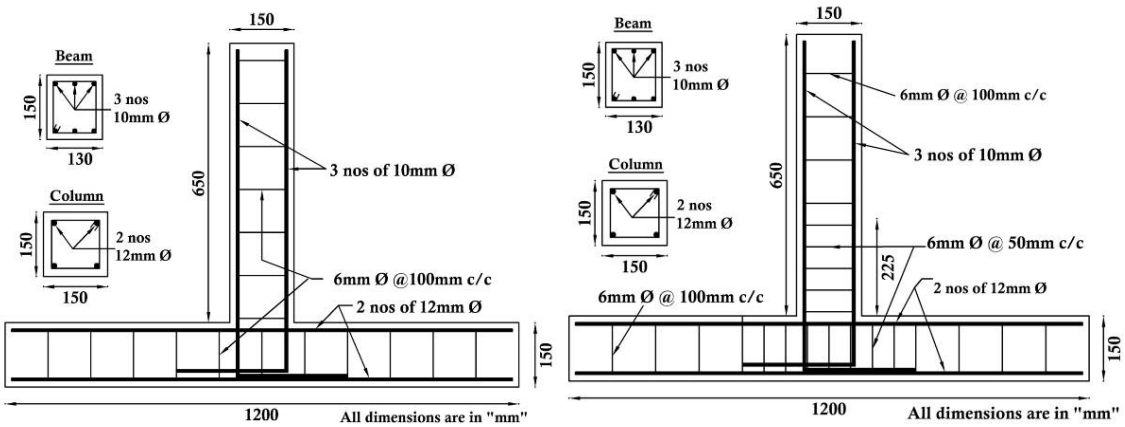

(a) EJ1-IS:456-2000 detailing (b) EJ2-IS:13920-1993 detailing

Figure 2.25: Reinforcement details of exterior beam-column joint specimens (a) EJ 1 (b) EJ 2.

(a) EJ 1-Conventional (b) EJ 3and EJ 4 partial geo-grid confinement

Figure 2.26: Typical details of beam-column joint specimens (a) EJ 1 (b) EJ 3 and EJ 4

In this test sequence, the first two beam-column joint specimens i.e. EJ 1 and EJ 2 were tested as conventional specimens with different spacing of transverse reinforcement as shown in Figure 2.25. The specimen EJ 3 was confined with geo-grid in addition to reinforcement details of specimen EJ 1, Figure 2.24. The specimen EJ 4 was similarly detailed as specimen EJ 3 but with 1% steel fiber. EJ 5 wais similarly detailed as EJ 1 with 2 % steel fibers. The previously tested beam-column joint specimens were repaired and retrofitted with geo-grid confinement with and without SFRC. The concrete and stirrups in

damaged portion of the previously tested joint specimens were thoroughly removed and recast with new lays of geo-grid confinement at different stirrups spacing. Polymer based cement slurry was used to create better bond between the old and fresh concrete.

Typical sectional details of retrofitted specimen are shown in Figure 2.27 while the details of the four retrofitted specimens are already given in Table 2.6.

Table 2.6: Configuration of geo-grid confined exterior beam-column joint specimens

Specimen ID	Spacing of Transverse Reinforcement (mm)	Special Configuration	Volume of Steel Fiber (%)	Description
EJ 1	100 mm C/C	×	×	Conventional confinement
EJ 2	50 mm C/C in joint hinge + 100 mm C/C in other region.	Ductile Detailing	×	Conventional confinement with ductile detailing
EJ 3	100 mm C/C	Geo-grid confinement in the hinge	×	Geo-grid confinement
EJ 4	100 mm C/C	Geo-grid confinement in the hinge.	1	Geo-grid confinement + SFRC
EJ 5	100 mm C/C	×	2	SFRC
REJ 1	150mm C/C stirrup spacing in the hinge region of beam and column and 100 mm C/C in other region	Geo-grid confinement in the hinge	×	Grid confinement
REJ 2	150mm C/C stirrup spacing in the hinge region of beam and column and 100 mm C/C in other region	Geo-grid confinement in the hinge.	1	Grid confinement + SFRC
REJ 3	200 mm C/C stirrup spacing in the hinge region of beam and 150mm C/C spacing in column hinge region and 100 mm C/C in other region	Geo-grid confinement in the hinge	×	Grid confinement
REJ 4	200 mm C/C stirrup spacing in the hinge region of beam and 150mm C/C spacing in column hinge region and 100 mm C/C in other region	Geo-grid confinement in the hinge.	1	Grid confinement + SFRC

In cyclic testing of beam-column joint specimens, beam portion was kept 90 deg vertical and the column portion of the joint was kept in the horizontal position held against the strong floor. Both ends of the column were supported using hydraulic jacks to apply axial load as shown in Figure 2.28. This test setup restricted column's horizontal movement and supported moment free rotation, and column was under fixed condition. The joints were tested under displacement controlled hydraulic actuator. One end of the

actuator was connected to the free end of the beam and the other end was connected to reaction wall. The cyclic loading was applied in the form of displacement control sine sweep wave at a very low frequency as shown in Figure 2.28. The amplitude of loading increased gradually from 5mm to the occurrence of failure with an interval of 5mm under displacement control to acquire the inelastic performance of the joint. All the specimens were tested up to failure and their corresponding load deformation response was recorded with the help of load cell and LVDT.

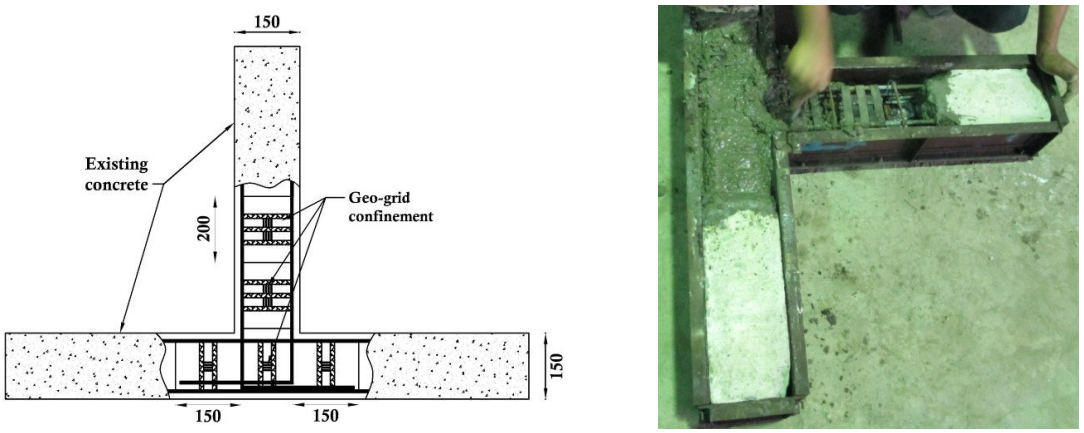

(a) Typical details (b) Construction method

Figure 2.27: Detailed configuration of retrofitted beam-column joint

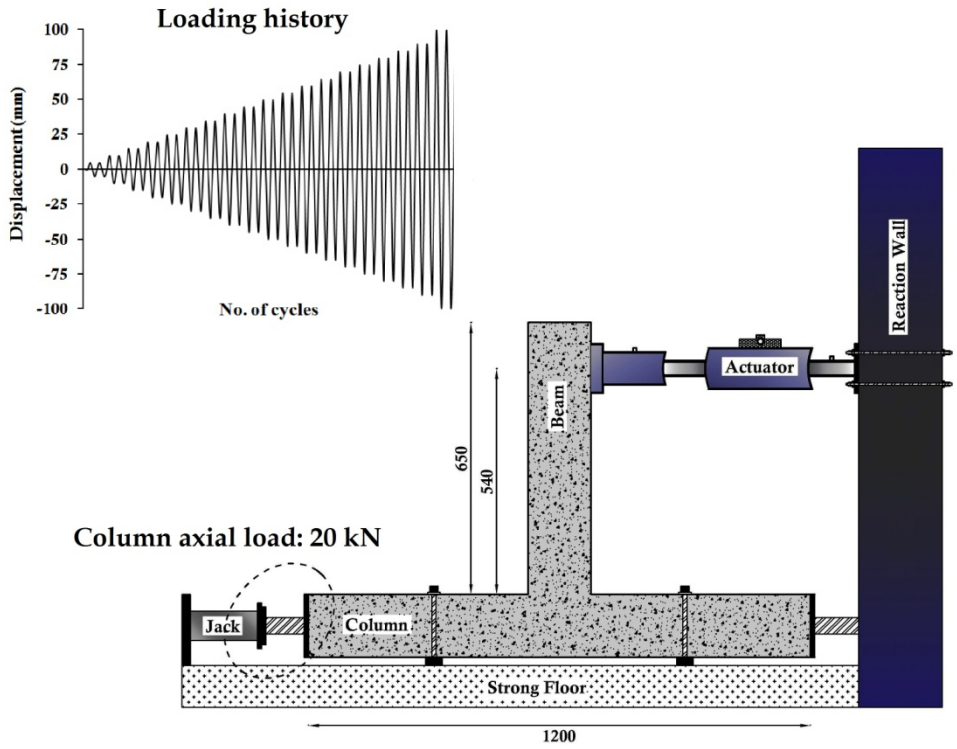

Figure 2.28: Experimental Test Setup of beam-column joint under Cyclic Loading

(All dimensions are in "mm")

Comparative cyclic performance of the tested beam-column joint specimens was evaluated on the basis of hysteresis behavior, load-deformation envelope curve, energy dissipation, strength and stiffness degradation, moment-rotation relationship and the damage characteristics with damage index.

2.5.1 Hysteresis Behavior of Beam-column Joint Specimens

The hysteresis behavior of the first five beam-column joint specimens (EJ 1 to EJ 5) under cyclic testing is presented in Figure 2.29 and the results are summarized in Table 2.7. It is observed that the load-deformation pattern after the yield of specimens is significantly improved by the use of geo-grid confinement and it is further improved by the use of SFRC as compared to conventional specimens with and without ductile detailing. However, the initial behavior upto pre yielding stage is nearly the same in all the test specimens. The use of ductile detailing (confinement) helps to improve the post yield load-deformation behavior of specimen EJ 2 in comparison to other conventional specimen EJ 1. However, the specimen still fails in shear in spite of confined reinforcement at the joint. There is sharp change in slope of descending branch of load deformation diagram in post peak region of the specimen. There is marked improvement in the hysteresis behavior of joint specimens after providing the confinement by the geo-grid. The geo-grid confinement not only helps in increasing the load carrying capacity of the specimen but also changes the mode of failure. The post peak behavior of specimen EJ 3 becomes gradual and shows ductile response before shear failure. The behavior is further improved in beam-column joint specimen EJ 4 by the use of SFRC at the joint in addition to geo-grid confinement. There is decrease in rate of degradation of load and stiffness after achieving the post -peak behavior with uniform distribution of minor diagonal shear cracking at the joint region of the specimen. The similar type of load-deformation behavior is observed in specimen EJ 5 with increased % of steel fiber. However, a minor reduction in deformation properties of the specimen is noticed as compared to specimen EJ 4. Therefore lesser volume of steel fiber can effectively be used along with geo-grid confinement that may help to increase the load-deformation performance of the joint.

The hysteresis behavior of the retrofitted beam-column joint specimens again confirms the efficacy of the geo-grid confinement under cyclic loading as shown in Figure 2.30. The tested joint specimens are retrofitted with new layer of geo-grid confinement with increased stirrups spacing. This shows that the geo-grid confinement works better even when the spacing of existing stirrups is higher than the conventional specimens. The

retrofitted specimens (REJ 2 and REJ 4) with grid confinement and SFRC show significant enhanced performance over the conventional specimens.

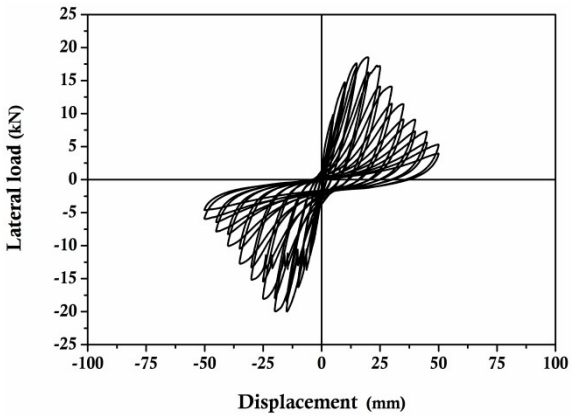

(a) EJ 1-IS 456 detailing

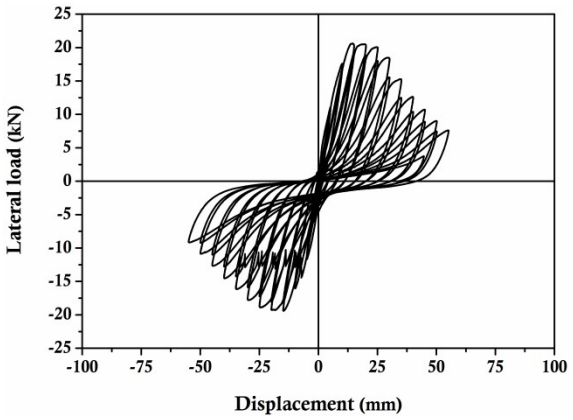

(b) EJ 2-IS 13920 detailing

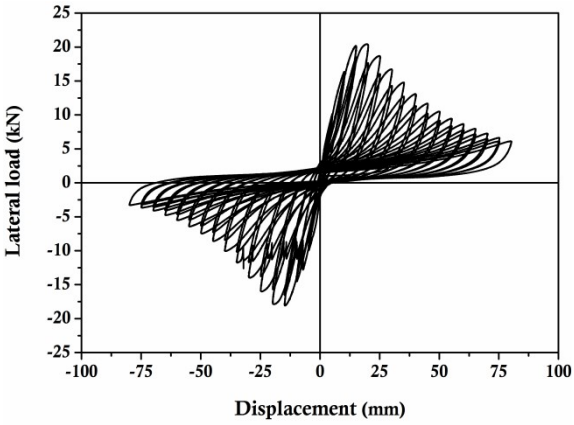

(c) EJ 3-Geo-grid confined

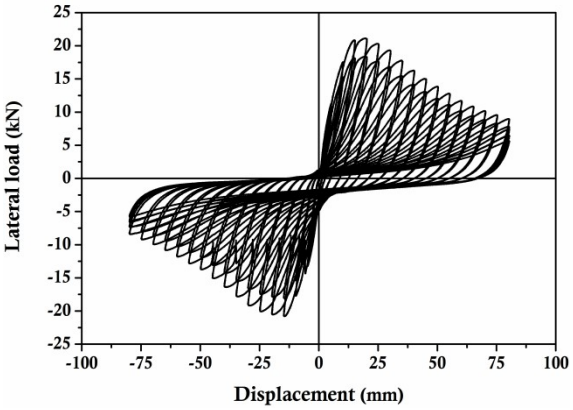

(d) EJ 4-Geo-grid confined with 1% steel fibers

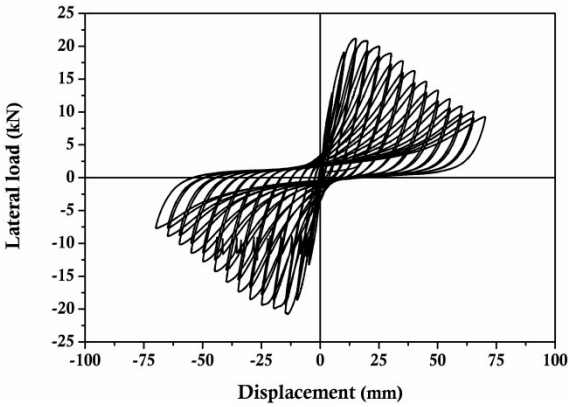

(a) EJ 5-2% steel fiber reinforced

Figure 2.29: Hysteretic curve of beam-column joint specimens with geo-grid confinement

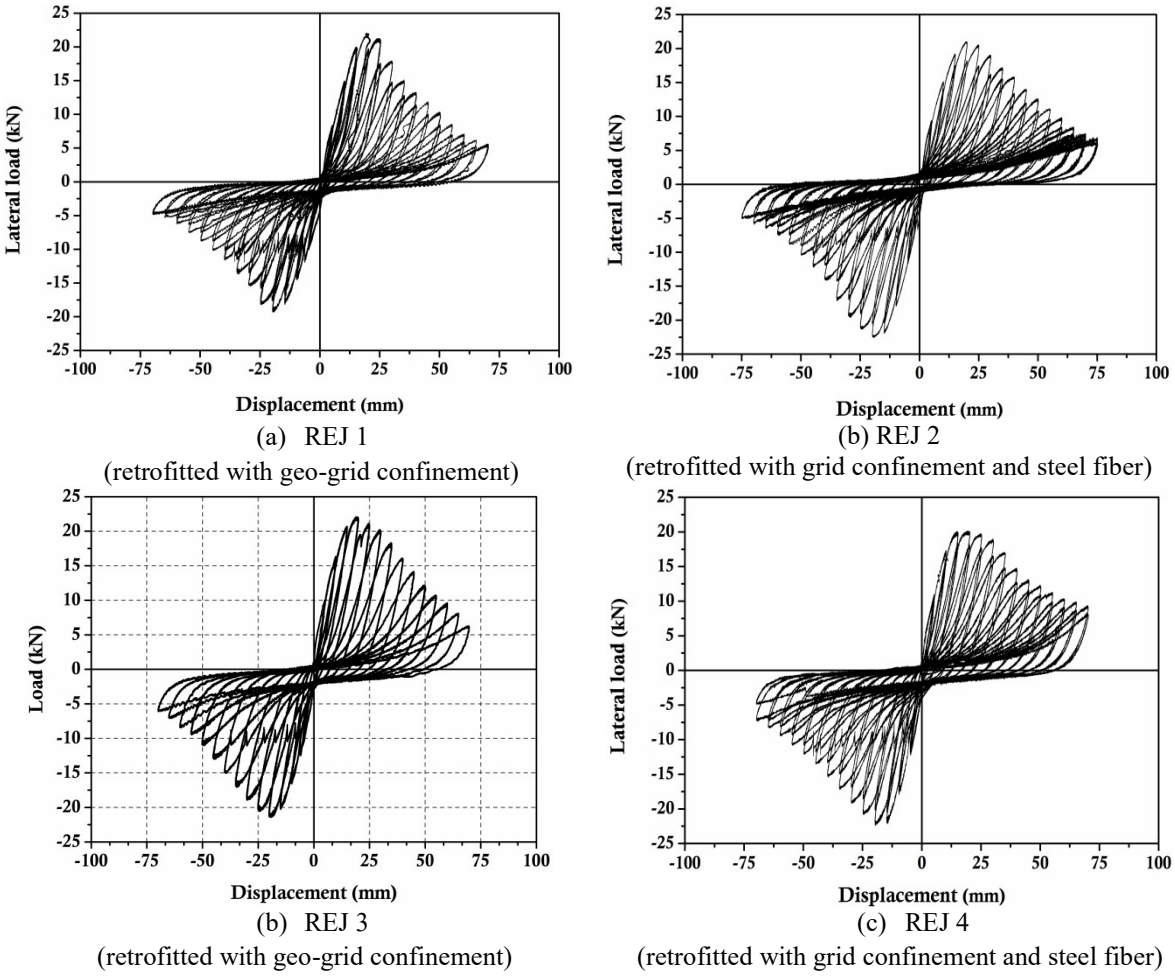

(a) REJ 1 (retrofitted with geo-grid confinement)

(b) REJ 2 (retrofitted with grid confinement and steel fiber)

(b) REJ 3 (retrofitted with geo-grid confinement)

(c) REJ 4 (retrofitted with grid confinement and steel fiber)

Figure 2.30: Hysteretic loop of retrofitted specimens with geo-grid confinement

Table 2.7: Cyclic test results of geo-grid confined beam-column joint specimens

S. ID	Maximum				Ultimate (experimental)				Displacement* calculated		Ductility*
	Positive		Negative		Positive		Negative		Δ_y	Δ_u	Δ_u/Δ_y
	P_m	Δ_m	P_m	Δ_m	P_u	Δ_u	P_u	Δ_u			
	kN	*mm*	*kN*	*mm*	*kN*	*mm*	*kN*	*mm*	*mm*	*mm*	
EJ 1	18.60	20	20.01	15	5.3	50	6.0	50	14.0	58.6	4.2
EJ 2	20.62	15	19.41	15	7.6	55	9.1	55	14.3	69.0	4.8
EJ 3	20.43	20	18.10	15	6.1	80	8.0	80	15.0	59.0	4.0
EJ 4	21.12	20	20.80	15	7.4	85	7.4	85	13.0	78.0	6.0
EJ 5	21.19	15	20.80	15	9.2	70	7.7	70	12.3	74.5	6.1
REJ 1	22.02	20	19.32	20	5.6	70	4.9	70	18.0	61.0	3.4
REJ 2	21.02	20	22.58	20	7.0	75	5.1	75	17.3	71.0	4.2
REJ 3	22.08	20	21.45	20	8.0	70	7.0	70	16.0	72.0	4.5
REJ 4	20.17	20	22.37	20	9.4	70	7.4	70	14.0	71.0	5.1

2.5.2 *Load-Deformation Envelope Curves*

The member ductility of all the tested specimens is calculated by the load-deformation envelops of the hysteresis behavior of the joint specimens as shown in Figure 2.31. The ductility parameter is an indication of the response after yield without significant reduction in peak strength of the specimens. Therefore, sometimes it is slightly misinterpreted since there is no well defined procedure for defining the yield and ultimate points in case of curvilinear type load-deformation envelop curves. In this study, a general procedure is defined for calculating the member ductility as shown in Figure 2.32 (Shannag et al. (2002)) and the calculated values are given in Table 2.7.

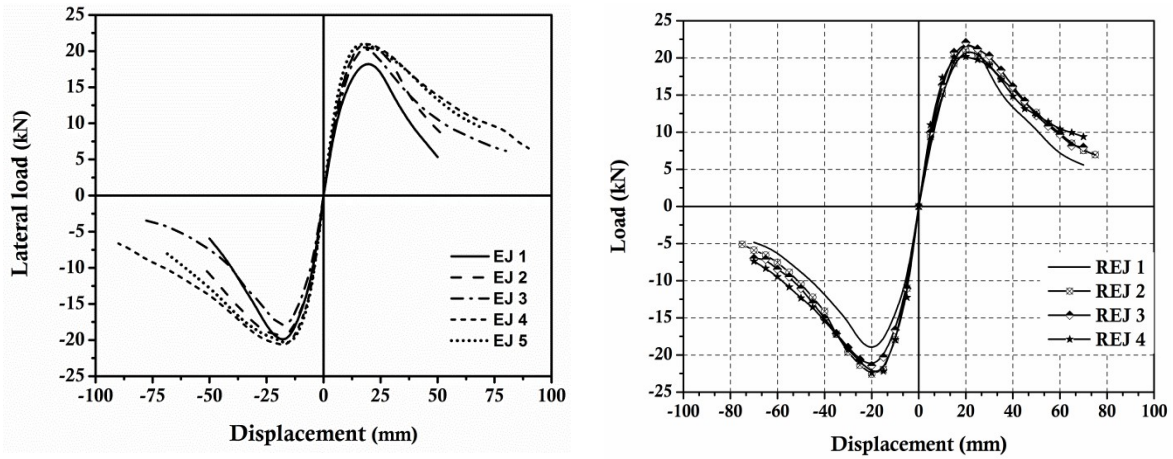

(a) Actual specimens EJ1-EJ6 (b) Retrofitted specimens (REJ1-REJ4)

Figure 2.31: Load-deflection envelope curve of geo-grid confined beam-column joint specimens

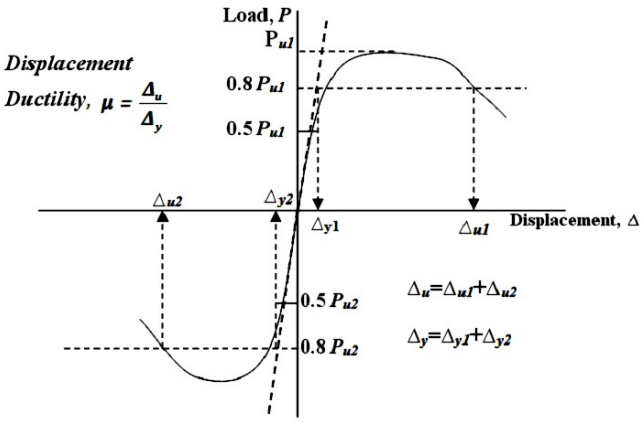

Figure 2.32: Procedure for the evaluation of ductility parameter (Shannag et al. (2002))

It is clearly observed that the geo-grid confined specimen with SFRC has much higher ductility (approximately one and half times) as compared to other conventional

specimens. The bridging action of steel fiber provides larger deflection without sudden loss in strength possessing higher ductility. The retrofitted specimens also illustrate comparative ductile response over other conventional specimens. In particular, the retrofitted specimens REJ 3 and REJ 4 show better ductile response over other two retrofitted specimens.

2.5.3 Strength and Stiffness Degradation

The strength and stiffness degradation versus post elastic drift for each tested specimen is plotted in Figure 2.33-2.34

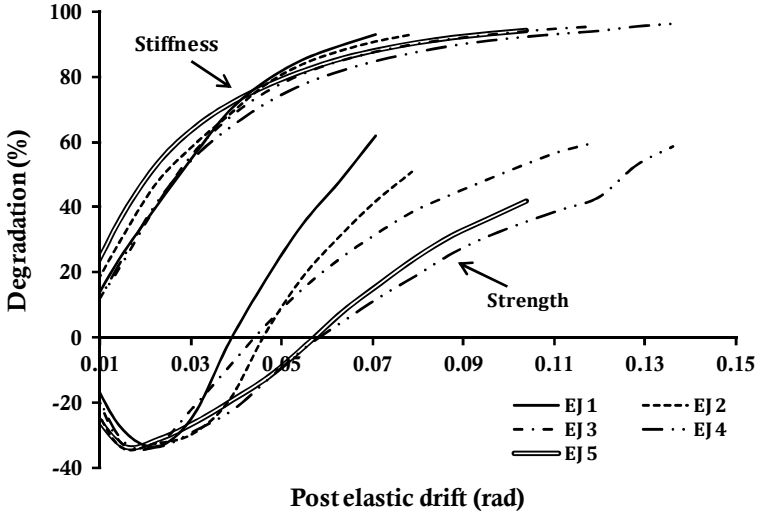

(a) Positive push

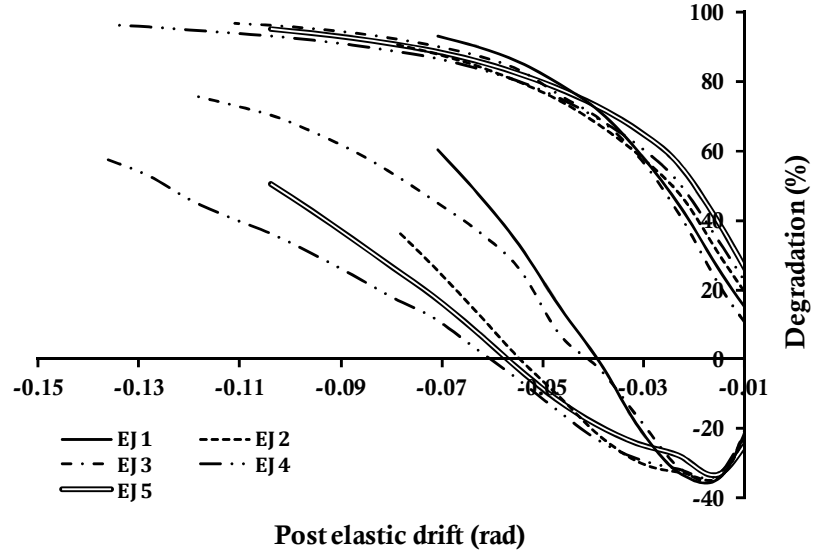

(b) Negative pull

Figure 2.33: Strength and stiffness degradation of actual geo-grid confined joint specimens

The degradation plot elevates the effectiveness of grid confinement in stiffness retention property. The joint specimen EJ 2 with conventional confinement reinforcement has low rate of degradation as compared to specimen EJ 1. The influence of geo-grid confinement is clearly visible from the rate of strength and stiffness degradation over post elastic drift as shown in Figure 2.33. It exhibits that the loss of 90% stiffness in conventionally confined specimens occurs at 0.06 radian whereas in geo-grid confined specimens at 0.08-0.09 rad.

Figure 2.34 authenticates the influence of geo-grid confinement in retrofitting work. The degradation plots of joint specimens REJ 3 and REJ 4 have low rate of strength degradation as compared to other two retrofitted specimens REJ 1 and REJ 2. The retrofitted specimens exhibit 70% loss in stiffness at 0.04 radian which increases to 95% at 0.12 radian. It manifests that geo-grid confinement decelerates the rate of stiffness degradation and holds the specimens to sustain upto 0.12 rad. This observed response of retrofitted specimens emphasizes the effectiveness of geo-grid confinement in structural engineering application along with existing stirrups with higher spacing.

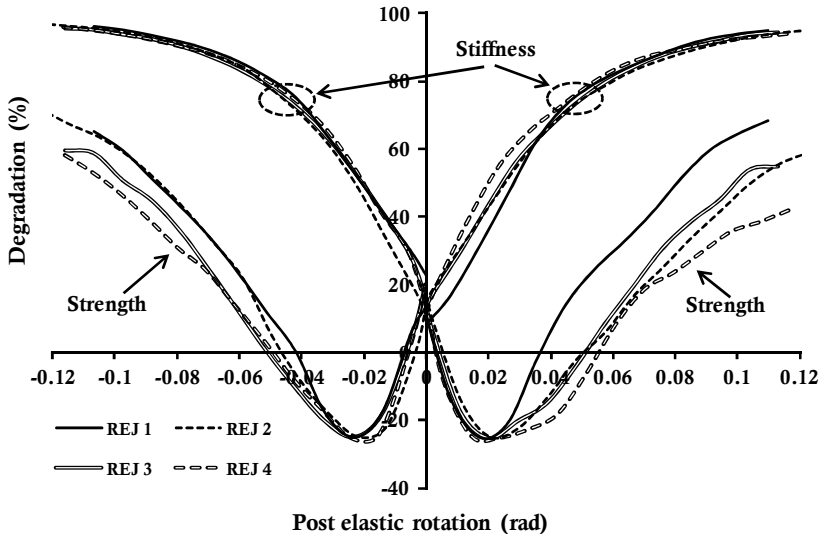

Figure 2.34: Strength and stiffness degradation of retrofitted joint with geo-grid confinement

2.5.4 *Energy Dissipation and Damping Behavior*

The energy dissipation capacity of a component is a significant parameter for the measurement of its response after yielding. Ductile response is governed by higher energy dissipation in subsequent cycles as deformation increases after yielding where the reverse of it manifests the brittle shear mode of failure of the component. Cumulative Energy

Dissipation [CED] parameter relates to cumulative energy after each subsequent cycle. The energy dissipation in each cycle is calculated on the basis of area enclosed by the hysteresis loop. The cumulative energy dissipation parameters for all the joint components with increased cyclic displacement are plotted in Figure 2.35.

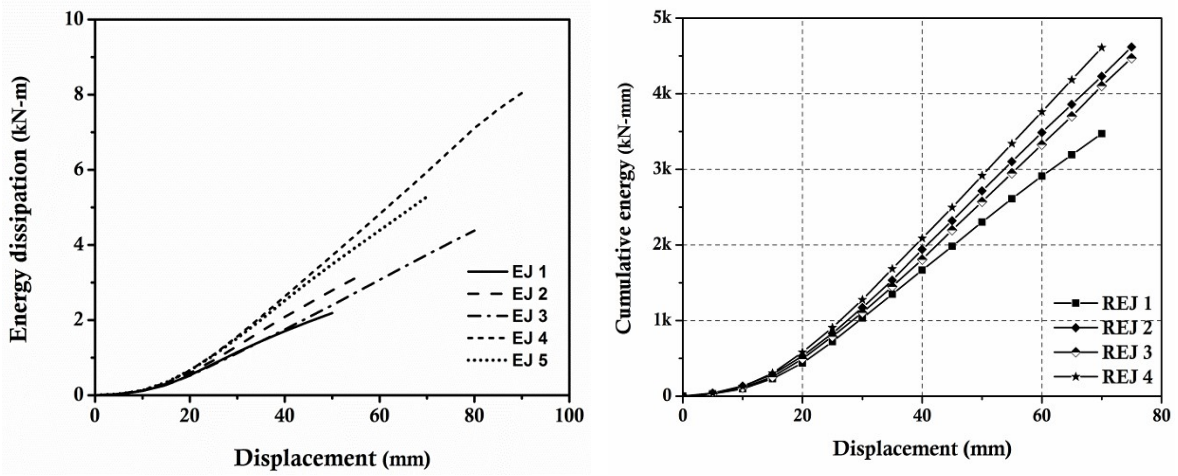

(a) Geo-grid confined specimens (b) Retrofitted joint with geo-grid confinement

Figure 2.35: Cumulative energy dissipation geo-grid confined joint specimens

It clearly manifests that the conventional joint specimens (EJ 1 and EJ 2) with and without ductile detailing have much lower ductile performance as compared to geo-grid confined specimens with steel fibers, however the performance of the joint EJ 2 is improved with ductile detailing. The geo-grid confined specimen EJ 3 exhibits two times higher energy dissipation over conventional joint specimens. The dissipated energy of EJ 3 is comparatively lower as compared to EJ 4 possibly because of the presence of steel fiber along with geo-grid confinement. It shows more stable and consistent energy dissipation without sudden change or drop. The specimen EJ 5 shows considerably better energy dissipation as compared to the conventional and geo-grid confined specimen but it is considerably lower as compared to geo-grid with lesser volume steel fiber specimen EJ4.

It is evident from Figure 2.35 (b) that the geo-grid confinement with higher stirrups spacing in retrofitted specimens is capable to dissipate higher energy as in the case of newly constructed specimens which also authenticates that the composite action works credibly in dissipating energy during cyclic loading. The retrofitted specimens REJ 1 and REJ 2 show enhanced CED level over conventional specimen EJ 1 and EJ 2.

The equivalent damping coefficient based on the relative energy dissipation (RED) parameters obtained from the hysteresis behavior of beam-column joint is also calculated and shown in Figure 2.36. It is evident that the average equivalent damping coefficient

with conventional confinement of joint specimen is in the range of 8 to 12% and it increases from 15% to 25% in geo-grid confined specimens with and without steel fibers. Figure 2.36 (b) shows geo-grid confinement with fibers in the damping behavior of retrofitted specimens. The increase in damping coefficient reflects the effectiveness of confinement and load-deformation capability of the specimens.

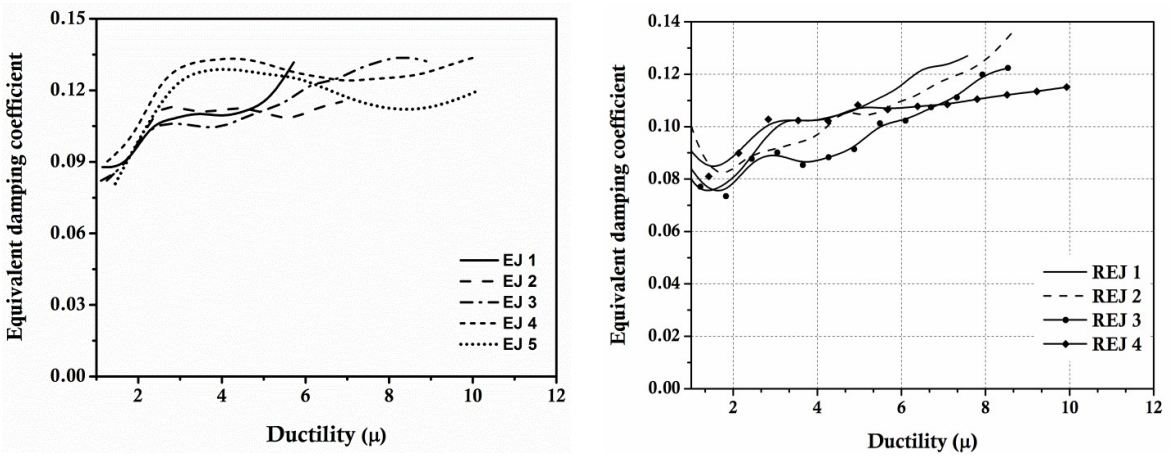

(a) Geo-grid confined specimens (b) Retrofitted joint with geo-grid confinement

Figure 2.36: Equivalent damping coefficient of geo-grid confined joint specimens

2.5.5 *Moment-Rotation Behavior*

The moment- plastic rotation relationships of all the tested joint specimens are compared with the specified values in ASCE/SEI 41-06 as shown in Figure 2.37.

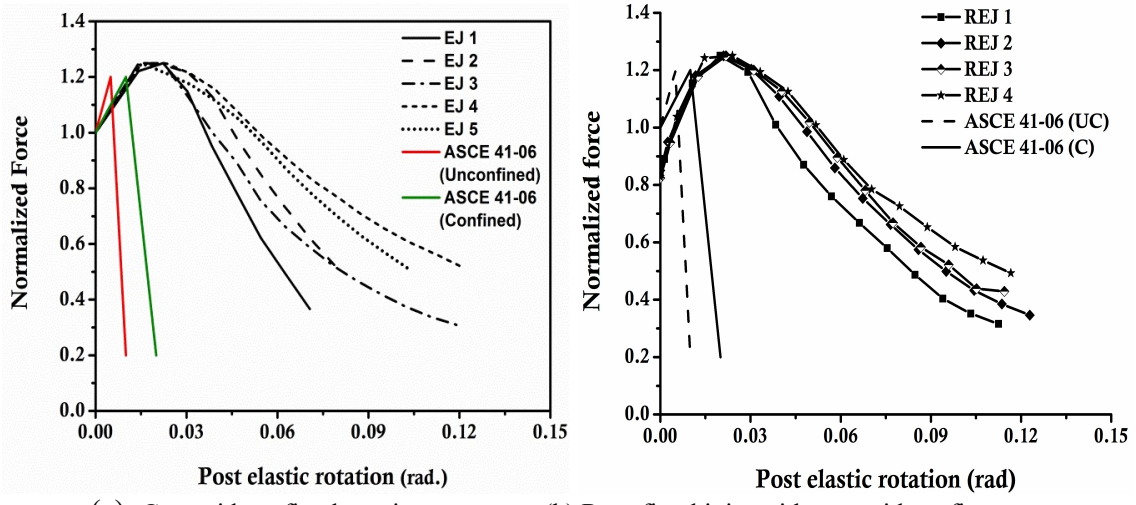

(a) Geo-grid confined specimens (b) Retrofitted joint with geo-grid confinement

Figure 2.37: Moment–rotation behavior of geo-grid confined joint specimens

The maximum value of moment reaches at the rotation of 0.03 radian and the range of post peak behavior i.e. no significant loss of moment capacity is noticed in the rotation of 0.03 – 0.08 radians. The experimentally obtained plastic rotation capacity of

geo-grid confined beam-column joint specimens is higher than the specified values in ASCE/SEI 41-06 in which the limit of linear elastic behavior of conventional joints is 0.015 and the range of post peak behavior is 0.015 to 0.02 radians, as shown in Figure 2.42 It is evident that the geo-grid confinement with steel fibers significantly improves the M-Θ relationship against the conventional specimens. The geo-grid confinement increases the moment capacity as well as post peak behavior of specimens which is further improved by the steel fibers. The higher ductility with better post peak response in the specimen may be achieved with steel fiber even in higher spacing of transverse reinforcement. The increase in rotational capacity with lower rate of moment degradation represents the sign of ductile behavior of joint which is really difficult to achieve by conventional confinement.

2.5.6 *Crack Formation Mechanism and Failure Analysis*

Crack patterns of tested beam-column joint specimens at failure level under cyclic testing are shown in Figure 2.38-2.39. Apparently, the specimens fail finally in shear with different load-deformation characteristics. The crack patterns of conventionally confined specimens and geo-grid confined specimens with and without steel fiber are distinct in terms of their failure mechanism. In conventionally confined specimen even with ductile detailing, the initial flexure cracks develop in beam component of the joint which are transferred to joint core as the moment or applied load increases. The joint core subjected to cyclic shear force which is resisted by the shear strength of core concrete is a function of concrete strength and steel resistance. In case of conventional specimen without ductile detailing, the shear strength of core concrete is relatively less as compared to confined concrete; therefore the joints fail in shear with spalling of concrete cover. In conventionally confined specimen EJ 2, there is a slight delay in shear failure with less intense cracking. In geo-grid confined specimens, the failure mechanism is the same but the shear resistance of core concrete increases significantly and further increases with the use of steel fiber in concrete due to bridging action. Therefore, the shear failures of joint in geo-grid confined specimen have higher load and deformation as compared to conventionally confined specimens. The intensity and severity of cracking are also reduced by an increase in sustaining the shear capacity of the core concrete.

The crack pattern and failure behavior of retrofitted specimens (REJ) are similar to the above discussed failure mechanism of specimens. The concrete cover of geo-grid confined retrofitted specimens spall during large drift, as a result of the specimen undergoing higher volumetric enlargement in the joint core region as shown in Figure 2.39.

However, the presence of steel fiber holds the cracked concrete portion to be intact with the core concrete. In specimen REJ 4 the intensity of flexural cracks in the beam hinge region shows that the synergetic effect of geo-grid confinement and steel fiber allow flexural cracks to occur in the beam region in spite of joints' failure in shear. This cracking behavior validates the success of confinement effect of grid confinement under cyclic loading.

(a) EJ 1-IS 456 detailing

(b) EJ 2-IS:13920 detailing

(c) EJ 3-Geo-grid confinement

(d) EJ 4-Geo-grid confinement +steel fibers

(e) EJ 5-Steel fiber reinforced

Figure 2.38: Crack pattern and mode of damage of actual beam-column joints

(a) REJ 1

(b) REJ 2

(c) REJ 3

(d) REJ 4

Figure 2.39: Crack pattern and failure mode of retrofitted specimens

2.5.7 *Damage Tolerance Capacity*

Damage and failure mechanisms are useful in intensity and safety assessment for reutilization and energy loss assessment (Saurabh et al. (2012). Park and Ang damage (1999) index calculates the comparison of relative performance of beam-column joint specimen with different confinements plotted in Figure 2.40**.** The corresponding damage index is expressed as

$$D = \frac{\delta_M}{\delta_u} + \frac{\beta}{F_y \delta_u} \int dE \qquad \textbf{2.5}$$

The damage index [*DI*] values vary from 0 to 1, whereas "0" indicates no damage and "1" indicates complete damage. In this study it is assumed that the 0 < DI < 0.20 represents elastic behavior or no damage in specimens, 0.20 < DI < 0.40 represents slight damage, 0.40 < DI < 0.60 represents moderate damage, 0.60 < DI < 0.80 represents severe damage and DI> 0.8 represents complete damage. It is observed that the DI values of the joint specimens in elastic region (I) show no damage. Both the conventional specimens reach moderate damage and other specimens show slight damage level in yield to peak region (III) as shown in Figure 2.40(a). The beam-column joint specimens reach severe damage to collapse level during post peak behavior (IV).

It is observed that the joint specimen EJ 1 and EJ 2 with conventional confinement have similar damage pattern with slight improvement due to ductile detailing of joint. The damage tolerance level is further improved by the use of SFRC along with geo-grid confinement in specimen EJ 4. It is observed from the DI plot that the conventional joint specimens have complete damage at the deformation of 50mm, at the same time the geo-grid confined specimens are under the limit of severe damage and complete damage is observed beyond 65 mm in post peak region (IV). Similarly, in displacement range of 25mm to 50mm, the conventional specimens undergo severe damage while the geo-grid confinement specimens show moderate damage. The measured damage index shows that the retrofitted specimens have better damage tolerance capacity over conventional specimens EJ 1 and EJ 2. Figure 2.40(b) shows that the damage tolerance capacity of retrofitted specimens REJ 2 and REJ 4 competes with the damage tolerance capacity of SFRC specimen EJ 5. It is interpreted that the geo-grid confined specimens have undergone damage one level lower as compared to conventionally confined specimens at the same range of displacement.

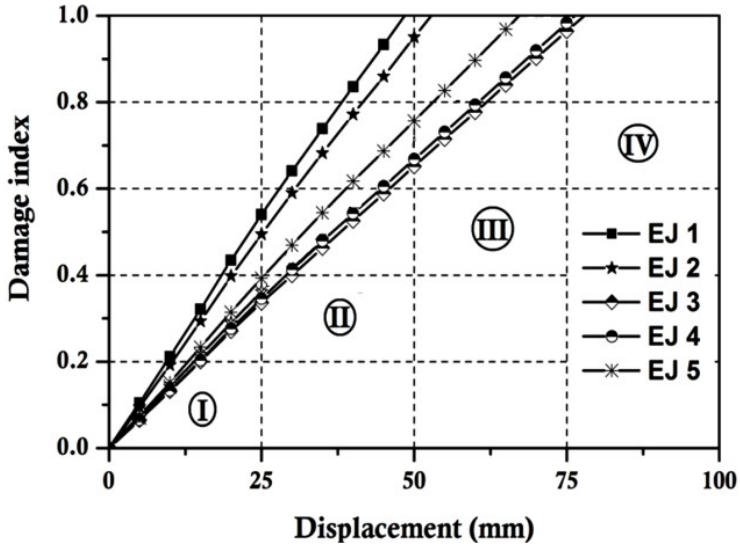

(a) Actual specimens

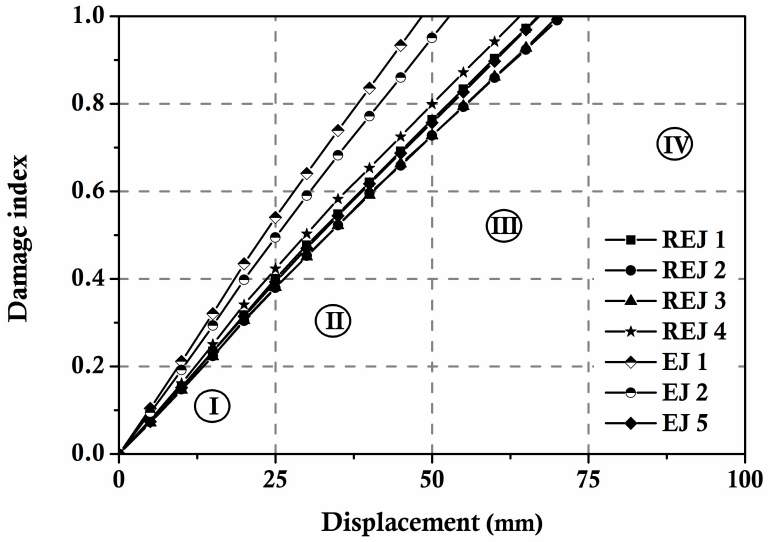

(b) Retrofitted specimens

Figure 2.40: Damage index (DI) plot vs displacement of joint specimens

2.6 Findings

An experimental investigation is carried out to study the effect of geo-grid confinement of concrete specimens with and without steel fibers. Some of the important observations of the study are summarized as follows;

1) There is a significant improvement in the axial stress-strain behavior of specimens under compression after confining the specimens by geo-grid as compared to conventional concrete specimens or even with the steel fibers. The maximum stresses in the geo-grid confined specimens increase upto 1.5 times and strain 3.0 times

more/less as compared to conventional specimens. There is a remarkable improvement in the inelastic behavior of geo-grid confined specimens as the failure stain reaches upto 0.035 against the failure strain 0.002 as conventional. The geo-grid along with steel fibers is able to reverse the failure mechanism from sudden brittle failure to ductile without significant loss of strength.

2) The effect of geo-grid confinement with and without steel fibers is also observed in the split tension behavior of respective concrete specimens as tested under compression. The geo-grid confinement does not contribute to increase the tensile strength of specimens but also help to sustain the deflection at a larger extent. The observed crack width clearly proves the effect of geo-grid confinement tension resistant capacity.

3) The deflection at failure of geo-grid confined specimens increases by about 5-6 times as compared to the deflections at peak while the conventional specimen does not reflect any post peak behavior.

4) In case of type-A beam specimens, remarkable improvement in post yield behavior and energy dissipation capacity is observed after additional confinement by geo-grid with low percentage (0.50 %) of steel fibers. The same type of post yield behavior of beam specimen is also observed with the sole use of SFRC but with higher percentage (1%) of steel fibers. However, there is no significant effect on increase in yield and ultimate load capacity of geo-grid confined SFRC beam specimens. The geo-grid with the use of SFRC maintains nearly the same type of performance in case of type-B (moderately confined) beam specimens.

5) The load - deformation behavior of geo-grid confined SFRC beam specimens of type-C and type-D (lightly confined) significantly improve as the strength of geo-grid and % of steel fibers increase. There is about 2 to 2.5 times improvement in load and deformation capacity of geo-grid confined SFRC beam specimens as compared to control shear deficient beam specimens with remarkable increase in energy dissipation capacity. It may be inferred from the test results that geo-grid and SFRC are able to increase the flexure and shear capacity of a deficient beam specimens effectively.

6) It is observed that the rate of degradation in strength and stiffness of conventionally confined beam specimens decreases as the amount of transverse reinforcement increases. The geo-grid confined beam specimens with and without steel fibers show a gradual and stable loss in strength and stiffness as the post yield rotation increases even in the specimens with large spacing transverse reinforcement.

7) There is a drastic change in the cracks pattern of type-C beam specimens (lightly confined) with the use of geo-grid confinement and SFRC. The complete shear failure of control beam specimen gradually changes towards flexural– shear failure as the specimens confined with geo-grid and SFRC depend on the strength of geo-grid and % of steel fibers. In type-D specimens the pattern of failure remains same as conventional specimens but the deflection after shear crack formation shows the significance of grid confinement.

8) There is an effective enhancement in the post peak behavior of beam-column joint specimen confined with geo-grid and steel fibers. The deformation capacity of geo-grid confined specimen increases upto 1.5 times as compared to conventionally confined specimens. The bond slippage failure of embedded longitudinal reinforcement in the joint region reduces due to the confining pressure of geo-grid in the joint core. There is also remarkable improvement in the ductility of geo-grid confined specimen with steel fiber.

9) The geo-grid confined joint specimens with and without steel fibers show lower rate of degradation in strength and stiffness as the post yield rotation increases even in the retrofitted specimens with large spacing of transverse reinforcement in the plastic hinge region.

10) The energy dissipation capacities of geo-grid confined specimen increase nearly 2 times as compared to other conventionally confined specimens. It is also evident that the average internal damping coefficient increases by 12 to 15% in geo-grid confined specimens with and without SFRC.

11) The specified values of plastic rotation capacity for the linear elastic behavior and post peak behavior of conventional and confined joints as per ASCE/SEI 41-06 are much lower as compared to geo-grid confined beam-column joint. The rotation at failure of geo-grid confinement specimens reaches upto 0.12 radian as against 0.07-0.08 radian in conventional specimens with and without ductile detailing. In addition, the rate of strength degradation of geo-grid confined specimen with SFRC considerably reduces as compared to other specimens.

12) The geo-grid confined beam-column joint specimens have more damage tolerance capacity. The observed damage index and mode of failure prove that the geo-grid confinement can resist upto peak load without severe damage in the joint region. It is understood that the geo-grid confined specimen has undergone at least one level lower

damage in comparison to conventional specimens with and without ductile detailing at the same range of displacement.

13) This study is focused on the application of geo-grid with steel fibers in RC structural members to enhance shear capacity particularly in plastic hinge zones. The test results prove that the geo-grid with steel fiber not only effectively achieves the desired objectives but also improves the damage tolerance capacity. This study paves the path of geo-grid in structural components in reinforced concrete but for its versatility and reliability, more experiment tests are needed under various types of load applications.

References

ACI Committee 544 (1997) “State-of-the-art report on fiber reinforced concrete”, (ACI 544.1R-96). *American Concrete Institute*, Farmington Hills, Mich, 1-60.

Adebar, P., Mindess, S., St.Pierre, D., and Olund, B., (1997), “Shear tests of fiber concrete beams without stirrups,” *ACI Structural Journal*, 94(1) ,68-76.

Ali, K., Shahab, F., and Fereidoon, M. N., (2009), “Effects of geosynthetics on reduction of reflection cracking in asphalt overlays,” *Geotextiles and Geomembrane*, 27,1–8.

ASCE/SEI 41-06 (2007), “Seismic rehabilitation of existing buildings,” *American Society of Civil Engineers*, Reston, USA, 2007.

Bensaid, B., Mostefa, H. M. C., and Sofiane, A., (2010), “Flowability of fiber-reinforced concrete and its effect on the mechanical properties of the material,” *Construction and Building Materials*, 24, 1664–1671.

Dinh, H. H., Parra-Montesinos, G. J., and Wight, J. K., (2010), “Shear behavior of steel fiber-reinforced concrete beams without stirrup reinforcement,” *ACI Structural Journal,* 107, (5), 597-606.

Dinh, H. H., Parra, M. G. J., and Wight, J. K., (2011), “Shear strength model for steel fiber reinforced concrete beams without stirrup reinforcement,” *Journal of Structural Engineering,* 137, (10), 1039-1051.

El-Niema, I. E., (1991), “Reinforced concrete beams with steel fibers under shear,” *ACI Structural Journal,* 88, (2), 178-183.

Fadel, A., and Mohammad, R. E., (1991), “High strength RC connections subjected to inelastic cyclic loading,” *Journal of Structural. Engineering*, 117, 829-849.

Fatih, A., Tefaruk, H., and Kamura, A., (2007), “Effects of steel fiber addition on mechanical properties of concrete and RC beams,” *Construction and Building Materials*, 21, 654–661.

Ganesan, N., Indira, P. V., and Ruby, A., (2007), “Steel fibre reinforced high performance concrete beam-column joints subjected to cyclic loading,” *ISET Journal of Earthquake Technology,* 44, 445-456.

Giuseppina, A., Giuseppe, C., Liborio, C., and Giovanni, M., (2011), “Flexural behaviour of external RC steel fibre reinforced beam-column joints,” *European Journal of Environment and Civil Engineering,* 15, 1253-1276.

Gregoria, K., and Harris, M., (2012), “Seismic design of RC external beam-column joints,” *Bulletin of Earthquake Engineering*, 10, 645-677.

Gerald, R., and Issa, I., (2003), “The effect of geogrid reinforcement on unbound aggregates,” *Geotextiles and Geomembrane*, 21, 355–380.

Giuseppe, C., (2008), “Simplified flexural response of steel fiber–reinforced concrete beams,” *Journal of Materials in Civil Engineering*, 200 (4), 283-293.

Hoe, I. L., and Zheng, L., (2001), “Performance of geosynthetic-reinforced asphalt pavements,” *Journal of Geotechnical and Geo-environmental Engineering*, 127 (2), 177-184.

Hwang, S. J., Lee, H. J., and Wang, K. C., (2004), "Seismic design and detailing of exterior reinforced concrete beam-column joints," *13th World Conference on Earthquake Engineering*, Vancouver, B.C., Canada.

Hwang, S. J., Lee, H. J., Liao, D. F., Wang, K. C., and Tasi, S. H., (2005), "Role of hoops on shear strength of reinforced concrete beam-column joints for seismic resistance," *ACI Structural Journal*, 102, 445-453.

Jung, Y. L., Jin, Y. K., and Gi, J. O., (1991), "Strength deterioration of reinforced concrete beam-column joints subjected to cyclic loading," *Engineering Structures,* 31, 2070-2085.

Jiuru, T., Chaobin, H., Kaijian, Y., and Yongcheng, Y., (1992), "Seismic behavior and shear strength of framed joint using steel-fiber reinforced concrete," *Journal of Structural Engineering*, 118 (2), 341-358.

Li, V. C., Ward, R., and Hamza, A. M., (1992), "Steel and synthetic fibers as shear reinforcement," *ACI Materials Journal*, 89 (5), 499-508.

Murty, C. V. R., Rai, D. C., Bajpai, K. K., and Jain, S. K., (2003), "Effectiveness of reinforcement details in exterior reinforced concrete beam–column joints for earthquake resistance," *ACI Structural Journal*, 100(2), 149-156.

Meski, F. El., and Chehab, G., (2014), "Flexural behavior of concrete beams reinforced with different types of geogrids," *Journal of Materials in Civil Engineering*, 26(8).

Nicholas, J. B., Les, M. M., and Jason, M. I., (2006), "Bond Performance of Interior Beam-column Joints With High Strength Reinforcement," *ACI Structural Journal,* 103(4), 596–603.

Naaman, A. E., Reinhardt, H. W., and Fritz, C., (1992), "Reinforced concrete beams with a SIFCON matrix," *ACI Structural Journal*, 89(1), 79-88.

Narayanan, R., and Darwish, I. Y. S., (1987), "Use of steel fibers as shear reinforcement," *ACI Structural Journal*, 84 (3), 216-227.

Saurabh, S., and Ravi, S., (2012), "Seismic damage index for classification of structural damage-closing the loop," *Proceedings of 15th Conference on Earthquake Engineering*, Portugal.

Saurabh, S., and Ravi, S., (2012), "Detailed evaluation of available seismic damage indices," *Proceedings of ISET Golden Jubilee Symposium*, Roorkee.

Shannag, M. J., Barakat, S., and Abdul K. M., (2002), "Cyclic behavior of HPFRC repaired interior beam-column joints," *Materials and Structures*, 35, 348-356.

Shyh, J. H., Hung, J. L., and Kuo, C. W., (2004), "Seismic design and detailing of exterior reinforced concrete beam-column joints," *13th World Conference on Earthquake Engineering*, Canada, paper no.397.

Shin, E. C., and Das, B. M., (2000), "Experimental study of bearing capacity of a strip foundation on geogrids reinforced sand," *Geosynthetics International*, 7 (1), 59-71.

Siva, C. K. R., and Thirugnanam, G.S., (2012), "Comparative study on behaviour of reinforced beam-column joints with reference to anchorage detailing," *Journal of Civil Engineering Research*, 2, 12-17.

Somma, G., (2008), "Shear strength of fiber reinforced concrete beam-column joints under seismic loading," *14th World Conference on Earthquake Engineering*, Beijing, China

Surya, K. D. V. V. S., and Pankaj, A., (2013), "Influence of reinforcement characteristics on non-linear performance evaluation of confined beam-column joints under cyclic loading," *Advances in Civil Engineering Materials*, 2, 201–217.

Surya, K. D. V. V. S., and Pankaj, A., (2013), "Cyclic performance evaluation of unconfined and confined beam-column joint specimens with different type of reinforcing characteristics as per ASCE/SEI 41-06," *Australian Journal of Structural Engineering,* 14, 1-16.

Tang, X., Chehab, G. R., and Kim, S., (2008), "Laboratory study of geo-grid reinforcement in Portland cement concrete," *RILEM International Conference on Cracking in Pavements*,769-778.

Xiaochao, T., Ghassan, R. C., and Angelica., (2008), "Evaluation of geogrids for stabilizing weak pavement subgrade," *International Journal of Pavement Engineering*, 9 (6), 413–429.

Yoon, K.K., Marc, O.E., Woo, S.K. and Jubum, K., (2002), "Shear strength of steel fiber-reinforced concrete beams without stirrups," *ACI Structural Journal*, 99 (4), 530-538.

Chapter 3

Cyclic Behavior of Exterior Beam-column Joint with Fiber Reinforced Concrete

3.1 Introduction

Shear strength of the joint can be enhanced by providing a closely spaced transverse reinforcement in the plastic hinge region. This critical confinement in the hinge region leads to steel congestion and construction problem. The joints could at times remain the weak link even for structures designed in accordance with current model building codes (Tsons 2006, Vijay et al. 2012). Also the brittleness of conventional concrete matrix significantly affects the inelastic response of the structural members even though with closely spaced shear reinforcement. The use of steel fibers in concrete improves the tensile behavior and enhances the shear strength without critical reinforcement detailing in the joint plastic hinge region. This randomly distributed discontinuous fiber increases the tensile strength by arresting the crack formation and by bridging the cracks after initiation (Ganesan et al. (2007), Holschemacher et al. (2010) and Adel et al. (2014)). Moreover, the additional anchorage by the different fibers such as crimpled, hooked end steel fiber improves the effectiveness of the fiber bridging ability. The steel fiber reinforced concrete (SFRC) improves shear strength and inelastic response of the structural member with optimum volume of fibers. Otherwise, fibers affect the workability of concrete and lead to fiber segregation and excessive air entrainment that loses its efficiency in higher deformation. The entire performance of fiber reinforced concrete (FRC) depends on its dispersion and location for effective resisting of applied loads (Mohammad (2007)). In the present study, the inelastic behavior of the joint is evaluated by using fiber reinforced concrete. The effectiveness of fiber hybridization using poly propylene fiber along with steel fiber and macro synthetic fiber is also studied.

3.2 Early Studies

Paul et al. (1986) investigated the application of SFRC in joints with higher stirrup spacing and suggested that the joint with SFRC could be considered in seismic prone areas. Jiru et al. (1992) studied the influence of SFRC on the cyclic behavior of beam-column

joint and concluded that the use of SFRC in the joint core might improve the ductility without steel congestion. Andre et al. (1994) studied the seismic performance of code-designed fiber-reinforced concrete joints and observed that the crack bridging mechanism of fibers in concrete improved the shear resistance capacity diminishing the need of closer confinement in the joint region. The performance of the SFRC is based on the volume and aspect ratio of fibers. Andre et al. (1995) tested four full scale beam-column joint with and without SFRC and reported that the use of SFRC in the joint increased the ductile performance during earthquake excitation. Liu et al. (2006) conducted research on the seismic behaviour of beam-column joint reinforced with steel fibres and concluded that the bridging action and tensile behavior of SFRC effectively controlled the cracks formation significantly arresting the diagonal cracks. SFRC can enhance shear strength and reduces the steel congestion in the joint region. Ganesan et al. (2007) conducted experimental study on steel fibre reinforced high performance concrete beam-column joints subjected to cyclic loading and concluded that the steel fibers in joint increased the stiffness retention, dimensional stability and imparted ductility. Yung et al. (2007) investigated the effect of ultra high strength steel fiber reinforced concrete (UFC) in beam-column joint strengthening and examined the cyclic behavior of UFC beam-column joint and concluded that the use of UFC improved rebar bond strength and shear strength of joint. Ganesan et al. (2014) investigated the influence of fiber hybridization on the cyclic behavior of joints and observed better strength and ductility enhancement and also suggested that the use of hybrid fibers in concrete could avoid the steel congestion. Bilal et al. (2015) examined the significance of SFRC and CFRP sheet on the performance of beam-column joint. The test results stated that the use of steel fiber increased the joint strength than external CFRP confinement. Dhaval et al. (2015) studied the use of hybrid fiber reinforced concrete on ductility enhancement of beam-column connection and observed improved ductility and damage tolerance capacity. The hybrid fiber reinforced concrete could be used in the seismic prone zone without critical shear reinforcement in the joint.

3.3 Compression and Flexure Behavior of FRC Composites

The mechanical properties of different fiber reinforced concrete composites are examined under compression, split tension and bending after conducting the standard tests on cylindrical and prism specimens.

3.3.1 Compression and Split Tension Behavior of FRC

Standard sizes of 100 × 200 mm concrete cylindrical specimens were used to obtain the axial stress-strain behavior and split tensile behavior of different concrete composites. Ordinary Portland Cement (OPC) as cementitious material, coarse aggregate with maximum size of 20 mm and locally available river sand as fine aggregate were used in conventional concrete preparation with water-cement ratio of 0.45. Water reducing admixture (CONPLAST 430) with a volume of 1% was used to increase the workability of FRC. Four different types of fibers such as hooked end steel fiber, crimpled steel fiber, macro synthetic fiber and micro synthetic polypropylene fiber were used in FRC preparation, shown in Figure 3.1. The hooked end and crimpled steel fiber with an aspect ratio of 60 with nominal tensile strength of 1100 MPa was used. The detailed mix ratio of fiber composite is given in Table 3.1 and 3.2.

Table 3.1: Detailed mix ratio of concrete and FRC

Specimen details	Cement	Sand	Coarse aggregate	Water binder ratio	Super plasticizer	Fibers
Conventional concrete	1	1.45	2.25	0.45	0.5	-
FRC	1	1.35	2.15	0.45	0.5	Refer Table no 3.2

A total of nine different types of concrete specimens were prepared, five FRC, three hybrid fiber reinforced concrete (HyFRC) and one conventional concrete specimen. The cylindrical specimens were tested under uni-axial compression and strain to be measured with the help of LVDT. The detailed configuration of the FRC composite is presented in Table 3.2.

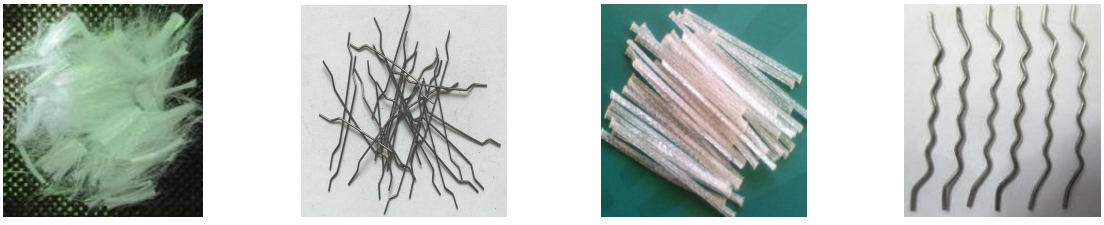

(a) Polypropylene fiber (b) Hooked end steel fiber (c) Macro synthetic fiber (d) Crimpled steel fiber

Figure 3.1: Materials used in FRC preparation

Table 3.2: Compression and split tensile strength of different FRC composites

Specimen ID	Description	Volume of fiber				Compressive strength	Split tensile strength	Flexural strength
		PP*	HSF*	CSF*	MSF*			
		%				MPa	MPa	MPa
FC 0	Conventional	×	×	×	×	30.5	3.4	4.0
FC 1	FRC I	×	×	**1**	×	50.6	5.7	8.4
FC 2	FRC II	×	×	**2**	×	48.0	6.1	8.0
FC 3	FRC III	×	**1**	×	×	48.1	4.9	7.2
FC 4	FRC IV	×	**2**	×	×	54.3	5.6	8.4
FC 5	FRC V	×	×	×	**1**	35.8	3.4	6.4
FC 6	Hybrid I	**0.2**	×	**1**	×	51.6	5.9	6.8
FC 7	Hybrid II	**0.2**	×	×	**1**	35.8	5.1	4.8
FC 8	Hybrid III	**0.2**	**1**	×	×	42.2	5.3	7.2

** **PP**- Polypropylene; **HSF**- Hooked end steel fiber; **CSF**-Crimpled steel fiber; **MSF**-Macro synthetic fiber*

The axial stress-strain curves of the compression specimens are shown in Figure 3.2 and the test results are summarised in Table 3.2. The average compressive strength of conventional concrete specimen FC 0 is 30.5 MPa. The post peak curve of FC 0 shows the brittle nature of plain concrete. FRC specimens possess better post peak strain behavior over conventional concrete. The presence of crimpled steel fiber in specimen FC 1 shows 50 MPa peak strength at 0.004 strains, whereas at the same strain the conventional concrete fails completely. The higher % of crimpled steel fiber in specimen FC 2 shows increased modulus of elasticity with lesser compressive strength over FC 1. It emphasises that the presence of higher volume steel fiber controls the cracks effectively and increases the stiffness behavior. Similar kind of response is observed with specimens FC 3 and FC 4. The higher volume hooked end steel fiber increases the strength and stiffness over lesser volume steel fiber specimen FC 3. The comparison of stress strain behavior of crimpled steel fiber and hooked end steel fiber specimens emphasises that the percentage of fiber and its anchorage behavior decides the performance enhancement. The observed compressive strength of SFRC shows 50-65% higher strength over conventional concrete. The specimen FC 5 (MFRC) shows unique stress strain behavior over other FRC. The compressive strength of MFRC is comparatively lesser than SFRC but post peak curve shows steady rate in strength retention without sudden loss in strength. This phenomenon describes the bridging effect of macro synthetic fiber on the enhancement of post peak behavior over strength enhancement.

The hybridization of polypropylene fiber with steel and macro synthetic fiber shows different behavior over fiber reinforced concrete specimens. The presence of micro synthetic fiber significantly influences the axial behavior of concrete specimens. The peak strength of hybrid macro synthetic fiber enabled specimen FC 6 is 35 MPa and also the rate of post peak degradation is rapid as compared to other hybrid fiber reinforced concrete specimens. The synergetic effect of hooked end steel fiber and polypropylene fiber shows lesser compressive strength as compared to FC 7 but shows improved post peak strain behavior. The compressive strength of FC 8 is 50 MPa which has higher rate of post peak retention over conventional specimen FC 0.

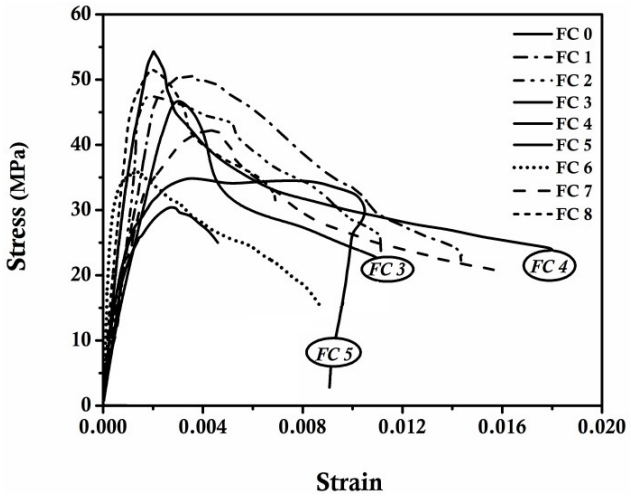

Figure 3.2: Stress-strain behavior of FRC compression specimens

The observed split tensile strength of concrete composite specimen varies from 11-14% of its compressive strength. The tensile behavior of MFRC specimen FC 5 exhibits lesser tensile response over other FRC specimens. The hybrid specimens, FC 6, FC 7 and FC 8 exhibit better tensile strength to compressive strength ratio than other fiber reinforced concrete specimens. It shows that the hybridization of fibers increases the tensile behavior irrespective of its compression behavior.

3.3.2 Flexural Behavior of FRC Prisms

The flexural tensile behavior of all composites is evaluated using a plain concrete beam with a size of 100×100×500 mm under two point static loading. The flexural behavior of specimens are plotted against corresponding deflection as shown in Figure 3.3 and test results are summarised in Table 3.2. The flexural strength of conventional concrete is 4 MPa which is 13% of its compressive strength. In plain concrete specimen load drops suddenly after initial crack. The fibers in the FRC show different flexural strength to

compressive strength ratio (f_s / c_s) with respect to its anchorage behavior. The average f_s / c_s ratio of crimpled fiber reinforced concrete is 16%, whereas it is 15% for hooked end steel fiber and 18% for macro synthetic fiber concrete. After initial crack, the presence of fiber hinders the crack growth and enhances the post peak deformation. FRC specimens exhibit post peak performance with different rate of post peak strength degradation. The anchorage of crimpled fiber improves the post peak degradation over hooked end steel fiber concrete. The f_s / c_s of MFRC is 18% which is better than other FRC but the load-deflection curve shows rapid post peak degradation over other FRC. It authenticates the influence of fiber anchorage on the bending behavior.

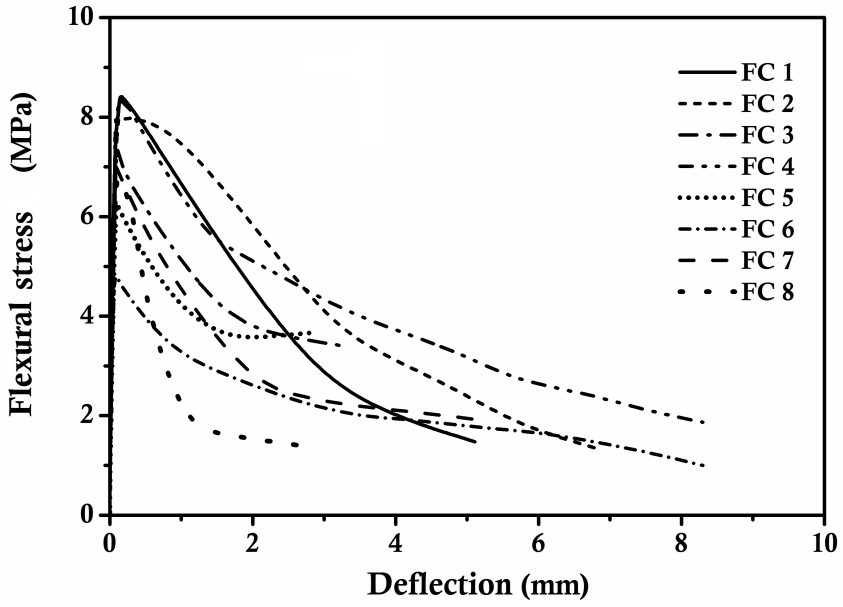

Figure 3.3: Flexural behavior of FRC prism specimens

The compressive behavior of hybrid concrete is similar to FRC but flexural behavior is significantly improved with FRC of 1% fiber volume. The observed average f_s / c_s ratio of hybrid concrete varies from 13-17%. In particular, the specimen FC 7 shows better flexural response over other hybrid and also the f_s / c_s ratio is 17% which is 1.3 times higher than FC 6 and FC 8. The micro synthetic fiber significantly improves the flexural performance and competes with the response of FRC specimen with 1% fiber volume.

Figure 3.4 shows the comparison of flexural energy absorption of flexural specimens on the basis of area under load-deflection curves. This energy absorption defines the post peak performance of different composites. The brittle failure of

conventional concrete fails to show post peak behavior. The FRC and HyFRC specimens have tremendous energy absorption capacity over the conventional concrete. The FRC with higher volume of steel fiber (FC 2 and FC 4) absorbs higher energy than other FRC and HyFRC. The higher volume steel fiber restricts the crack growth and its propagation after peak load and enhances the energy absorption behavior. The lesser volume of fiber fails to bridge the cracks effectively after peak in the cracked region (because of lesser volume in FC 1 and FC 3); thus it shows comparatively lesser energy absorption over FC 2 and FC 4. The sudden degradation after peak strength due to the absence of fiber anchorage causes less energy absorption in specimen FC 5 (MFRC). The energy absorption of hybrid concrete specimens is lesser as compared to FRC specimen because of the presence of micro synthetic fiber. It affects the dispersion of steel fiber in concrete and makes the steel fibers fail in bridging the cracks in the cracked region.

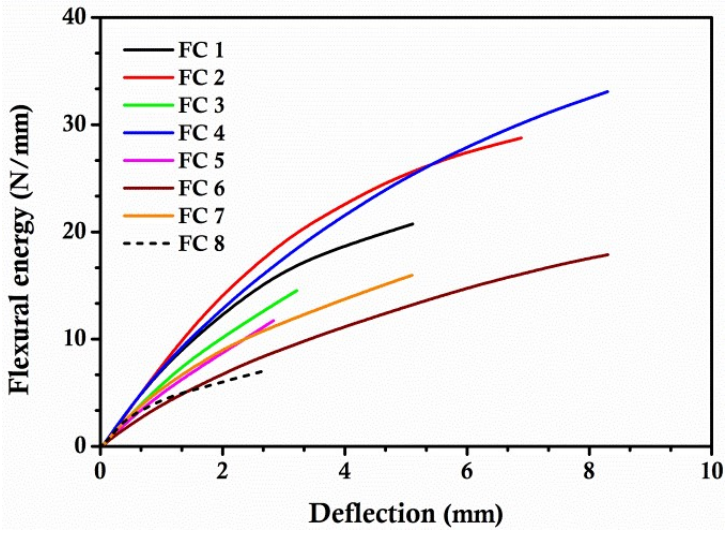

Figure 3.4: Flexural energy dissipation of FRC prism specimens

3.4 Cyclic Testing of Beam-column Joint specimens with Different FRC Composites

Ten exterior beam-column joint specimens are cast and tested under cyclic loading in quasi-static test facility to evaluate the hysteresis behavior of different FRC. The complete details of beam-column joint specimens with different types of concretes are given in Table 3.3. The reinforcing details of two conventional specimens with different transverse reinforcement ratio are shown in Figure 3.5.To quantify the influence of ductile detailing, the first conventional specimen is detailed as per IS: 456-2000 (unconfined) whereas the second conventional specimen is detailed as per IS: 13920-1993 (confined).

The unconfined reinforcing details are used in preparation of specimens with different FRC. The FRC is used only at joint region of beam-column connection and the remaining area is cast with conventional concrete. The beam-column joint test setup and cyclic loading history are shown in Figure 3.6

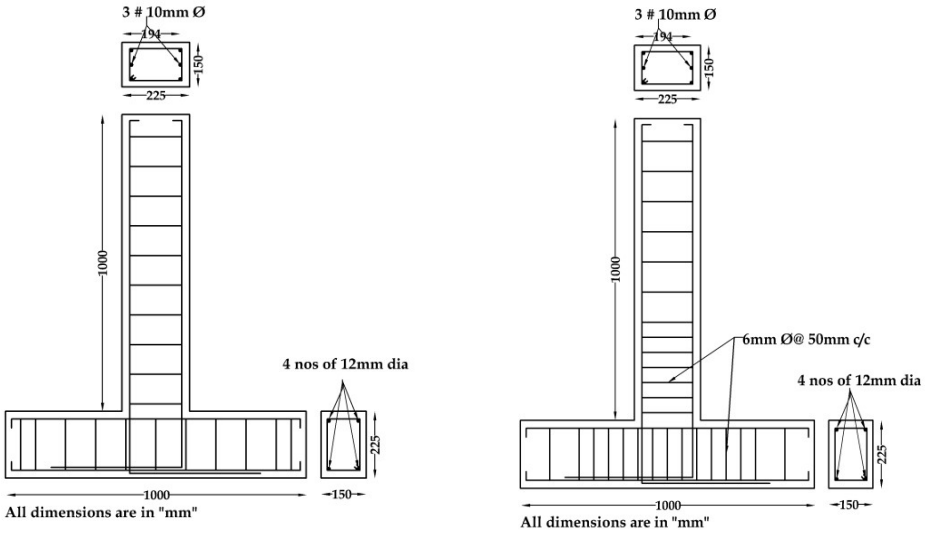

(a) IS:456-2000 detailing (b) IS:13920-1993 detailing

Figure 3.5: beam-column joint reinforcement detailing of (a) HYJ 1 (b) HYJ 2

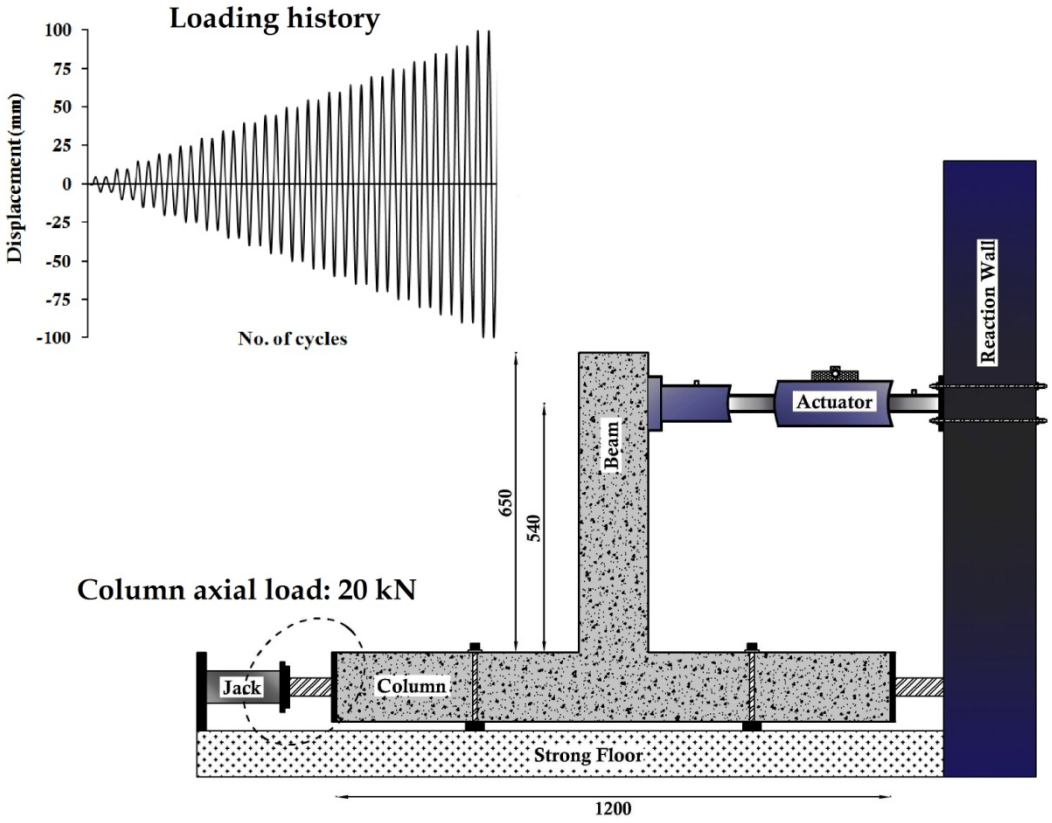

Figure 3.6: Experimental test setup and loading history of beam-column joint

. The amplitude of loading is increased gradually from 5 mm/10mm till occurrence of failure with an interval of 5 mm/10mm under displacement control. The specimens are tested up to failure and their corresponding load deformation response is recorded with the help of load cell and LVDT. The test results are examined in terms of hysteresis behavior, strength and stiffness degradation, energy dissipation and damping, moment-rotation relationship, failure pattern and damage index.

Table 3.3: Detail of exterior beam-column joint specimen with different configurations

ID	Transverse reinforcement	Concrete in joint hinge region	Reinforcement		Remarks
			Beam	Column	
Type 1 Conventional specimens					
HYJ 1	Ø6mm @100mm C/C	Conventional 1	3 # of 10mm Ø @ top and bottom	4 # of 12mm Ø	Unconfined
HYJ 2	Ø6mm @100mm C/C and 50mm C/C in the hinge region	Conventional 2			Confined
Type 2 Fiber reinforced concrete (FRC) specimens					
HYJ 3	Ø6mm @100mm C/C	FRC I			SFRC (1%) - Crimpled steel fiber
HYJ 4		FRC II			SFRC (2%) - Crimpled steel fiber
HYJ 5		FRC III			SFRC (1%) – Hooked end steel fiber
HYJ 6		FRC IV			SFRC (2%) - Hooked end steel fiber
HYJ 7		FRC V			Macro synthetic steel fiber (MFRC)
Type 3 Hybrid fiber reinforced concrete (HyFRC)					
HYJ 8	Ø6mm @100mm C/C	Hybrid I			Macro synthetic + Micro synthetic
HYJ 9		Hybrid II			Hooked end fiber + Micro synthetic
HYJ 10		Hybrid II			Crimpled fiber + Micro synthetic

3.4.1 Crack Pattern and Failure Mode

In conventional specimens HYJ 1 and HYJ 2 fine flexural cracks are noticed along the beam hinge region followed by shear cracks at the joint region. The spalling of concrete cover in the beam hinge region along with inadequate confinement leads the

longitudinal reinforcement to buckle in specimen HYJ 1, as shown in Figure 3.7a. The buckling of longitudinal reinforcement is because of inadequate confinement during severe loading. The closer confinement in the hinge region restricts early spalling of concrete and allows resisting the load to a higher extent without reinforcement buckling in specimen HYJ 2. The crack pattern of specimen HYJ 2 shows the dense cracks in the beam hinge region and joint connection with concrete crushing. The absence of reinforcement buckling and delayed spalling of concrete improve the damage tolerance capacity over HYJ 1, shown in Figure 3.7.b.

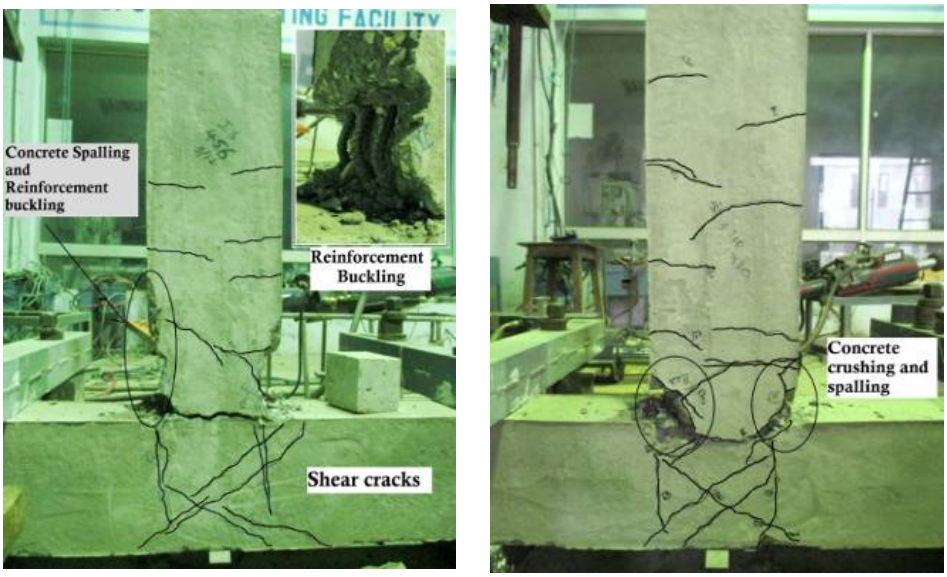

(a) HYJ 1-Unconfined (IS 456 detailing)

(b) HYJ 2 -Confined (IS 13920 detailing)

Figure 3.7: Failure pattern of conventional specimens HYJ 1 and HYJ 2

The presence of fibers in concrete internally improves the aggregate interlocking by restricting the crack formation at initial stage of loading. As a result of fibers, fine flexural cracks develop in the plastic hinge region of beams rather than diagonal cracks in the joint. However, no spalling of concrete cover is noticed, instead of the crack at the beam-column joint connection which widens during larger deflection. In specimen HYJ 4, the denseness of flexural cracks is comparatively lesser as compared to specimen HYJ 3 due to the fiber volumetric difference. In specimen HYJ 3, the crack formation exactly occurs at joint connection and in HYJ 4 the crack widening is observed in beam region. During larger deflection the reinforcement at joint connection starts to yield and finally exhibits ductile failure. Similar trend of cracking behavior is observed with specimen HYJ 5 and HYJ 6, but as the deformation increases a horizontal crack along the longitudinal direction of beam is observed as shown in Figure 3.8. The crack widening is severe after 50 mm

deflection because of the lesser anchorage capacity of hooked end steel fiber over crimpled steel fiber. The cracking behavior of specimen HYJ 6 is nearly identical with specimen HYJ 5. The higher volume fiber restricts crack growth and turns the reinforcement to yield at failure. It is also observed that in specimens HYJ 4 and HYJ 6, the denseness of flexural cracks in beam is reduced as compared to specimens HYJ 3 and HYJ 5. This implies that the higher volume of fiber in the concrete increases the tensile behavior and more effectively bridges the cracks and restricts its formation and propagation. In specimen HYJ 7 enormous flexural cracks are noticed in beam span but the macro synthetic fiber fails to restrict the formation of shear cracks in the joint region. As a result vast diagonal cracks are observed in the joint region as shown in Figure 3.8e.

(a) HYJ 3
(Crimpled steel fiber-1%)

(b) HYJ 4
(Crimpled steel fiber-1%)

(c) HYJ 5
(Hooked end steel fiber-1%)

(d) HYJ 6
(Hooked end steel fiber-1%)

(e) HYJ 7
(Macro synthetic fiber-1%)

Figure 3.8: Crack pattern and mode of failure of FRC joint specimens

The synergetic effect of polypropylene fiber with steel and macro synthetic fiber shows diverse cracking behavior. The hybridization of macro and micro synthetic fiber (HYJ 8) fails to control the occurrence of early shear cracks as a result of poor tensile nature of composite (Figure 3.9a). The absence of fiber anchorage and less pull out strength of macro synthetic fiber as compared to steel fiber result in shear crack formation in the joint. The formation of shear cracks encourages the beam's longitudinal

reinforcement slip instead of reinforcement yielding. However the specimens HYJ 9 and HYJ 10 experience ductile failure with immeasurable fine inclined cracks in the joint region as shown in Figures 3.9 (b) and (c). This implies the efficient synergetic action of steel fiber with micro synthetic fiber in improving the tensile stress capacity.

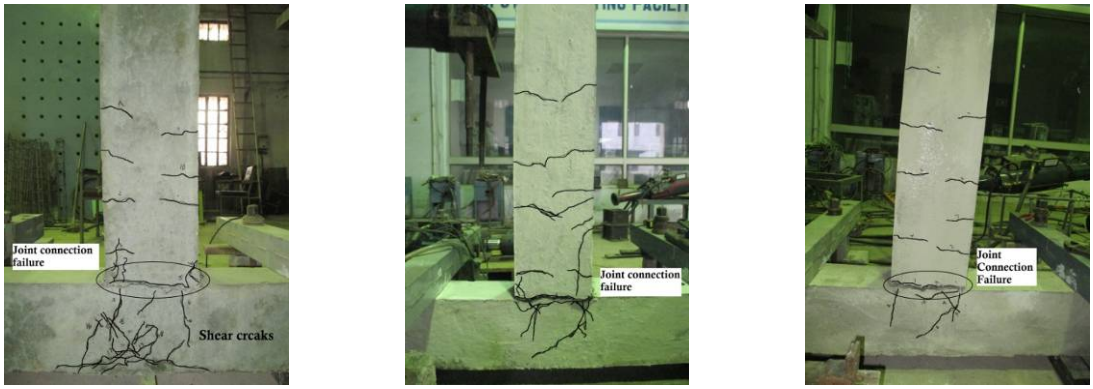

(a) HYJ 8 (Macro + Micro fiber)

(b) HYJ 9 (Hooked end +Micro fiber)

(c) HYJ 10 (Crimpled +Micro fiber)

Figure 3.9: Failure pattern of hybrid fiber reinforced concrete joint specimens

3.4.2 Damage Tolerance Capacity

Modified Park and Ang damage index (1987) is used to examine the damage level that compares the relative performance beam-column joint specimens with different configuration. Figure 3.10 shows the damage index versus ductility comparison.

$$DI = \frac{\delta_M - \delta_y}{\delta_f - \delta_y} + \beta \int \frac{dE}{F_y \delta_f} \qquad 3.1$$

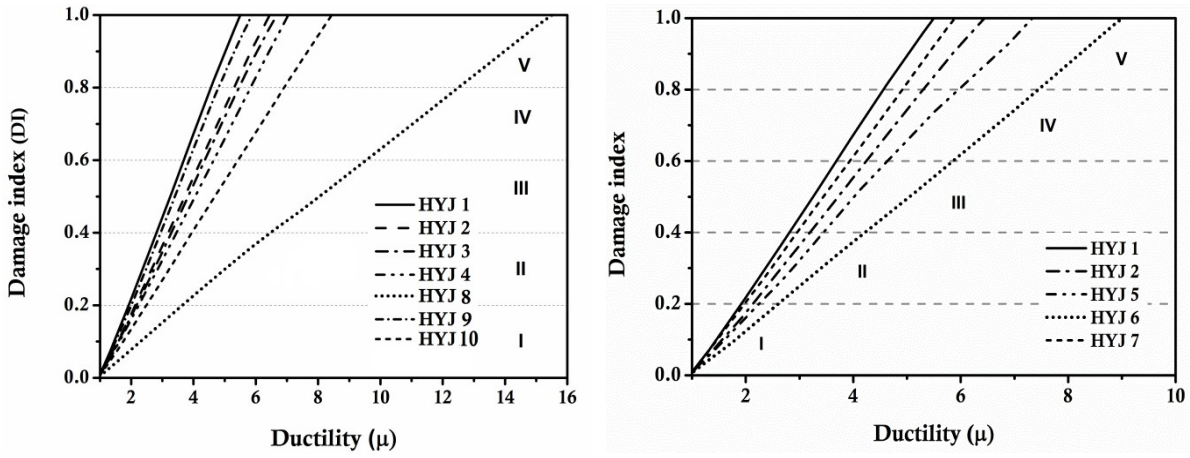

Figure 3.10: Damage index vs. ductility plot of beam-column joint specimens

The damage index [*DI*] values vary from 0 to 1, whereas "0" indicates no damage and "1" indicates complete damage. In this study it is assumed that 0 < DI < 0.20 represents elastic behavior or no damage in specimens, 0.20 < DI < 0.40 represents slight damage, 0.40 < DI < 0.60 represents moderate damage and 0.60 < DI < 0.80 represents severe damage and DI> 0.8 represents complete damage. The inherent crack resisting and bridging characteristics of FRC specimens show superior damage tolerance capacity without ductile detailing in the joint hinge regions as compared to conventional specimens. But in case of specimen HYJ 7, the early diagonal cracks in the joint at early stage of loading significantly affect the damage tolerance capacity and show lesser DI than HYJ 2. Hybrid fiber reinforced concrete enhances the damage tolerance capacity as compared to conventional specimens and shows comparable performance with fiber reinforced concrete specimens even with lesser volume of fibers. This proves that the use of fibers in conventional way or by hybridization in concrete effectively improves the damage tolerance capacity without closely spaced stirrups.

3.4.3. Hysteretic Behavior of Tested Specimens

Figure 3.11 shows the hysteresis behavior of conventional specimens HYJ 1 and HYJ 2. In specimen HYJ 1, post peak load degradation starts after 40 mm deflection while the same is observed after 50 mm deflection in specimen HYJ 2. The degradation is more gradual in specimen HYJ 2 as compared to specimen HYJ 1 that can be evident from the load deflection envelope curve as shown in Figure 3.12.

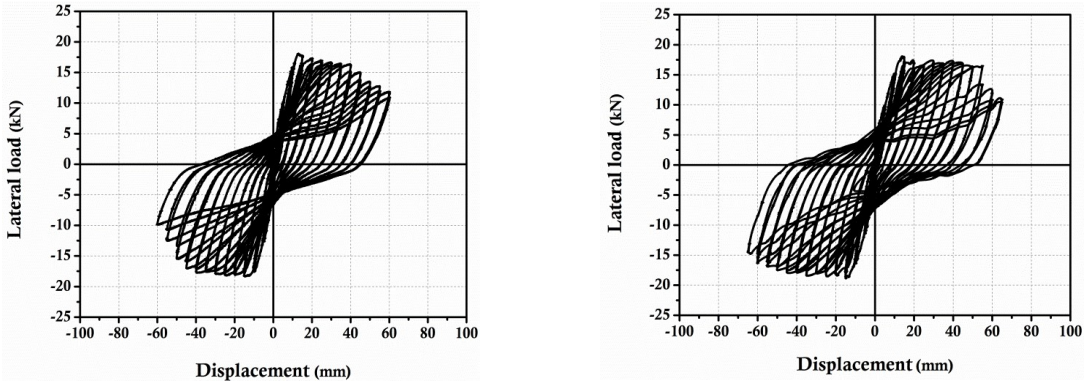

(a) HYJ 1- Unconfined (b) HYJ 2- Confined

Figure 3.11: Hysteresis curve of conventional joint specimens HYJ 1 and HYJ 2

The SFRC specimens (HYJ 3 to HYJ 6) having different volume of crimpled and hooked end steel fiber without critical confinement show higher shear strength and post yield strength (Figure 3.13) compared to conventional specimens. In FRC, fiber bridges the

crack well and transfers the stress until the fiber gets pulled out. Thus it enhances the first and second cycle load as large as 18% over conventional specimens. The volumetric differences of fiber do not show much difference in the load enhancement as compared to lesser volume specimens. It shows that irrespective of volume of fiber, the presence of steel fiber in the cracked region and the pull out strength of fibers decide the performance.

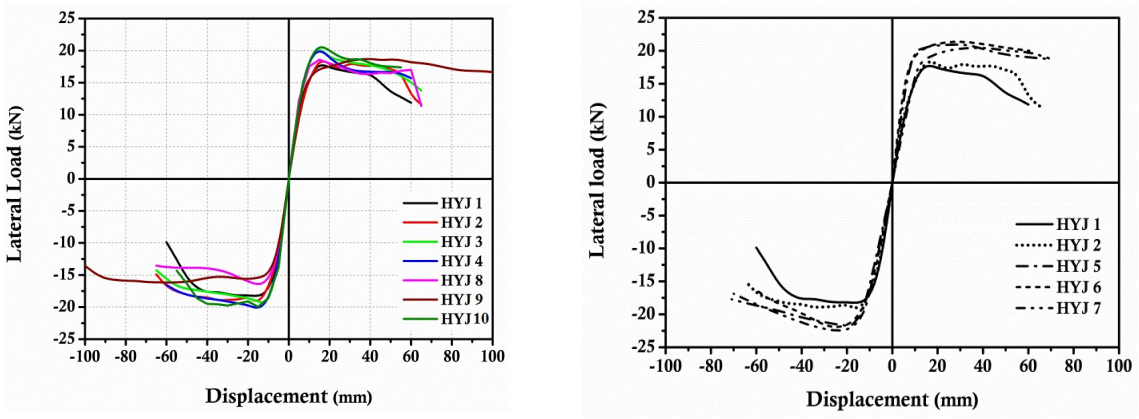

(a) (b)

Figure 3.12: Load-deflection envelope curve of FRC and HyFRC joint specimens

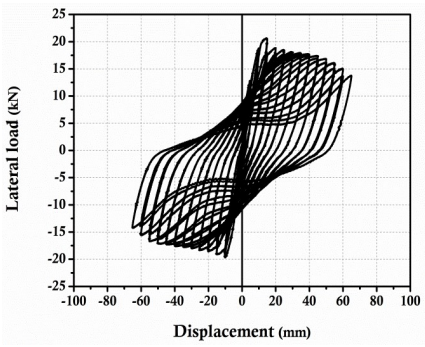

(a) HYJ 3-Crimpled steel fiber-1%)

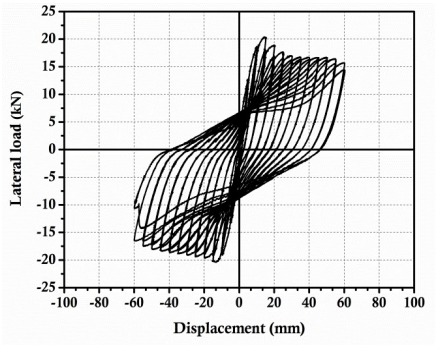

(b) HYJ 4-Crimpled steel fiber-2%)

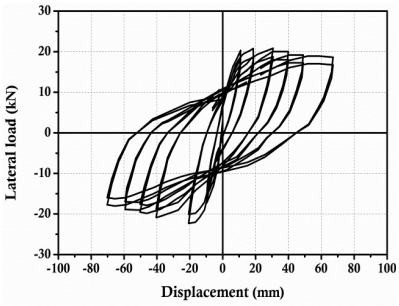

(c) HYJ 5-Hooked end fiber-1%)

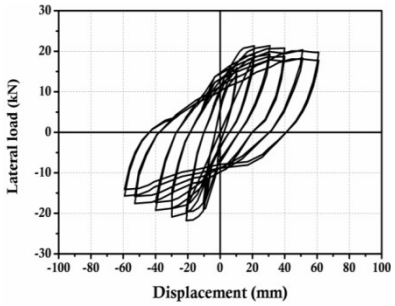

(d) HYJ 6-Hooked end fiber-2%)

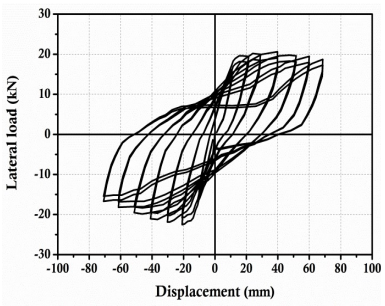

(e) HYJ 7- Macro synthetic fiber

Figure 3.13: Hysteresis curve of beam-column joint specimens

In joint specimens the concentration of major cracks is noticed at the joint connection region than joint shear zone. The presence of fibers and its anchorage property enhance the shear strength of the joint region that can be clearly understood from the

hysteresis loop of SFRC over MFRC. The poor anchorage and bonding behavior of MFRC fails to restrict the crack formation and propagation thus it fails in transferring the stress across the crack. The shear cracks in the joint region and concrete crushing in connection region in specimen HYJ 7 show reduced area of loop but has comparable shear strength enhancement similar to SFRC specimen. It shows that macro fiber has lesser influence on restricting the crack growth but has considerable load resistance capacity as in case of steel fibers. The hysteresis curve of specimens HYJ 8 to HYJ 10 shows different behaviors (Figure 3.14). The peak load of all the three specimens differs irrespective of its compressive strength as compared to FRC specimens. The mechanical properties of macro synthetic fiber enabled hybrid specimen are comparatively lesser than other fiber reinforced concretes. The observed peak load of specimen HYJ 8 is comparable with the specimen HYJ 9. The measured load at first and second cycle in this hybrid concrete specimen shows similar response of FRC specimens.

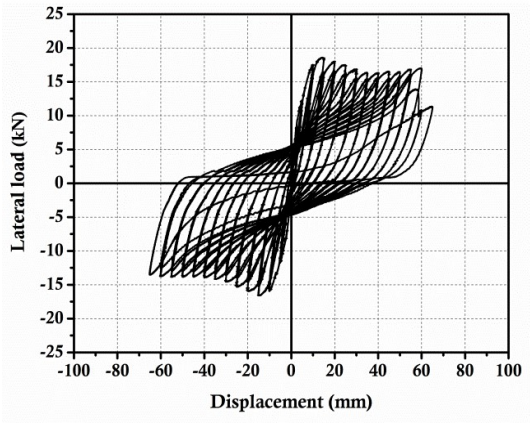

(a) HYJ 8
(Macro + micro fiber)

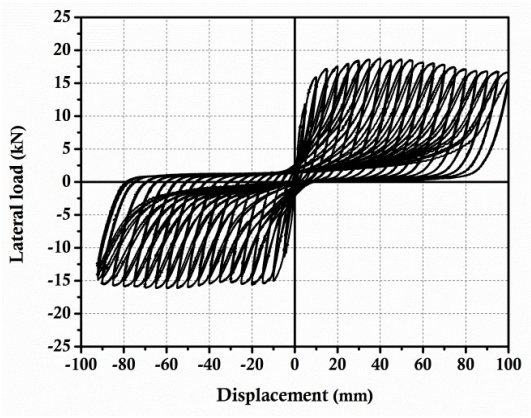

(b) HYJ 9
(Hooked end + micro fiber)

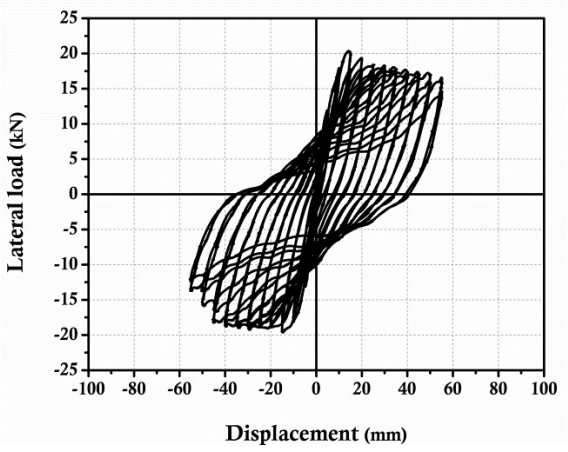

(c) HYJ 10
(Crimpled + micro fiber)

Figure 3.14: Hysteresis curve of hybrid fiber reinforced concrete joint specimens

3.4.4 Energy Dissipation and Damping

The Cumulative Energy Dissipation (CED) is calculated by summing the energy after each subsequent cycle and is plotted against cyclic displacement as shown in Figures 3.15 and 3.16. The equivalent damping coefficient is also calculated on the basis of relative energy dissipation and shown in Figures 3.15 and 3.16.

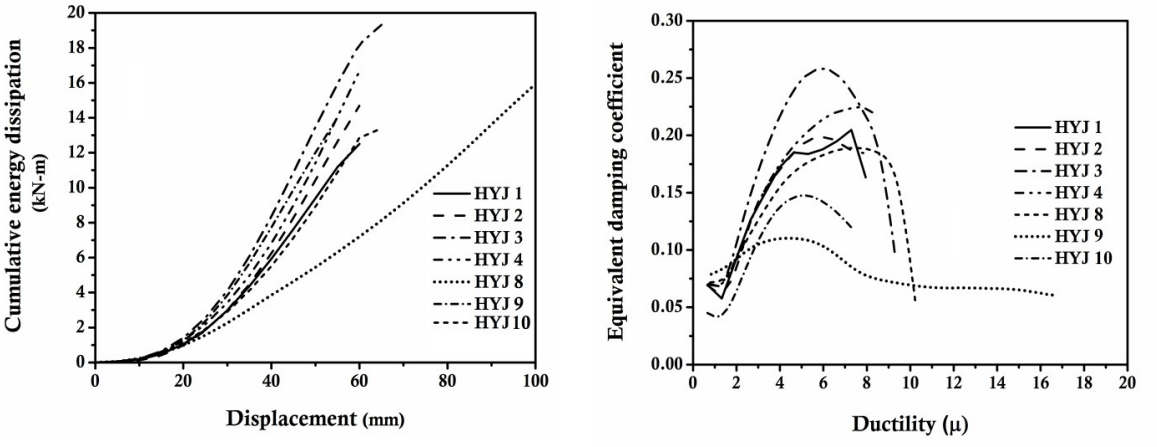

(a) Cumulative energy dissipation (b) Equivalent damping coefficient

Figure 3.15: Energy dissipation and damping response of FRC and HyFRC joint specimens

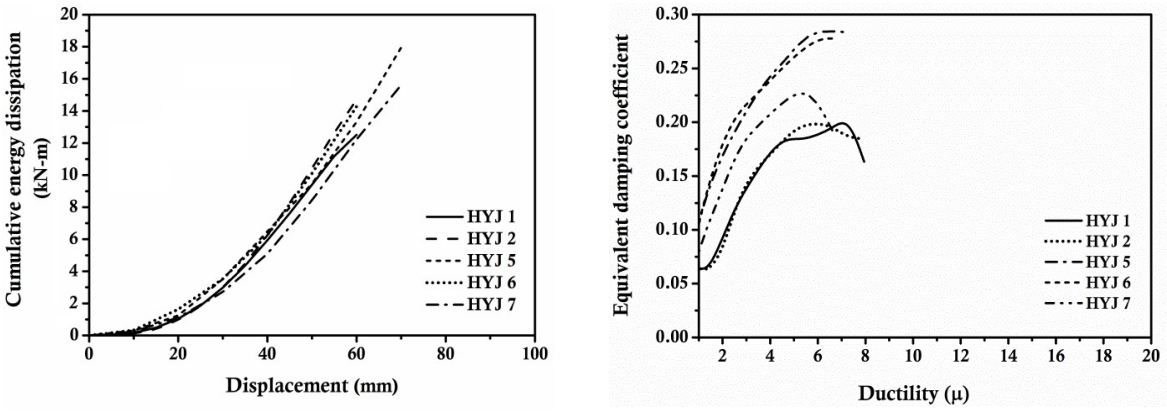

(a) Cumulative energy dissipation (b) Equivalent damping coefficient

Figure 3.16: Energy dissipation and damping response of FRC joint specimens

The hysteresis loop of specimens HYJ 3 and HYJ 4 shows the volumetric difference in specimens in terms of enlarged loop area. This shows 30 to 45% increased energy dissipation over specimen HYJ 1 and 10 to 25% increase in energy dissipation over specimen HYJ 2. The equivalent damping coefficient of FRC specimens are nearly 25%. In particular the energy dissipation of HYJ 3 and HYJ 5 is higher at early stage as compared to specimens HYJ 4 and HYJ 6. It emphasises that, the presence of higher

volume steel fiber in concrete plays pivotal role in resisting the applied load effectively at early stage than energy dissipation.

Figure 3.16 shows slow and steady energy dissipation capacity of specimen HYJ 7. The hysteretic curve of HYJ 7 shows the negative effect of early shear cracks on the energy dissipation characteristics. At 60 mm deflection the specimen HYJ 7 dissipates one third level of SFRC specimen's energy dissipation level. But CED of HYJ 7 at 100 mm deflection shows comparative performance with SFRC specimens. The fiber hybridization in specimens HYJ 8 to HYJ 10 shows better energy dissipation over conventional specimens and exhibits comparative energy dissipation capacity over SFRC specimens. This authenticates that the fiber hybridization can improve energy dissipation and damping without increasing the volume of fiber and critical detailing in the hinge region.

3.4.5 Strength and Stiffness Degradation

The post-elastic strength degradation over yield and post-elastic stiffness degradation over yield stiffness are calculated to estimate the inelastic behavior of test specimens. The inelastic performances of structural components are measured using the rate of change in strength and stiffness degradation over the post elastic rotation. Low rate of change in degradation shows ductile performance of structural component and vice-versa. Figure 3.17 and 3.18 shows the measured degradation versus post-elastic rotation.

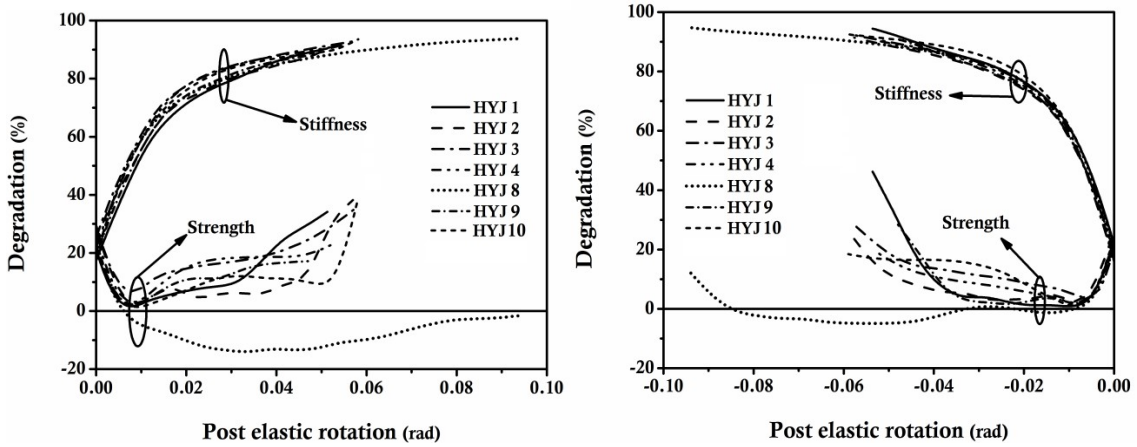

(a) Positive (push) (b) negative (pull)

Figure 3.17: Strength and stiffness degradation of FRC and HyFRC joint specimens

The degradation plot shows that the specimens with FRC and HyFRC illustrate improved strength and stiffness retention response over conventional specimens. In SFRC specimens the higher volume steel fiber in HYJ 4 and HYJ 6 shows lower rate of

degradation as compared to specimens HYJ 3 and HYJ 5. However, the strength and stiffness retention ability of specimen HYJ 7 signifies the influence of MFRC in improving the inelastic behavior and stiffness retention capacity. Even though with shear cracks in the joint region this MFRC restricts the sudden loss of stiffness in the early stage of loading and improves the retention capacity in the post yield region. Figure 3.17 shows that the hybrid fiber reinforced concrete joint specimens exhibit better strength and stiffness retention. The HYJ 8 shows comparable stiffness degradation response with better post elastic rotation over all other specimens. The steel fiber enabled HyFRC specimens HYJ 9 and HYJ 10 show slow rate of degradation over HYJ 8 but the ultimate post yield rotation of these specimens is lesser because of reinforcement yielding at 0.06 rad.

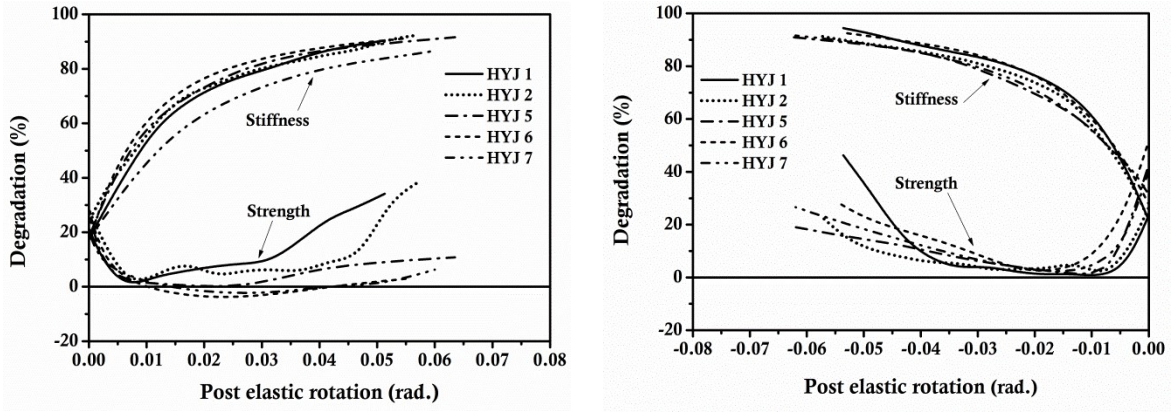

(a) positive (push)

(b) negative (pull)

Figure 3.18: Strength and stiffness degradation of FRC joint specimens

3.4.6 Moment-Rotation Behavior

The moment-plastic rotation relationships of all the tested beam-column joint specimens are compared with the specified values in ASCE/SEI 41-06 as shown in Figure 3.19. The maximum value of moment reaches as the rotation reaches 0.01 radian. The range of post peak behavior is noticed between 0.01 and 0.06 radians where there is no significant loss of moment capacity. The experimentally obtained plastic rotation capacity of the beam-column joint specimens is higher than the specified values in ASCE/SEI 41-06. The limit of linear elastic behavior of conventional joints is 0.015 and the range of post peak behavior is 0.015 to 0.02 radians, as shown in Figure 3.19. It is evident that the FRC and HyFRC in the joint significantly improve the *M-ø* relationship against the conventional specimens. The rate of moment degradation is deliberate as compared to the moment degradation of control specimens. FRC specimens exhibit better moment

resistance behavior over the defined range of ASCE 41-06. The higher ductility with better post peak response of specimen with FRC and HyFRC without ductile detailing in the hinge region shows increase in rotational capacity with lower rate of moment degradation. It represents the sign of ductile behavior of joint which is really difficult to achieve by conventional confinement.

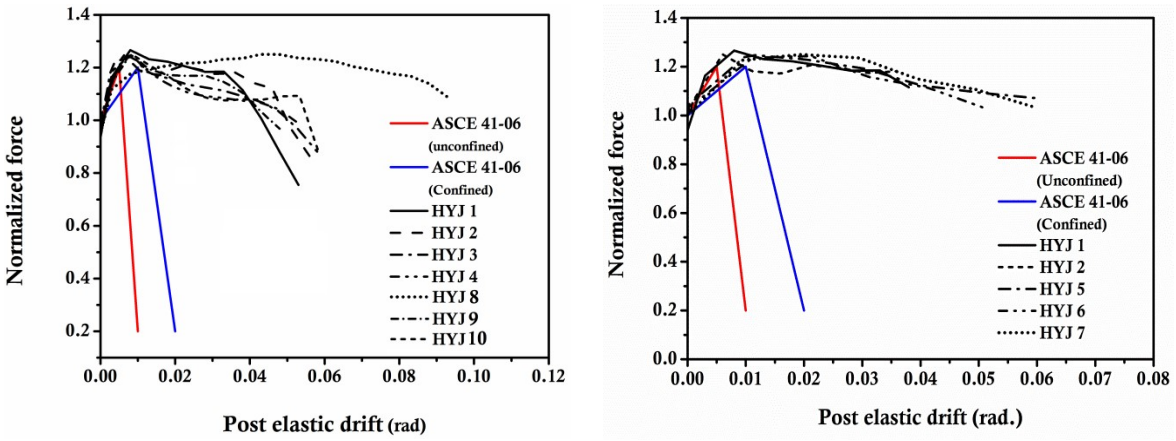

(a) (b)

Figure 3.19: Moment-rotation behavior of FRC and HyFRC joint specimens

3.5. Findings

The objective of this experimental investigation is to examine the influence of different fibers on the cyclic performance of exterior beam-column joint. The following are the main observations of the study;

1. There is a significant improvement in the axial stress-strain behavior of specimens under compression with fibers as compared to conventional concrete specimens. The SFRC specimens are able to sustain 66% more stress at four times of failure strain of conventional specimens. The steel fibers are able to reverse the failure mechanism from suddenly brittle to ductile with gradual post peak degradation. The effectiveness of macro synthetic fiber is not significant as compared to SFRC under axial compression as it fails to resist the applied load effectively.
2. There is a significant improvement in the flexural tension behavior of FRC beam specimens. The observed post peak degradation after initial cracking depends upon fiber volume and its physical property. There is a significant improvement in the peak load capacity and ultimate deflection of the specimens. The load-deformation performance and the energy dissipation of SFRC specimens are drastically improved

with the increase in volume of steel fibers as compared to the hybrid concrete specimens.

3. There is an effective enhancement in the post peak behavior of beam-column joint specimens with fibers. The post peak deformation capacity of SFRC specimens increases as compared to conventionally confined specimens without significant loss in strength. The bond slippage failure of embedded longitudinal reinforcement in the joint region is reduced due to the FRC in the joint core. There is also remarkable improvement in the ductility of hybrid concrete specimen with steel fiber.
4. The joint specimens with steel fibers show lower rate of degradation in strength and stiffness as compared to hybrid concrete specimens with large spacing of transverse reinforcement in the plastic hinge region.
5. The energy dissipation capacities of SFRC specimen increase nearly 1.5 times as compared to other conventionally confined specimens. It is also evident that the average internal damping coefficient increases by 15 to 30% in specimens with SFRC.
6. The specified values of plastic rotation capacity for the linear elastic behavior and post peak behavior of conventional and confined joints as per ASCE/SEI 41-06 are much lower as compared to beam-column joint with FRC.
7. The SFRC specimen and hybrid concrete specimens have more damage tolerance capacity. The observed damage index and mode of failure prove that the FRC can resist peak load without severe damage in the joint region. It is clearly observed that the SFRC specimen has undergone two level lower damage in comparison to conventional specimens with and without confining detailing of reinforcement.

References

ASCE/SEI 41-06 (2007), "Seismic rehabilitation of existing buildings," *American Society of Civil Engineers*, Reston, USA, 2007.

Adel, K., Djamel, A., Francois, D., and Lidia, R., (2014), "Effect of mineral admixtures and steel fiber volume contents on the behavior of high performance fiber reinforced concrete," *Materials and Design*, 63,493–499.

Andre, F., Karim, L., and Bruno, M., (1994), "Seismic performance of code-designed fiber-reinforced concrete joints," *ACI Structural Journal*, 91(5), 564-571.

Andre, F., Sylvain, P., and Jules, H., (1995), "Seismic behavior of steel-fiber reinforced concrete interior beam-column joints," *ACI Structural Journal*, 92(5), 543-552.

Bilal, S. H., and Elias, Y. A. H., (2015), "Bond studies of high-strength concrete joints confined with stirrups, steel fibers, or fiber-reinforced polymer sheets," *Journal of Structural Engineering*, 04015098.

Dhaval, K., Richard, H. S., Deb, S. K., and Anjan, G., (2015), "Ductility enhancement in beam-column connection using hybrid fiber reinforced concrete," *ACI Structural Journal*, 112(2), 167-178.

Ganesan, N., Indira, P. V., and Ruby, A., (2007), "Steel fibre reinforced high performance concrete beam-column joints subjected to cyclic loading," *ISET Journal of Earthquake Technology*, 44, 445-456.

Ganesan, N., Indira, P. V., and Sabeena, M. V., (2014), "Behaviour of hybrid fibre reinforced concrete beam–column joints under reverse cyclic loads," *Materials and Design*, 54, 686-693.

Holschemacher, K., Mueller, T. and Ribakov, Y., (2010), "Effect of steel fibres on mechanical properties of high-strength concrete," *Materials and Design*, 31, 2604-2615.

IS: 456:2000, "Indian Standard code for plain and reinforced concrete code of practice," 4th Revision, *Bureau of Indian Standard*, New Delhi.

IS:13920:1993 (Reaffirmed 1998), "Ductile detailing of reinforced concrete structures subjected to seismic forces - code of practice," *Bureau of Indian Standard*, New Delhi.

Jiru, T., Chaobin, H., Kaijian, Y., and Yongcheng, Y., (1992), "Seismic behavior and shear strength of framed joint using steel-fiber reinforced concrete," *Journal of Structural Engineering*, 118 (2), 341-358.

Liu, C., (2006), "Seismic behaviour of beam-column joint reinforced with steel fibres," *M.E Thesis*, University of Canterbury, Christchurch, New Zealand.

Mohammad, J. A., (2007), "Durability of steel fiber reinforced concrete in sulfate environment," *Final Research Report No. 38/426*, King Saud University, Saudi Arabia.

Park, Y. J., Ang, A. H. S., and Wen, Y. K., (1987), "Damage limiting aseismic design of buildings," *Earthquake Spectra*, 3, 1-26.

Paul, R. G., and Melvin, R., (1986), "Ramey increased joint hoop spacing in type 2 seismic joints using fiber reinforced concrete," *ACI Structural Journal,* 86(2), 168-172.

Tsonos, A., (2006), "Cyclic load behaviour of reinforced concrete beam-column joint designed according to modern codes," *European Earthquake Engineering*, 20(3), 3.

Vijay, N. K., Yogendra, S., and Dominik, H. L., (2012), "A comparative study of design base shear for RC buildings in selected seismic design codes," *Earthquake Spectra*, 28(3), 1047-1070.

Vijay, N. K., Yogendra, S., and Dominik, H. L., (2012), "A comparative study of code provisions for ductile RC frame buildings," *Proceedings of 15th World Conference on Earthquake Engineering*, Lisbon, Portugal.

Yung, C. W., and Ming, G. L., (2007), "Ultra high strength steel fiber reinforced concrete for strengthening of RC frames," *Journal of Marine Science and Technology*, 15(3),210-218.

Chapter 4

Inelastic Behavior of RC Structural Components using High Performance Fiber Reinforced Cementitious Composites

4.1 Introduction

In high performance fiber reinforced cementitious composites (HPFRCC), the presence of higher volume of fibers, mineral admixtures and the absence of coarse aggregate improve tensile strength and post elastic strain by strain hardening and softening behavior. Different types of composites such as slurry infiltrated fiber reinforced concrete (SIFCON); engineered cementitious composites (ECC) etc. are classified under this HPFRCC category. The performance of these composites is different and depends on the materials used. In SIFCON preparation steel fibers varying from >4-15% in volume have been used whereas in ECC preparation synthetic fibers such as Poly-Vinyl Alcohol (PVA) fiber and Poly- Ethylene (PE) fiber varying from 2-3% are preferred. In both the composites the addition of fine mineral admixtures and chemical admixtures are desired to fill the pores and to improve the strength without increasing the water content. The SIFCON composites have superior compression, tension and shear strength that dissipates higher energy in inelastic range. Many experimental studies have been conducted to explore the effect of different HPFRCC on structural members under large deformation. The test results indicate that HPFRCC have higher energy dissipation that enables to retard the degradation in strength and stiffness of structural member even without the special confining reinforcement.

In this study, behavior of RC beams and exterior beam-column joints with different types of HPFRCC i.e. Engineered Cementitious Composites (ECC) and Hybrid Cementitious Composites (HCC) is examined under cyclic loading. These composites are prepared by using Polypropylene fiber and steel fibers such as hooked end, crimpled and brass coated steel fiber varying from 2-3% percentage in volume. The load-deflection envelope behavior, hysteresis pattern, stiffness degradation, damage tolerance and energy dissipation are obtained and compared with conventional specimens.

4.2 Early Studies

Victor et al. (1993, 1994 and 1998) conducted many experimental and theoretical studies on ECC and its application in structural components. The ECC strain hardening behavior increased the ductile behavior of this composite over conventional fiber reinforced concrete. Maalej et al. (1995) proposed a new design for reinforced concrete flexural members to improve durability using strain-hardening cementitious composite and observed limited crack widths under service load conditions which were never before achieved using conventional steel reinforcement and concrete. Hiroshi et al. (2000) used ECC for seismic structural application and found better damage tolerance and ductility. The ECC increased the tension strain capacity by 1.5%. Malej et al. (2005) stated that while using ECC in RC beams the de-bonding was delayed and deflection behavior was improved. Maalej et al. (2005) studied the characteristics of ECCs subjected to dynamic tensile loading and high-velocity projectile impact and reported that ECC provided much higher enhancement in tensile strength enabling to maintain pronounced tensile strain-hardening behavior with tight crack width of about 0.1 mm. The results from high-velocity (300-750 m/s) impact tests demonstrated the potential of ECC in shatter resistance with reduction in damage arising from scabbing, spalling, and energy absorption associated with distributed micro cracking. Maalej et al. (2010) conducted an experimental study on improvement of out-of-plane resistance behavior of unreinforced masonry (URM) walls using ECC with hybrid fibers subjected to point load, uniformly-distributed load and low-velocity projectile impact. The results showed that ECC strengthening systems were effective in increasing the ultimate load-carrying capacity of URM walls, improving their ductility, enhancing their resistance against multiple low-velocity impacts and preventing sudden and therefore catastrophic failure. Maalej et al. (2012) conducted a review on potential application of hybrid ECC on various structural applications and suggested that the hybrid fiber ECC can significantly enhance the performance of structures incorporating these materials. Sameer et al. (2010) investigated the deflection behavior of concrete beams reinforced with PVA micro fibers and observed that the presence of micro-fibers in the composites delayed the development of micro cracks and enhanced the strength and crack resistance behavior. Giovanni et al. (2010) examined the application of HPFRC in strengthening of RC beams and observed enhanced strength and stiffness. Sun et al. (2011) experimentally investigated the application of strain-hardening cement-based composite in flexure dominant RC beam repairing work and observed dense minor cracks without concrete spalling and enhanced moment with delayed reinforcement yielding.

Raymond et al. (2008) studied the behavior of HPFRCC for RC coupling beams in earthquake-resistant structural wall systems and showed that the HPFRCC can be used in structural element due to susceptibility to seismic events and its energy dissipating capacity. Gregor et al. (2002) and Gregor et al. (2003) examined the effect of ECC on column members under cyclic loading and observed relatively stable inelastic deformation and large deflection response. Gregor et al. (2003) evaluated intrinsic response of moment resisting frame using advanced composite materials and introduced intended deformation mechanism theoretically. Hiroshi et al. (2000) investigated seismic response of ECC using reinforced concrete beam and observed better crack resisting mechanism and ductile behavior. Shannag et al. (2002) retrofitted interior beam-column joints with HPFRCC jackets (V_f = 2%) and observed high load carrying capacity, displacement ductility with slower stiffness degradation. Afsin et al. (2004) investigated the effect of HPFRCC using polyethylene and twisted steel fiber in precast coupling beams under cyclic loading observing higher shear strength and stiffness retention without additional transverse reinforcement. Shannag et al. (2005) experimentally studied the cyclic response of interior beam-column joints with HPFRCC using hooked end steel fiber and brass coated steel fiber. A better ductile and damage tolerance behavior was observed over conventional specimens. Patodi et al. (2008) studied mechanical properties of steel fiber reinforced ECC with RECRON 3s fiber reinforced ECC and confirmed that the RECORN 3s fiber reinforced ECC enhanced behavior under tension and impact over steel fiber reinforced ECC. The post - yield behavior of ECC using Recron fiber in moment resisting frame was studied and enhanced ductile performance over steel fiber reinforced ECC was observed. Fang et al. (2013) studied the behavior of exterior beam-column joints without stirrups using ECC in the joint zone under reverse cyclic loading and observed higher shear strength and damping property.

4.3 Behaviour of HPFRCC under Compression and Flexure

Mechanical properties of different concrete composites were examined under compression, split tension and bending using standard cylindrical and prism specimens.

4.3.1 Compression and Split Tension Behavior of HPFRCC

The axial stress-strain behavior and split tensile behavior of different composites were studied on cylindrical specimen with a standard size of 100 × 200 mm. Engineered Cementitious Composites (ECC) and Hybrid Cementitious Composites (HCC) using

different metallic fibers and synthetic fibers were used in the preparation of composites as presented in Table 4.1. A total of seven composites were prepared and the results were compared with conventional concrete specimens. The cylindrical specimens were tested under uni-axial compression. LVDT was used with a gauge length of 100 mm to measure the axial strain. In preparation of HCC, hooked end, crimpled steel fiber and brass coated steel fiber were used with polypropylene fiber in the desired mix ratio.

The detailed configuration of all composites is summarized in Table 4.2.The nomenclature of HCC is modified on the basis of type of fibres used in hybridization such as Hooked End Steel Fiber named as (HECC). Similarly, Crimpled and Brass Coated Steel Fiber in ECC composites are named as CECC and BECC respectively with Recron 3s poly-propylene fiber as shown in Figure 4.1. The hooked end and crimpled steel fiber of size 35mm length and 0.60 mm diameter (aspect ratio = 60) with nominal tensile strength of 1100MPa is used. Conventional concrete specimens are prepared using Ordinary Portland Cement (OPC) as cementitious material, coarse aggregate with maximum size of 20 mm and locally available river sand as fine aggregate. The water - cement ratio is kept at 0.45 in accordance with super-plasticizer to provide better workability.

The axial stress-strain curve of all HPFRCC specimens under compression is shown in Figure 4.2 and the test results are summarised in Table 4.3. The average compressive strength of conventional concrete CC1 is 27 MPa with sudden degradation in post yield capacity after attaining the peak stress which shows the brittle nature of plain concrete. All HPFRCC specimens possess better post peak strain behavior with low stiffness over conventional concrete because of presence of high volume synthetic fiber. In specimen CC2 (ECC), observed compressive strength is 25 MPa with ultimate strain of 0.02 which is nearly 1.5 times higher strain than conventional concrete. The compressive strength of HECC composites i.e. CC3 and CC 4 is also considerably low but initial stiffness is higher due to effective crack bridging property of metallic fiber over synthetic fiber in specimen CC2.

There is a significant improvement in compressive strength as well as post yield behaviour of BECC composite specimens (CC5 and CC6). The stress-strain behaviour of lesser volume brass coated steel fiber specimen CC5, exhibits a better response as compared to higher volume specimen CC6 of the same type of fiber. The compressive behavior of CECC composite specimens CC7 and CC8 is further improved due to the additional anchorage of crimpled fiber over other fibers.

Table 4.1: Cementitious materials mix proportions conventional concrete and HPFRCC

Specimen details	Cement	Sand	Coarse aggregate	Silica fume	Fly ash	Water binder ratio	Super Plasticizer	Fibers
Conventional Concrete	1	1.45	2.25	-	-	0.45	0.5	-
HPFRCC	1	0.5	-	0.1	0.2	0.45	1	Refer Table 4.2

(a) Polypropylene fiber (b) Hooked end steel fiber (c) Brass coated steel fiber (d) Crimpled steel fiber (e) Steel wool

Figure 4.1: Materials used in the study

Table 4.2: Mix ratio of different fibers in HPFRCC preparation

Specimen ID	Description	Volume of fiber			
		Poly-propylene	Hooked end steel fiber	Brass coated steel fiber	Crimpled steel fiber
		%			
CC -1	Conventional	-	-	-	-
CC -2	ECC	3	×	×	×
CC -3	HECC -1	1	2	×	×
CC -4	HECC -2	1.5	1.5	×	×
CC -5	BECC -1	1	×	2	×
CC -6	BECC -2	1.5	×	1.5	×
CC -7	CECC -1	1	×	×	2
CC -8	CECC -2	1.5	×	×	1.5

In HPFRCC specimens, a volumetric enlargement is observed and the failure pattern is in the form of multiple cracks without spalling and crushing of concrete as shown in Figure 4.3. The HECC composite holds the cracked portion together and increases the post peak strain property while BECC composites impede the crack growth and the specimen shows higher volumetric enlargement. The additional anchorage of crimpled steel fiber in CECC composite increases the strength and also restricts the volumetric enlargement.

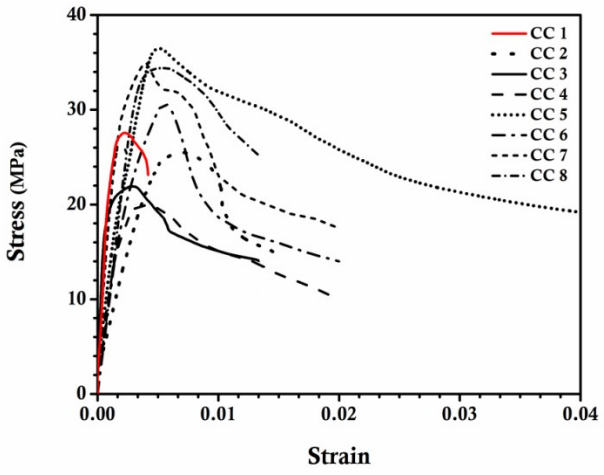

Figure 4.2: Stress-strain behavior of compression specimens

Table 4.3: Compression and flexural test results

Specimen ID	Compressive strength (MPa)	Split tensile strength (MPa)	Flexural strength (MPa)	Flexural energy (N/mm)
CC 1	27.5	3.4	4.0	0.22
CC 2	25.5	4.5	5.7	28.3
CC 3	22.0	4.2	4.9	26.4
CC 4	20.0	3.8	6.0	41.4
CC 5	36.4	4.7	7.0	24.0
CC 6	31.0	3.9	5.9	19.6
CC 7	35.0	5.6	6.7	39.0
CC 8	34.4	5.6	7.4	47.2

(a) HECC (b) BECC (c) CECC (d) Conventional

Figure 4.3: Failure patterns of different composites

The ratio of split tensile strength to compressive strength ratio differs with respect to composites. The split tensile strength of conventional concrete specimen CC1 is approximately 12.5 % while of ECC composite specimen CC2 is 17% of the respective compressive strength. The addition of steel fiber with synthetic fiber composites shows different tensile behavior with respect to their anchorage. The tensile strength of HECC and CECC composite ranges from 19-20% of its compressive strength, but the inadequate anchorage and lesser length of BECC have only 12% of its compressive strength.

4.3.2 Flexural Behavior of Composite Specimens under Two Point Loading

The flexural tensile behavior of different ECC composites is evaluated using prism of size 100×100×500 mm under two static point loading with centrally located LVDT to measure the corresponding deflection. The flexural tensile strength vs. deflection of HPFRCC composite is plotted in Figure 4.4 and the test results are summarised in Table 4.3. The flexural strength of conventional concrete is 4.0 MPa which is 14.5% of its compressive strength. The average flexural strength to compressive strength ratio (f_s / c_s) of HPFRCC composite specimens is about 20% with an improved and stable post yield deformation. The type of fibers, volume and anchorage of fibers play vital role in post peak behavior of HPFRCC composite specimen. Hybrid composite CECC possesses higher flexural strength due to the synergetic effect of crimpled fiber anchorage with synthetic fiber. The crimpled fiber anchorage effectively transfers the stress across the cracks and allows the specimen to deform gradually which can be observed from the post peak deflection curve of CC7 and CC8 in Figure 4.4. The flexural strength of CECC composite is nearly 1.8 times greater than conventional concrete. The post yield degradation of BECC composite specimen has a considerably higher rate than other hybrid composites due to its anchorage deficiency in bridging the cracks. The flexural energy of HPFRCC specimens is also calculated on the basis of area under the load-deflection curves. Figure 4.5 shows the comparison of flexural energy absorption of all HPFRCC composite specimens. The energy absorption capacity of HPFRCC composite is significantly higher than conventional concrete. The optimum amount of steel fiber along with synthetic fiber in cementitious composites may effectively improve the post-yield deformation with enhanced energy absorption capacity.

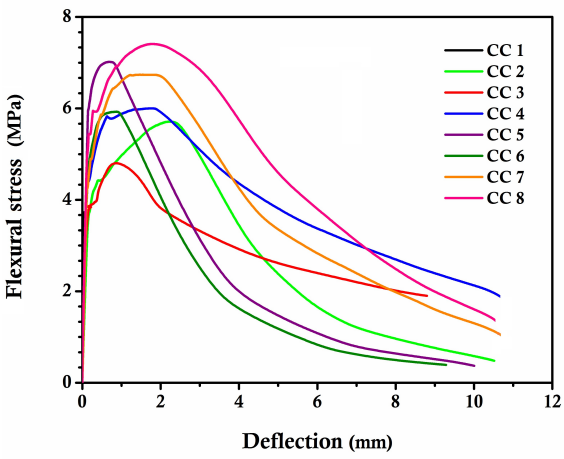

Figure 4.4: Flexural strength-deflection curve

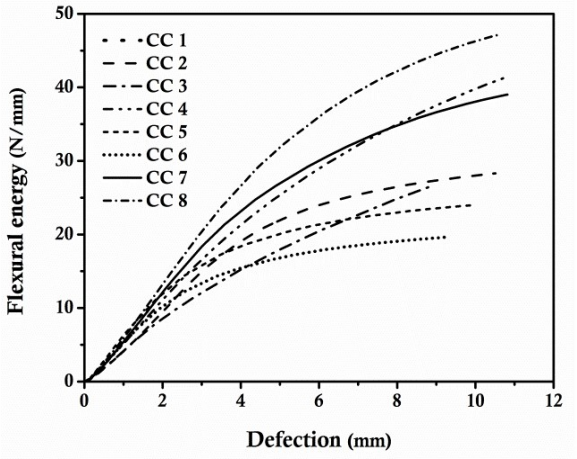

Figure 4.5: Flexural energy dissipation

4.4 Flexure behaviour of RC beam specimens with HPFRCC under Static loading

Eight types of RC beam specimens composed of different HPFRCC composites at the mid region with total length of 1.2m were tested under monotonic loading. Cross sectional detail of beam specimen remains the same in all the specimens but with different composites in the mid span region. Fe 500 grade steel was used as longitudinal reinforcement and Fe250 grade steel reinforcement was used for stirrups. The specimens were tested under single point static loading, shown in Figure 4.6, under load controlled in flexural testing machine with a test speed of 50N/s with a clear span length of beam specimens 1050 mm. The applied load was measured using inbuilt data acquisition and corresponding deflection was acquired using LVDT in three different locations.

The details of HPFRCC composite are given in Table 4.4.

Table 4.4**:** Detailed configuration of R.C beam specimen with different HPFRCC

ID	Transverse reinforcement	Composite in hinge region	Cross section and reinforcement details
SB 0	Ø6mm @150mm C/C	Conventional	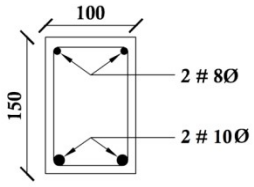
SB 1		ECC	
SB 2		HECC1	
SB 3		HECC2	
SB 4		BECC1	
SB 5		BECC2	
SB 6		CECC1	
SB 7		CECC2	

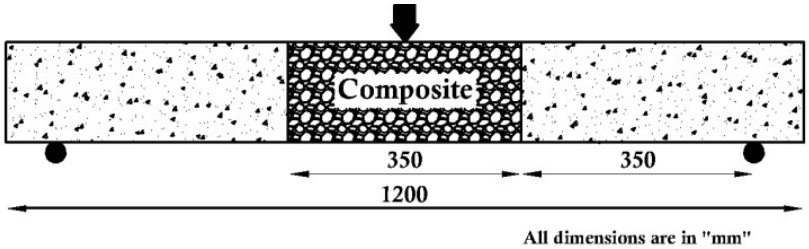

Figure 4.6: Detailed configuration of R.C beam specimen with test set up

4.4.1 Moment-Curvature Behavior of RC Beams

The moment-curvature response of beam specimens is shown in Figure 4.7 and the test results are summarized in Table 4.5. An early crack is formed at tension zone due to the brittle nature of plain concrete in conventional specimen SB 0. The propagation of inclined cracks across the cross section restricts the post yield behavior. The inelastic response of beam specimen with different HPFRCC is significantly improved and stable as compared to conventional specimen. The yield moment of HPFRCC specimens is comparatively higher than the conventional specimen. The composites in the hinge region resist the applied load and reduce the rate of crack propagation by bridging the cracks. The HPFRCC specimens experience ductile behavior even though with inclined cracks. The compressive strength of ECC is lesser than the conventional concrete but the specimen SB 1 shows 13% higher yield moment over conventional beam specimen. The first noticed crack moment (*fcm*) of specimen SB 1 and SB 0 is 13 kN-m and 10 kN-m respectively while in HECC composite specimens SB 2 and SB 3 it is 17 kN-m and 16 kN-m respectively. The absence of coarse aggregate, high volume fiber and blended dispersion restricts the crack formation, hinders its growth and allows the tension reinforcement to yield without significant loss in strength. Thus the HPFRCC beam specimens manifest enhanced ductile response over the conventional specimen.

The beam specimens (SB 4 and SB 5) with BECC encounter a sudden loss in moment after attaining the peak load. The uniform mixing of brass coated steel fiber increases the composite compressive strength but the lesser length and poor anchorage has lesser resistance in hindering the crack growth. However, higher volume of synthetic fiber in SB 5 shows improved post yield response over SB 4 but has lesser yield stiffness. The anchorage of crimpled fiber in the composite results is 1.7 times increased in *fcm* of specimens SB 6 and SB 7 over conventional specimen. In all the hybrid composite beams the first type (SB2, SB4 and SB6) composites have higher strength and stiffness as compared to second type of beam specimens (SB 3, SB5 and SB7). However, the second

type composites have better ductile behavior than first type composites. This is possible because of the volumetric difference of metallic fiber and synthetic fiber. The higher volume of metallic fiber increases the crack resistance and stiffness and higher volume of synthetic fiber increases ductility.

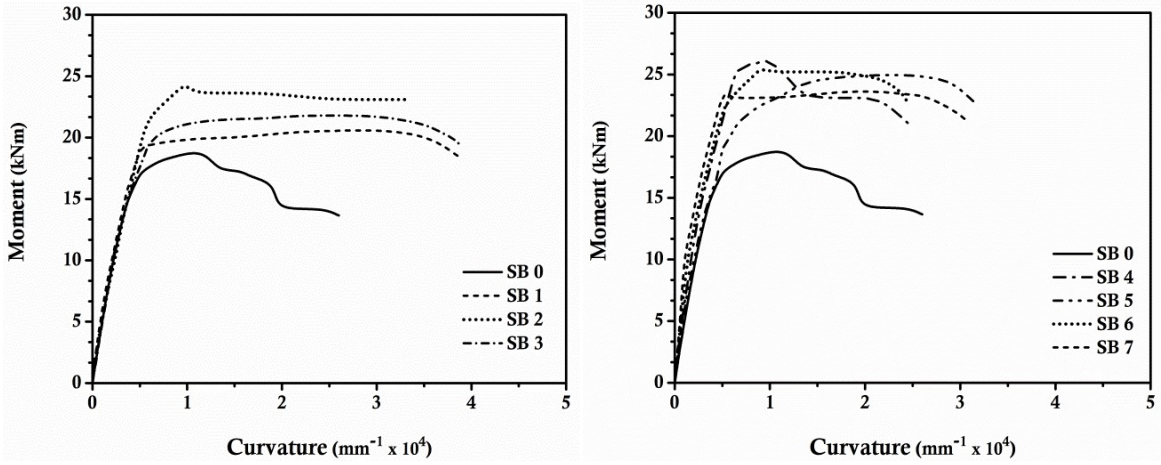

(a) (b)

Figure 4.7: Moment-curvature relationship of R.C beams

Table 4.5: Test results of R.C beams with different composites

Specimen ID	Moment *kNm*			Energy dissipation *(kN-mm)*	Curvature ductility
	First crack	Yield	Maximum		
SB 0	09.97	18.0	18.9	1051	5.4
SB 1	13.12	20.0	20.6	1950	11.1
SB 2	16.80	24.0	24.1	1868	6.3
SB 3	15.75	21.7	22.0	2041	8.4
SB 4	17.32	26.0	26.2	1553	5.4
SB 5	15.75	24.7	25.0	1830	6.4
SB 6	17.32	25.5	25.5	1449	6.3
SB 7	16.80	23.2	24.0	1765	10.2

4.4.2 Stiffness and Strength Degradation

The strength and stiffness degradation plot of beam specimens is shown in Figure 4.8. The HPFRCC enables beam specimens to exhibit steady and low rate of degradation in strength and stiffness. There is no sudden degradation in strength between the post yield rotation of 0.02 radian to 0.08 radian except in beam specimen SB 4. The conventional specimen has 90% degradation at 0.06 radian but the same is observed at 0.08 radian to 0.09 radian with HPFRCC specimens. This steady rate of degradation manifests the ductile

performance of the beam specimens. The stiffness degradation of all composite specimens shows similar kind of response, irrespective of fiber volume.

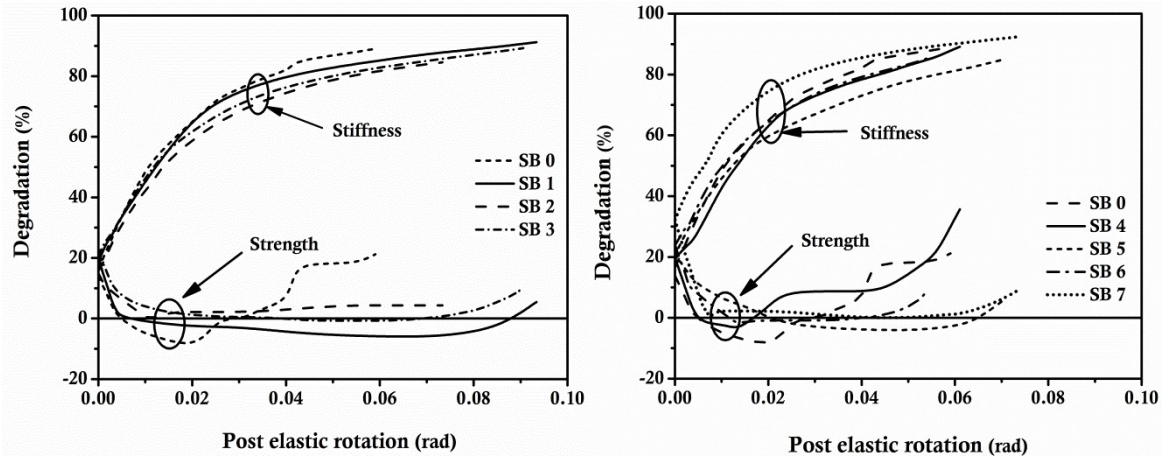

Figure 4.8: Stiffness and strength degradation response of R.C specimens

4.4.3 Energy Absorption and Ductility

The curvature ductility and energy absorption are calculated to examine the significance of composite on the ductility enhancement. Ductile behavior of a structural member is governed on the basis of post yield response and the amount of energy absorbed. The curvature ductility of beam specimens is calculated after the idealization of moment-curvature curves as shown in Figure 4.9. The energy absorption is calculated on the basis of area enclosed by the load-deflection curve. The measured curvature ductility and energy absorption of beam specimens are summarized in Table 4.5.

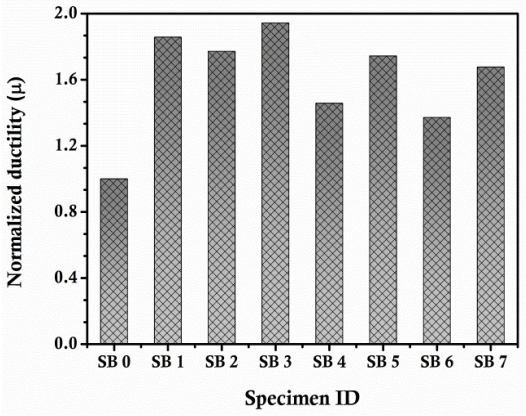

Figure 4.9: Comparison of curvature ductility

A 40% to 85% increase in ductility is observed on an average in fiber reinforced composite specimens as compared to conventional specimen. The composites with higher volume of synthetic fiber have higher ductility over composite with lesser volume of synthetic fiber. The conventional specimen has low ductile performance as compared to

specimens with HPFRCC as shown in Figure 4.9. The energy absorption in HPFRCC specimens is more stable and consistent without sudden drop of load, Figure 4.10. The type of fiber and its proportion governs the ultimate deflection and cumulative energy absorption. The composite beam specimens are able to show higher energy absorption as the post yield deflection increases.

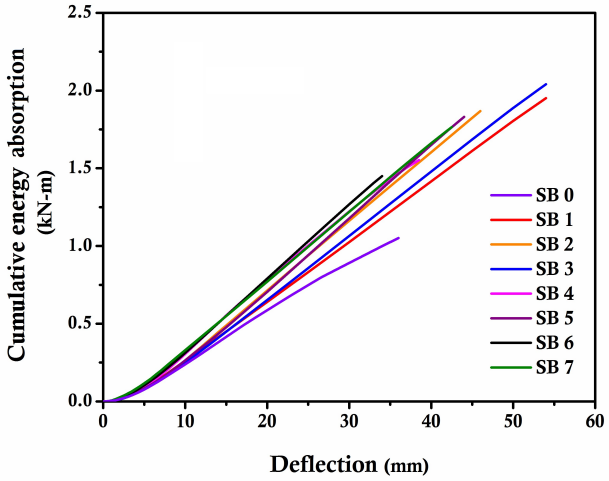

Figure 4.10: Energy dissipation of specimens

4.4.4 *Failure Pattern and Damage Index*

Crack patterns of tested beam specimens at failure are shown in Figure 4.11. The first crack load of conventional beam specimen is 20kN after initiating the vertical cracks in mid span. As the load increases, the cracks become inclined and wide as shown in Figure 4.11a. The failure mechanism of conventional beam specimen is flexural-shear while the HPFRCC composite enabled beam specimens exhibit flexural failure. In specimen SB 1 very dense flexural cracks are noticed in the composite region. In other hybrid composite enabled specimens, initially few vertical cracks are formed. This shows that the metallic fiber in the composites effectively bridges the cracks and restricts their growth and allowing the primary crack to propagate at a very slow rate towards loading direction. Figure 4.12 clearly demonstrates the crack bridging mechanism of different composites. Figure 4.12a shows the absence of effective crack bridging mechanism and gradual opening of cracks in synthetic fiber based composites (SB 1). Figure 4.12b shows the effectiveness of steel fiber with proper anchorage restricting the crack propagation in different stages. The lesser length of brass coated steel fiber without anchorage (SB 6) fails in restricting the cracks growth as shown in Figure 4.12c. In HPFRCC specimens, inclined shear cracks are also noticed but the growth of primary vertical cracks leads the specimen to fail in flexure.

SB 0- Conventional concrete

SB 1-Engineered cementitious composites (ECC)

SB 2-Hooked end + synthetic fiber (HECC-1)

SB 3-Hooked end + synthetic fiber (HECC-2)

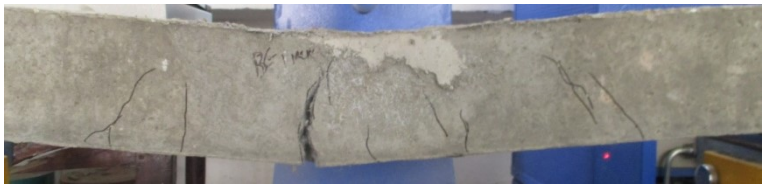

SB 4-Brass coated + synthetic fiber (BECC-1)

SB 5-Brass coated + synthetic fiber (BECC-2)

SB 6-Crimpled + synthetic fiber (CECC-1)

SB 7- Crimpled + synthetic fiber (CECC-2)

Figure 4.11: Failure pattern R.C beam specimens under bending

(a) ECC (b) HECC (c) BECC

Figure 4.12**:** Cracking pattern of different composite

Modified flexural damage ratio (MFDR) (Roufaiel et al. 1987) is also used to quantify the damage tolerance capacity of the beam specimens with and without HPFRCC. MFDR is the ratio of secant stiffness at the onset of failure (M_m/ϕ_m) to initial elastic stiffness(M_x/ϕ_x)**.** The MFDR values vary from 0 to 1, whereas "0" indicates no damage and "1" indicates the onset of failure of the member. The calculated MFDR of each specimen is plotted versus ductility as shown in Figure 4.13.

$$MFDR = \left[\frac{\frac{\phi_x}{M_x} - \frac{\phi y}{M_y}}{\frac{\phi_m}{M_m} - \frac{\phi y}{M_y}} \right] \qquad \textbf{4.1}$$

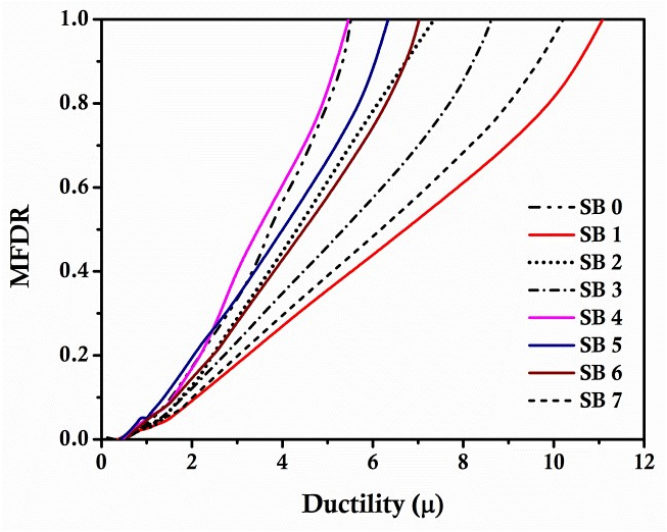

Figure 4.13: Modified flexural damage ratio vs. ductility comparison

The conventional specimen undergoes complete collapse state at the ductility level of 5 whereas HPFRCC beam specimens fail at much higher ductility levels. The measured ductility at collapse stage in HPFRCC beam specimen is nearly two times higher than conventional concrete beam specimen. A higher volume synthetic fiber based composite shows high damage tolerance capacity over the lesser volume synthetic fiber.

4.5 Cyclic Behavior of Beam-column Joint with HPFRCC

This experimental study investigates the influence of different HPFRCC in the potential hinge region of exterior beam-column joints to enhance its post elastic behavior. A quantitative assessment was carried out using different HPFRCC on the inelastic behavior of RC beam-column joints with nine exterior beam-column joint specimens tested under cyclic loading in quasi-static test facility to evaluate the hysteresis behavior of different HPFRCC under cyclic loading. In the HPFRCC joint specimen composites were used only in the joint hinge region and in the remaining places conventional concrete was used.

Table 4.6: Detail of exterior beam-column joint specimen with HPFRCC

ID	Transverse Reinforcement	Concrete in Joint	Beam Reinforcement	Column Reinforcement
HYCJ 1	Ø6mm @100mm C/C	Conventional 1	Specimens are reinforced with 3 # of 10mm Ø at top and bottom (Fe 500 grade steel)	Specimens are reinforced with 4 nos. of 12mm Ø (Fe 500 grade steel)
HYCJ 2	Ø6mm @100mm C/C & 50mm C/C in the hinge region	Conventional 2		
HYCJ 3	Ø6mm @100mm C/C (Fe 250 grade steel)	ECC		
HYCJ 4		BECC-1		
HYCJ 5		BECC-2		
HYCJ 6		CECC-1		
HYCJ 7		CECC-2		
HYCJ 8		HECC-1		
HYCJ 9		HECC-2		

Among the nine joint specimens two specimens were conventional specimens with different transverse reinforcement detailing. The first conventional specimen (HYCJ 1) was prepared with IS: 456-2000 (unconfined) detailing whereas the second conventional specimen (HYCJ 2) was configured with IS: 13920-1993 (confined) detailing. This was designed to quantify the influence of HPFRCC on the cyclic behavior of joint without ductile detailing. The same reinforcing details were used in preparation of specimens with different HPFRCC as in case of conventional-1 (unconfined) specimen. In HPFRCC beam-column joints different types of HPFRCC are used only in the joint and in hinge region and

in remaining places conventional concrete is used. The reinforcing details of two conventional specimens with different transverse reinforcement ratio are shown in Figure 4.14. The same reinforcing details as provided in conventional-1 specimen are used in preparation of specimens with different HPFRCC. Figure 4.15 shows the beam-column joint test setup and cyclic loading history. The amplitude of loading increases gradually from 10mm to occurrence of failure with an interval of 10mm under displacement control. The complete details of beam-column joint specimens with different types of concrete composites are given in Table 4.6.

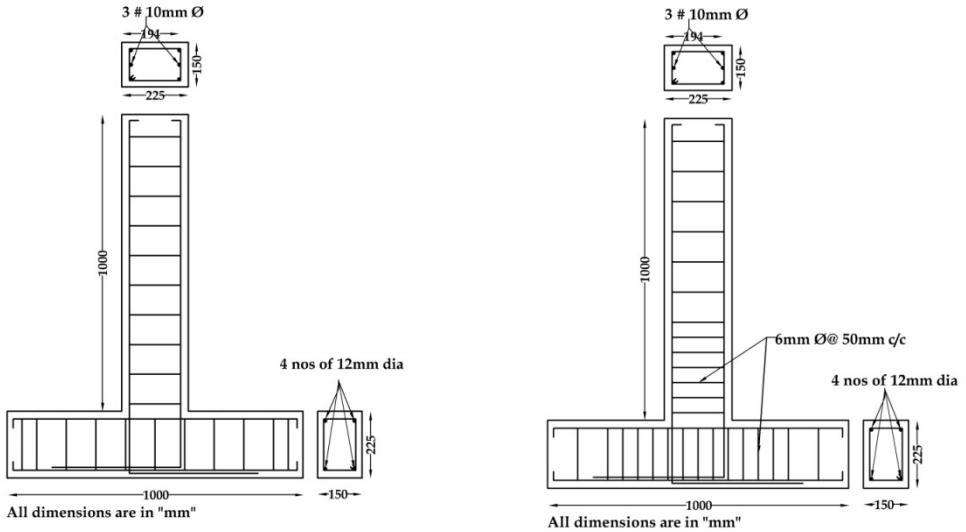

(a) HYCJ 1-IS 456:2000 detailing (Conventional-1)

(b) HYCJ 2-IS 13920:1993 detailing (Conventional-2)

Figure 4.14: Typical reinforcement details of joint specimen

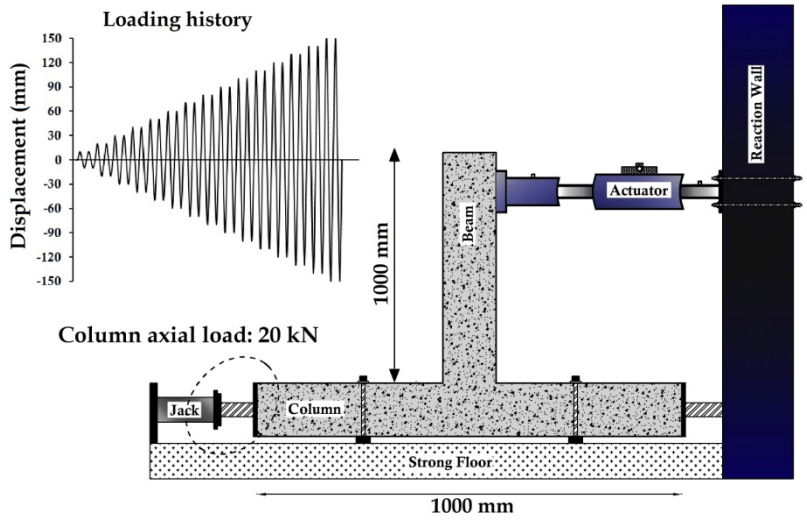

Figure 4.15: Beam-column joint test setup and loading history

4.5.1 Hysteresis Behavior

The hysteresis behavior of tested beam-column joint specimens is shown in Figure 4.16. The hysteresis behavior of conventional specimen (HYJ 1) shows meagre post yield performance over specimen HYJ 2. The post peak degradation of specimen HYJ 2 starts after 50mm whereas in HYJ 1 it is after 40mm. The rate of post peak degradation is also high in specimen HYJ 1 over the confined conventional specimen (HYJ 2). It demonstrates the influence of stirrups in the hinge region on the post elastic behavior of structural components.

The response of HPFRCC in joint without ductile detailing is remarkable in terms of strength and ductility. The higher tensile strength and tensile strain of ECC improve the resistance to early crack formation in specimen HYCJ 3 and show tremendous difference in the hysteresis behavior as compared to conventional. It (HYCJ 3) shows better and improved inelastic performance and very slow rate of post peak load degradation. Figure 4.16e shows enlarged loop and increased strength of joint specimen HYCJ 4 and HYCJ 5 constructed with BECC. The effect of BECC composite on strength enhancement is significant because of its perfect blending with synthetic fiber. Moreover, the higher volume of brass coated steel fiber has less impact on the workability as compared to crimpled and hooked end steel fiber. The BECC 1 shows 40% and 25% enhanced shear strength over conventional specimens HYCJ 1 and HYCJ 2 respectively.

The presence of brass coated steel fiber improves the composite compressive strength. It shows higher shear strength over ECC and other specimens. Also the enlarged loop of HYCJ 4 and 5 proves that the fiber hybridization has positive influence over ECC composites. Among the specimens HYCJ 4 and 5 the composite with higher steel fiber (HYCJ 4) shows wider loop over lesser steel fiber enabled composite. This observed difference in the loop area due to the volumetric difference demonstrates the role of fiber dosage in hybridization. In HPFRCC joints, the specimen with higher percentage of steel fiber shows higher strength and energy dissipation than the composite with lesser volume steel fiber. An average increase in strength of 40% and 25% is observed with HPFRCC joint specimens over conventional specimens HYCJ 1 and HYCJ 2 respectively. Irrespective of compressive strength, HPFRCC specimens exhibit better strength and ductility. In specimen with CECC composite, the hysteresis loop shows wider loops and higher strength over conventional specimens and ECC (HYCJ 3) specimen. The area difference in loop is observed with specimen HYCJ 7.

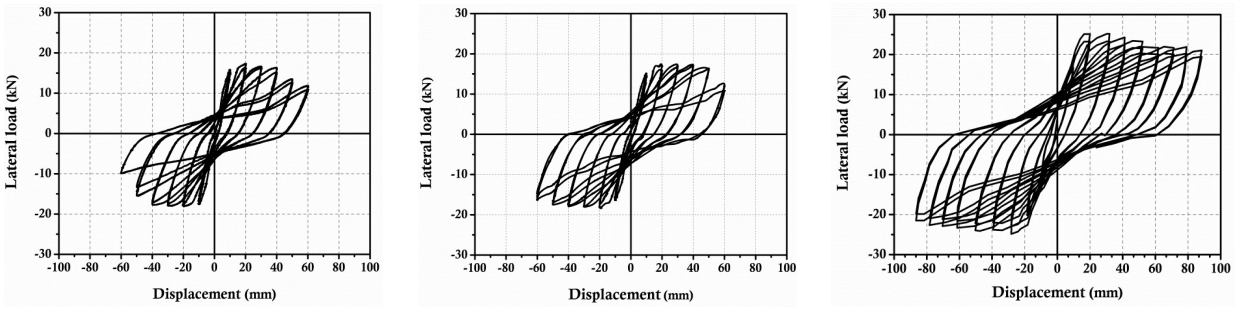

(a) HYCJ 1-IS 456 detailing

(b) HYCJ 2-IS 13920 ductile detailing

(c)HYCJ 3-ECC (3%)

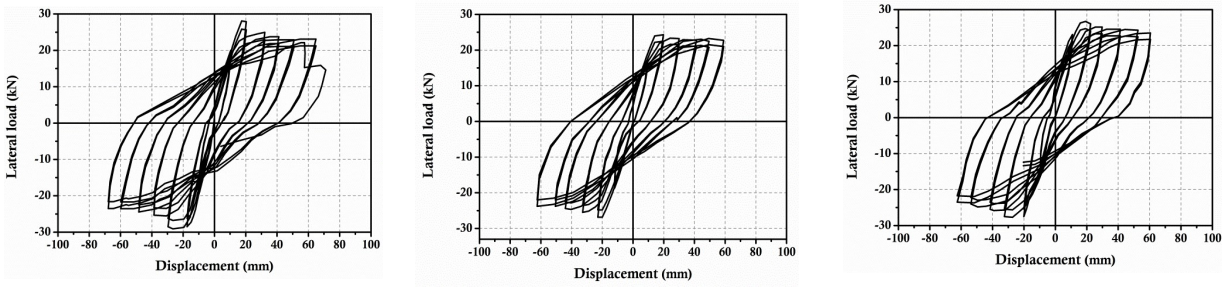

(d) HYCJ 4-BECC-1

(e) HYCJ 5-BECC-2

(f) HYCJ 6-CECC-1

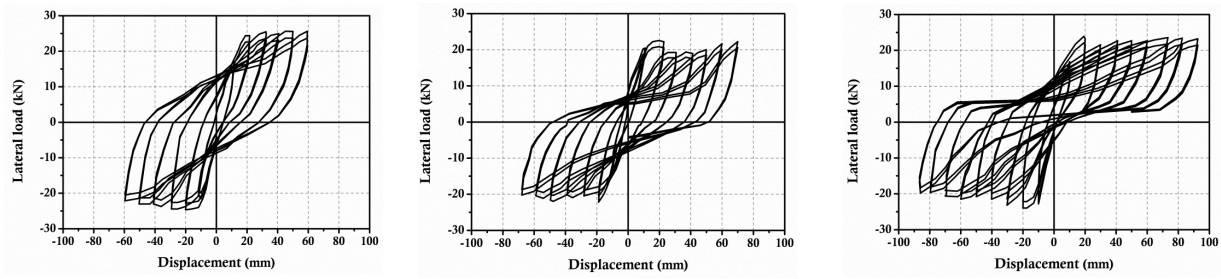

(g) HYCJ 7-CECC-2

(h) HYCJ 8-HECC-1

(i) HYCJ 9-HECC-2

Figure 4.16: Hysteresis curves of beam-column joint specimens with HPFRCC

The compressive strength of HECC 1 is lesser but shows comparable cyclic response. It shows that the tensile behavior due to the presence of fiber plays very important role in improving the post-yield performance. The hysteretic curve of HECC specimens looks different than the others and shows reduced loop area over other composites. Also irrespective of its low compressive strength the synergetic effect of hooked end steel fiber and synthetic fiber show better shear strength and post yield response over conventional specimens. This response authenticates that the tensile behavior of this composites has significant influence than compressive. The HPFRCC improves the reinforcement bond strength as is evident from the failure of joint specimens. The composite increases the bond strength and the crack bridging characteristics of fibers help in improving the tensile strength and can resist the tensile force from the flexural member.

4.5.2 Load-Deformation Envelope Curves

The load and deformation characteristics of each specimen with and without HPFRCC are estimated from envelops of the hysteresis curves as shown in Figure 4.17. The envelop curve explains the enhanced ductile behavior of HPFRCC over conventional specimens. It can be understood that the yield strength and ultimate deflection of HPFRCC specimens are considerably higher over conventional specimens. The post peak curve response is steady and rate of reduction in post yield strength authenticates the strength retention capacity of composite over conventional concrete.

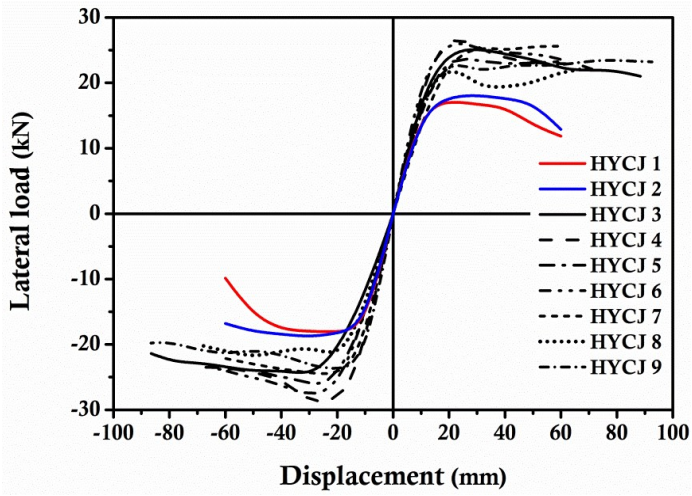

Figure 4.17: Load–displacement envelopes over ductility

4.5.3 Stiffness and Strength Degradation

The stiffness behavior of joint specimens shows the influence of HPFRCC on the post yield stiffness retention capacity. Figure 4.18 shows that the conventional specimens HYCJ 1 and HYCJ 2 almost lose 60% stiffness at 0.01 radians whereas HPFRCC specimens at 0.02 radians. In HPFRCC specimens 80% degradation is observed at 0.05 radians whereas the same is noticeable at 0.03 radians in conventional specimens. As evident from the Figure 4.18, ECC joint specimen HYCJ 3 has better stiffness retention over other composites. According to the nature of fiber and the composite strength other composites such as HECC, BECC and CECC show different stiffness and strength degradation behavior over ECC. In hybrid composites CECC plays better role in post yield stiffness retention. The additional anchorage of crimpled fiber effectively works in resisting the sudden loss in strength and stiffness. The degradation curve of CECC 2 (HYCJ 7) and HECC 2 (HYCJ 9) demonstrates that the composition with lesser steel fiber volume has

better post peak strength and stiffness retention over composite with higher volume of steel fibers. The stiffness response of BECC is commendable as compared to conventional specimens but not upto the level of other hybrid composites. It shows the deficiency of fiber anchorage and its ineffectiveness in bridging the cracks.

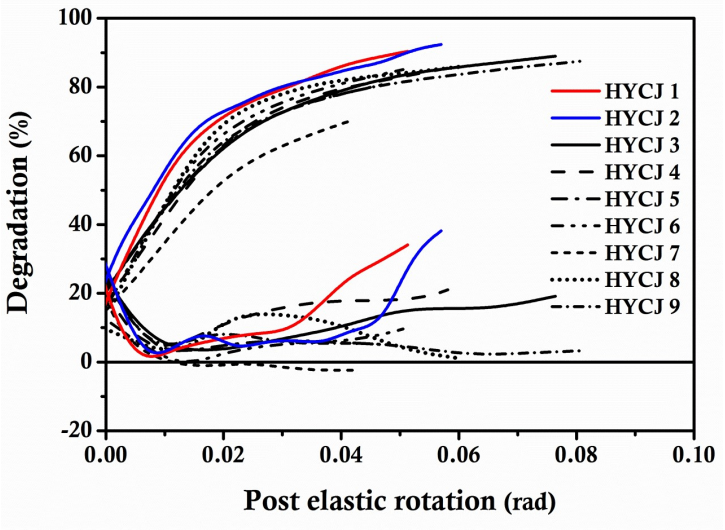

(a) Positive push

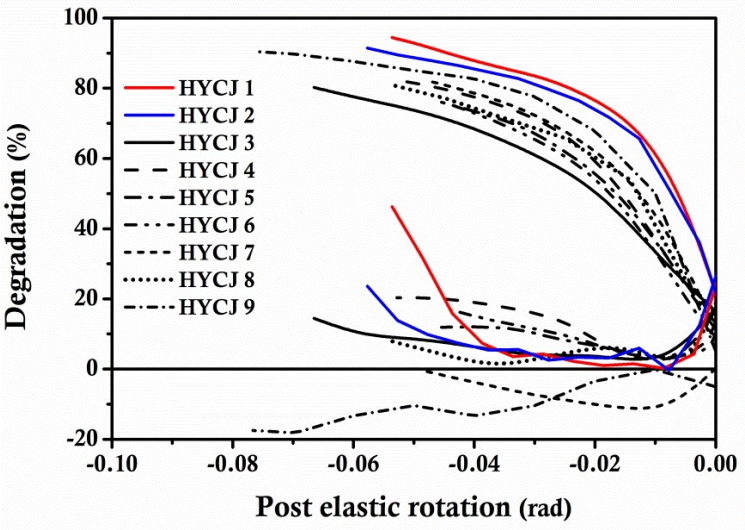

(b) Negative pull

Figure 4.18: Stiffness and strength degradation for type 2 joints.

4.5.4 Energy Dissipation and Damping

Figure 4.19 shows the comparison of cumulative energy dissipation of joint specimens. The energy dissipation of HPFRCC specimen shows a minimum of 50-100% increased energy dissipation over conventional specimens HYCJ 1 and HYCJ 2 respectively. The enlarged loop of BECC shows 15 kN-m energy at 60mm deflection and it is considerably higher than other composites at the same deflection. Except HECC, other

two hybrid composites BECC and CECC show improved energy dissipation over ECC composite enabled specimens. The dissipated energy of ECC specimen at 60mm deflection is 12.5kN-m and at 70mm deflection the energy level is 16kN-m. But at 70mm deflection, BECC and HECC show 20kN-m and 15kN-m. The performance of ECC lies between these two composites. The smaller loop of HECC results in lesser energy dissipation over other composites but the observed energy dissipation is 100% higher than HYCJ 1.

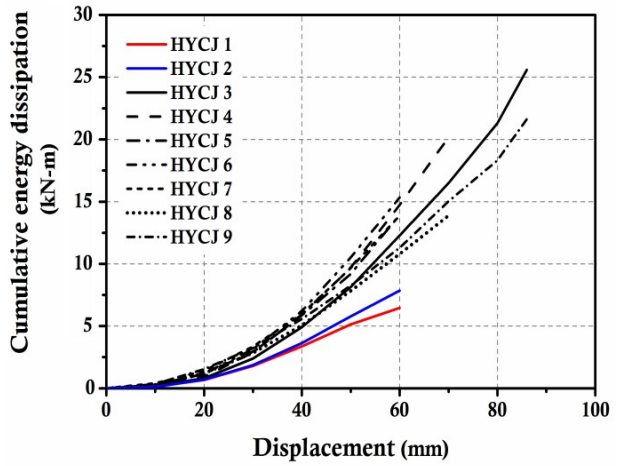

Figure 4.19: Energy dissipation plot over displacement of tested specimens

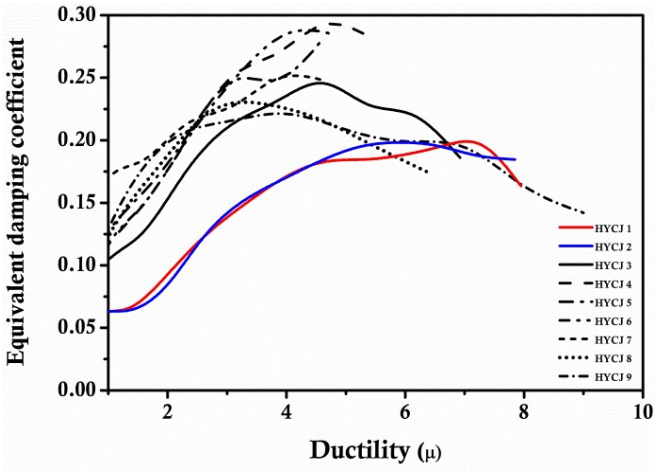

Figure 4.20: Equivalent damping coefficients over ductility

The equivalent damping coefficient based on the relative energy dissipation (RED) obtained from the hysteresis behavior of beam-column joint specimens is also calculated using the following equation 4.2 and the comparison is presented in Figure 4.20.

$$\xi_{eq} = \frac{1}{2\pi}\left\{\frac{area\ of\ loop}{area\ of\ triangle}\right\} \qquad 4.2$$

It is evident that the average equivalent damping coefficient with conventional confinement of joint specimen is in the range of 14 to 16% and 15-25% in HPFRCC joint specimen. The increase in damping coefficient reflects the effectiveness of HPFRCC on ductility and load-deformation capability of the specimens.

4.5.5 Moment-Rotation Behavior

Figure 4.21 shows the moment - rotation (M-Θ) relationships of beam-column joint specimens. It shows that the hybrid composites with lesser volume steel fiber and higher volume of synthetic fiber possess better post peak moment retention than the composite with higher volume of steel fiber. This is possible because of the high volume synthetic fiber blending and its effective stress transferring ability across cracks. The post peak moment degradation of conventional specimens starts after 0.04 radians but the HPFRCC shows no evidence of such post peak degradation upto 0.07-0.08 radians. This behavior authenticates the influence of HPFRCC on the post peak response of structural elements.

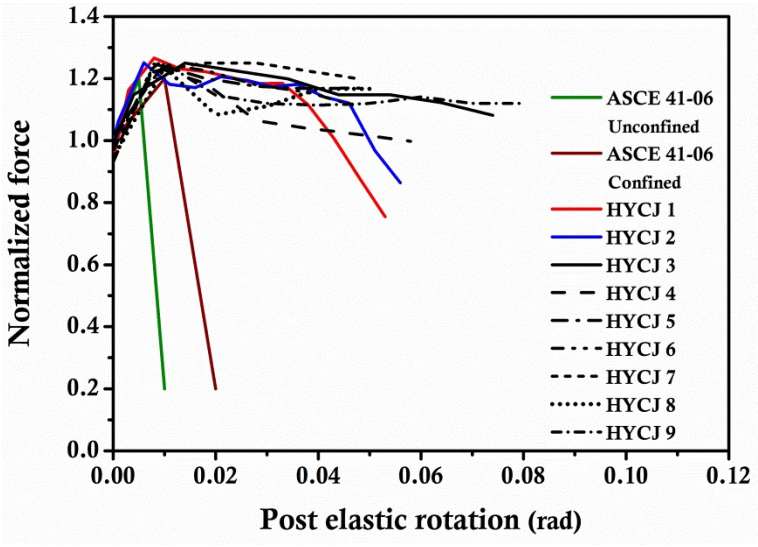

Figure 4.21: Moment-rotation behavior of test specimens

4.5.6 Crack Patten and Failure Analysis

Crack pattern of tested beam-column joint specimens at failure level under cyclic testing is shown in Figure 4.22. It is observed that the specimens with or without HPFRCC have different deformation characteristics, crack pattern and failure mechanism. In tested specimens initial flexural cracks are observed followed by joint connection crack. Two distinguished failure patterns are observed in conventional specimens.

(a) HYCJ 1

(b) HYCJ 2

(c) HYCJ 3

(d) HYCJ 4

(e) HYCJ 5

(f) HYCJ 6

(g) HYCJ 7

(h) HYCJ 8

(i) HYCJ 9

Figure 4.22: Crack pattern of HPFRCC joint specimens

The inadequate confinement in the hinge region of specimen HYCJ 1 experiences concrete cover spalling in the beam hinge region which is followed by reinforcement buckling at joint faces. Diagonal cracks are noticed in both the controlled specimens after 20mm deflection. In HYCJ 2 the seismic detailing restricts the rebar buckling at joint faces and crushing of concrete in the connection region is noticed as shown in Figure 4.22. In

addition to diagonal cracks vertical cracks along beam longitudinal reinforcement are also noticed. The cracking pattern of HPFRCC specimens is different from the conventional. The ECC composite in the joint region allows flexural crack formation along the beam span in the hinge region and as the deflection increases few diagonal cracks are also noticed in the joint. These cracks are immeasurable and hairline cracks develop as shown in Figure 4.22c. The cracks start at the joint after 40 mm deflection and finally fail. In other hybrid composite specimens, the concentration of failure is noticed at the joint connection region. There is no evidence of dense flexural cracks in the hinge region of the joint where the joint has HPFRCC. The flexural cracks in the beams are also observed above the composite region. There is no crack at the contact surface of composite and concrete, which proves the perfect bonding of two different concretes. The crack widening at joint connection in BECC specimens is considerably faster than other hybrid composite specimens due to its poor anchorage behavior.

4.5.7 Damage Index

Park and Ang, (1987) damage index is used for the comparison of relative performance of beam-column joint specimens with and without HPFRCC joint as shown in Figure 4.23.

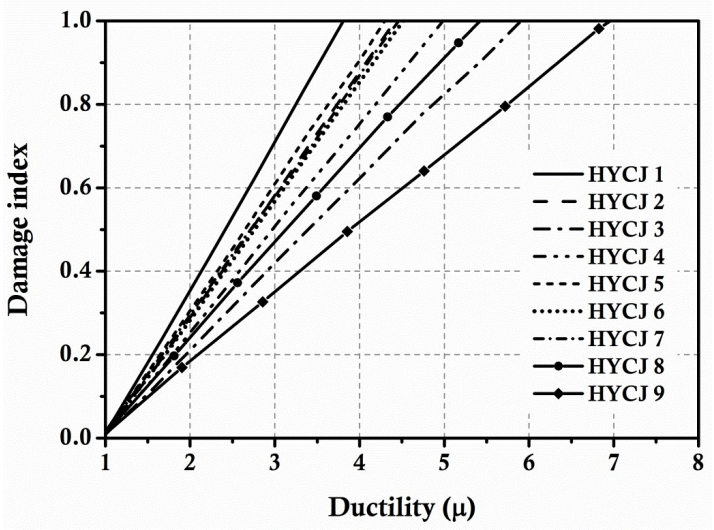

Figure 4.23: Damage index over ductility of all test specimens

The damage tolerance of HPFRCC is considerably higher even without seismic detailing in the joint region. Figure 4.23 shows that the conventional specimen HYCJ 1 reaches the collapsed stage before ductility 4. The HPFRCC specimens reach the collapse stage at ductility 4.5 to 7 with respect to the individual composites. The ECC, BECC and

HECC show high level damage tolerance than CECC composites. The HECC possesses better damage tolerance over other composites.

4.6 Cyclic Behavior of Shear Deficient Exterior Beam-column Joint with HPFRCC

This experimental program investigates the effect of different HPFRCC in the potential hinge region of shear deficient exterior beam-column joints to enhance its post elastic behavior. Six exterior beam-column joint specimens with different fiber reinforced cementitious (FRC) composites; steel fiber reinforced concrete (SFRC) and conventional concrete are tested under cyclic loading. The detailed mix ratios of concrete and fiber reinforced concrete with composites are presented in Table 4.7 and Table 4.8.

Table 4.7: Concrete mix proportions for SFRC and HPFRCC

Specimen details	Cement	Sand	Coarse aggregate	Silica fume	Steel wool	Fly ash	Water binder ratio	Super Plasticizer	Fibers
Conventional Concrete	1	1.45	2.25	-	-	-	0.45	0.5	-
SFRC	1	1.35	2.15	-	-	-	0.45	0.5	Refer Table no 2
HPFRCC (Beam)	1	0.5	-	0.1	-	0.2	0.45	1	

Table 4.8: Compressive and split tensile strength of HPFRCC I composites

Specimen ID	Description	Volume of fiber			Cylinder Compressive Strength	Split tensile strength
		PP*	HSF*	BSF*		
		%			MPa	MPa
SC -1	Conventional	-	-	-	27	3.8
SC -2	SFRC	-	2	-	36	4.8
SC -3	ECC	3	-	-	26	4.5
SC -4	HECC	1.5	2	-	39	6.5
SC -5	BECC	1.5	-	2	33	4.5

***Note:** PP- Polypropylene; **HSF**- Hooked end steel fiber; **BSF**-Brass coated steel fiber; **HECC-** HSF reinforced engineered cementitious composites; **BECC-** BSF reinforced engineered cementitious composites*

The HPFRCC is used only in the joint hinge region and in the remaining portion cast with conventional concrete. The complete details of beam-column joint specimens with different types of concrete composites are given in Table 4.9. The reinforcing details of two conventional specimens with different transverse reinforcement ratios are shown in Figure 4.24. Fe 500 grade steel is used as longitudinal reinforcement and Fe250 grade steel

reinforcement is used for stirrups. The joint specimens are tested under cyclic loading with amplitude of loading that increases gradually from 5mm to occurrence of failure with an interval of 5mm under displacement control.

Table 4.9: Configuration of beam-column joints with HPFRCC

ID	Transverse Reinforcement	Concrete in Joint	Beam Reinforcement	Column Reinforcement
SJ1	Ø6mm @100mm C/C	Conventional 1	All specimens are reinforced with 3 nos. of 10mm Ø at top and bottom	All specimens are reinforced with 4 nos. of 12mm Ø
SJ2	Ø6mm @100mm C/C & 50mm C/C in the hinge region	Conventional 2		
SJ3	Ø6mm @100mm C/C	SFRC		
SJ4		ECC		
SJ5		HECC		
SJ6		BECC		

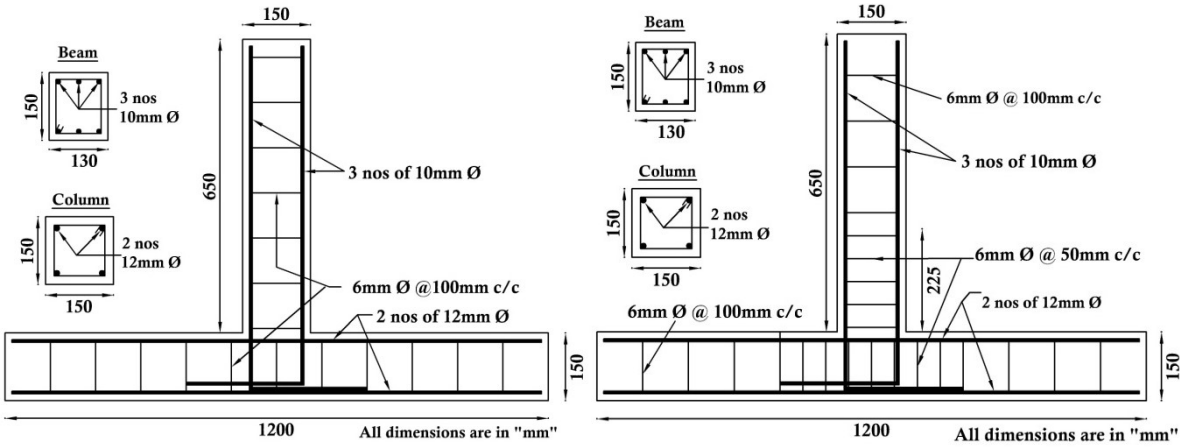

(a) SJ1 -Contro1(*Unconfined)* (b) SJ2 –Contro2(*Confined)*

Figure 4.24: Typical reinforcement details of joint specimen

4.6.1 Crack Pattern and Failure Analysis

Initially flexural cracks are noticed in beam portion of the joint specimens, as the deformation increases, diagonal shear cracks develop at the joint. In conventional specimen SJ1, complete brittle nature of shear crack formation initiates through the joint that accelerates the slippage of embedded longitudinal beam bar from the joint and spalling of joint cover concrete. In confined specimen SJ2, there is a slight delay in shear failure

with less intense cracking as compared to joint specimen SJ1. The presence of steel fiber and the fiber bridging characteristics along with hooked end anchorage in specimen SJ 3 restrict the occurrence of initial shear cracks and reduce the intensity of wider shear cracks with volume enlargement as compared to conventional specimens, shown in Figure 4.25c.

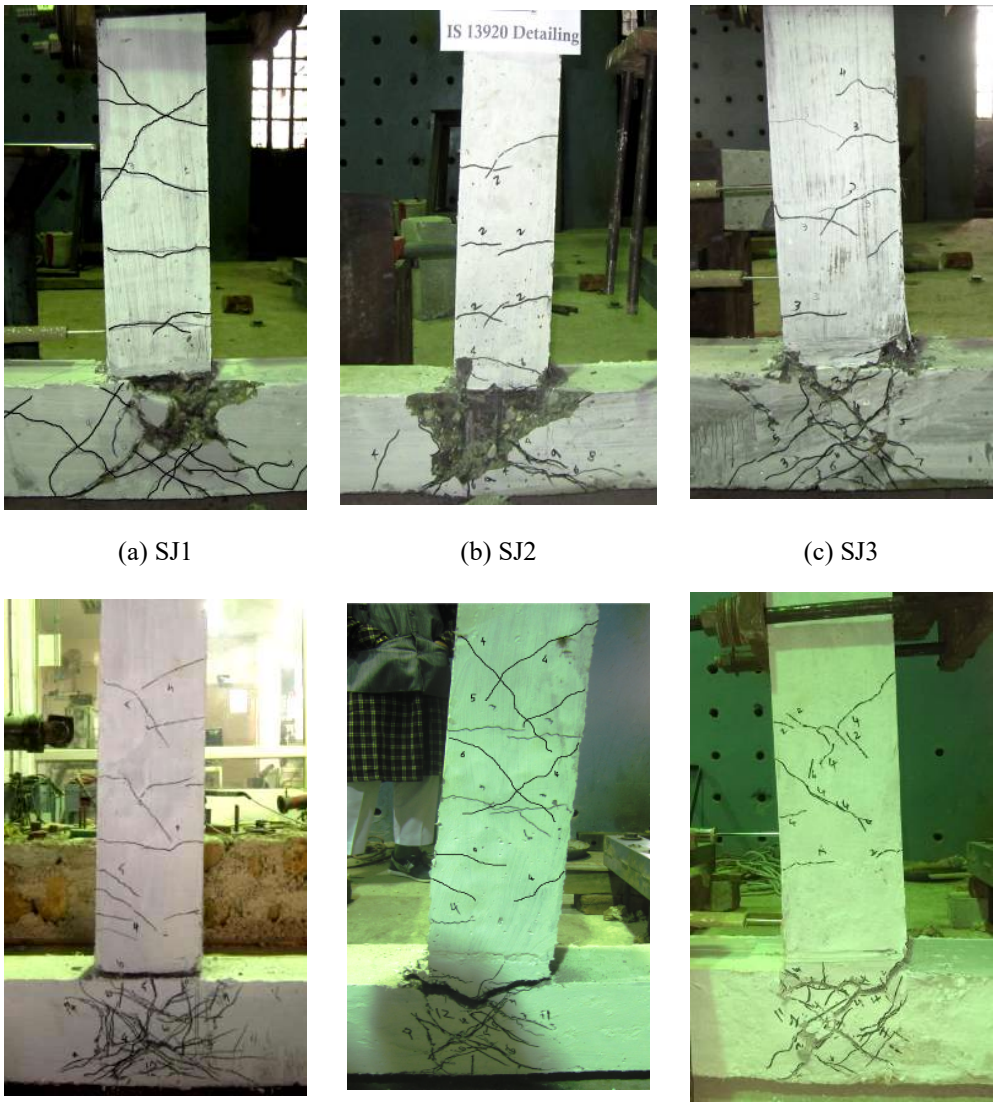

(a) SJ1 (b) SJ2 (c) SJ3

(d) SJ4 (e) SJ5 (f) SJ6

Figure 4.25: Crack pattern and failure mode

The failure pattern of ECC specimen shows considerably different cracking behavior over earlier specimens. The initial inclined crack occurs at the deformation of about 20mm with the widening of shear cracks at joint and continues upto the deformation of 50mm. During higher lateral drift, a number of micro cracks are also observed as shown in Figure 4.24d. The major failure takes place in HECC joint specimen SJ5 at the beam – column joint connection. This is due to toughness of hooked end steel fiber composite that restricts the crack width growth at the joint. The crack formation through energy

dissipation of beam-column joint is shown in Figure 4.25e. The toughness of joint may be because of higher tensile strain of composite and significant bridging ability of hooked end steel fiber. In BECC joint specimen SJ6, the presence of brass coated steel fiber works effectively in post peak performance and plastic rotation property and even cracks resistance property. However, due to deficient fiber anchorage strength it cannot bridge the cracks effectively like hooked end steel fiber as in specimen SJ5. The specimen allows the widening of shear cracks at the deformation of 35mm and as the deflection further increases, these cracks also widen and finally the joints fail in shear as shown in Figure 4.25f.

4.6.2 Hysteretic Behavior

The hysteresis behavior of conventional specimen (SJ1) shows brittle failure since there is a sudden drop in load carrying capacity after attaining the peak load with higher rate of degradation as compared to the confined conventional specimen (SJ2). A large hoop area of specimen SJ2 as compared to specimen SJ1 confirms the importance of confinement detailing in the joint hinge region. The occurrence of shear cracks at the initial stage of loading in conventional specimen SJ1 facilitates early slippage of longitudinal beam reinforcement and spalling of concrete in the joint region which lead to shear failure. The ductile detailing in the joint region of specimen SJ2 exhibits increased yield loading capacity and post peak load carrying capacity as compared to specimen SJ1.

The SFRC in beam-column joint specimen SJ3 is able to improve the load carrying capacity with higher loop area over conventional specimens SJ1 and SJ2. SFRC at the joint region acts as a potential barrier for crack growth and its propagation. Moreover, the bridging effect of steel fiber improves the interfacial bond strength of embedded beam reinforcement and concrete as well as post peak load carrying capacity of specimen SJ3. The area under every cycle of hysteresis loop (Figure 4.26c) shows the improved ductile behavior of specimen SJ3 over conventional specimens SJ1 and SJ2.

The anchorage strength of brass coated steel fiber in BECC is considerably lesser than the hooked end fiber in HECC, thus it cannot effectively resist the occurrence of initial diagonal cracks as in the case of specimen with HECC i.e. SJ5. At 80 mm deflection longitudinal bar failure takes place at one side, Figure 4.26e. This composite enables to hold the load upto 100 mm deflections. The BECC joint specimen SJ6 is not able to further improve the hysteresis behavior over specimen SJ5 but it maintains better post peak load-deformation behavior than SFRC and ECC specimens respectively.

The ECC at the joint region significantly improves the load-deformation capacity as compared to conventional specimens SJ1, SJ2 and SFRC specimen SJ3. The lower rate in loss of load carrying capacity with increased post peak deformation in specimen SJ4 with ECC is comparatively better than other specimens. Figure 4.27 shows a reduction of 25% ultimate load at deformation of 50 mm in ECC specimen, whereas at the same deformation 50% and 75% reduction of ultimate load is observed in conventional specimens (SJ1 and SJ2) respectively. As compared to SFRC specimen SJ3, 25% higher load is observed at the deformation of 70mm whereas at the same deformation the conventional specimens (SJ1 & SJ2) completely fail. At 90 mm deflection, ECC joint specimen completely fails and its load resisting capacity is reduced to 10kN.

The tensile strain of ECC and its crack resisting behavior prevent the early slippage of embedded beam anchorage reinforcement and improve the post peak load carrying capacity of specimens as compared to conventional and SFRC specimens. The hysteresis behavior of HECC joint specimen SJ5 shows comparatively improved performance over ECC specimen, as shown in Figure 4.26e. The specimen SJ5 reaches its peak load at 20 mm deflection but is able to resist the considerable load upto 100 mm deflection. The observed load at 100 mm deflection is 48% of peak load and the loop area emphasises the effectiveness of HECC in preventing early slippage of embedded reinforcement from the joint and better post - yield behavior. It is noteworthy to mention that in specimen SJ5, one of the tension sides of the flexural reinforcement fails at 80 mm deflection with a load of 17.5kN and at 100mm deflection, the measured load at tension side is 13 kN. It proves the effectiveness of steel fiber reinforced hybrid composites on the ductility in specimen SJ4 with ECC in joint region. The sudden drop in load after reinforcement failure in specimen SJ4 shows the ineffectiveness of composite strength which is improved by the hybrid composite in specimen SJ5.

It is observed from the test results that there is significant improvement in the post - yield behavior of specimens with HPFRCC joint as compared to conventional specimens with and without confinement. The ductility of the specimen SJ5 (HECC) is increased more than 2 times as compared to conventional specimens as shown in Figure 4.26. The ultimate deformation of specimens with ECC is about 2 times more as compared to conventional specimens with much higher residual strength. The specimen with SFRC joint shows significant improvement in the load-deformation characteristics as compared to conventional specimens. However, the post - yield performance of SFRC is slightly lower than the specimen SJ4.

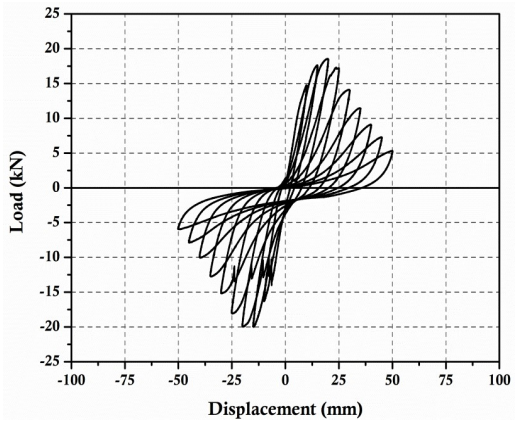

(a) SJ1-IS 456 detailing

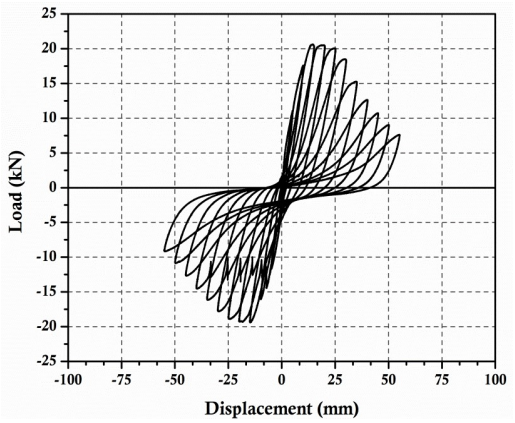

(b) SJ2-IS 13920 detailing

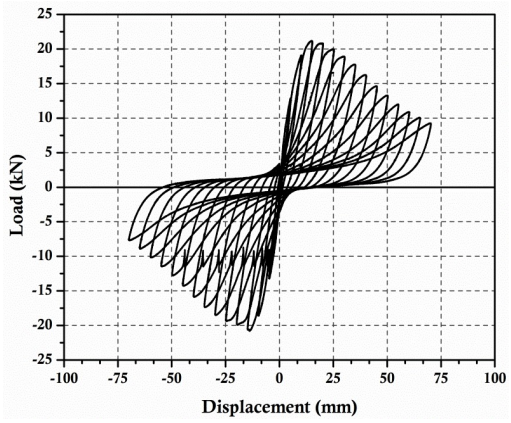

(c) SJ3-SFRC

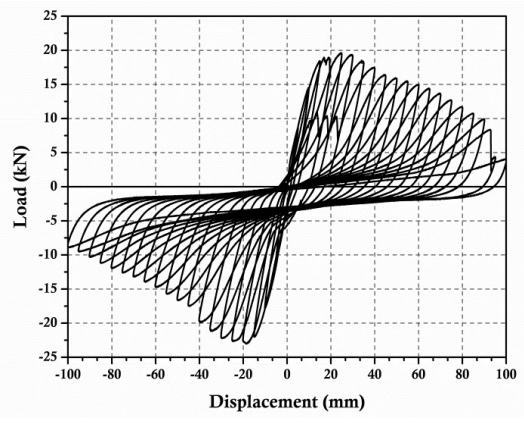

(d) SJ4-ECC

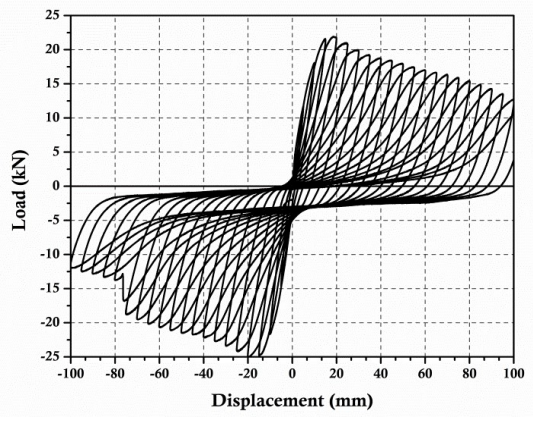

(e) SJ5-HECC

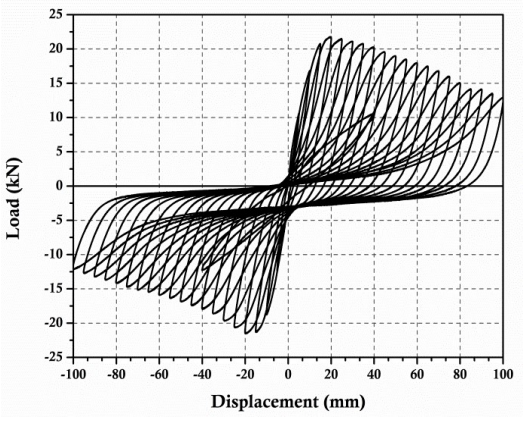

(f) SJ6-BECC

Figure 4.26: Hysteresis curves of tested specimens

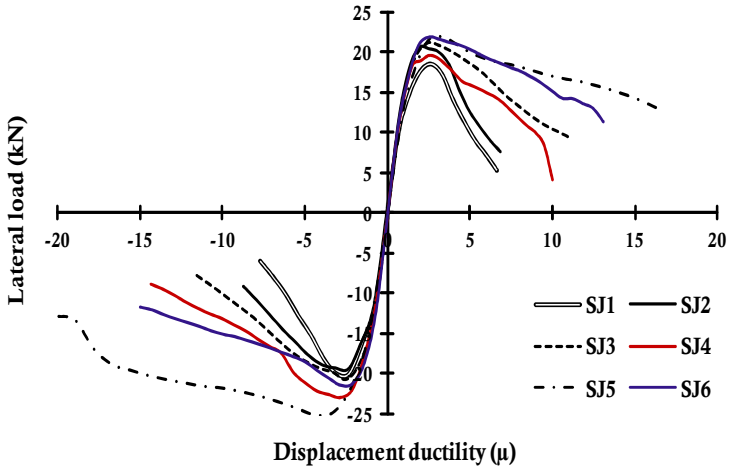

Figure 4.27: Load–displacement envelopes over ductility

4.6.3 Stiffness and Strength Degradation

Figure 4.28 and 4.29 show the strength and stiffness degradation over post elastic drift for each test specimens. The specimen SJ3 has considerably lower rate of degradation than conventional specimens SJ1 and SJ2. Figure 4.21 also shows that the loss of 90% stiffness and strength takes place at 10% drift i.e. 30% higher than conventional specimen SJ1 and SJ2. This shows that the SFRC at the joint is effective to further improve the post - yield behavior of specimen without ductile detailing.

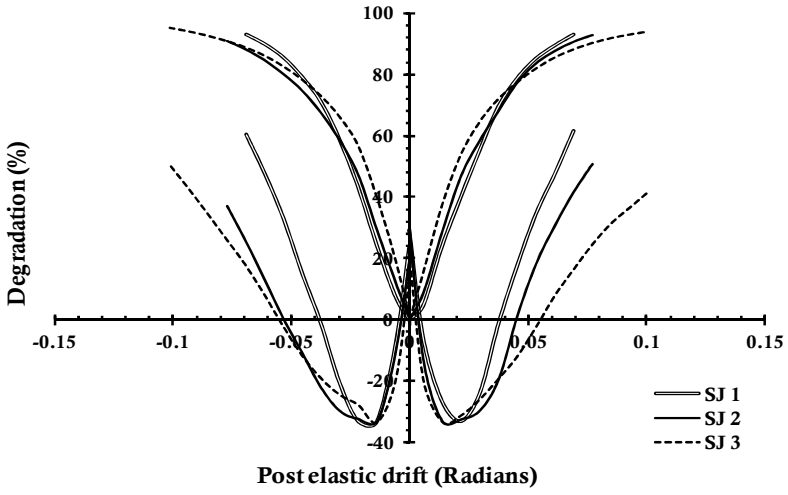

Figure 4.28: Stiffness and strength degradation over drift for SJ1-SJ3

As evident from Figure 4.28, the use of ECC at joint is more effective to reduce the rate of degradation over the same range of deformation as compared to other specimens, even specimen with SFRC in joint. Figure 4.29 also clearly demonstrates that the hybrid cementitious composites with hooked end steel fiber (HECC) have considerably higher

stiffness and higher post - yield strength as compared to other composite specimens SJ4 and SJ6. The BECC specimen SJ6 also exhibits better rate of degradation over specimen SJ4, but not as exhibited by the specimen SJ5 because of scarcity in fiber anchorage capacity. However, the entire HPFRCC specimens demonstrate more gradual and stable post - yield response as compared to conventional specimens. The ECC joint specimens lose 90% of stiffness at 15% drift and it is 1.8 times higher than the measured drift of conventional specimens. The crack resistance behavior as well as tensile strain capacity of HPFRCC specimens improves the post- yield stiffness behavior of specimen as well as in restricting the sudden loss of post - yield strength.

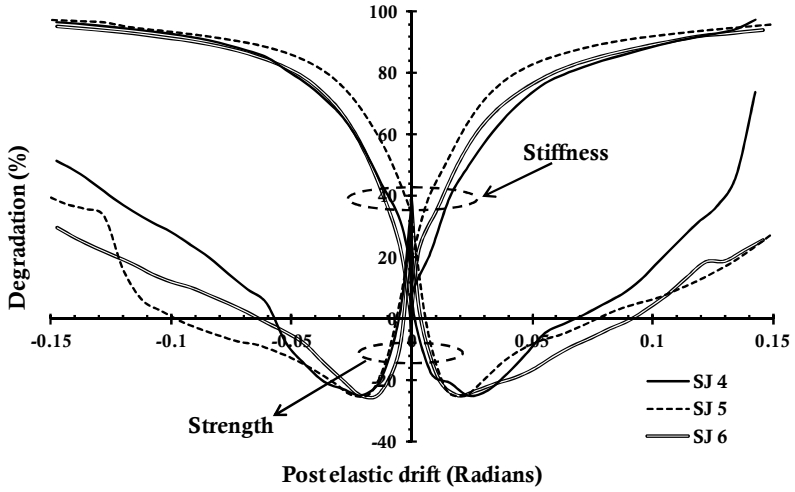

Figure 4.29: Stiffness and strength degradation over drift for SJ4, SJ5 and SJ6

4.6.4 Energy Dissipation and Damping

The relative and cumulative energy dissipation parameters for the beam-column joint specimens are plotted and shown in Figure 4.30. It is clearly evident from Figure 4.30a that the conventional joint specimens (SJ1 and SJ2) with and without confining reinforcement have low ductile performance as compared to specimens with HPFRCC. The energy dissipation in specimens with SFRC and HPFRCC i.e. (SJ3 to SJ6) is more stable and consistent without sudden change or drop. Figure 4.30a also clearly exhibits effectiveness of HECC over other HPFRCC joint specimens. The relative energy dissipation capacity after yield in ECC and BECC joint specimen i.e. SJ4 and SJ6 is comparatively lesser than HECC joint specimen SJ5. As the displacement increases after yielding, ECC joint specimens are able to sustain higher energy dissipation capacity as compared to SFRC specimen. It is evident from Figure 4.25a that ECC joint specimens have 5 times higher cumulative energy dissipation than conventional specimens. It is

evident that the average equivalent damping coefficient with conventional confinement of joint specimen is in the range of 10 to 12% and it increases upto 15-16 % in HPFRCC joint specimen. The increase in damping coefficient reflects the effectiveness of HPFRCC on ductility and load-deformation capability.

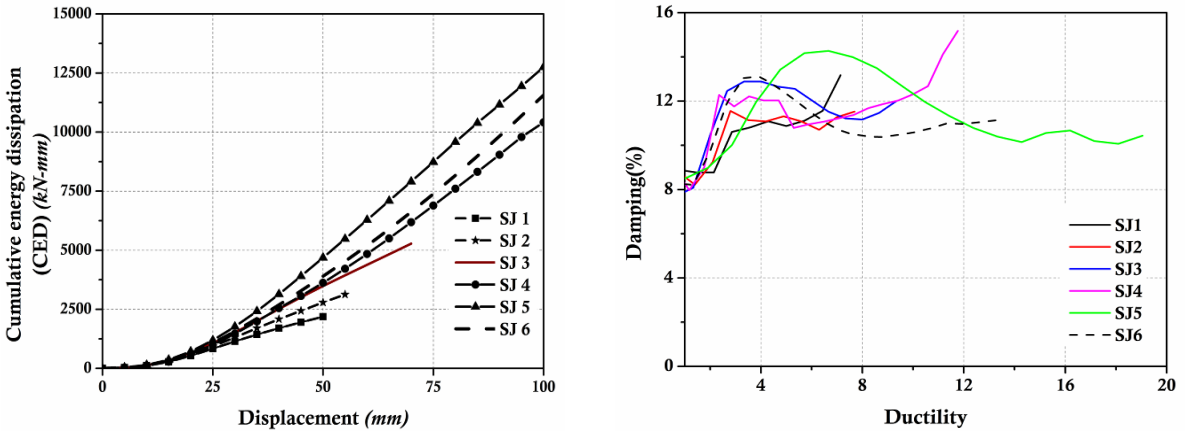

(a) Cumulative energy dissipation (b) Equivalent damping coefficient

Figure 4.30: Energy dissipation and damping coefficient of shear deficient beam-column joint with HPFRCC

4.6.5 Moment-Rotation Behavior

Figure 4.31 shows the moment - rotation *(M-Θ)* relationships of beam-column joint specimens and the values are compared with the specified values in ASCE/SEI 41-06. The maximum value of plastic rotation at yield moment is 0.02 radian and there is no significant loss of moment capacity in the post - peak range of 0.02 to 0.06 radians.

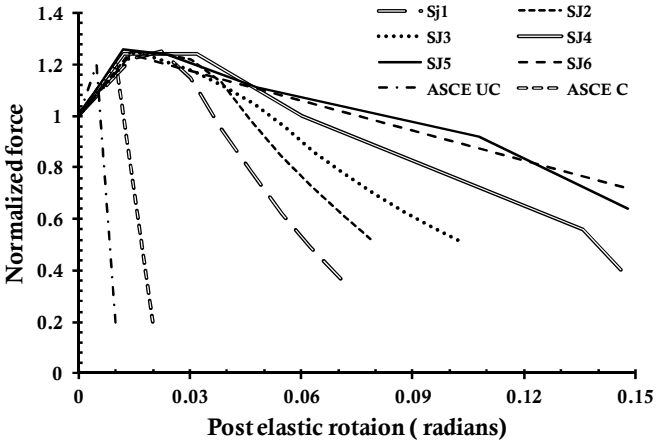

Figure 4.31: Moment-rotation behavior of test specimens

The experimentally obtained plastic rotation capacity of HPFRCC beam-column joint specimens is much higher than the specified values in ASCE/SEI 41-06. As per the

ASCE 41-06, the limit of linear elastic behavior conventional joints is 0.015 and the range of post - peak behavior is about 0.015 to 0.02 radians, as shown in Figure 4.31. The ECC joint specimen has significantly improved the *M-Θ* relationship against the conventional and SFRC joint specimens. The HPFRCC significantly increases the moment carrying capacity as well as post peak behavior of specimens. The moment carrying capacity of ECC joint (SJ 4) is considerably equal to HECC and BECC upto 0.05 radian, later the rate of moment degradation is considerably higher than the hybrid composite specimens SJ 5 and SJ6 respectively. The unique toughness property of steel fiber and its anchorage across the cracks is provided by the hooked end that supports the specimen (SJ 5) to enhance rotation capacity without significant loss in moment. The performance of BECC joint specimen SJ 6 is also able to withstand upto 0.15 radian of rotation. It is clearly understood from Figure 4.30 that steel fiber has played efficient role in maintaining the post - peak behavior even in higher transverse reinforcement spacing. The increase of rotational capacity with low rate of moment degradation represents the ductile behavior of joint which is difficult to achieve by providing the closely spaced stirrups or with SFRC in joint.

4.6.6 Damage Index

Figure 4.32 shows the damage index of shear deficient beam-column joint specimens. The conventional specimen undergoes moderate damage, severe damage and complete collapse state at the ductility level of 4, 6 and beyond 6 while SFRC joint specimen SJ3 undergoes one stage lower damage at the same level of ductility.

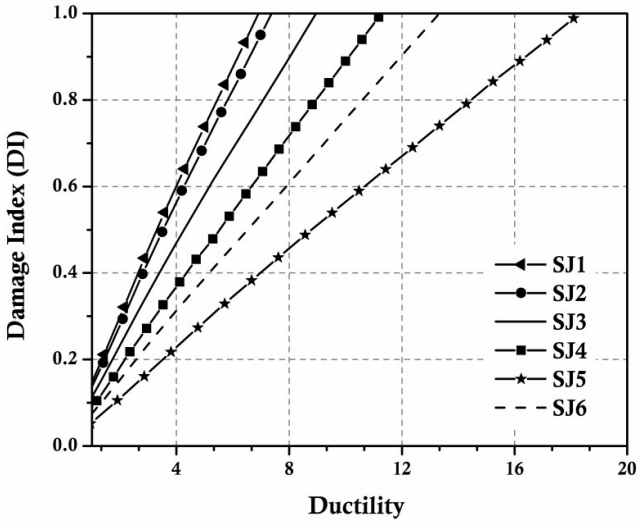

Figure 4.32: Damage index over ductility of all test specimens

The damage index plot of ECC joint specimen SJ4 validates the damage tolerance under cyclic loading over other specimens. The measured ductility at collapse stage increases

about 1.5 times than other specimens. The HECC joint specimen SJ5 reaches moderate damage at a ductility level of 11, which is about 2 times higher than the conventional specimen at complete collapse stage. It is inferred that hybrid composite specimens has 50% reduction in damage as compared to conventional and other fiber reinforced concrete joint specimens

4.7 Findings

This experimental study is focused on the static behavior of RC beams and cyclic behavior of external beam-column joints with different HPFRCC in hinge region. The objective of the study is to examine the effectiveness of different HPFRCC in improving of inelastic behavior of the structural members. The plots of load-deformation characteristics, strength and stiffness degradation, energy dissipation and equivalent damping, moment-rotation analysis, crack pattern etc are prepared to evaluate the comparative behavior of the joints. Following are the main conclusions of the study;

4.7.1 Flexural Behavior of RC Beams

1. The combination of hybrid composites improves mechanical properties and damage tolerance. The stress strain of axial compression shows 100% higher failure strain over conventional concrete and the failure pattern authenticates the crack resistance and damage tolerance of the hybrid composites under compression.
2. The flexural strength of HPFRCC specimens is 19% of its compressive strength. The post peak deflection and its rate of degradation show the efficacy of the hybrid fiber in enhancement of ductility and energy dissipation.
3. The HPFRCC enhances the moment and retards the tension reinforcement yielding by crack bridging property of fibers.
4. The tensile behavior of HPFRCC and the anchorage of hooked end fiber and crimpled fiber improve the first crack moment and yield moment effectively. This is because of the tensile strength and strain property of composites. The flexural tensile property of HPFRCC under bending shows improved post-peak strength and the ductile behavior.
5. The HPFRCC in hinge region of beam specimen shows slower rate of strength and stiffness degradation. The composite specimens show that 20% reduction in peak load capacity is observed over the post elastic drift of 0.02 to 0.07 radian. The loss of stiffness i.e. 60% to 90% occurs over the post elastic range from 0.02 to 0.08

radian. This degradation in strength and stiffness plot clearly mentions the effectiveness of HPFRCC beam specimen over the conventional specimen.

6. The crack pattern and failure mechanism of HPFRCC specimens manifest a uniform dissipation of energy with resistance for crack growth and reduced rate of crack propagation at the hinge region. This slower rate of crack propagation increases the post peak deformation without loss in strength.
7. The damage index of different composite specimens manifests that the composite with higher volume synthetic fiber has better damage tolerance capacity. The damage level of HPFRCC is much lower than the conventional beam specimen at the same ductility level. As the ductility level increases beyond 4, the conventional specimen completely collapses. At the same damage state, ECC joint specimen undergoes the ductility level of 11 whereas in hybrid composites the ductility level varies from 6-10. It may be inferred that the HPFRCC specimen becomes 1.5- 2.5 times more damage resistant as compared to conventional specimen.
8. The higher energy dissipation, slower stiffness and strength degradation, higher post elastic rotation authenticate the ductile behaviour of HPFRCC with enhanced damage tolerance capacity.

4.7.2 Cyclic Behavior of Exterior Beam-Column Joints

1. There is significant enhancement in strength of HPFRCC specimen tested under split tension compared to conventional concrete. The HPFRCC specimens have higher tensile strain over conventional concrete. The composite action of hybrid cementitious composites (hooked end steel fiber reinforced) shows two-fold increase in strength and incomparable strain over conventional and other composites. Even with the same mix ratio the hooked end steel fiber enables composites to have 50% higher compressive strength over conventional and other composites.
2. Hysteresis behavior of the HPFRCC joint specimens shows that there is a significant improvement in the pre and post- peak behavior of external beam-column joint specimen under cyclic loading. This improvement is not only in the form of increase in resisting the peak load but also stabilizes the post -peak behavior with gradual loss of strength and stiffness. The hysteresis performance of hybrid composite BECC, CECC and HECC joint specimen shows remarkable improvement as compared to conventionally confined joint specimens. Hybrid

cementitious composites may be an effective alternative possibility to enhance the performance of shear deficient seismic joint of the building under earthquake loading.

3. The load-deformation envelop curve of HPFRCC joint specimens reveals major impact on the post-yield behavior than pre-yield load-deformation characteristics. The ductility and post-yield deformation capacity of BECC, CECC, and HECC joint specimens are approximately 2 times greater as compared to confined joint specimens. The other types of HPFRCC joint specimens are also able to improve the post-yield behavior of the joint with varying effectiveness.
4. The strength and stiffness degradation plot of conventionally confined joint specimen as well as SFRC joint specimen show that the peak load is about 1.4 times the yield load over the post elastic drift of 0.02 rad. After attaining the peak load, reduction of 40% load capacity is observed as the post elastic drift increases from 0.02 to 0.05 radians in conventional specimens. However, the same loss in load carrying capacity of SFRC joint specimen is also observed over the post elastic drift of 0.02 to 0.05. There is a sharp reduction in load capacity of the joint specimens beyond the post elastic drift of 0.05 rad. There is 60% reduction in yield load as the post elastic drift increases from 0.05 to 0.08 rad. There is a very sharp reduction in the stiffness and the specimen loses 80% of stiffness over the post elastic drift of 0.08 radian. However, this reduction is slightly gradual in case of SFRC joint specimen.
5. The strength and stiffness degradation plot of HPFRCC joint specimen shows that the joints reach at peak load (= 1.2 times the yield load) over the post elastic drift of about 0.02 radian and further 20% reduction in peak load capacity is observed over the post elastic drift of 0.02 to 0.05 radian. The specimens further lose in load capacity (= 0.4 times of yield load) over the post elastic drift of 0.05 to 0.15 radian. Similarly, the loss of stiffness i.e. 0 to 80% occurs over the post elastic range from 0.02 to 0.05 radian and after that there is a gradual loss of strength from 80 to 90 % over the post - yield 0.05 to 0.15 radian. The plot clearly mentions the effectiveness of ECC joint specimen over the conventionally confined specimens as well as SFRC joint specimen.
6. The hysteresis damping of HPFRCC joint specimens varies from 8 to 15 % as the yielding increases. The hysteresis damping of joint specimen SJ5 increases to 15% at the ductility level of about 6 and gradual loss in hysteresis damping coefficient is

noticed as the ductility increases from 6 to18. However, in other HPFRCC specimens the pattern of variation of hysteresis damping is nearly the same but over a low range of ductility level. The conventional and confined specimens have a variation in hysteresis damping from 8 to 12% over the maximum ductility of 8.

7. The post elastic rotation modelling parameter ‘b or a” for HPFRCC joint specimens is higher than the conventional and confined beam-column joints as well as values prescribed in ASCE/SEI 41-06. The value of non-linear modelling parameter “b or a**”** as per ASCE/SEI 41-06 for the exterior beam-column joint for non-confirming ‘NC’ (unconfined) conforming ‘C’ (confined) lies between 0.015 – 0.02 while the same value for HPFRCC joint specimens varies between .02 to 0.06 radian. The value of residual strength parameter ‘c’ as per ASCE/SEI 41-06 is about 0.2 for the deformation of 0.015 – 0.02 for the unconfined and confined specimens. The value of parameter ‘c’ for HPFRCC specimen is about 0.5 to 0.8 over the post-elastic range of 0.09 to 0.15 depending on the type of HPFRCC.
8. The crack pattern and failure mechanism of HPFRCC joint specimens manifest a uniform dissipation of energy with wide spread cracks at the joint. It forms a horizontal crack at the junction of beam-column joint along with minor cross diagonal shear cracking which intensifies as the deformation increases.

References

Afsin, C. B., Gustavo, J. P. and James, K. W., (2004), "Behavior of precast high-performance fiber reinforced cement composite coupling beams under large displacement reversals," *13th World Conference on Earthquake Engineering*, Vancouver, B.C., Canada, 2004.

ASCE/SEI 41-06 (2007), "Seismic rehabilitation of existing buildings," American Society of Civil Engineers, Reston, USA, 2007.

Fang, Y., Jinlong, P., Luoting, D., and Leung, C. K. Y., (2014), " Mechanical behaviors of steel reinforced ECC or ECC/concrete composite beams under reversed cyclic loading," *Journal of Materials in Civil Engineering.*

Giovanni, M., Alberto, M., Giovanni, A. P., Zila, R., (2010), "Strengthening and repair of RC beams with fiber reinforced concrete," *Cement and Concrete Composites,* 32,731-739.

Gregor, F., Hiroshi, F., and Victor, C. L., (2002), "Effect of matrix ductility on the performance of reinforced ECC column under reverse cyclic loading condition," *Proceedings of JCI International Workshop on Ductile Fiber Reinforced Cementitious Composites—Application and Evaluation*, 269–278.

Gregor, F., and Victor, C. L., (2003), "Intrinsic response conventional of moment-resisting frames utilizing advanced composite materials and structural elements," *ACI Structural Journal*, 100(2), 166–176.

Hiroshi, F., Yukihiro, S., Victor, C, L., Yasuhiro, M., and Hirozo, M., (2000), "Ductile engineered cementitious composite elements for seismic structural application," *World Conference on Earthquake Engineering ,New Zealand,* Paper no. 1672.

Maalej, M., and Victor, C, L., (1995), "Introduction of strain hardening engineered cementitious composites in design of reinforced concrete flexural members for improved durability," *ACI Structural Journal*, 92(2), 167-176.

Maalej, M., and Leong, K.S., (2005), "Engineered cementitious composites or effective frp-strengthening of RC beams," *Composites Science and Technology,* 65, 1120–1128.

Maalej, M., Quek, S.T., and Zhang, J., (2005), "Behavior of hybrid-fiber engineered cementitious composites subjected to dynamic tensile loading and projectile impact," *Journal of Materials in Civil Engineering*, 17(2), 143-152.

Maalej, M., Lin, V. W. J., Nguyen, M.P., and Quek, S.T., (2010), "Engineered cementitious composites for effective strengthening of unreinforced masonry walls," *Engineering Structures*, 32(8),2432-2439.

Maalej, M., Quek, S.T., Ahmed, S.F.U., Zhang, J., Lin, V. W. J., and Leong, K. S., (2012), "Review of potential structural applications of hybrid fiber engineered cementitious composites," *Construction and Building Materials*, 36(11), 216–227.

Park, Y. J., Ang, A. H. S. and Wen, Y. K., (1987), "Damage limiting aseismic design of buildings," *Earthquake. Spectra*, 3, 1-26.

Patodi, S. C., and Rathod, J. D., (2008), "Response of engineered cementitious composites with steel reinforcement and concrete in moment resisting frames," *New Building Materials in Construction World*, 13 (12), 232–242.

Raymond, R., Foltz., Jesse, M. G., and James, M. L., (2008), "Behavior of high-performance fiber-reinforced cementitious composites for RC coupling beams in earthquake-resistant structural wall systems," *The 14 the World Conference on Earthquake Engineering, Beijing, China.*

Roufaiel, M., and Meyer, C., (1987), "Analytical modeling of hysteretic behavior of R/C frames," *Journal of Structural Engineering,* 113(3), 429–444.

Sameer, H., Taher, A., Toney, C., (2010), "Deflection behavior of concrete beams reinforced with PVA micro-fibers," *Construction and Building Materials,* 24, 2285–2293.

Shannag, M. J., Barakat, S., and Abdul, K. M., (2002), "Cyclic behavior of HPFRCC repaired interior beam-column joints," *Materials and Structures*, 35,348–356.

Shannag, M. J., Nabeela, A.D., and Ghazi, A.F., (2005), "Lateral load response of high performance fiber reinforced concrete beam–column joints," *Construction and Building Materials*, 19,500–508.

Sun,W., Kim., Hyun, D., and Yun., (2011), "Crack-damage mitigation and flexural behavior of flexure-dominant reinforced concrete beams repaired with strain-hardening cement-based composite," *Composites: Part B,* 42,645–656.

Victor, C. L., (1993), "From micromechanics to structural engineering the design of cementitious composites for civil engineering applications," *JSCE Journal of Structural Mechanics and Earthquake Engineering,* 10, 37-48.

Victor, C. L., Mishra, D. K., Naaman, A. E., Wight, J. K., LaFave, J. M., Wu, H. C., and Inada, Y., (1994), "On the shear behavior of engineered cementitious composites," *Journal of Advanced Cementitious Based Materials,*1 (3),142–149.

Victor, C. L., and Tetsushi, K., (1998), "Engineered cementitious composites for structural applications," *ASCE Journal of Materials in Civil Engineering*, 10, 66-69.

Chapter 5

Cyclic Performance Evaluation of SIFCON Core Enabled Beam-column Joint Specimens

5.1 Introduction

Slurry In-Filtrated CONcrete (SIFCON) is categorized as a High Performance Fiber Reinforced Cementitious Composite (HPFRCC). SIFCON is a composite made by using high volume of steel fiber fraction, V_f (volumetric percent of fibers) with low viscosity cement based slurry binder. Higher volume steel fibers (5% to 30%) are used without coarse aggregate in SIFCON preparation (Homrich et al. 1987; Naaman et al. 1991). In SIFCON, fibers are preplaced in the frame work with proper orientation and low viscosity cement rich fine slurry is poured or pumped into the forms with optimum pressure. This SIFCON composite possesses high strength and ductility to resist dynamic loads (Schneider et al. 1989). The strength and ductile property of SIFCON composite is mainly based on five parameters namely (a) strength of cement based slurry binder, (b) volume of fiber, (c) orientation of fiber aligned normal to loading or parallel to loading, (d) type of fiber and (e) a leak proof form work. The economical strategy restricts the application of SIFCON within the critical region of structures. Precast SIFCON element may be an efficient way to be used in cast-in-place concrete structure at the critical region such as beam-column joint that eliminates the execution problem. The precast SIFCON is a composite made with 8% steel fiber by volume with low viscosity cement and mineral admixtures based slurry binder. In the present study, the pre and post yield behavior of beam-column joints with precast SIFCON core elements is evaluated under cyclic loading. The hysteresis behaviour of the SIFCON enabled beam-column joints is compared with conventionally confined joints on the basis of shear strength behavior, failure pattern and energy dissipation.

5.2 Early Studies

Lankard (1984) studied the potential benefits of SIFCON in structural applications. Balaguru et al. (1987) examined the mechanical properties of SIFCON and concluded that the SIFCON was ductile in compression, tension and flexure. Naaman et al. (1987) studied

the SIFCON connections for seismic resistant frames using precast and pre-stress technique and observed better damage tolerance and failure away from the face of column in joint frame. Mondragon (1988) studied the flexural properties of SIFCON. Naaman et al. (1989) examined the tensile stress-strain behavior of SIFCON using different volumes of steel fibers and observed tensile strength ranging from 11 to 16MPa with 1 to 2% strain. Schneider et al. (1989) reported bridge deck design and slab designing with SIFCON. Due to high strength, toughness, and ability to resist penetration by fragments and ballistics, SIFCON was an ideal material for building new hardened military structures, or for economically upgrading existing facilities. Parameshwaran et al. (1990) studied the behaviour of 6-8% volume fiber cement mortar in flexure and observed 5 time's higher flexural strength and greater ductility over plain concrete and ferrocement specimens. Naaman et al. (1991) examined the elastic modulus of SIFCON in tension and compression and achieved tensile strength over 35MPa and elastic modulus of 35GPa using 12 to 27% fiber volume. Naaman et al. (1992) investigated the influence of SIFCON matrix in R.C beams and observed better ductility and energy dissipation. He noticed smaller crack width in the flexural region and suggested improvement in the behavior of tension and compression zone reinforcement. Wang et al. (1994) studied the shear behavior of SIFCON using cylinder under torsion and beams under two point loading. The test results showed that the torsion test provided a reliable lower-bound shear strength that may be used for design purposes. The fiber size and specimen diameter had a greater effect on results. The size of cored-cylinder SIFCON specimens for torsion tests should be at least three times the fiber length to ensure consistent results. Naaman et al. (1995) examined shear response of dowel reinforced SIFCON and observed better energy dissipation with 400% peak shear slip. Thirugnanam et al. (2000) studied the influence of SIFCON composite in the beam-column joint of RC frames under cyclic loading and observed enhanced energy dissipation and ductility over the conventional RC frame. Mohammed et al. (2009) studied the use of SIFCON in RC corner joint connection and observed increased joint efficiency and ductility.

5.3 Mechanical Properties of SIFCON under Compression and Flexure

The physical properties of conventional concrete and SIFCON composites are examined using standard cylindrical and prism specimens under static loading.

5.3.1 Stress-Strain Behaviour of SIFCON Composite under Compression

In order to study the performance difference between steel fiber reinforced concrete (SFRC) and SIFCON, SFRC with 2% steel fibers was prepared and tested. The water cement ratio was kept as 0.45 with 1% super plasticizer to increase the workability.

The mix ratio of SIFCON composite and details of conventional concrete mix ratio are summarized in Table 5.1.

Table 5.1: Matrix for SIFCON compositions under compression and flexure

Composites ID	Cement	Sand	C.A	Steel Fiber %	S.W*	S.F*	Compressive strength (MPa)	Flexural strength MPa
Control	1	1.45	2.25	-	-	-	27	4.5
SFRC	1	1.35	2.20	2	-	-	35	-
SIFCON	1	0.7	-	8	0.1	0.1	56	31-36

Note: C.A- Coarse aggregate; S.W-Steel Wool; S.F: Silica Fume.

Hooked end steel fiber with an aspect ratio (*l/d*) of 60 with 8% of volume fraction (V_f) was used in preparation of SIFCON core elements. To estimate the compressive strength of SIFCON composites, cylindrical specimens of size 100×200 mm were cast and tested under compression. Three LVDTs were used with a gauge length of 100 mm to measure the strain under compression. The average compressive strength of SIFCON composite was 56 MPa.

Figure 5.1 shows the stress-strain behaviour of SIFCON composite with 8% of volume of steel fiber fraction, V_f. The addition of discrete steel fiber in the concrete (SFRC) improves strength and post peak strain as compared to conventional concrete. It can be understood from Figure 5.1 that the presence of steel fiber shows strain softening behavior whereas the conventional concrete fails abruptly after peak in complete brittle mode. The fibers in SFRC specimen restrict spalling of concrete and allow the volumetric enlargement during post peak degradation. Figure 5.2b shows the failure pattern of SFRC specimen under compression. The stress-strain behavior of SIFCON composite is also in contrast to the response of conventional and SFRC concrete. The absence of coarse aggregate and the presence of high volume steel fiber (V_f) show strain hardening behavior with enhanced strength and ductility. After attaining the peak load, the strength of

conventional concrete and SFRC degrades whereas SIFCON increases with huge volumetric enlargement as shown in Figure 5.2.

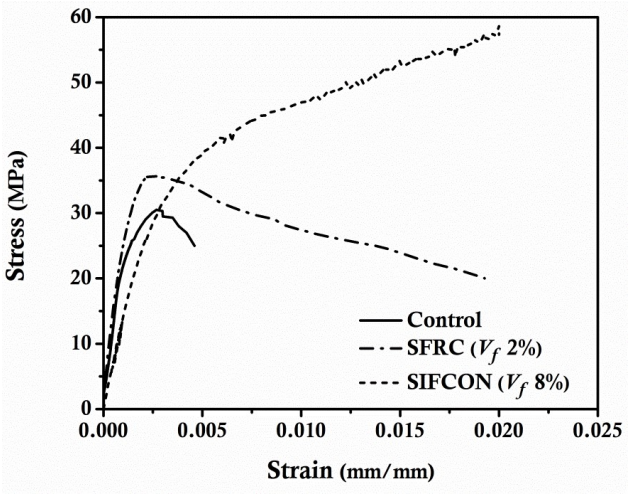

Figure 5.1: Stress-strain curve under compression of SIFCON composite, SFRC and convention concrete

(a) Conventional concrete (b) SFRC (c) SIFCON

Figure 5.2: Failure pattern under compression of SIFCON composite, SFRC and conventional concrete

5.3.2 Flexural Behaviour of SIFCON Composite

The flexural strength of conventional concrete and SIFCON composite are evaluated by preparing a standard prism of size 100 × 100 × 500 mm and tested under two point loading. A weld mesh is also used in SIFCON core preparation for fiber alignment and for the perfect fiber orientation. This flexural study is carried out on three types of specimens such as conventional specimen (F0), SIFCON (V_f -8%) specimen (F1) and SIFCON with three weld mesh layers (F2). The specimens are tested after 28 days of curing under two point static loading.

After initial crack, conventional concrete specimen encounter sudden failure with a maximum flexural strength of 4.5 MPa. The higher volume of steel fiber and bridging effect of hooked end steel fiber in SIFCON composite resist the applied load without any sudden degradation to a higher extent as shown in Figure 5.3. The response of SIFCON specimen with weld mesh is similar to the specimen F1 without mesh but shows quite enhanced strength. The observed flexural strength is seven times higher than the conventional concrete. Failure pattern of flexural specimen is shown in Figure 5.4.

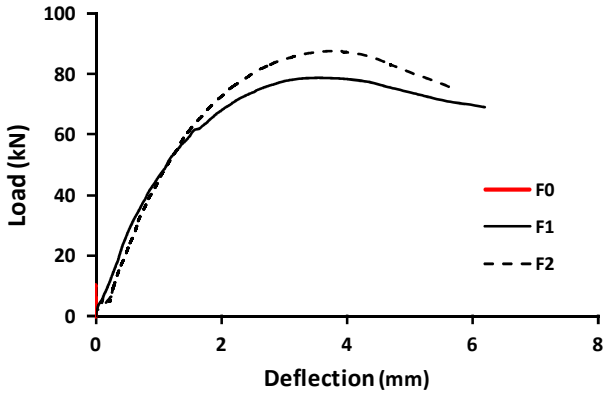

Figure 5.3: Load-deflection behavior of SIFCON specimens under flexure

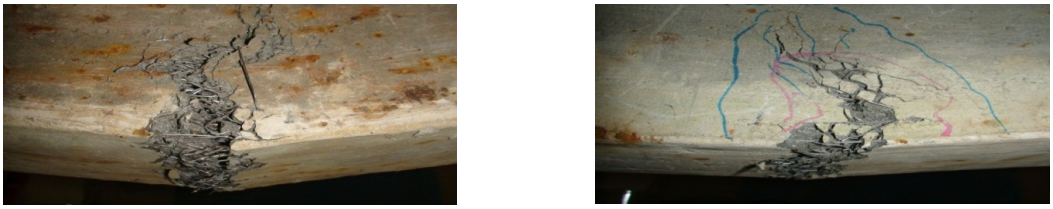

(a) SIFCON (b) SIFCON with mesh

Figure 5.4: Failure pattern of SIFCON specimens under flexure

5.4 Cyclic Behaviour of Beam- Column Joints with and without SIFCON Core Element

The test program consisting of six full scale exterior beam-column joint specimens is constructed with and without SIFCON inner core element. This SIFCON core is a precast unit with a cross section of 150mm×150mm. The cross section details of SIFCON core are one half of actual cross section of beam-column joint specimen. The shape of the core element resembles the exterior joint as shown in Figure 5.5. The length of core element is as per the plastic hinge length as given in IS 13920:1993. In SIFCON core preparation 8% steel fibers with weld mesh as fiber aligner are used. In core preparation fibers are placed layer by layer with cement slurry to avoid slurry infiltration problem and to eliminate the voids. The weld mesh perfectly helps to keep the fibers in the desired

direction. The procedure for inserting the core in beam-column joint is shown in Figure 5.5. A pre-hole is made in the core during construction of core element to insert the beam longitudinal bar anchorage length and is carefully placed into the reinforcement cage. The core surface is rubbed with steel wire brush before placing the core inside the reinforcement gauge and a polymer based cement slurry coating is applied to create a better bond between the precast core and the cast-in-situ concrete during casting. Two types of specimens are prepared and tested under cyclic loading i.e. (a) flexure specimens detailed as per Indian Standard code consisting of four specimens and (b) shear deficient specimens consisting of two specimens. The complete details of beam-column joint specimens with and without SIFCON core element under cyclic testing are summarized in Table 5.2. Figure 5.6 shows the detailed configuration of all beam-column joint specimens. The joint specimens are tested under cyclic loading using automated hydraulic actuator under displacement control with an interval of 5mm as shown in Figure 5.7.

Figure 5.5: Construction technique of SIFCON core enable specimen

Table 5.2: Details of beam-column joint specimens with and without SIFCON core

Sp.ID	Reinforcement Ast %		Reinforcement details (Fe 500 grade)		Shear reinforcement detailing (Fe 500 grade)	Description
	Beam	Column	Beam	Column		
Type I						
SP1	0.31	0.7	3# 10mmØ @top and bottom	2# 20mmØ @top and bottom	Unconfined	Conventional specimen - I
SP2	0.31	0.7			Confined	Conventional specimen - II
SP3	0.31	0.7			Unconfined	SIFCON Core enabled - I
SP4	0.31	0.7			Confined	SIFCON Core enabled - II
	Type II		2# 20mmØ @top and bottom			
SP5	0.83	0.7			Unconfined	Conventional specimen - III
SP6	0.83	0.7			Unconfined	SIFCON Core enabled - III

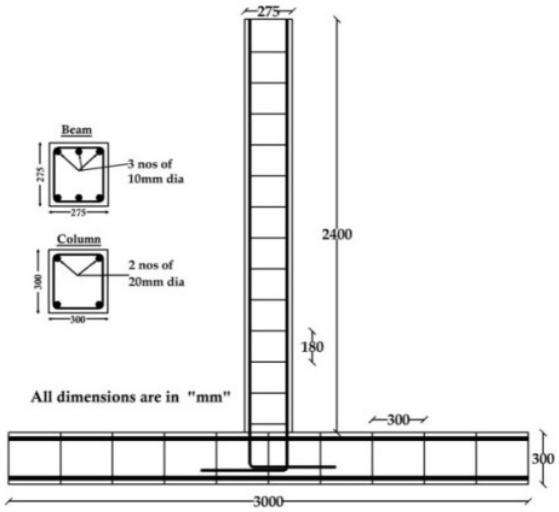

(a) SP1- IS 456:2000 detailing

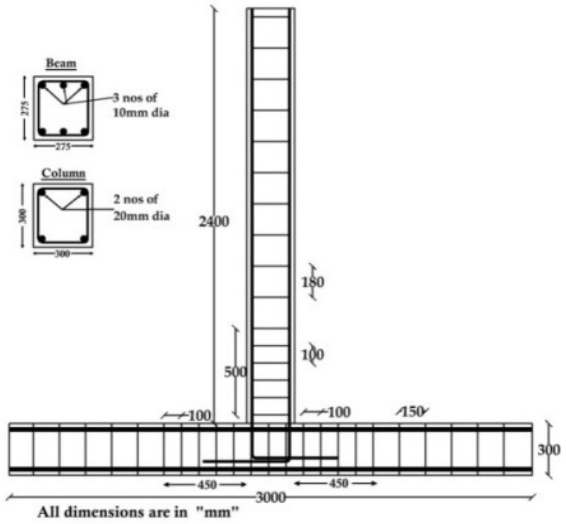

(b) SP2- IS13920:1993 detailing

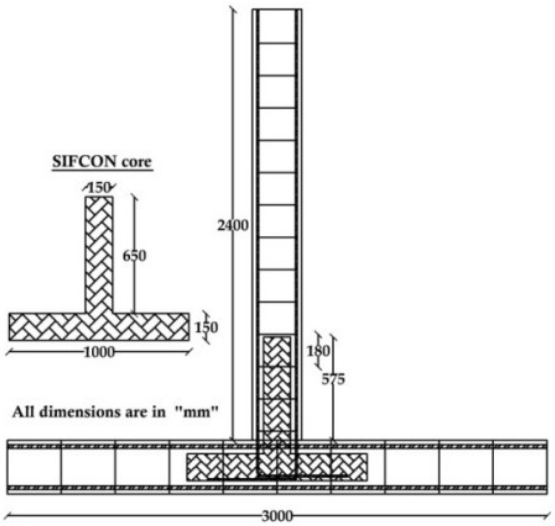

(c) SP3- SIFCON Core + IS 456 detailing

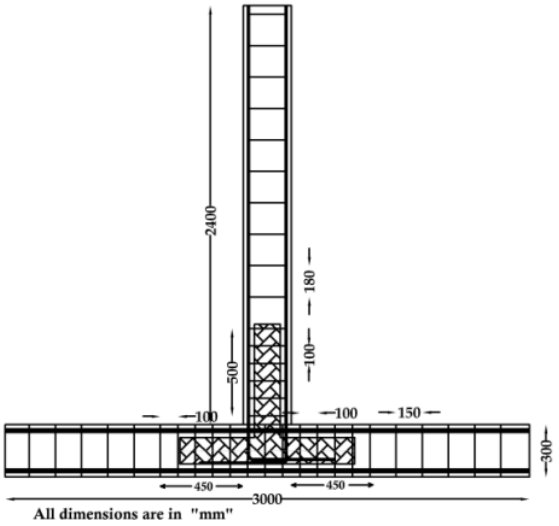

(d) SP4- SIFCON Core + IS 13920 detailing

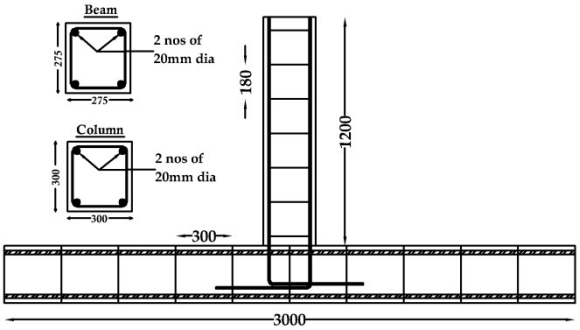

(e) SP5- IS 456:2000 detailing

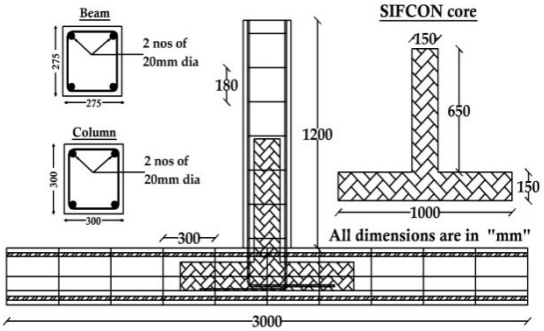

(f) SP6- SIFCON Core + IS 456 detailing

.

Figure 5.6: Cross section and reinforcement details of Type I and Type II specimens

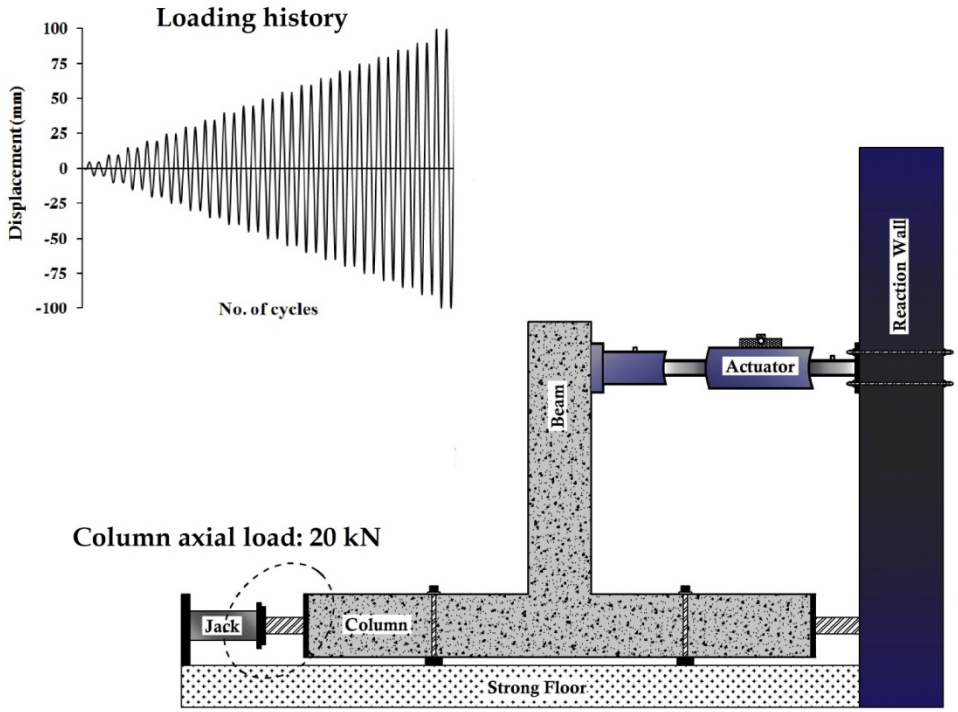

Figure 5.7: Test set-up for beam-column joint specimens and loading history

5.4.1 Cracking Behavior and Failure Analysis

The yielding of reinforcement is observed in both the unconfined and confined conventional beam-column joint specimens SP1 and SP2 along with numerous flexural and shear cracks at the joint region as shown in Figure 5.8a and 5.8b. These cracks are noticed after a displacement of 50 mm which widen as the displacement reaches 90mm. The specimen SP1 fails by yielding of longitudinal reinforcement. In case of confined specimen SP2, flexural cracks are noticed in the joint region with a few inclined shear cracks and the beam transfers the load beyond 90mm displacement as a result of ductile detailing.

The failure pattern of SIFCON core enabled beam-column joint specimens is completely different from the conventional specimens. The confinement plays a vital role in failure pattern of core enabled specimen. In SIFCON core specimens SP3 and SP4, the cracking behavior remains the same upto 80 mm displacement and afterwards the crack in the beam at the end of the core element propagates differently. This crack widening at the end of core in beam hinge region decides further performance of the joint. As the deflection increases beyond 80mm in specimen SP3, spalling of concrete cover takes place and subsequently buckling of longitudinal reinforcement occurs at 90mm displacement as shown in Figure 5.9a.

(a) SP 1 (b) SP 2 (c) SP 3 (d) SP 4

Conventional specimen I Conventional specimen II SIFCON Core enabled I SIFCON Core enabled II

Figure 5.8: Cracking behavior of Type 1 specimens

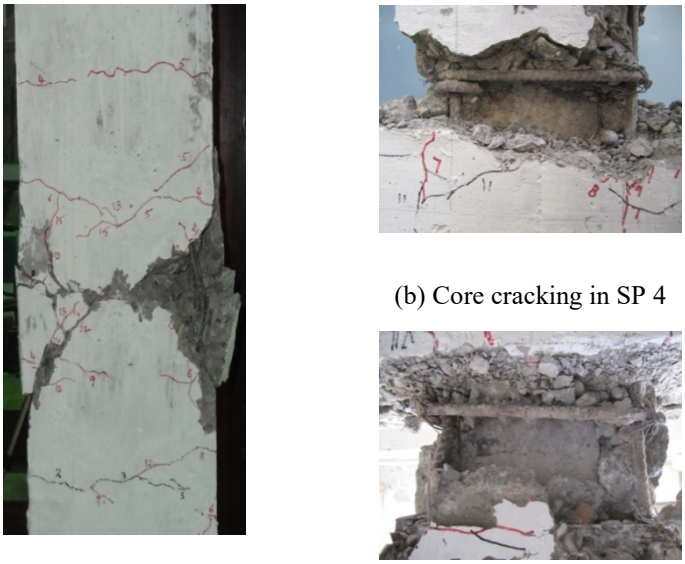

(a) Beam bar buckling in SP3

(b) Core cracking in SP 4

(c) Reinforcement buckling in connection SP4

Figure 5.9: Cracking behavior of SIFCON core enable specimen SP4

The buckling of longitudinal bar in beam hinge region restricts further load transfer to the joint after 110 mm deflection. Finally, failure occurs in beam of the SIFCON core enabled joint specimen SP3 at plastic hinge region rather than at joint. Another SIFCON core enabled joint specimen SP4 also experiences similar type of cracking behavior as specimen SP3 with dense flexural cracks in plastic hinge region of beam as shown in Figure 5.8d. There is no buckling of longitudinal reinforcement in plastic hinge region of

beam as in case of specimen SP3. At 50 mm deflection, the crack near the end of the core region widens, but the additional confinement in specimen restricts buckling of reinforcement and allows the beam to rotate. This large rotation leads to crack formation in the SIFCON core and the joint rotates to a higher extent. After 100 mm deflection, the cracks develop and widen in core along the pushing direction with increase in deflection. The cracking behavior of core in pushing direction is in contrast with pulling direction and there is no cracking in pulling direction. It shows crack growth in onset direction and does not propagate in opposite direction. This cracking behavior buckles the reinforcement near connection region as shown in Figure 5.9c.

In Type 2, shear type joint specimens SP5 and SP6, initially a few flexural cracks are noticed in beam portion but finally the occurrence of diagonal cracks in the joint region severely reflects on the post yield behavior. The inclined cracks in joint region of specimen SP5 widen after 20mm deflection and lead the concrete cover spalling to an early stage. As the displacement increases, the reinforcement loses the contact with the concrete surface and finally joint collapses as shown in Figure 5.10. The specimen SP6 experiences extensive flexural cracks as depicted in Figure 5.11. It shows that the core mechanism restricts the occurrence of early inclined cracks by allowing numerous flexural cracks in the hinge region. Inclined cracks in joint region are noticed at 30mm deflection, but the spalling of concrete in joint region occurs.

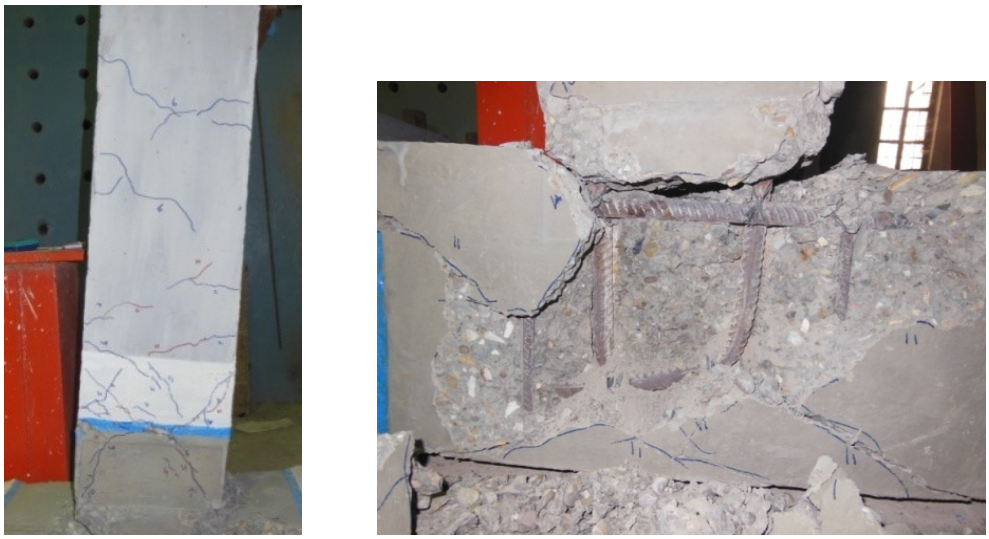

(a) Flexural cracks in beam (b) Joint shear failure and beam–column connection failure

Figure 5.10: Failure pattern of specimen SP5

(a) Shear cracks widening (b) Joint concrete cover failure

Figure 5.11: Cracking and failure behavior of Type-II joint specimen SP6

At failure stage, the concrete in the joint is completely crushed and the core fails near the joint connection region. The vertical member of the core connects the top and bottom portions of column as shown in Figure 5.11b and remains active in transferring the load. There is no evidence of failure or cracking of core in the column and in beam region except the connection failure. Figure 5.10b shows the dislocation of longitudinal rebar due to the larger deflection whereas in Figure 5.11b the nonexistence of rebar dislocation is due to large deflection at failure. It demonstrates the efficacy of the core in resisting the shear and supporting the reinforcement performance.

5.4.2 Hysteresis Behavior

Figure 5.12 shows the hysteresis behavior of all the tested beam-column joint specimens. The adequate confinement in the plastic hinge region of joint in specimen SP2 shows increased load and deformation over unconfined specimen SP1. In specimen SP2, the yielding starts at 30mm deflection and corresponding lateral load of 14kN remains nearly constant upto a deflection of 110 mm against 90 mm deflection in specimen SP1.

In SIFCON core enabled specimen SP3, yielding occurs at approximately 40 mm displacement and corresponding load is 20kN that continues upto 80mm deflection without any significant degradation. The crack widening in the beam hinge region has significant influence on the post elastic behavior of specimen SP3 that can be understood from the hysteretic curve shown in Figure 5.12c. In reference to specimen SP1 and SP2, the longitudinal reinforcement yields and joint connection fails after 80mm deflection with flexural cracks in beam hinge region. The ductile detailing in plastic hinge region of

specimen SP4 demonstrates different nonlinear behavior than SP3. The linear portion of both the specimens is likely to be the same but the confinement plays vital role in non linear range. The specimen SP4 develops anticipated primary crack near the end of core in beam section where specimen SP3 encounters failure.

Figure 5.6d shows consistent load carrying capacity of specimen SP 4 upto 100mm in both positive and negative sides. Later the rate of load degradation is relatively faster than positive loading. The observed load at 140mm deflection in "+" ive side is 14kN while in "-"ive side is 7.5kN. At the negative side, load degradation is quite higher than the positive push because of rebar buckling in the connection region as shown in Figure 5.9c. Generally in SIFCON, the high volume steel fiber restricts uniform crack opening at twin sides and hence crack opening continues on the onset cracking direction though under cyclic loading it restricts the rotation of core and encourages the reinforcement buckling near the connection location in opposite direction. This reinforcement buckling has remarkable influence on the rate of load degradation in post yield range.

The shear deficient Type II conventional specimen SP5 shows sudden post yield load degradation after reaching peak load at 20mm deflection. Figure 5.13 shows that there is no gain in load after 20mm deflection. The hysteretic loop of specimen with core SP6 shows diverse behavior over specimen SP5. The specimen attains peak load at 30mm deflection and remains the same upto 45 mm deflection. At 60mm deflection the measured load is more than 50% of its maximum load. The difference can be understood from the load envelope curve shown in Figure 5.13b.

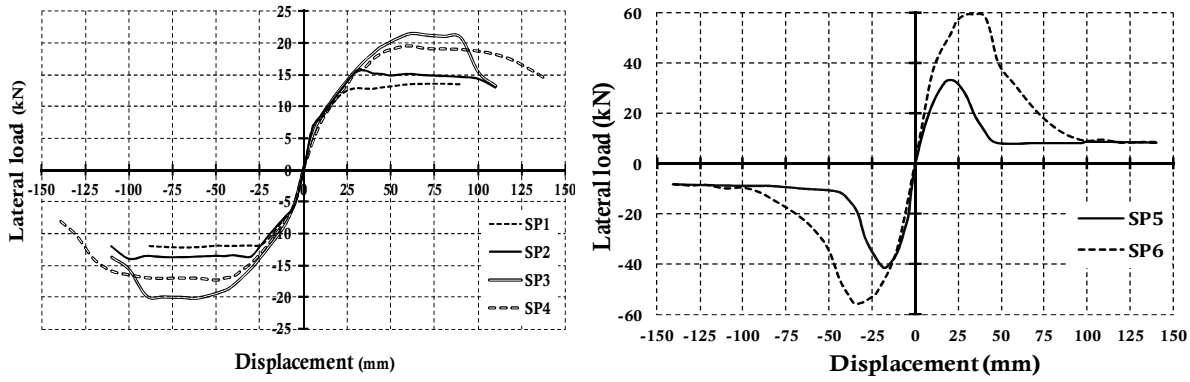

(a) Type I - Flexure (b) Type II - Shear deficient

Figure 5.13: Load-deflection envelope curves of tested beam-column joint specimens

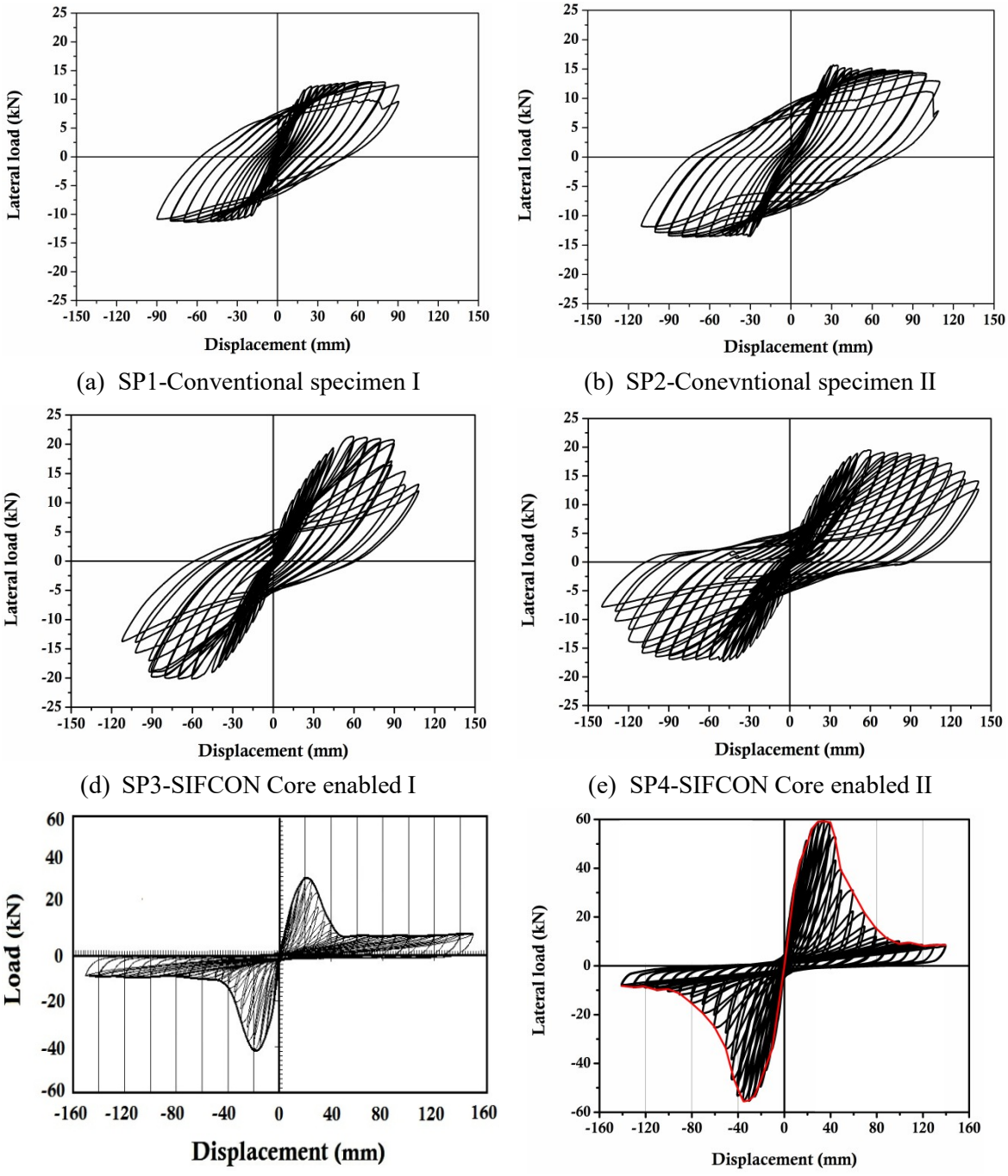

(a) SP1-Conventional specimen I

(b) SP2-Conevntional specimen II

(d) SP3-SIFCON Core enabled I

(e) SP4-SIFCON Core enabled II

(e) SP5-Conventional specimen III

(f) SP6-SIFCON Core enabled III

Figure 5.12: Hysteretic curve of all test specimens

5.4.3 Strength and Stiffness Degradation

The inelastic performances of joint specimens are measured using the rate of change in strength and stiffness degradation over the post-elastic range. Figure 5.14 and 5.15 show the strength and stiffness degradation over post elastic drift of all the tested specimens. In specimen SP1, nearly 50% degradation reaches at the rotation of 0.01 radian while 70% degradation at 0.02 radian and finally the specimen fails at 0.03 radian. The conventional

specimen SP2 shows lower rate of degradation and large drift over specimen SP1. The maximum 80% stiffness degradation reaches at 0.035 radian and afterwards sudden failure is observed with the yielding of longitudinal reinforcement. The SIFCON core enabled specimens SP3 and SP4 show lower rate of degradation over conventional specimens SP1 and SP2.

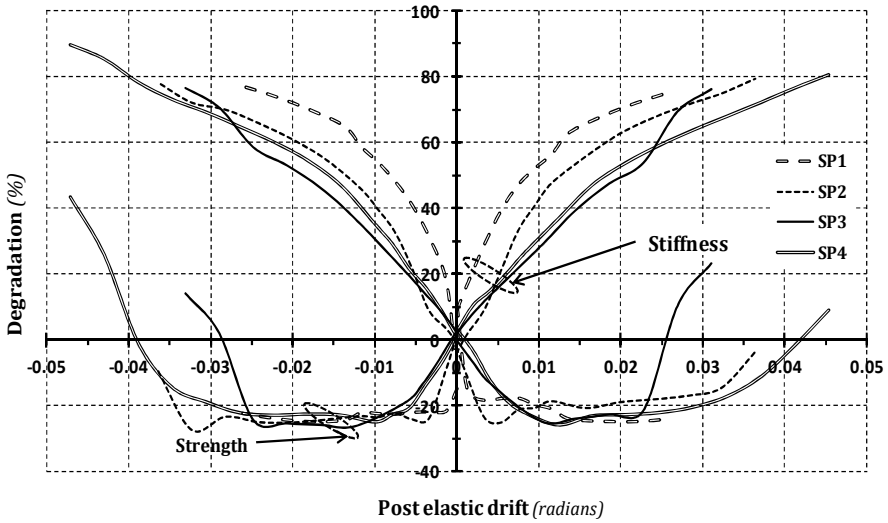

Figure 5.14: Stiffness and strength degradation plot of Type I specimens

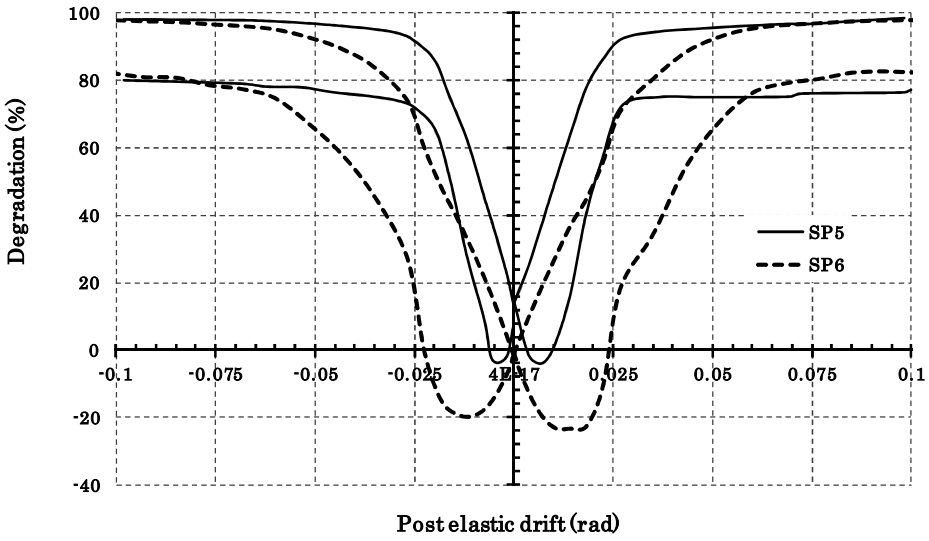

Figure 5.15: Stiffness and strength degradation plot of Type II specimens

The specimen SP3 reaches 50% stiffness degradation at 0.02 radian and afterwards a sudden increase in rate of degradation is noticed as shown in Figure 5.14. In specimen SP4, nearly 80% of stiffness degradation reaches at 0.045 radian that shows increased rotation with lower rate of degradation. The degradation plot of SP5 as shown in Figure 5.15 reflects the shear failure of specimen i.e. about 95% stiffness and strength degradation

occurs at 0.025 radian. The effectiveness of SIFCON core is also shown in shear deficient specimen SP6 by lowering its rate of degradation in stiffness and strength. The specimen SP6 shows 70% degradation at 0.025 rad. and 95% degradation at 0.075 radian.

5.4.4 Cumulative Energy Dissipation

The energy dissipation of each specimen can be assessed by computing the relative and cumulative area of hysteretic loop. Figure 5.16 presents the comparison of cumulative energy dissipation (CED) level of two types of specimens. The seismically detailed specimen SP2 dissipates 80% higher CED than conventional specimen SP1. The specimen SP1 fails at 3.7% drift by yielding whereas specimen SP2 fails at 4.5% drift. The higher rotation of specimen SP2 helps to dissipate higher energy than unconfined specimen SP1.The core enabled specimen exhibits extremely different behavior than anticipated. The problem associated with longitudinal bar buckling at hinge region restricts further load transfer and hence the hysteresis loop area shrinks in specimen SP3. This effect has a negative impact on the post yield energy dissipation behavior. As expected, specimen SP4 also demonstrates similar response until 3.7% drift. Afterwards, the confinement influences large rotation with enhanced energy dissipation capacity over other specimens. As a result of higher rotation, 30% higher CED level is noticed at failure stage with higher drift over conventional specimens.

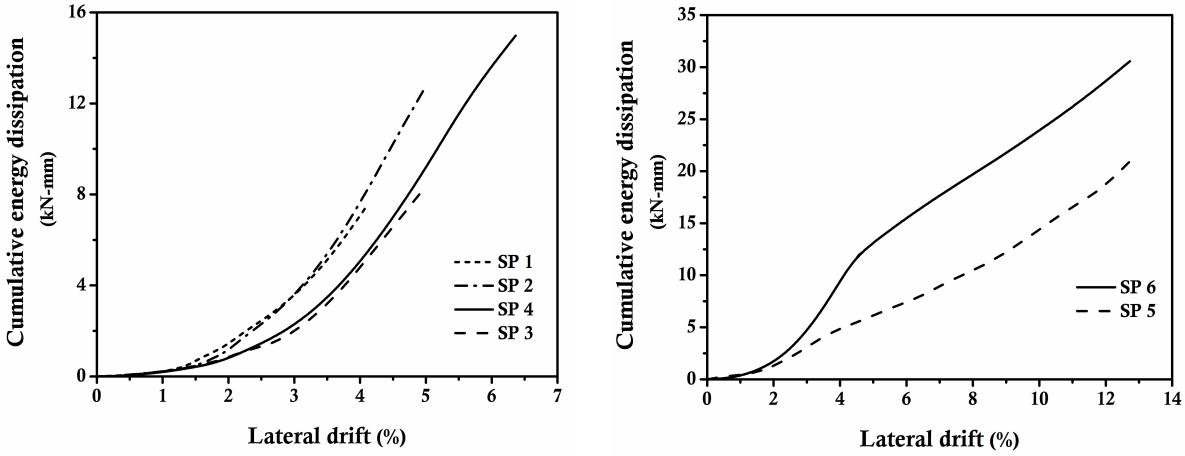

(a) Type I Specimens (b) Type II Specimens

Figure 5.16: Energy dissipation plot of tested specimens

Figure 5.16b shows the energy dissipation plot of specimens SP5 and SP6 respectively. The earlier shear failure in specimen SP5 dissipates lesser energy and shows 50% lesser CED than specimen SP6. The CED of SP6 shows sudden increase in energy

dissipation after 50mm deflection. This is because of crack formation of core in joint connection at 50mm deflection. This crack allows the specimens to dissipate higher energy in the subsequent cycle. Finally observed CED of specimen SP6 shows 50% higher dissipated energy than conventional specimen SP5.

5.4.5 Moment-Rotation Behavior

Figure 5.17 and 5.18 shows the moment- rotation relationships of all beam-column joint specimens and the corresponding values are compared with the specified values in ASCE/SEI 41-06.

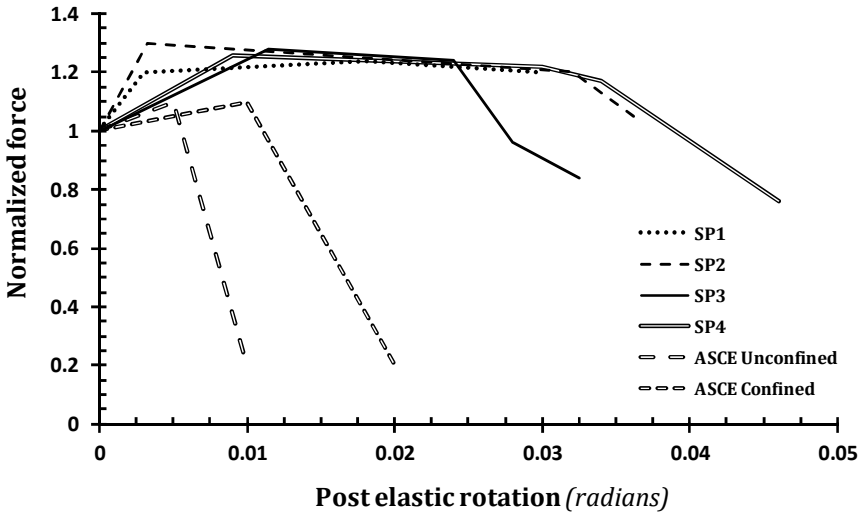

Figure 5.17: Moment-rotation response of Type I specimens

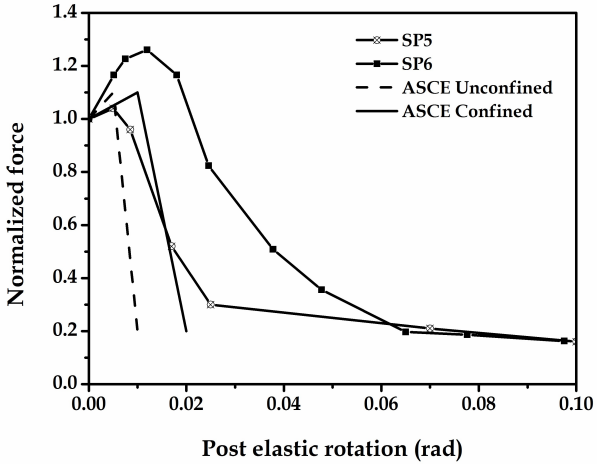

Figure 5.18: Moment-rotation response of Type II specimens

The specimen SP1, SP2 and SP4 show stable moment carrying capacity upto 0.03 radians whereas specimen SP3 experiences degradation of moment after 0.025 rad. due to

the early buckling of reinforcement. The specimen SP4 with confinement shows higher rotation over the other specimens and it reaches upto 0.05 rad. The degradation of SP4 starts after 0.0375 radian at a lower rate as compared to the specified values of ASCE/SEI41-06. As Figure 5.18 shows, specimen SP5 encounters sudden moment degradation after 0.01 rad. The rate of degradation is nearly equal to the specified value of ASCE/SEI41-06. The specimen SP6 shows better moment degradation response over the specimen SP5. The peak moment reaches nearly at 0.015 radian, later gradual degradation in moment is observed. At 0.03 rad the SP6 shows 80% moment retention whereas SP5 shows 30% moment capacity. This authenticates the effectiveness of SIFCON core in resisting the applied shear force and improving the post elastic behavior.

5.4.6 Damage Tolerance Capacity

Modified Park and Ang (1987) damage index is used to examine the damage level that compares the relative performance of beam-column joint specimen with different configuration. Figure 5.19 shows the damage index versus ductility comparison.

$$DI = \frac{\delta_M - \delta_y}{\delta_f - \delta_y} + \beta \int \frac{dE}{F_y \delta_f} \qquad 5.1$$

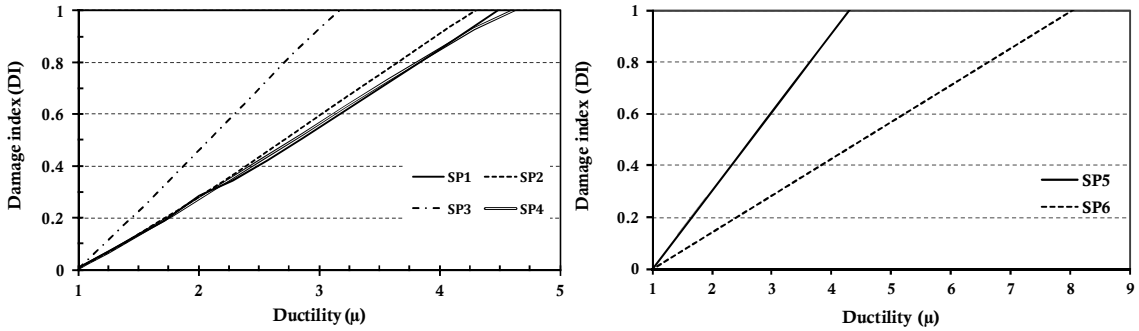

(a) Type I - Flexure (b) Type II- Shear deficient

Figure 5.19: Modified Park and Ang damage index plot vs. Ductility

The damage index [*DI*] values vary from 0 to 1, whereas "0" indicates no damage and "1" indicates complete damage. In this study, it is assumed that 0 < DI < 0.20 represents elastic behavior or no damage in specimens, 0.20 < DI < 0.40 represents slight damage, 0.40 < DI < 0.60 represents moderate damage and 0.60 < DI < 0.80 represents severe damage and DI> 0.8 represents complete damage. The conventional beam-column joint specimens SP1 and SP2 fail at ductility level 4.5 whereas core enabled specimen SP3 completely fails at the ductility level of 3.5. According to the damage index equation 5.1, the calculation is based on the energy dissipation, yield strength and yield deflection. These three variables act as primary source to decide the damage level of structural

components. In SIFCON core enabled specimen, the failure occurs at 450mm away from the column face and restricts the load transfer at the joint that may negatively influence the energy dissipation capacity of the specimen. The presence of SIFCON core in joint region makes it rigid and the yielding is transferred to beam region above the core. Therefore, the damage index plot shows early damage in the specimen SP3. Actually there is neither damage at joint region nor is failure transfer to beam hinge region. The damage index of specimen SP4 is nearly at equal level as in case of conventional specimen. The exact damage tolerance response of core enabled specimens SP5 and SP6 can be understood from the DI plot. The earlier joint shear failure in specimen SP5 reflects the poor damage tolerance capacity over the specimen SP6. The specimen SP5 reaches collapse stage nearly at the ductility level of 4.0; however specimen SP6 shows the same damage at ductility level 5.0.

5.5 Findings

The cyclic behavior of external beam-column joints with SIFCON inner core in joint region is evaluated. The complete hysteresis behavior of SIFCON core joint specimens is compared with the conventional joint specimens. Load-deformation characteristics, strength and stiffness degradation, energy dissipation and equivalent damping, moment-rotation analysis, crack pattern etc are plotted and evaluated for the study of comparative behavior of joints. Following are the main conclusions of the study;

1. Hysteresis behavior of the SIFCON core enabled joint specimens show that there is a significant improvement in the pre and post- peak behavior of external beam-column joint specimen under cyclic loading. The hysteresis performance of SIFCON core joint specimen with confinement in the hinge region is particularly remarkable as compared to other core enabled specimens. The hysteresis behaviour of core enabled shear deficient specimens also proves that SIFCON core at the joint may be an effective and alternative possibility to enhance the performance of shear deficient seismic joint of the building.
2. The strength and stiffness degradation plot of conventionally confined joint specimens degrade about 70% at 2% of drift whereas the SIFCON core enabled specimens degrade about 60% at the same amount of drift. The core with ductile detailing is able to sustain larger deformation (at 4.5% of drift) with lower stiffness degradation. The conventional shear deficient joint specimens also lose about 90%

of its stiffness at 2.5% of drift whereas core enabled specimen degrades about 70% in stiffness with a lower rate of degradation.

3. The strength and stiffness degradation plot of HPFRCC joint specimen shows that the joints reach at peak load (1.2 times the yield load) over the post-elastic drift of about 0.02 radian and further 20% reduction in peak load capacity is observed over the post- elastic drift of 0.05 radian.
4. The core enabled specimens show increased energy dissipation over conventional specimens with different failure mechanisms. The damage in core joint specimens is also much lower than the conventionally confined joint specimens at the same ductility level. The conventional specimens completely collapse even at half of the ductility level of core joint specimens. The core joint specimen becomes 2-3 times more ductile as compared to conventionally confined specimens.

References

ASCE/SEI 41-06 (2007), "Seismic rehabilitation of existing buildings," ASCE Standard, *American Society of Civil Engineers*, Reston, USA

Balaguru, P., and Kendzulak, J., (1987), "Mechanical properties of slurry infiltrated fiber concrete (SIFCON)," *SP-105, American Concrete Institute*, Detroit,pp. 247-268.

Homrich, J. R., and Naaman, A. E., (1987), "Stress-strain properties of SIFCON in compression," *Fiber reinforced concrete properties and applications, ACI, SP-105*, *American Concrete Institute*, Detroit.

IS: 456:2000 (2000), "*Indian Standard code for plain and reinforced concrete,"* 4th Revision, Bureau of Indian Standard, New Delhi

IS: 13920:1993 (1998), "*Ductile detailing of reinforced concrete structures subjected to seismic forces,*" Bureau of Indian Standard, New Delhi

Lankard, D. R., (1984), "Slurry infiltrated fiber concrete (SIFCON)," *Concrete International*, 6(12), 44-47.

Mohammed, A. E., Hamed, M. S., Ahmed, M. F., and Ashrat, H. E., (2009), "Use of slurry infiltrated fiber concrete in reinforced concrete corner connection subjected to opening moments," *Journal of Advanced Concrete Technology*, 7(1),51-59.

Mondragon, R., (1988), "Development of material properties for slurry-infiltrated fiber concrete (SIFCON) - flexural strength," *AFWL-TR-87-79*, Air Force Weapons Laboratory, Kirtland Air Force Base, New Mexico.

Naaman, A. E., Wight, J. K., and Abdou, H., (1987), "SIFCON connections for seismic resistant frames," *Concrete International*, (11),34-39.

Naaman, A. E., Otter, D., and Najm, H., (1989), "Elastic modulus of SIFCON in tension and compression," *ACI Materials Journal*, 88(6),603-612.

Naaman, A. E., and Homrich, J. R., (1989), "Tensile stress-strain properties of SIFCON," *ACI Materials Journal*, 86(3), 244-251.

Naaman, A. E., Otter, D., and Najm, H.,(1991), "Elastic Modulus of SIFCON in Tension and Compression," *ACI Materials Journal*, 88(6),603-612.

Naaman, A. E., Reinhardt, H. W., and Fritz, C., (1992), "Reinforced concrete beams with a SIFCON matrix," *ACI Structural Journal*, 89(1), 79-88.

Naaman, A. E., and Baccouche, M. R.,(1995), "Shear Response of Dowel Reinforced SIFCON," *ACI Structural Journal*, 92(3),587-596.

Parameswaran, V. S., Krishnamoorthy, T.S., and Balasubramanian, K., (1990), "Behaviour of high volume fibre cement mortar in flexure," *Cement and Concrete Composites,* 12, 293- 301.

Park, Y. J., Ang, A. H. S., and Wen, Y. K., (1987), "Damage limiting aseismic design of buildings," *Earthquake Spectra,* 3, 1-26.

Schneider, B., and Mondragon, R., (1988), "Design and Construction Techniques of SIFCON," *AFWL-TR-88-88*, Air Force Weapons Laboratory, Kirtland Air Force Base, New Mexico.

Thirugnanam, G. S., Govindan, P. and Sethurathnam, A., (2001), "Ductility behavior of SIFCON structural members," *Journal of Structural Engineering*, 28(1),27-32.

Wang, M. L., and Maji, A. K., (1994), "Shear properties of slurry-infiltrated fibre concrete (SIFCON)," *Construction and Building Materials,* 8(3),161-168.

Chapter 6

Shear Strength Model for Beam-Column Joints using High Performance Materials

6.1 Introduction

The shear resisting mechanism of beam-column joints is generally based on either strut-and-tie approach or empirical/ semi-empirical models. This mechanism is considered in the combined action of the normal and shear forces through the compressive zone of beam and column elements. Five main parameters are generally considered for the development of joint shear strength models namely, concrete compressive strength (f_c'), joint stirrups ratio (ρ_s), beam longitudinal reinforcement (ρ_t), column axial load (N) and joint index (h_b/h_c) (Vollum et al. 1999; Bakir et al. 2002 and 2003; Hegger et al. 2003; Attaalla 2004; Tran et al. 2014). In this study, a joint shear prediction model is proposed by considering the synergetic action of joint core with other conventional variables. The results of proposed shear strength model of joint are compared with the models given by American Concrete Institute (ACI), New Zealand Standard (NZS), and the Architectural Institute of Japan (AIJ).

6.2 Shear Strength Model for Exterior Beam-Column Joints

The joint shear strength V_{jh} is usually composed of two main components, equation 6.1

$$V_{jh} = V_{jh,uc} + V_{jh,s} \qquad \text{.....6.1}$$

V_{jh} is the horizontal shear strength of exterior beam-column joint. $V_{jh,uc}$ is the shear strength of un-confined exterior BEAM-COLUMN joint and, $V_{jh,s}$ is the contribution of stirrups or confinement in shear strength. Equation 6.2 predicts the shear strength of un-confined exterior BEAM-COLUMN joint based on the joint index (h_b/h_c), percentage of reinforcement (ρ_t), column axial load ratio (n_x) and compressive strength of concrete (f_c'). These are considered with multiplier constant.

$$V_{jh,uc} = \left(\alpha \left\{ \rho_t^{\,y} \times A_j \times \beta \times \left(1 - \frac{N}{A_g \times f_c'} \right) \times (f_c')^r \right\} \right) \qquad \text{.....6.2}$$

where, value of "α" is based on joint index ***(h_b/h_c).*** "ρ_t" is the percentage of beam reinforcement and on the basis of it the value of power constant ***"y"*** is defined. "A_j"is the area of the joint and ***"β"*** is the axial load constant which is based on the axial load ratio defined as $\left(\frac{N}{A_g * f_c'}\right)$. ***"r"*** is compressive strength constant. Table 6.1 presents the value of proposed constants used in the joint shear strength model by employing multiple regression analysis.

Table 6.1: Constants for proposed shear strength model

h_b/h_c	"α" (joint index constant)	% longitudinal. reinforcement	"γ" (reinforcement constant)	Axial load ratio (n_x)	"β" (axial load ratio constant)	f_c'	"r" (Concrete strength constant)	% hoop	S(stirrups ratio constant)
<1	**0.9**	< 0.5	**0.8**	0	**0.5**	<25	**0.475**	0-0.4	**1**
1-1.45	**1.1**	0.5 - 2	**0.4**	0-0.1	**0.75**	30-40	**0.45**	0.4-0.5	**0.7**
1.45-1.5	**1.2**	>2	**0.25**	0.1-0.2	**0.8**	40-50	**0.425**	0.5-0.6	**0.5**
1.5-1.6	**1.25**	Unconfined Joint	**0.8**	0.2-0.3	**0.9**	60-70	**0.35**	0.7-1.9	**0.4**
>1.6	**1.2**	(no stirrups)		>0.3	**1**			2-2.5	**0.3**
								>3	**0.2**

The contribution of confinement in shear resistance can be estimated by using Equation 6.3.

$$V_{js} = \left(s \times \left\{ \frac{\pi d^2}{4} \right\} \times n_b \times n_{sl} \times f_{sy} \right) \quad \text{.....6.3}$$

$$s = \frac{A_{str} \times n_b \times n_{sl}}{A_j} \quad \text{.....6.4}$$

where, A_{str}: area of stirrups, n_b: number of bar, n_{sl}: number of leg, f_{sy}: yield strength of stirrups

The summation of Equation 6.2 and 6.3 gives the joint shear strength model of confined beam-column joints, equation 6.5

$$V_{jh} = \left(\alpha \left\{ \rho_t^{\,y} \times A_j \times \beta \times \left(1 - \frac{N}{A_g \times f_c'} \right) \times (f_c')^r \right\} \right) + \left(s \times \left\{ \frac{\pi d^2}{4} \right\} \times n_b \times n_{sl} \times f_{sy} \right) \quad \text{.....6.5}$$

A comparison is also made between the proposed model and the model given by American Concrete Institute's building code requirements (ACI), the Concrete structures standard of New Zealand (NZS), and Architecture Institute of Japan (AIJ).

Joint Shear Strength Model as per ACI 369 R-11

This code provides the following Equation 6.6 for calculating the joint shear force.

$$V_j = 0.083 \lambda \gamma \sqrt{f_c'} A_j \quad \text{.....6.6}$$

Where, λ: 0.75 light weight aggregate and 1 for normal weight aggregate; A_j : is the effective horizontal area, γ : 6 for unconfined joints and 12 for confined joints.

Joint Shear Strength Model as per NZS 3105:1995 (SNZ 1995)

The probable horizontal shear force ($V_{p,jh}$) resisted by interior and exterior beam-column joints, equation 6.7

$$V_{pjh} = 0.85 v_{ch} b_j h \quad \text{.....6.7}$$

Where, v_{ch} is the horizontal joint shear stress carried by a diagonal compressive strut mechanism crossing the joint. b_j : effective width of the joint, *h*: depth of column. The equation can be re-written as

$$V_{pjh} = 0.85 k \sqrt{f'} \sqrt{1 + \frac{N'}{A_g \sqrt{f'}}} b_j h \le 1.92 \sqrt{f' b_j h} \quad \text{.....6.8}$$

Where, b_j : effective width of the joint, h: depth of column, *k*: 0.4 for exterior and 1 for interior joints, *N*: axial load on column, f_c': concrete compressive cylinder strength, A_g: gross area of column.

Joint Shear Strength Model as per AIJ 2010

The recommended nominal joint shear strength in the form of Equation 6.9

$$V_{ju} = k \phi F_j b_j h_j \quad \text{.....6.9}$$

In Equation 6.9, ***k*** is the factor dependent on the shape of in-plane geometry (1.0 for interior connections, 0.7 for exterior connections and T-shape of the joints, and 0.4 for comer knee connections); ø is the factor for the effect of out-of-plane geometry (1.0 for joints with transverse beams on both sides and 0.85 for other types of joints); F_j is the standard value of the joint shear strength (as a function of concrete compressive strength); b_j is the effective joint shear width; and h_j: joint depth ($0.75h_c$ for T- joints). The standard value of the joint shear strength (F_j) is suggested as Equation (6.10); that is:

$$F_j = 0.8 \times f_{ck}^{0.7} (N/mm^2) \quad \textbf{.....6.10}$$

The effective joint width (b_j) is defined as $b_j = b_b + b_{a1} + b_{a2}$ .Where b_{a1} & b_{a2} are smaller one-quarter of column depth and one-half of distance between beam and column face on. In this study the value of k: 0.7 for T-shape joints, ø: 0.85, b_j: effective width of beam-column joint, h_j: joint depth ($0.75h_c$ for T- joints) is considered.

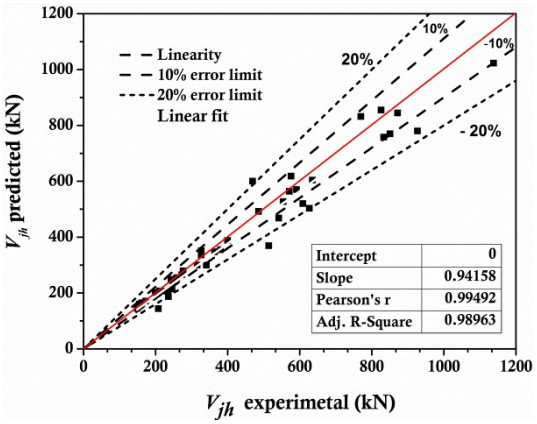

(a) Proposed equation

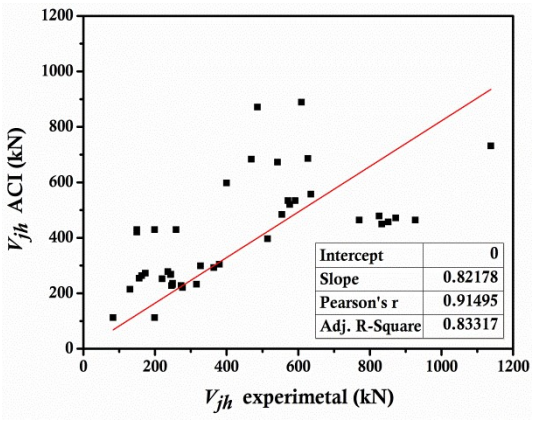

(b) ACI 369-R11

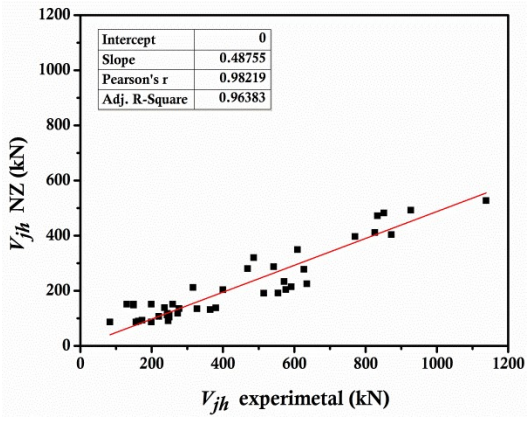

(c) SNZ 1995

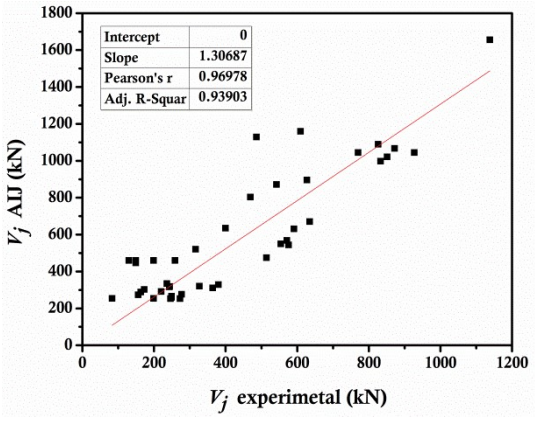

(d) AIJ 2010

Figure 6.1: Comparison of predicted shear strength of beam-column joint with existing experimental data base and codal values

An experimental database on beam–column joints is compiled for the validation of proposed Equation 6.4. The comparative results of the proposed model are summarized in Table 6.2. In the collected experimental data base, the compressive strength (f_c') varies from 22 to 67 MPa and axial load ratio (a_x) varies from 0 to 3. The percentage of beam longitudinal reinforcement (ρ_t) varies from 0.3 to 2% and (h_b/h_c) ratio varies from 0 to 2. The results of the proposed model are also compared with the results of the present experimental work. The experimental shear strength versus predicted shear strength of the proposed models is shown in Figure 6.1.

The Coefficients of Variation (CoV) and average values are the main parameters to examine the effectiveness of proposed model. The CoV for the proposed model is 10% which is comparatively lower than other existing models for determining the shear strength of joint. The CoV of ACI, AIJ and NZ model are 48%, 43%, and 35% respectively. The maximum calculated shear strength values lie within 10% difference limit. The proposed model is able to predict the joint shear strength with more accuracy. The average result of proposed model and other models are shown in Figure 6.2.

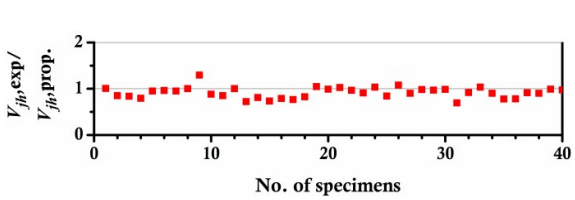

(a) Siva – Pankaj proposed model

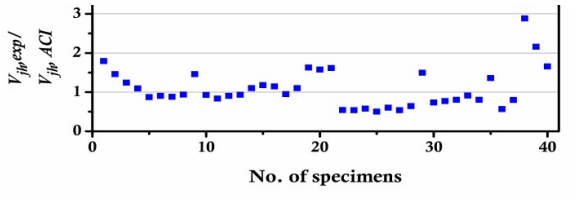

(b) Experimental results vs. ACI

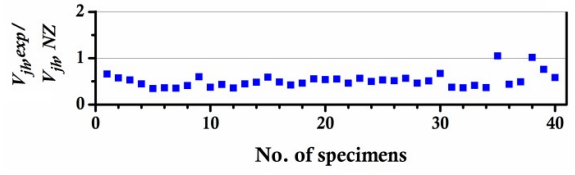

(c) Experimental results vs. NZ

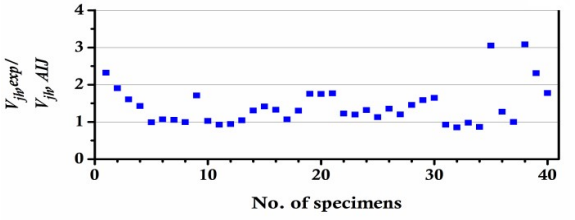

(d) Experimental results vs. AIJ

Figure 6.2: The average result of predicted shear strength of beam-column joint with existing experimental data base and codal values

Table 6.2: Experimental verification of proposed joint shear model with past studies

Reference	Specimen	h_b	b_b	h_c	b_c	b_e	f_c'	$V_{jh,exp}$	$V_{jh,cal}$	V_{ACI}/V_{exp}	$V_{jh,NZS}/V_{jh,exp}$	$V_{jh,AIJ}/V_{jh,exp}$	$V_{jh,SP}/V_{jh,exp}$
Esahani et al. 1987	**1**	480	300	340	340	320	64.7	486	**488**	1.79	0.66	2.32	1.00
	2	480	300	340	340	320	67.3	609	**516**	1.46	0.57	1.90	0.85
	3	440	260	300	300	280	64.7	542	**454**	1.24	0.53	1.61	0.84
	4	440	260	300	300	280	67.3	627	**497**	1.09	0.44	1.43	0.79
Eshani et al. 1985	**1B**	480	259	300	300	279.5	33.6	554	**526**	0.87	0.35	0.99	0.95
	3B	480	259	300	300	279.5	40.9	591	**568**	0.90	0.36	1.07	0.96
	4B	439	259	300	300	279.5	44.6	635	**602**	0.88	0.35	1.06	0.95
	5B	480	300	340	340	320	24.3	571	**571**	0.94	0.41	1.00	1.00
	6B	480	300	340	340	320	39.8	469	**607**	1.46	0.60	1.71	1.29
Fuji et al. 1991	**B1**	250	160	220	220	190	30	246	**217**	0.93	0.37	1.03	0.88
	B4	250	160	220	220	190	30	273	**232**	0.84	0.43	0.93	0.85
Megget 1974	**Unit A**	460	255	380	330	292.5	22.1	576	**576**	0.90	0.36	0.94	1.00
Kaku et al. 1991	**1**	220	160	220	220	190	31.1	249	**179**	0.93	0.44	1.04	0.72
	2	220	160	220	220	190	41.7	244	**198**	1.10	0.48	1.31	0.81
	4	220	160	220	220	190	44.7	236	**173**	1.18	0.59	1.42	0.73
	5	220	160	220	220	190	36.7	220	**174**	1.15	0.49	1.32	0.79
	7	220	160	220	220	190	32.2	249	**191**	0.95	0.42	1.07	0.77
	8	220	160	220	220	190	41.2	243	**201**	1.10	0.46	1.30	0.83
Murthy et al. 2003	**Q1**	400	200	250	200	200	26	156	**163**	1.63	0.56	1.76	1.05
	R1	400	200	250	200	200	30	173	**171**	1.58	0.54	1.75	0.99
	S1	400	200	250	200	200	28	163	**167**	1.62	0.55	1.77	1.03
Pentelides et al. 2002	**Test Unit 1**	406	406	406	406	406	33	872	**843**	0.54	0.46	1.22	0.97
	Test Unit 2	406	406	406	406	406	30	833	**757**	0.54	0.57	1.20	0.91
	Test Unit 3	406	406	406	406	406	34	826	**854**	0.58	0.50	1.32	1.03
	Test Unit 4	406	406	406	406	406	32	927	**779**	0.50	0.53	1.13	0.84
	Test Unit 5	406	406	406	406	406	32	770	**831**	0.60	0.52	1.36	1.08
	Test Unit 6	406	406	406	406	406	31	851	**768**	0.54	0.57	1.20	0.90
Hwang et al. 2004	**28-0T0**	500	380	550	550	465	33	1138	**1117**	0.64	0.46	1.45	0.98
Vatani et al. 2010	**1**	400	350	350	350	350	24	400	**388**	1.49	0.51	1.59	0.97
Kuang et al. 2006	**BS-L**	450	260	300	300	280	31	316	**311**	0.74	0.67	1.65	0.99
Alva et al. 2007	**LVP2**	400	200	300	200	200	44	514	**356**	0.77	0.37	0.92	0.69
	LVP3	400	200	300	200	200	24	364	**334**	0.80	0.36	0.85	0.92
	LVP4	400	200	300	200	200	25	327	**338**	0.91	0.41	0.98	1.03
	LVP5	400	200	300	200	200	26	380	**342**	0.80	0.36	0.87	0.90
Karayansis et al. 2008	**A0**	300	200	200	200	200	32	83	**65**	1.36	1.05	3.05	0.78
	B0	300	200	200	200	200	32	199	**155**	0.57	0.44	1.27	0.78
Hegger et al. 2003	**RK7**	400	150	200	150	150	54.7	277	**253**	0.80	0.49	1.00	0.91
Surya et al. 2010		275	275	300	300	287.5	25	149	**145**	2.88	1.02	3.09	0.97
		275	275	300	300	287.5	25	199	**202**	2.16	0.76	2.31	1.01
		275	275	300	300	287.5	25	259	**254**	1.66	0.58	1.78	0.98
Result Output							**Avg.**			**1.14**	**0.54**	**1.51**	**0.95**
							COV			**0.48**	**0.35**	**0.43**	**0.11**

6.3 Model for Contribution of SIFCON Core in Joint Shear Strength

The presence of SIFCON core in the joint region changes the shear stress resisting mechanism as shown in Figure 6.3. The core is well packed composite and there is no stirrup influence to resist the applied load directly. After the failure of core, a sudden decrease in load is observed as in case of conventional specimens.

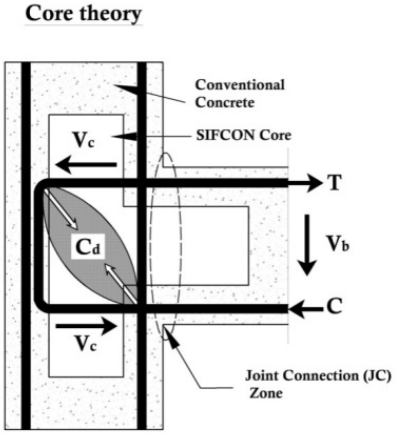

Figure 6.3: Shear resisting mechanism of SIFCON Core enabled beam-column sub-assemblage

The load- deformation behavior of both types of SIFCON core enabled specimens (flexure and shear) underlines the contribution of core in resisting the shear forces. The shear strength contribution of SIFCON core is evaluated and predicted analytically through a modified joint shear strength model and the results are validated with present experimental work. The contribution of SIFCON core is considered as per Equation 6.11

$$V_{core} = \left(\frac{0.6 \times b_{co} \times d_{co} \times (f_{co}')^{0.45}}{1000} \right) \quad \text{.....6.11}$$

Where, b_{co} is the breadth of the core; d_{co} is the depth of the core element; f_{co}' is the compressive strength of the SIFCON.

The summation of Equation 6.5 and 6.11 gives the core enabled joint shear strength as per Equation 6.12 given below;

$$V_{jh} = \left(\alpha \left\{ \rho_t^{\,y} \times A_j \times \beta \times \left(1 - \frac{N}{A_g \times f_c'} \right) \times (f_c')^r \right\} \right) + \left(s * \left\{ \frac{\pi d^2}{4} \right\} \times n_b \times n_{sl} \times f_{sy} \right) + \left(\frac{0.6 \times b_{co} \times d_{co} \times \sqrt{f_{co}'}}{1000} \right) \quad \text{.....6.12}$$

In Equation 6.10, the influence of SIFCON core and beam longitudinal reinforcement is taken into account for shear strength prediction. The proposed model

shows relatively close response over experimental results with an average of 0.99 and CoV is 6.5% as shown in Table 6.3. Figure 6.4 shows the comparison of proposed model with codal values as given in ACI and NZS.

Table 6.3: Experimental Validation of proposed model

Specimen	V_{jh},exp.	V_{jh},prop.	V_{jh},prop./ V_{jh},exp
S1	130	117	0.9
S2	150	146	0.97
S3	210.9	207.9	0.99
S4	195.4	214	1.10
S5	226.7	234	1.03
S6	326.2	322	0.98
		average	0.995
Output		Cov	0.065
		R^2	0.99

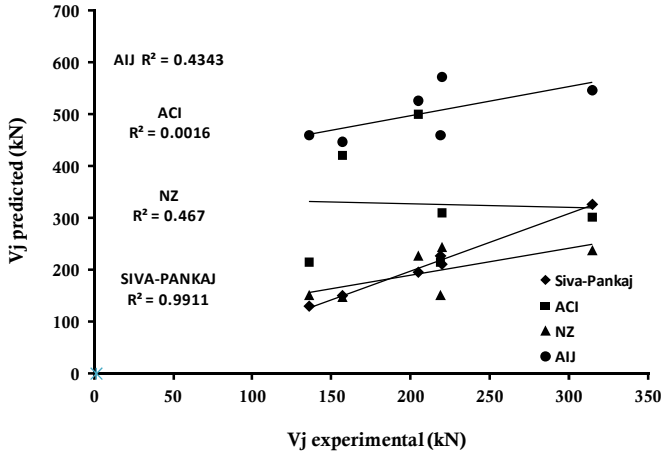

Figure 6.4: Comparison of predicted shear strength of SIFCON core enabled specimens and the experimental values with other codal models

6.4 Model for Predicting the Contribution of Steel Fiber Reinforced Concrete (SFRC)

A number of experimental studies are focused on the use of SFRC as structural component. Very limited study is carried out to predict the shear strength model for SFRC. Jiru et al., 1992, has proposed a shear strength model for exterior beam-column joint with SFRC as follows:

$$V_j = V_c + V_f + V_s \qquad \text{.....6.13}$$

Where, V_j: ultimate shear strength of the SFRC joint; and V_c: shear carried by concrete and defined as by Equation.

$$V_c = 0.1\times\left(1+\frac{N}{b_c h_c f_c}\right) b_j h_j h_c \qquad \text{.....6.14}$$

Where, N is the axial load; b_c is the column breadth; h_s is the depth of the column; f_c is the compressive strength of concrete; b_j is the joint width; h_j is the depth of the joint.

The contribution of steel fibers (V_f) is considered with respect to its aspect ratio, percentage of fibers and area of the joint as follows

$$V_f = 2\frac{l_f}{d_f} v_f b_j h_j \qquad \text{.....6.15}$$

Where, l_f is the length of the fiber; d_f is the diameter of the fiber; v_f is the volume of the fiber; b_j is the joint width; h_j is the depth of the joint.

and (Vs) shear carried by the joint stirrups and may be defined as

$$V_s = f_y \frac{A_{sh}}{S}(h_o - a_s') \qquad \text{.....6.16}$$

Where, A_{sh} is the area of stirrups; S is the spacing of the stirrups; f_y is the yield strength of the stirrup reinforcement.

The contribution of SFRC on the shear resistance depends on the fiber dispersion, type of fiber, crack bridging capacity of fiber irrespective of compressive strength of concrete. The experimental study of SFRC shows that the addition of steel fiber varying from 1-2% in volume enhances the tensile strength and flexural strength of concrete. The split tensile strength (s_t) to compressive strength (c_s) ratio (s_t / c_s) of SFRC ranging from 10 -13% and flexural strength (f_t) to compressive strength ratio (f_t / c_s) of crimpled fiber reinforced concrete is 15 - 16%, whereas it is 14 -15% for hooked end steel fiber.

The proposed model to predict the shear strength of beam-column joint with confinement may also be applicable to predict the shear strength of beam-column joint with SFRC. The contribution of SFRC with its enhancement in strength is considered along with compressive strength of concrete, percentage of longitudinal reinforcement and stirrups in the joint. In addition, column axial load and joint index are also considered. The proposed Equation 6.17 is as follows;

Without considering the stirrups

$$V_{jh} = \left(\alpha\left\{\rho_t^{\,y} \times A_j \times \beta \times \left(1-\frac{N}{A_g \times f_c'}\right)\times (f_c' \times f_t)\right\}\right) \qquad \text{.....6.17}$$

With stirrups

$$V_{jh} = \left(\alpha \left\{ \rho_t^{\,y} \times A_j \times \beta \times \left(1 - \frac{N}{A_g \times f_c{}'} \right) \times (f_c{}' \times f_t) \right\} \right) + \left(s \times \left\{ \frac{\pi d^2}{4} \right\} \times n_b \times n_{sl} \times f_{sy} \right)$$

…...**6.18**

The constant value of f_t varies according to the concrete compressive strength and the contribution of beam longitudinal reinforcement is considered with a multiplier that depends on the unconfined and confined state along with the percentage of reinforcement. The constants used in the proposed Equation are given in Table.6.4.

Table 6.4: Constants for proposed SFRC shear strength model

h_b/h_c	**"α"** (Joint index constant)	**% longitudinal. reinforcement**	**"y"** (Reinforcement constant)	**Axial load ratio (n_x)**	**"ß"** (Axial load ratio constant)	**f_c'**	**"ft"** (Flexural strength constant)	**% hoop**	**S**(Stirrups ratio constant)
<1	**0.7**	< 0.5	**0.8**	0	**0.6**	20-40	**0.125**	0-0.4	**1**
1-1.45	**0.9**	0.5 - 2	**0.4**	0-0.1	**0.7**	40-50	**0.1**	0.4-0.5	**0.7**
1.45-1.5	**1.0**	>2	**0.25**	0.1-0.2	**0.8**	>70<81	**0.075**	0.5-0.6	**0.5**
1.5-1.6	**1.1**	Unconfined Joint (no stirrups)	**0.8**	0.2-0.3	**0.9**			0.7-1.9	**0.4**
>1.6	**1.2**			>0.3	**1**	Unconfined Joint (no stirrups)	**0.2**	2-2.5	**0.3**
								>3	**0.2**

The proposed Equation 6.17 is validated with an experimental database of twenty four RC beam–column joints. A comparison is made to predict the shear strength of SFRC beam-column joint with available test results as given in Table 6.5 and shown in Figure 6.5. In the collected data the compressive strength varies from 21 to 81 MPa and the axial load ratio varies from 0 to 3. The percentage of beam longitudinal reinforcement varies from 0.5 to 1.85 % and (h_b/h_c) ratio varies from 0.5 to 1.5.The coefficient of variation (CoV) for the proposed model is 9% with 93% average value. It proves the efficiency of the proposed equation in shear strength prediction. The maximum calculated shear strength values lie within 20% difference limit. The average result of proposed model with experimental details is shown in Figure 6.6.

Table 6.5: Experimental verification of proposed model from available data

S.ID	h_b	b_b	h_c	b_c	f_c	Axial ratio	h_b/h_c	% Fiber	V_{jh} exp.	V_{jh} pred	exp. /pred.
Kheni et al. 2014											
1	240	200	200	200	34.2	0.014	1.2	1.0	131	119	**0.910**
Andreu 2012											
SF3	450	350	350	350	36	0.084	1.28	1.0	602	590.28	**0.98**
Kwon et al. 2011											
NC2											
F1.0	300	250	250	250	26.41	0	1.2	1.0	237	224	**0.945**
F1.5	300	250	250	250	28.65	0	1.2	1.5	245	235	**0.960**
NC0											
F1.0	300	250	250	250	26.41	0	1.2	1.0	229	212	**0.928**
F1.5	300	250	250	250	28.65	0	1.2	1.5	237	230	**0.973**
Tang et al. 1992											
SF1	350	200	350	250	21.3	0.133	1	1.2	327	294	**0.900**
SF2	350	200	350	250	32.1	0.133	1	1.5	422	430	**1.020**
SF3	350	200	350	250	32.1	0.133	1	1.5	296.9	340	**1.145**
SF5	350	200	350	250	21.3	0.133	1	1.5	221	225	**1.018**
Ganesan et al. 2007											
F4 HPR	200	150	200	150	81	0.01	1	1.0	132.74	134	**1.009**
Siva and Pankaj(2015)											
C1	225	150	225	150	50.6	0.015	1	1.0	99.63	111.5	**1.119**
C2	225	150	225	150	48	0.015	1	2.0	99.63	106	**1.063**
H1	225	150	225	150	48.1	0.015	1	1.0	104.61	106	**1.013**
H2	225	150	225	150	54.3	0.015	1	2.0	104.61	118.6	**1.134**
S1	150	130	150	150	36	0.025	1	2.0	120.31	122	**1.016**
Junichiro et al. 2012											
TJ 1	200	168	250	250	23.5	0	0.8	1.0	91.93	97.8	**1.064**
TJ 1.5	200	168	250	250	30	0	0.8	1.5	105.06	124.9	**1.189**
Craig et al. 1984											
SP2	254	203	203	203	34.6	0.249	1.25	1.5	209.8	190	**0.908**
SP4	254	203	203	203	26.5	0.325	1.25	1.5	245.7	206	**0.840**
SP10	254	203	203	203	38.33	0.224	1.25	1.5	196.7	218	**1.112**
Balouch et al. 2009											
J4	300	200	250	200	46.2	0.08	1.2	0.92	238.45	208	**0.873**
										Avg.	**1.005**
										Cov.	**0.094**

Table 6.6: Experimental validation of proposed model

Specimen	V_{jh},exp.	V_{jh},prop.	V_{jh},exp/ V_{jh},prop.
C1	99.63	111.5	1.119
C2	99.63	106	1.063
H1	104.61	106	1.013
H2	104.61	118.6	1.134
S1	120.31	122	1.016
		Average	**1.06**
		Cov.	**0.05**

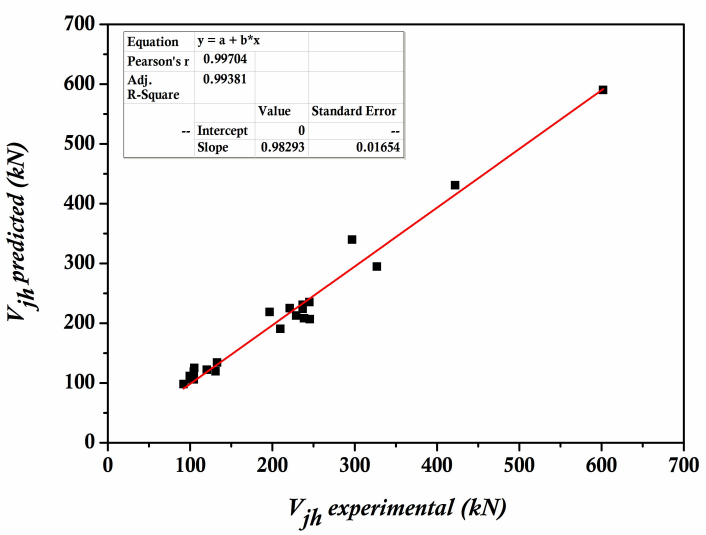

Figure 6.5: Comparison of predicted shear strength of SFRC joint specimens and the experimental values

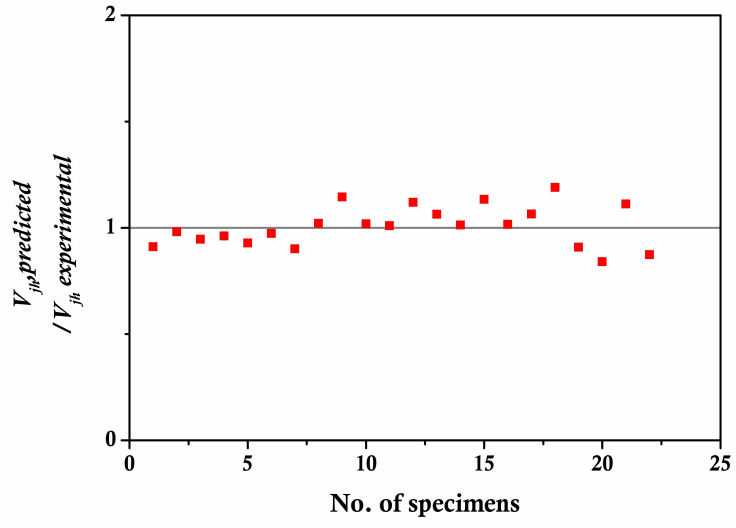

Figure 6.6: The average result of experimental values of shear strength of SFRC joint specimens vs. predicted values

6.5 Numerical Validations

Numerical validations of the proposed models for the evaluation of shear strength of beam-column joint with different types of core with experimentally obtained values are given as under;

Unconfined Beam-column joint [Surya et al. 2010]

h_b-275mm ; h_c-300; b_b-275; b_c-300; be-287.5; % beam reft.-0.47; h_b/h_c-0.916; N-25kN; f_c'-25

Parameters

- **"α"** is based on $\mathbf{h_b/h_c}$ ratio. The $\mathbf{h_b/h_c}$ ratio in this problem is 0.916 which is less than 1, hence the **"α"**is taken as 0.9.
- The percentage of beam reinforcement is given as 0.71; but it is unconfined so directly **"y"** can be taken as 0.8.
- The beta value is taken as 0.75 because the axial load ratio is 0.0133 which lies between 0.01-0.1.
- The compressive strength is 25MPa; hence **"r"** is taken as 0.475.

On the basis of Equation 6.2 the shear strength of unconfined BEAM-COLUMN joint as shown below

$$\boldsymbol{V_{jh,uc}} = \left(0.9\left\{0.47^{0.8}\times 300\times 287.5\times 0.75\times\left(1-0.0133\right)\times(25)^{0.475}\right\}\right)$$

$$\boldsymbol{V_{jh,uc}} = 144.8\boldsymbol{kN} \approx 145\boldsymbol{kN}$$

Confined Beam-column joint [Ehsani et al. 1985]

h_b - 440 mm ; h_c - 340; b_b - 259; b_c - 300; be - 279.5; % beam reft. - 1.5; h_b/h_c - 1.46; axial load ratio: 0.0603; f_c'- 44.6; stirrups diameter:12.7mm; yield strength of stirrups: 437MPa. number of legs: 2 and number of bars: 3 nos.

Parameters

- **"α"** is based on $\mathbf{h_b/h_c}$ ratio. The $\mathbf{h_b/h_c}$ ratio in this problem is 1.466 hence the **"α"**is taken as 1.25.
- The percentage of beam reinforcement is given as 1.5 also it is unconfined so **"y"** is be taken as 0.4.

The value of "s" depends on the basis of $\frac{A_{str} \times n_b \times n_{sl}}{A_j}$. It is 0.9, hence the value of "s" chosen as 0.4.

- The beta value is taken as 0.75 because the axial load ratio is 0.063 which lies between 0.01-0.1.
- The compressive strength is 44.6 MPa; hence **"r"** is taken as 0.425.

On the basis of Equation 6.4 the shear strength of unconfined BEAM-COLUMN joint as shown below

$$V_{jh,uc} = \left(1.25\left\{1.5^{0.4} \times 300 \times 279.5 \times 0.75 \times \left(1-0.0603\right) \times (44.6)^{0.425}\right\}\right)$$

$$V_{js} = \left(s \times \left\{ \frac{\pi d^2}{4} \right\} \times n_b \times n_{sl} \times f_{sy} \right)$$

$$V_{jh,c} = 469.2 + 132.79kN = 602kN$$

Beam-column Joint with SIFCON Core [Siva and Pankaj 2015]

h_b-275mm ; h_c-300; b_b-275; b_c-300; be-287.5; % beam reft.-0.83; h_b/h_c-0.916; N-25kN; f_c'-25 ; d_{co}-150; b_{co}- 150; f_{co}' of SIFCON core - 48

Parameters

- **"α"** is based on $\mathbf{h_b/h_c}$ ratio. The $\mathbf{h_b/h_c}$ ratio in this problem is 0.916 which is less than 1, hence the **"α"**is taken as 0.9.
- The percentage of beam reinforcement is given as 0.833; but it is unconfined so directly **"y"** can be taken as 0.8.
- The beta value is taken as 0.75 because the axial load ratio is 0.011 which lies between 0.01-0.1.
- The compressive strength is 25MPa; hence **"r"** is taken as 0.475.

On the basis of Equation 6.2 and 6.9 the shear strength of unconfined BEAM-COLUMN joint with SIFCON core is shown below

$$V_{jh,SIFCON} = \left(0.9\left\{0.833^{0.8} \times 300 \times 287.5 \times 0.75 \times \left(1-0.011\right) \times (25)^{0.475}\right\}\right) + \left(\frac{0.6 \times 150 \times 150 \times \sqrt{48}}{1000} \right)$$

$$V_{jh,SIFCON} = 322.35kN \approx 322kN$$

Beam-column joint with SFRC [Tang et al. 1992]

h_b-350 mm; h_c-350; b_b-200; b_c-300; be-225; % beam reft.-1.81; h_b/h_c-1;axial load ratio:0.133; f_c'-32.1; stirrups diameter: 8mm; yield strength of stirrups: 290MPa; Number of legs:2 and number of bars : 3nos.

Parameters

- **"α"** is based on $\mathbf{h_b/h_c}$ ratio. The $\mathbf{h_b/h_c}$ ratio in this problem is 1 hence the **"α"**is taken as 0.9.
- The percentage of beam reinforcement is given as 1.5 and it is confined so **"y"** is being taken as 0.4.

The value of "s" depends on the basis of $\frac{A_{str} \times n_b \times n_{sl}}{A_j}$. It is 0.76, hence the value of "s" chosen as 0.4.

- The beta value is taken as 0.7 because the axial load ratio is 0.133 which lies between 0.1-0.2.
- The compressive strength is 32.1MPa; hence **"f_t"** is taken as 0.125.

On the basis of Equation 6.16 the shear strength of unconfined beam-column joint with SFRC as shown below

$$V_{jh,SFRC} = \left(0.9 \times \left\{1.81^{0.4} \times 350 \times 225 \times 0.7 \times (1-0.133) \times (32.1 \times 0.125)\right\}\right) + (1 \times 87417.6)$$

$$V_{jh,SFRC} = 430kN$$

6.5.1 Performance Comparison of Joints with Different Configurations

Unconfined Beam-Column Joint [HYJ 1,HYJ 2, HYJ 6 in Chapter 3]

h_b-225mm ; h_c-225; b_b-150; b_c-150; be-150; % beam reft.-0.81; h_b/h_c-0.1; f_c'-27.5

Parameters

- **"α"** is based on $\mathbf{h_b/h_c}$ ratio. The $\mathbf{h_b/h_c}$ ratio in this problem is 1 which is less than 1, hence the **"α"**is taken as 0.9.
- The percentage of beam reinforcement is given as 0.81; but it is unconfined so directly **"y"** can be taken as 0.8.
- The beta value is taken as 0.75 because the axial load ratio is 0.015 which lies between 0.01-0.1.
- The compressive strength is 27.5 MPa; hence **"r"** is taken as 0.45.

On the basis of Equation 6.2 the shear strength of unconfined beam-column joint as shown below

$$V_{jh,uc} = \left(0.9\left\{0.81^{0.8} \times 225 \times 150 \times 0.75 \times \left(1-0.015\right) \times (27.5)^{0.45}\right\}\right)$$

$V_{jh,uc} = 81.4kN$ (Predicted)

$V_{jh,uc} = 87.17kN$ (Experimental)

The joint with confining reinforcement in the joint region. Stirrups diameter:6 mm; yield strength of stirrups: 250 MPa. number of legs: 2 and number of bars: 2 nos.

- **"α"** is based on $\mathbf{h_b/h_c}$ ratio. The $\mathbf{h_b/h_c}$ ratio in this problem is 1 which is less than 1, hence the **"α"**is taken as 0.9.
- The percentage of beam reinforcement is given as 0.81; but it is confined so directly **"y"** can be taken as 0.4.
- The beta value is taken as 0.75 because the axial load ratio is 0.015 which lies between 0.01-0.1.
- The compressive strength is 25.5 MPa; hence **"r"** is taken as 0.45.

The value of "s" depends on the basis of $\frac{A_{str} \times n_b \times n_{sl}}{A_j}$. It is 0.33, hence the value of "s" chosen as 1.

$$V_{jh,uc} = \left(0.9\left\{0.81^{0.8} \times 225 \times 150 \times 0.75 \times \left(1-0.015\right) \times (27.5)^{0.45}\right\}\right)$$

$$V_{js} = \left(1 \times \left\{\frac{\pi \times 6^2}{4}\right\} \times 2 \times 2 \times 250\right)$$

$V_{jh,c} = 95kN$ (predicted)

$V_{jh,c} = 101.3kN$ (experimental)

The joint with SFRC in the joint region. Stirrups diameter:6 mm; yield strength of stirrups: 250 MPa. number of legs: 2 and number of bars: 1nos.

- **"α"** is based on $\mathbf{h_b/h_c}$ ratio. The $\mathbf{h_b/h_c}$ ratio in this problem is 1 which is less than 1, hence the **"α"**is taken as 0.9.
- The percentage of beam reinforcement is given as 0.81; but it is confined so directly **"y"** can be taken as 0.4.
- The beta value is taken as 0.7 because the axial load ratio is 0.015 which lies between 0.01-0.1.

- The compressive strength is 48.1 MPa; hence **"f_r"** is taken as 0.1.

The value of "s" depends on the basis of $\frac{A_{str} \times n_b \times n_{sl}}{A_j}$. It is 0.16, hence the value of "s" chosen as 1.

$$V_{jh,SFRC} = \left(0.9 \times \left\{0.81^{0.4} \times 225 \times 150 \times 0.7 \times (1-0.015) \times (48.1 \times 0.1)\right\}\right) + (1 \times 14130)$$

$V_{jh,sfrc} = 106kN$ (Predicted)

$V_{jh,sfrc} = 104.61kN$ (experimental)

6.6 Findings

An analytical model is proposed for predicting the shear strength of BEAM-COLUMN sub-joint under unconfined and confined conditions after considering the five main variables i.e. concrete compressive strength (f_c'), joint stirrups ratio (ρ_s), beam longitudinal reinforcement (ρ_t), column axial load ***(N)*** and joint index (h_b/h_c). The predicted results are compared with the model as proposed in American Concrete Institute (ACI), New Zealand (NZS), and the Architectural Institute of Japan (AIJ). The variables in the proposed equation are determined on the basis of regression analysis of past experimental data base of beam-column joints.

The coefficient of variance (CoV) of ACI, NZS and AIJ are 0.48, 0.35 and 0.43 with an average of 1.14, 0.54 and 1.51 respectively. The co-variant of proposed model is 0.10 with an average of 0.95. The R^2 of the proposed model is 0.98 whereas this is 0.83, 0.96 and 0.93 for ACI, NZS and AIJ models respectively. The ratio of slope of R^2 for proposed model is 0.96 whereas this is 0.98, 0.50 and 1.39 for ACI, NZS an AIJ respectively. The covariant and R^2 for the present experimental data is 0.065 and 0.99.

The proposed model is further modified for the SIFCON core enabled beam-column joints after considering the contribution of SIFCON core in shear resisting mechanism. The results are validated with present experimental work with an average of 0.99 and CoV is 6.5%.

A more rational shear strength prediction model is also proposed for SFRC BEAM-COLUMN joint after considering the contribution of SFRC along with five main variable parameters. The proposed equation is again validated with other sets of experimental database with coefficient of variance (CoV) which is 9% with an average of 0.93.

References

ACI 369 R-11, "Guide for seismic rehabilitation of existing concrete frame buildings and commentary" *American Concrete Institute*.

AIJ 2010, "Standard for structural calculation of reinforced concrete structures," *Architectural Institute of Japan.*

Alva, G. M. S., Debs, A. L. H. D. C., and Debs, M. K. E., (2007), "An experimental study on cyclic behaviour of reinforced concrete connections," *Canadian Journal of Civil Engineering*, 34(4), 565–565.

Attaalla, S. A., (2004), "General analytical model for nominal shear stress of type 2 normal-and high-strength concrete beam-column joints," *ACI Structural Journal*, 101(1),65-75.

Bakir, P. G., and Boduroglu, H. M., (2002), "A new design equation for predicting the joint shear strength of monotonically loaded exterior beam-column joints," *Engineering Structures*, 24(8), 1105-1117.

Bakir, P. G., (2003), "Seismic resistance and mechanical behaviour of exterior beam-column joints with crossed inclined bars," *Structural Engineering and Mechanics*, 16(4), 493-517

Balouch, D. S. U., (2009), "Strengthening of BEAM-COLUMN joint with steel fibre reinforced concrete during earthquake loading," *Post Doctoral Report*, University of Leeds, UK.

Craig, R., Mahadev, S., Patel, C. C., Viteri, M., and Kertesz, C., (1984), "Behavior of joints using reinforced fibrous concrete," *Proc. of Fiber Reinforced Concrete International Symposium*, *SP-81, American Concrete Institute*, 125–167.

Ehsani, M. R., Moussa, A. E., and Vallenilla, C. R., (1987), "Comparison of inelastic behavior of reinforced ordinary and high-strength concrete frames," *ACI Structural Journal,* 84(2), 161-169.

Ehsani, M. R., and Wight, J.K., (1985), "Exterior reinforced concrete beam-to-column connections subjected to earthquake type loading," *ACI Structural Journal,* 82(4), 492–499.

Fujii, S., and Morita, S., (1991), "Comparison between interior and exterior RC Beam-column Joint Behavior," *Design of Beam-column Joints for Seismic Resistance, SP-123*, J.O.Jirsa ed., AMCI Farminton Hills, Mich., 145-165.

Ganesan, N., Indira, P. V., and Abraham, R., (2007), "Steel fibre reinforced high performance concrete beam-column joints subjected to cyclic loading," *ISET Journal of Earthquake Technology*, 44(3-4), 445-456.

Hegger, J., Sherif, A., and Roeser, W., (2003), "Nonseismic design of beam–column joints," *ACI Structural Journal,* 100(5), 654 –664.

Hwang, S. J., Lee, H. J., and Wang, K. C., (2004), "Seismic design and detailing of exterior reinforced concrete beam–column joints," *Proceedings of 13th World Conference on Earthquake Engineering*, Vancouver BC, Canada.

Jiru, T., Chaobin, H., Kaijian, Y., and Yongcheng, Y., (1992), "Seismic behavior and shear strength of framed joint using steel-fiber reinforced concrete," *Journal of Structural Engineering*, 118(2), 341-358.

Junichiro, N., Kabir, S., and Ken, W., (2012), "Experimental study on the possibility of using steel fiber-reinforced concrete to reduce conventional rebars in beam-column joints," *Journal of Materials in Civil Engineering*, 24(12), 1461-1473.

Kaku, T., and Asakusa, H., (1991), "Ductility estimation of exterior beam–column joint in reinforced concrete frames," *In: Design of beam-column joints for seismic resistance (SP-123). Detroit (MI): American Concrete Institute*, 167-185.

Karayannis, C. G., and Sirkelis, G. M., (2008), "Strengthening and rehabilitation of RC beam–column joints using carbon-FRP jacketing and epoxy resin injection," *Earthquake Engineering and Structural Dynamics*, 37(5), 769–790.

Kheni, D., Scott, R. H., Deb, S. K., and Dutta, A., (2015), "Ductility enhancement in beam-column connections using hybrid fiber-reinforced concrete," *ACI Structural Journal*, 112(2), 167.

Kuang, J. S., and Wong, H. F., (2006), "Effects of beam bar anchorage on beam-column joint behavior," *Proceeding of the Institution of Civil Engineers-Structures and Buildings* 159(2),115-124.

Kwon, W. H., Kim, W. S., Kang, T. H. K., Hong, S. G., Kwak, Y. K., (2011), "Behavior of steel fiber-reinforced concrete exterior connections under cyclic loads," *Journal of the Korea Concrete Institute*, 23(6),711-722.

Megget, L. M., (1974), "Cyclic behaviour of exterior reinforced concrete beam–column joints," *Bulletin of the New Zealand National Society for Earthquake Engineering,* 7(1), 27-47.

Murty, C. V. R, Rai, D. C, Bajpai, K. K and Jain, S. K., (2003), "Effectiveness of reinforcement details in exterior reinforced concrete beam–column joints for earthquake resistance," *ACI Structural Journal*, 100(2), 149-156.

Pantelides, C. P, Hansen, J., Nadauld, J., and Reaveley, L. D., (2002), "Assessment of RC building exterior joints with substandard details," *PEER Report No. 2002/18*, College of Engineering, University of California, Berkely.

Surya, V. V. S., (2010), "Nonlinear modelling of soft storey RC frame based on cyclic testing of components," *PhD.Thesis,Dept. of Earthquake Engineering, IIT Roorkee*, Roorkee, India.

SNZ 1995. Concrete structures standard NZS 3101:1995, Volume 1 Code of Practice and Volume 2 Commentary. Standards New Zealand, Wellington.

Tran, T., Hadi, M. N. and Pham, T. M., (2014), "A new empirical model for shear strength of reinforced concrete beam-column connections," *Magazine of Concrete Research*, 66(10), 514-530.

Vatani, O. A., (2010), "Repairing of seismically damaged RC exterior beam–column connection using CFRP," *Journal of Reinforced Plastics and Composites*,29(21),3257–3274.

Vollum, R. L. and Newman, J. B., (1999), "Strut and tie models for analysis/design of external beam-column joints," *Magazine of Concrete Research*, *51*(6), 415-425.

Chapter 7

Influence of Mechanical Rebar Coupler on the Static and Cyclic Behavior of R.C Components

7.1 Introduction

An extensive experimental investigation is carried out to examine the effectiveness of mechanical coupler under flexure as well as in beam-column joint in the present chapter. The proposed coupler may be effective as a practical solution for retrofitting of structural member with buckled, broken or corroded reinforcement. Threaded bolts used in mechanical coupler not only hold the existing reinforcing bar in its position but also resist the externally applied load by applying the laterally confined pressure on existing reinforcement. The influence of coupler in rebars connection at different locations of beams and beam-column joints is examined. The test results reveal that the mechanical coupler using threaded bolt with epoxy (as filler) can be effectively used in retrofitting of structural member and can be an alternative solution of welding or splicing in the critical region.

7.2 Early Studies

Many research works were carried out on lap splicing in R.C beams which suggested different splice length according to the strength of concrete. Ezeldin et al. (1989) studied the bond behavior of normal and high-strength concrete made with and without fibers and observed that the addition of silica fume results in higher bond strength but results in brittle bond failure. Fibers improved post peak behavior and ductility of spliced beam to a considerable extent and the slip at maximum bond load increased with increase in fiber content. Azizinamini et al. (1993) investigated the effect of several variables on bond capacity of reinforcing bars embedded in high-strength concrete and concluded that proper confinement in splice region proved effective. Additionally it was concluded that the current trend in ACI of making the splice length longer to compensate for having small cover and spacing might not be an effective approach. Zuo et al. (2000) investigated the splice strength of conventional and high relative rib area bars in normal and high-strength

concrete and observed that the splice strength of bars confined by transverse reinforcement increased with an increase in relative rib area and bar diameter. The use of stronger coarse aggregate resulted in an increase in splice strength for bars both with and without confining reinforcement. Esfahani et al. (1998) proposed bond strength models by considering the influence of concrete strength, splice length, concrete cover, ratios between side cover, bottom cover, and the spacing between the spliced bars, rib face angle of the reinforcing bar, and admixtures in the concrete mix on bond in splices. Bilal et al. (2001) studied the effect of fiber reinforcement on bond strength of tension lap splices in high-strength concrete and the test results indicated that the use of steel fibers in the splice region increased the bond strength, ductility and mode of failure. Harajli (2005) investigated the effect of confinement using steel, FRC, or FRP on the bond stress-slip response of steel bars under cyclic loading. The test results showed improved seismic performance and reduced bond strength degradation when confining the concrete with transverse steel, steel fiber reinforcement and external confinement using FRP composites within the splice region. Tarabia et al. (2010) studied the behavior of reinforced concrete beams with lap splice reinforcement with different stirrups spacing and observed drastic increase in ductility when transverse reinforcement was used in splice region. Hosny et al. (2012) proposed equation to predict the required development of length in the lap splice region. Ahmed et al. (2014) experimented different splice length and diameter of rebars in high strength concrete RC beams and experienced better ductility with increased splice length and observed no effect due to the diameter of the bar on ductility.

7.3 Uni-axial Tensile Behavior of Mechanical Couplers

Uni-axial stress-strain tensile behaviour of mechanical couplers is studied on reinforcing bar of 12 mm and 16 mm with different size of couplers. The length, number of threaded bolts and wall thickness of coupler differ with respect to the size of the reinforcing bar. The complete details of test program on mechanical coupler are summarized in Table 7.1. The interfacial bond strength between the rebar and coupler is increased by carrying out (a) thread at the inner surface of coupler, (b) using external threaded bolts and (c) using high strength epoxy at the gap between coupler and reinforcement. The inner threaded surface of the coupler increases frictional resistance, external threaded bolt and provides a confining pressure. Moreover, the epoxy increases the bond strength that helps to reduce the length of couplers. Figure 7.1 provides the cross-

section details and Figure 7.2 shows the typical details of rebar coupler. The epoxy in coupler is only pumped after tightening the bolts.

Table 7.1: Summarized tensile strength results of rebars

Sl. No	Rebar size	Coupler size				Bolts		Yield Strength	Ultimate strength	UTS /YTS
		Inner dia	Outer dia	Wall thickness	Length	No. of bolts	Size of bolts			
	mm	*mm*	*mm*	*mm*	*mm*		*mm*	MPa	MPa	
1	10	15	30	7.5	120	4	8	530	585	1.10
2	12	-	-	-	-	-	-	500	520	1.04
3	12	15	30	7.5	120	6	8	550	660	1.20
4	16	-	-	-	-	-	-	550	660	1.20
5	16	20	35	7.5	160	8	8	540	620	1.13

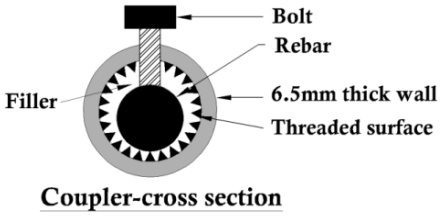

Figure 7.1: Typical cross sectional details of rebar coupler

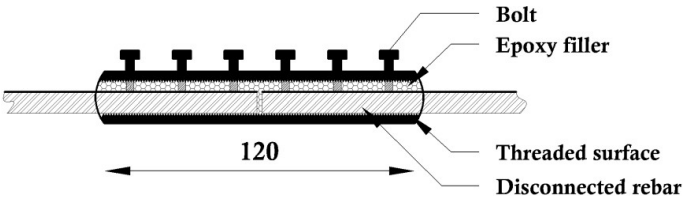

(a) Typical details of coupler for 10 mm and 12 mm diameter rebar

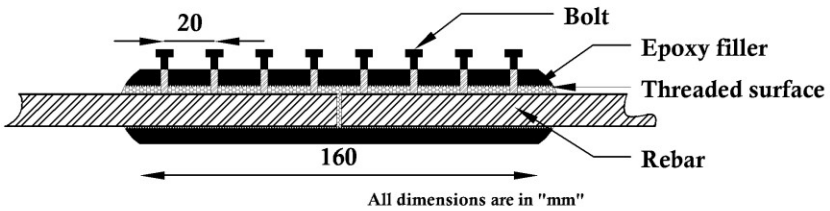

(b) Typical details of coupler for 16mm diameter rebar

Figure 7.2: Typical details of coupler

The tensile tests of different diameters of TMT rebar with and without couplers are carried out under uni-axial tension and the results are summarized in Table 7.1. The uni-axial tensile stress-strain behavior of reinforcing bars of 12 mm and 16 mm diameter exhibits complete ductile behavior as shown in Figure 7.3.

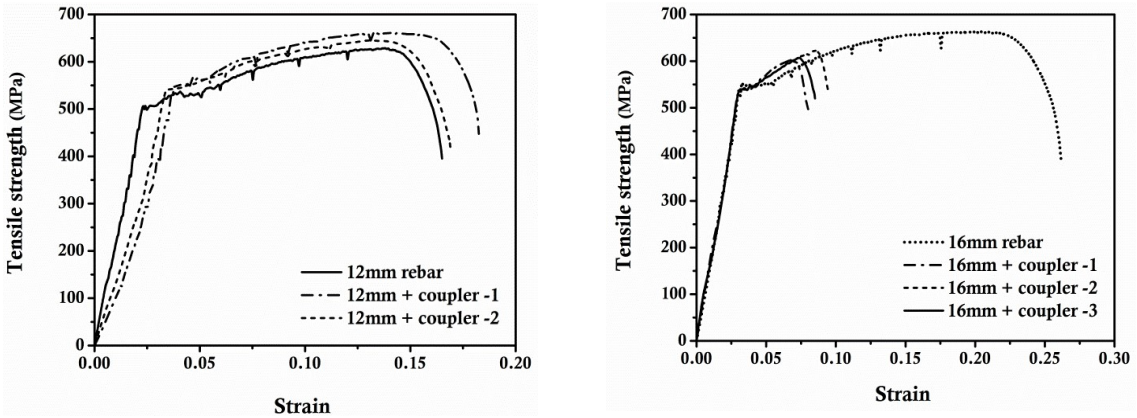

(a) Stress – strain of 12mm diameter (b) Stress – strain of 16mm diameter

Figure 7.3: Tensile behavior of rebar with and without coupler

The tensile behavior of reinforcing bar of 12 mm diameter with couplers exhibits nearly similar responses as observed in original reinforcing bar. An initial slip is observed but as the load increases, the reinforcing bar yields in similar fashion as in case of original reinforcing bar without failure of coupler that can be evident from the failure pattern of the specimen shown in Figure 7.4. The yield and ultimate strength of reinforcing bar of 12 mm with coupler is about 540 MPa and 640 MPa respectively with a 1.2 UTS/YTS ratio.

(a) Control rebar failure (b) Rebar slipping (c) Rebar yielding failure

Figure 7.4: Failure pattern of tensile specimens

A low post-yield deformation is observed under the tensile test of reinforcing bar of 16mm diameter with couplers as compared to original companion specimen. The coupler specimen starts to slip after attaining the peak load instead of yielding as in the case of original companion specimen as shown in Figure 7.5. However, the yield and ultimate strength of coupler specimen is 540 MPa and 620 MPa respectively which is nearly close of original companion specimens. As per code-of-practice, the considered tensile strength of reinforcing bar in design is 0.87 f_y. A slight improvement in tensile behaviour is also observed with the increase of length of coupler, number of bolts and strength of epoxy.

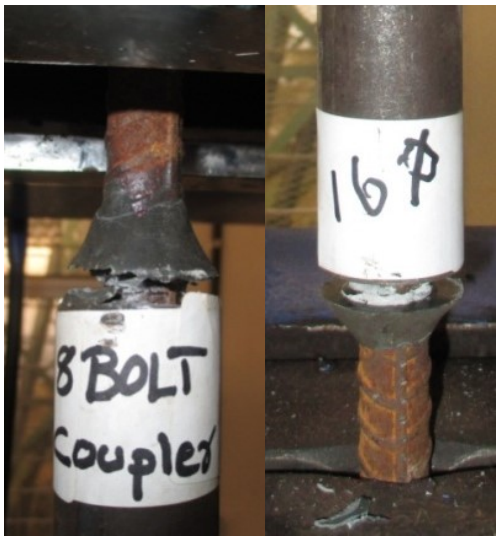

Figure 7.5: Failure pattern of 16mm dia. rebar with coupler under tension

7.4 Behavior of RC Beam Specimens with Coupler under Flexure

Four types of RC beam specimens with different reinforcement configurations were tested to evaluate the flexure behaviour of coupler as summarized in Table 7.2. The cross sectional size of the first three types of beam specimens was kept 100 mm x 150 mm with a span length of 1200 mm. Uniform 6mm diameter (Fe 250 grade) stirrups were provided at spacing of 150 mm but with different percentage of tension reinforcement (Fe 500 grade) as shown in Figure 7.6a. The cross section size of fourth specimen remained 150 mm x 200 mm with span length of 1400 mm as shown in Figure 7.6b. The couplers were used at two different locations, one at the centre of span and the other at the corner as shown in Figure 7.7.

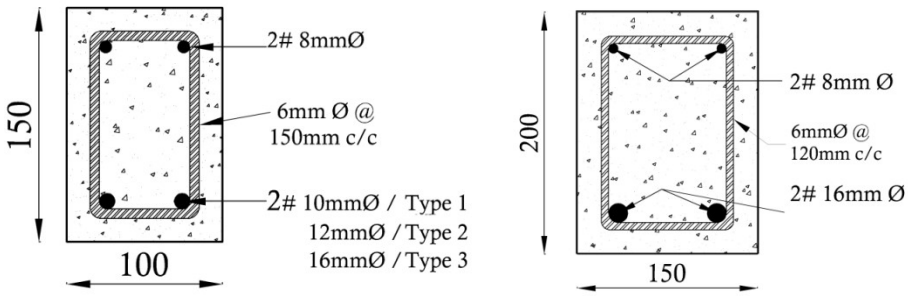

(a) Type 1-3 (b) Type 4

Figure 7.6: Typical cross section and reinforcement details of all types of RC beams

One specimen of each type of beam known as conventional specimen was also tested under similar conditions for the comparison of test results with the coupler beam specimens. The same type of couplers were used to connect the 10 mm and 12 mm

diameter longitudinal reinforcement in first two types of beam specimens with a typical detail of coupler connection as shown in Figure 7.7-7.8. The sequence of coupler connection at the two ends of reinforcing bar consisted of (a) inserting each end of reinforcing bar into the coupler, (b) tightening of external bolts (c) sealing of both sides of the coupler with a sealant and (d) pumping of epoxy into the coupler through a bolt hole.

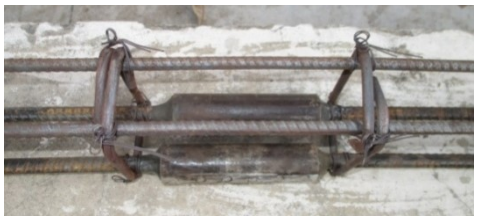

(a) CB 121

(b) CB 122

(c) LB 162

Figure 7.7: Details of rebar coupler connection in second and third type

(a) Rebar connection using coupler at center in CB 102 and CB122

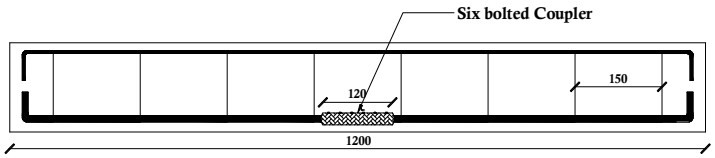

(b) Typical details of beam specimen CB 121

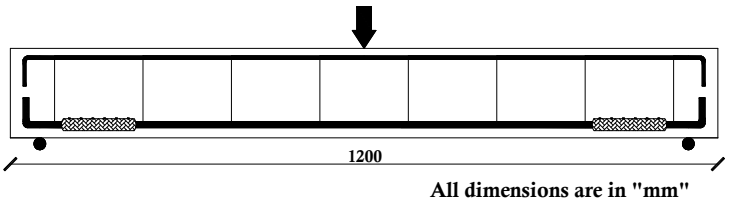

(c) Typical details of beam specimen CB 122

Figure 7.8: Typical RC beam specimen's reinforcement and coupler connection details

Table 7.2: Detailed configuration of RC beams with and without coupler

Specimen		Reinforcement Configuration *(Fe 500 grade)*	Stirrups *(Fe 250 grade)*	Length of the beam	Configuration	Coupler location in tension rebars
Type 1						
CB 101		2 # 8Ø @ top 2 # 10Ø @ bottom	6 Ø @ 150mm c/c	1200 mm	Control beam I	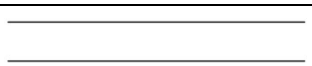
CB 102	**1**				Couplers connected the rebar@ centre	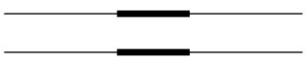
	2					
Type 2						
CB 121		2 # 8Ø @ top 2 # 12Ø @ bottom	6 Ø @ 150mm c/c		Control beam II	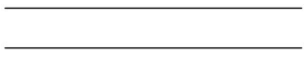
CB 122	**1**				Couplers connected the rebar @ centre	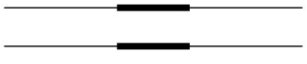
	2					
CB 123	**1**				Couplers connected the rebar @ corner	
	2					
Type 3						
CB 161		2 # 8Ø @ top 2 # 16Ø @ bottom	6 Ø @ 150mm c/c		Control beam III	
CB 162	**1**				Couplers connected the rebar @ corner	
	2					
Type 4						
LB 161		2 # 8Ø @ top 2 # 16Ø @ bottom	6 Ø @ 120mm c/c	1400 mm	Control beam IV	
LB 162	**1**				Couplers connected the rebar @ corner	
	2					

7.4.1 Moment-Curvature Behavior of RC Beam Specimens

The moment-curvature response of each type of beam specimen reflects the efficacy of the coupler connection in 10 mm diameter rebar as shown in Figure 7.9. The conventional specimen CB101 shows gradual degradation in moment after peak because of the inclined shear cracks. In presence of coupler, vertical cracks form and widen at the mid span that show improvement in the post elastic behavior. The observed curvature at failure in specimen CB102 shows the enhanced inelastic response of about 25% as compared to conventional beam specimens CB101. The rebar connected beam specimens withstand higher deflection without any rebar slip or pull out from the coupler that clearly manifests the efficacy of the coupler in lower diameter of reinforcing bar.

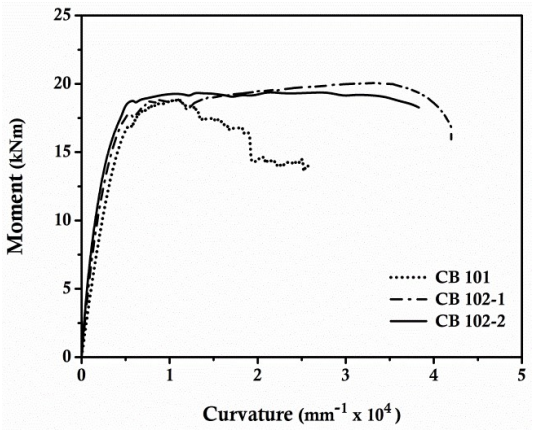

(a) 10 mm dia. coupler RC beams

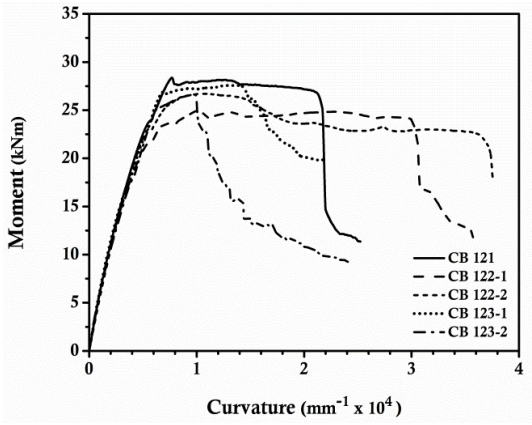

(b) 12 mm dia. coupler RC beams

Figure 7.9: Moment curvature relationship of (a) Type 1 and (b) Type 2 specimens

The conventional specimen CB 121 exhibits ductile response up to curvature 2 $\times 10^4$ mm^{-1} followed by shear cracks in hinge region. Post yield deflection without any sudden drop is noticed in beam specimen CB 122 with coupler connection in 12 mm dia. rebars. The beam specimens (CB 122) at the centrally located coupler encounter sudden drop in moment at curvature 3×10^4 mm^{-1} whereas the conventional specimen (CB 121) fails at curvature 2×10^4 mm^{-1}. It authenticates the effectiveness of the coupler even after yielding of specimen. Beam specimen (CB 123) i.e. coupler at both the corner shows reduction in moment after peak due to the formation of early shear cracks. The post yield behaviour of beam specimens (CB 123) is slightly lower as compared to conventional specimen.

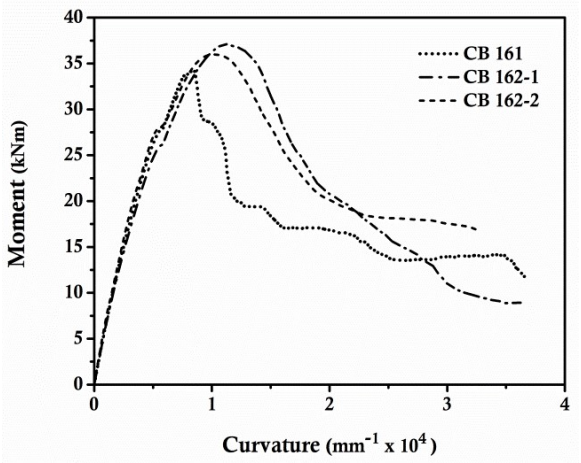

(a) 16 mm dia. coupler RC beams

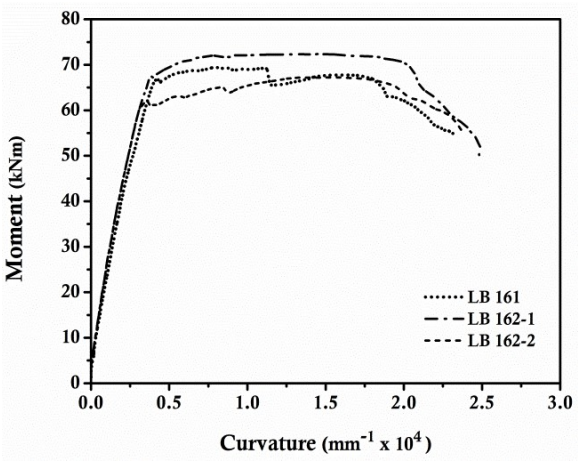

(b) 16 mm dia. coupler RC beams

Figure 7.10: Moment curvature relationship of (a) type 3 and (b) type 4 beam specimens

The moment-curvature behavior of beam specimens with and without couplers (CB 161 and CB 162) is nearly the same as shown in Figure 7.10a. In both types of beam specimens a sharp decrease in moment carrying capacity is observed as curvature increases. This may be due to the short span of beam specimen with moderate confinement and higher percentage of tension reinforcement. In long span beam specimens with and without couplers (LB 161 and 162), nearly the same and stable post-yield behavior is observed as shown in Figure 7.10b. It proves that the couplers are able to transfer the load effectively in flexure under large deflection.

7.4.2 Stiffness and Strength Degradation

The post elastic strength degradation over yield load [$F_{Deg\%}$] and post elastic stiffness degradation over yield stiffness [$K_{Deg\%}$] are estimated the inelastic behavior of all test specimens. The measured stiffness and strength degradation over post-elastic drift for all test specimens are shown in Figure 7.11. In conventional beam specimen (CB 101), there is a reduction of 30% in strength at the post yield rotation of 0.06 radian. However, the coupler beam specimens (102) sustain a load upto a curvature of 0.10 radian without significant loss in strength. It underlines the efficacy of coupler under flexure even after yielding of beam specimens.

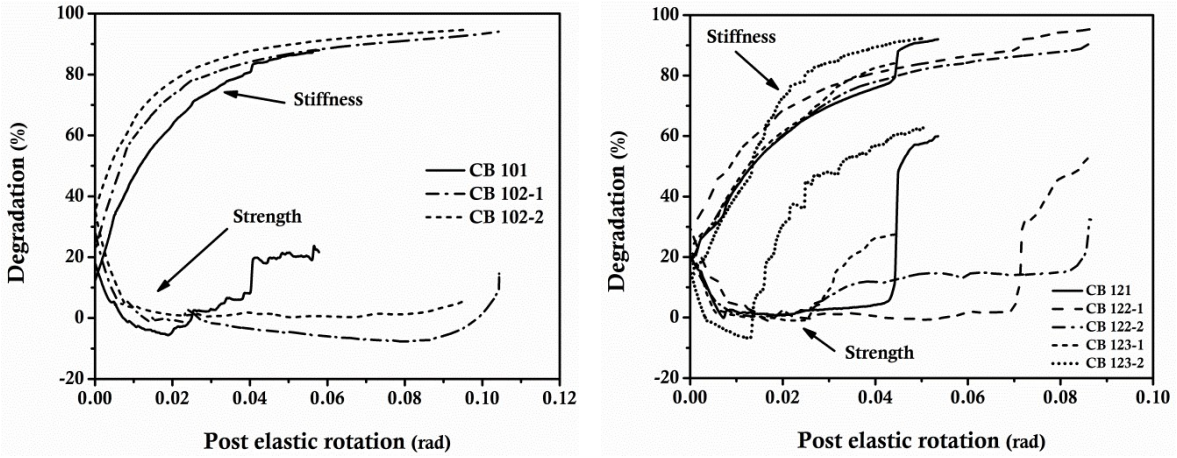

(a) 10 mm dia. coupler RC beams (b) 12 mm dia. coupler RC beams

Figure 7.11: Strength and stiffness degradation of (a) Type 1 and (b) Type 2 specimens

The strength and stiffness degradation plots of beam specimens with couplers (122 and 123) are more stable and the rate of degradation is low even at the higher rotation as compared to conventional specimens (CB 121) as shown in Figure 7.13b. The couplers are effective to connect the reinforcing bar and able to resist the load under the flexure similar

to beam specimen without coupler. A higher rate of strength and stiffness degradation after yielding is observed in conventional beam specimen (CB 161) as compared to coupler enabled beam specimen (CB 162) as shown in Figure 7.12. At the rotation of 0.02 radian the loss of stiffness in beam specimen (CB 162) is 60% in comparison to 80% in conventional specimen.

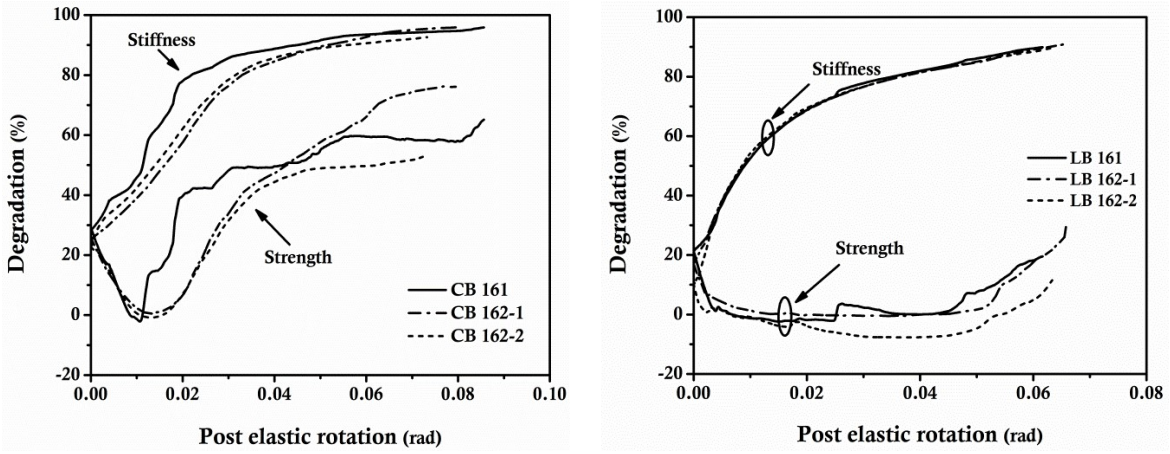

(a) 16 mm dia. coupler RC beams (b) 16 mm dia. coupler RC beams

Figure 7.12: Strength and stiffness degradation of (a) Type 3 and (b) Type 4 specimens

The stiffness and strength degradation plot of Type 4 specimen shows that the performance of both conventional (LB 161) and coupler connected specimen (LB 162) remains comparable even after post yield rotation. The stiffness degradation plot of Type 4 beam specimen (CB 161) unveils the actual response of 16 mm coupler connection under flexure. The large cross sectional area and increased span length allow the beam specimens to deflect under flexure without any shear failure.

7.4.3 Energy Absorption

The post yield behavior of a structural member can be estimated in terms of energy absorption calculated on the basis of area enclosed by the load-deflection curve and shown in Figure 7.13. The energy dissipation in coupler beam specimens is nearly 2 times higher as compared to conventional beam specimen (CB 101). The dissipated energy of coupler specimens (CB 122-1/2) is also comparatively higher as compared to conventional specimens (CB 123). The shear cracks in the conventional beam specimen (CB 121) of Type 2 restrict the post yield response and are unable to dissipate higher energy as compared to coupler beam specimen CB 122. The specimens CB 123 exhibits similar response as shown by the specimen CB 121 in dissipation of energy. The energy

absorption of coupler beam specimens of Type 3 (CB 162) and Type 4 (LB 162) is comparable to respective conventional specimens (CB 161 and LB 162).

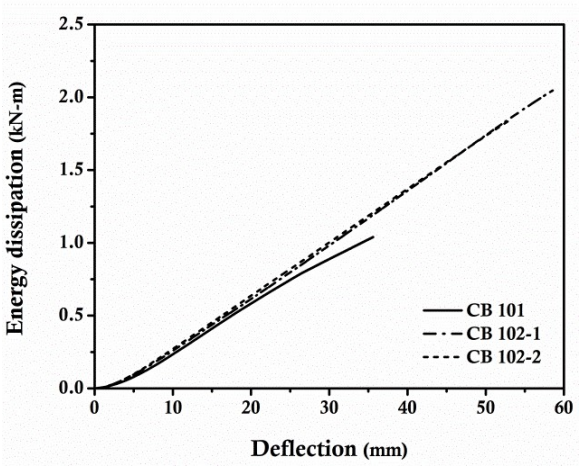

(a) 10mm dia. coupler RC beams

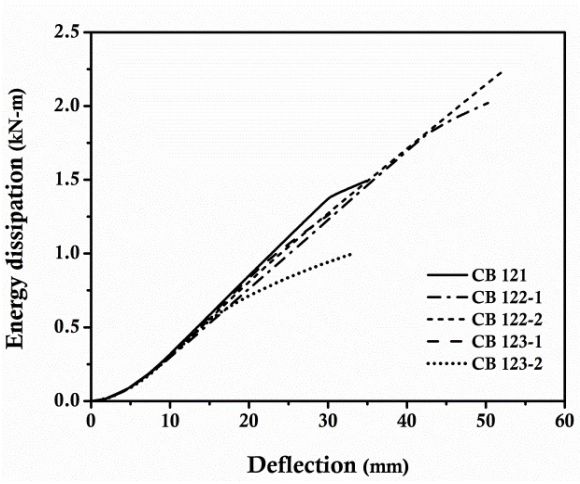

(b) 12mm dia. coupler RC beams

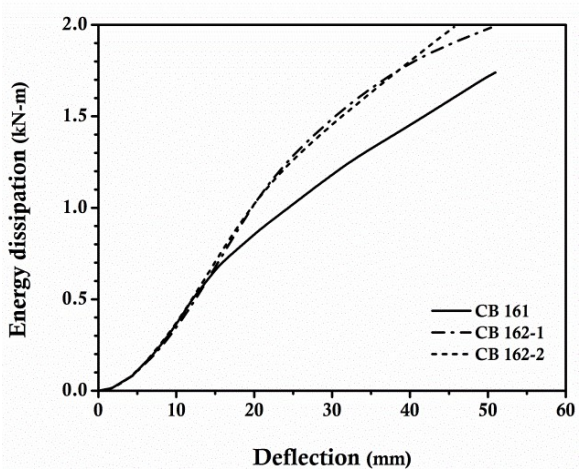

(c) 16 mm dia. coupler RC beams

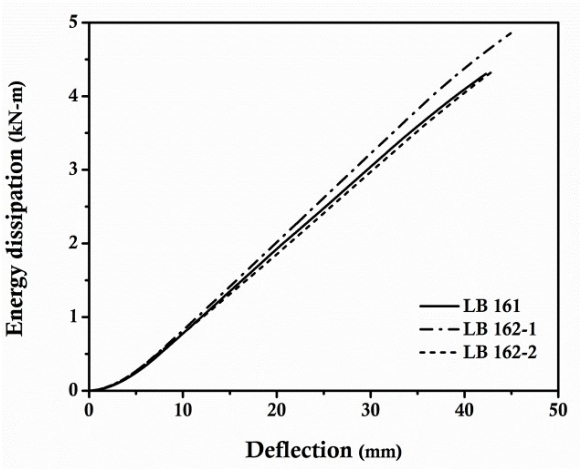

(d) 16 mm dia. coupler RC beams

Figure 7.13: Energy dissipation of all test specimens

7.4.4 Crack Pattern and Damage Index

The formation of cracks and its propagation are monitored and marked on the surface of the beam specimens during testing. The observed crack patterns and mode of failure of all tested beam specimens are shown in Figure 7.14. In conventional beam specimen CB 101, initially vertical cracks are observed which turn inclined as the load increases near the point of loading as shown in Figure 7.14a. The widening of inclined cracks reduces the load carrying capacity of the specimen. In centrally located coupler beam specimen (CB 102), the cracks initiate at both the ends of the coupler as depicted in Figure 7.15 and widen towards the loading point.

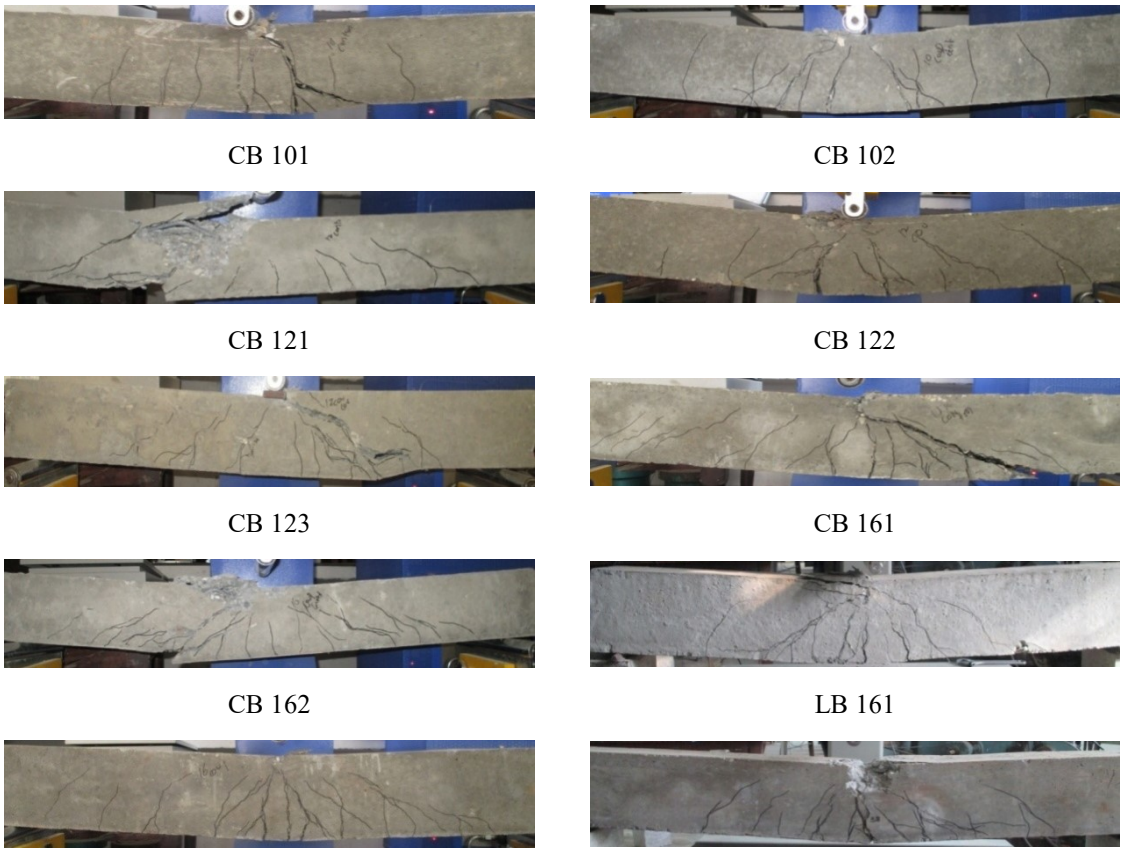

Figure 7.14**:** Crack pattern of RC beam specimens

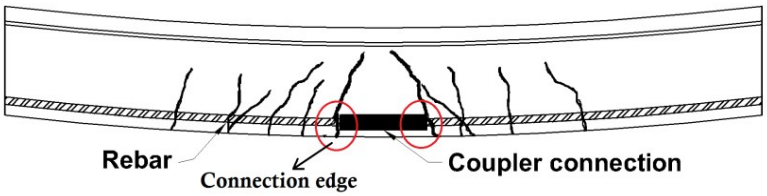

Figure 7.15: Cracking behavior of CB 102

As the load continues, the deflection increases, the reinforcement starts to bend at the edge of coupler without any deformation in coupler and finally the specimen fails in flexure as shown in Figure 7.16. The close-up view of the coupler connection allows the reinforcing bar to bend without slip. The conventional beam specimen (CB 121) fails in shear with the growth of inclined cracks while coupler enabled beam specimen (CB 122) exhibits vertical flexure cracks as shown in Figure 7.14. The cracking and failure behavior of coupler beam specimen (CB 122) are nearly the same as exhibited by beam specimen (CB 102) in Figure 7.15. The cracking behavior and crack formation near the ends of coupler are clearly shown in Figure 7.16 as marked in black color. There is no indication of any slip of reinforcing bar at the couplers in specimen CB 122. In corner located coupler

beam specimen (CB 123), inclined cracks initiate at the ends of the coupler and widen as the deflection increases as shown in Figure 7.17. The coupler specimen significantly resists the load and transfers the applied stress effectively through the connection without failure slip of reinforcing bar as exhibited in Figure 7.18.

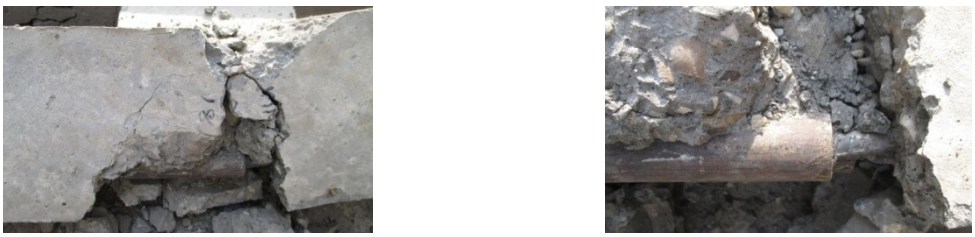

(a) coupler connection after failure (b) Close-up view of connection

Figure 7.16: Coupler connection after beam failure

(a) coupler connection after failure (b) Close-up view of connection

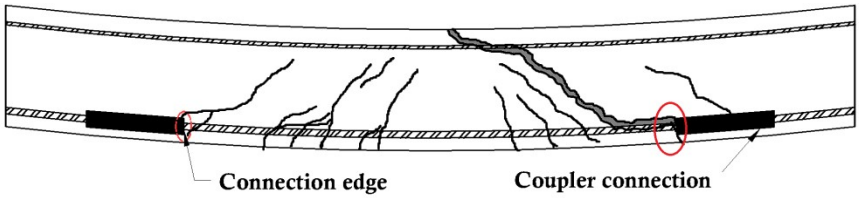

(c) Cracking behavior and failure pattern of CB 123

Figure 7.17: Cracking behavior and failure pattern RC beams

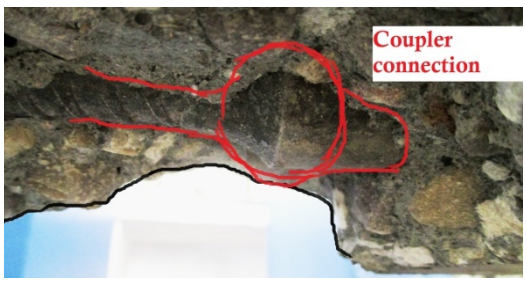

Figure 7.18: Coupler connection in CB 162 after specimen failure

The coupler beam specimens (CB 161 and 162) of Type 3 and beam specimens (LB161 and LB 162) show similar kind of cracking and failure pattern. Initially flexural

cracks are observed in the middle region but as the load increases further cracks are noticed across the span and finally specimens fail in flexure as shown in Figure 7.19. This failure pattern proves the active coupler connection in stress transfer without any brittle failure. There is no significant difference in crack pattern between the control and coupler enabled specimens.

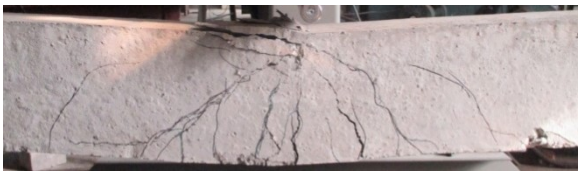

(a) LB 161

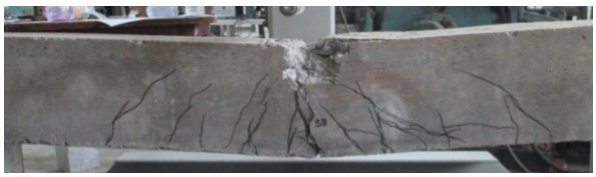

(a) LB 162

Figure 7.19: Failure pattern of Type 4 beams

7.4.5 Damage Index

Modified flexural damage ratio (MFDR) of beam specimen with and without coupler is used to compare the damage vs. post yield deformation in the form of ductility as given in Equation 6.1.

$$MFDR = \left[\frac{\frac{\phi_x}{M_x} - \frac{\phi y}{M_y}}{\frac{\phi_m}{M_m} - \frac{\phi y}{M_y}} \right] \qquad \textbf{7.1}$$

This MFDR is defined as the ratio between the secant stiffness at the onset of failure (M_m/ϕ_m) and the minimum secant stiffness (M_x/ϕ_x). The term (M_y/ϕ_y) is the initial elastic stiffness of the member. The MFDR values vary from 0 to 1, whereas "0" indicates no damage and "1" indicates the onset of failure of the member. The calculated MFDR of each specimen is plotted against ductility as shown in Figure 7.20. The MFDR results indicate that the coupler enabled specimens possess better damage tolerance capacity over respective control specimens. It proves that the proposed couplers are able to effectively connect the two ends of reinforcing bar and participate actively in stress transfer mechanism.

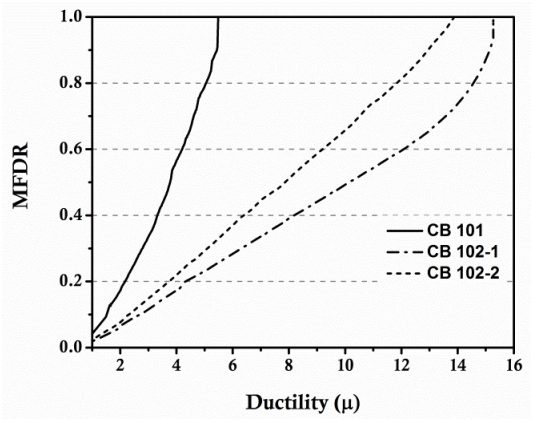

(a) 10 mm dia. coupler RC beams

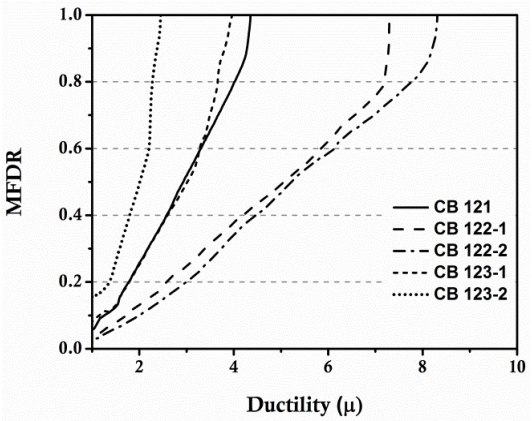

(b) 12 mm dia. coupler RC beams

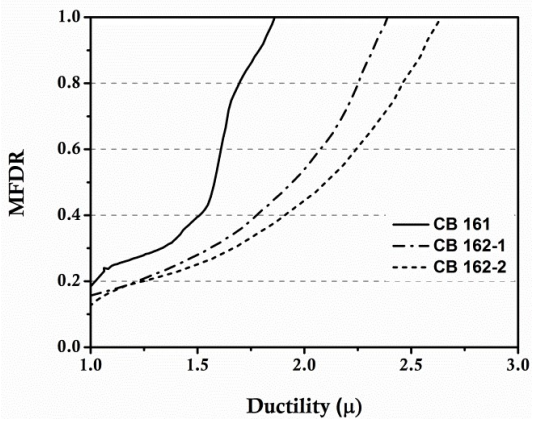

(c) 16 mm dia. coupler RC beams

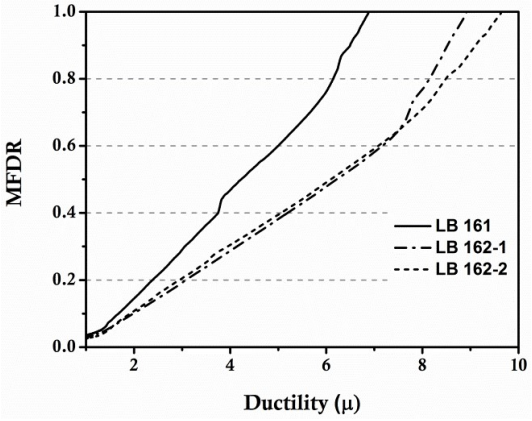

(d) 16 mm dia. coupler RC beams

Figure 7.20: Damage index of all type beam specimens

7.5 Cyclic Behavior of beam-column joint specimens with Coupler

Two types of exterior beam-column joint specimens are tested under cyclic loading in quasi-static test facility to evaluate the hysteresis behavior of coupler enabled joint specimens under cyclic loading. The complete details of beam-column joint specimens with different types of coupler connections are given in Table 7.3. The reinforcing details of both types of beam-column joint specimens (CEJ2 and CEJ3) are the same except the position of the coupler at the joint as shown in Figure 7.21. In beam-column joint specimens CEJ 2 and CEJ 3, both the longitudinal reinforcing bars of left side are intentionally cut near the joint but within plastic hinge region at two different locations (110 mm and 80 mm). They are connected with the help of couplers with the same procedure as described in previous section. Figure 7.21 (c) shows the typical coupler connection in beam-column joint specimens. In cyclic testing of beam-column joint specimens with and without coupler, beam portion is kept 90° vertical and the column portion of the joint is kept in the horizontal position held against the strong floor. Both

ends of the column are supported using hydraulic jacks to apply axial load as shown in Figure 7.22. The joints are tested under displacement controlled hydraulic actuator. One end of the actuator is connected to the free end of the beam and the other end is connected to reaction wall. The specimens are tested up to failure and their corresponding load deformation response is recorded with the help of load cell and LVDT.

Table 7.3: Detailed configurations of beam-column joint specimens

Specimen	Reinforcement configuration	Stirrups	Length of the beam	Configuration	Coupler location in tension rebars
CEJ 1	2#12Ø @ top and bottom of beam and column	6 Ø @ 100mm c/c	1000	Conventional specimen	-
CEJ 2				Coupler enabled specimen	Couplers connected the rebar @ joint faces in pushing direction
CEJ 3				Coupler enabled specimen	Couplers connected the rebar @ joint faces in pulling direction

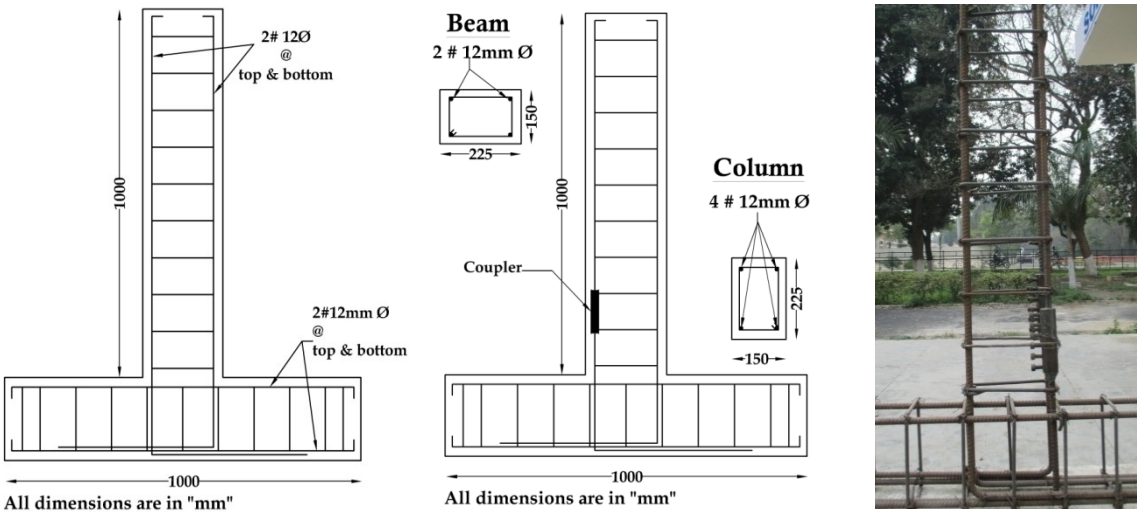

(a) CEJ 1 (b) CEJ 2 (c) Typical connection

Figure 7.21: Detailed configuration of beam-column joint with and without coupler

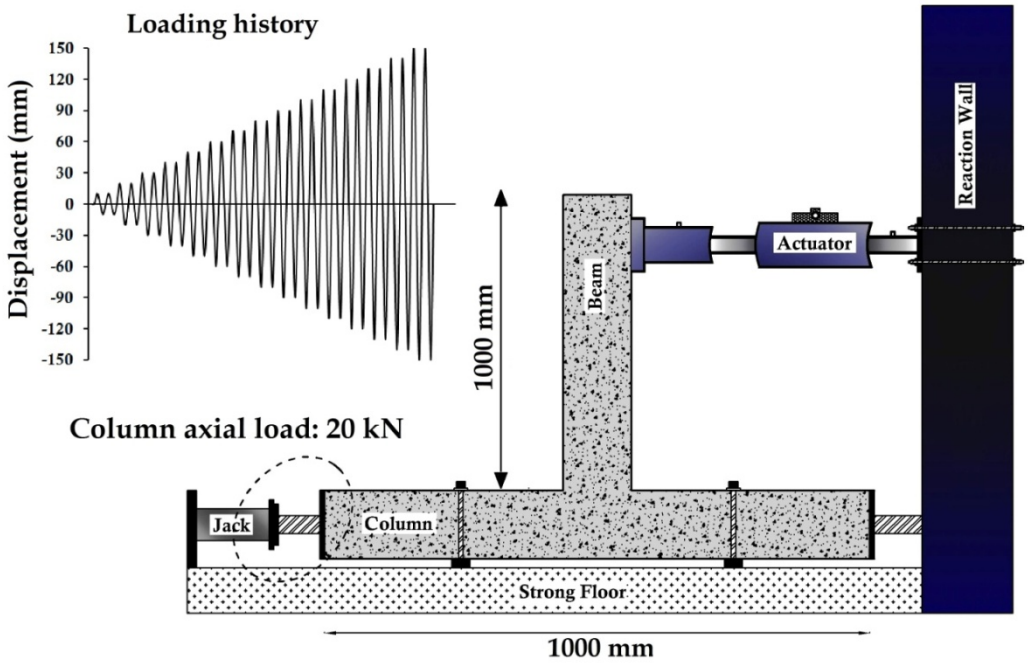

Figure 7.22: Beam-column joint cyclic test setup

In the three beam-column joint specimens, flexural cracks are noticed initially in the beam hinge region as shown in Figure 7.23a. As the deformation increases, formation of diagonal cracks also begins in the joint region as shown in Figure 7.23b. A spalling of concrete cover in the joint region is observed at a deformation of 60 mm. Afterwards a sharp decrease in load capacity is noticed in the specimens. The pattern of failure of coupler enabled specimens CEJ 2 and CEJ3 is nearly the same as conventional specimen. There are no additional cracks due to the presence of coupler in the hinge region. Figure 7.24 shows the post failure analysis of coupler connection; it authenticates the coupler activeness in rebar connection. It proves the effectiveness of the coupler in the beam-column joint region.

The load-deformation hysteresis curves of tested joint specimens are shown in Figure 7.25. There is minor punching effect in the specimen CEJ 3 due to the formation of early shear cracks in the joint region that affects the inelastic performance of the joint. It is also observed from the envelop of load-deformation curves that the performance of coupler enabled specimens is completely at par with the conventional specimen CEJ 1 even with improved post-yield behaviour. The coupler enabled specimens are tested up to 80 mm deformation to ensure the coupler activeness until failure. There is no evidence of connection failure and rebar slip from the coupler which is observed after the removal and chipping off the damaged concrete.

(a) CEJ 1 (b) CEJ 2

Figure 7.23: Failure pattern of CEJ 1 and CEJ 2

(a) Coupler location (b) Rebar buckling (c) Active coupler connection

Figure 7.24: Post failure analysis

Figure 7.26 shows energy dissipation of all the three beam-column joint specimens with and without coupler. The curves are identical up to a displacement of 40 mm and even afterwards there is no significant difference. Thus the energy dissipation of coupler enabled specimens is nearly same as conventional specimen that again confirms the effectiveness of coupler in connecting the reinforcing bars even in the joint region. Figure 7.27 shows the stiffness and strength degradation plots of coupler enabled beam-column joint tested specimens. There is no early degradation in stiffness and strength as compared to conventional joint. The couplers are able to transfer the forces from one member to another without any slip and failure with better stiffness retention capacity as compared to

conventional specimen. Again there is no remarkable difference in strength and stiffness degradation plot of coupler enabled specimen and conventional specimen. The damage index (DI) vs. post yield deformation curves as shown in Figure 7.28 also exhibits that the damage tolerance capacity of coupler enabled specimen is comparable to conventional specimen. In view of the discussed parameters about the effectiveness of coupler under tension, flexure and shear pave the path for further confidence in the use of coupler in the retrofitting of buckled reinforcement at the plastic hinge region of structural member.

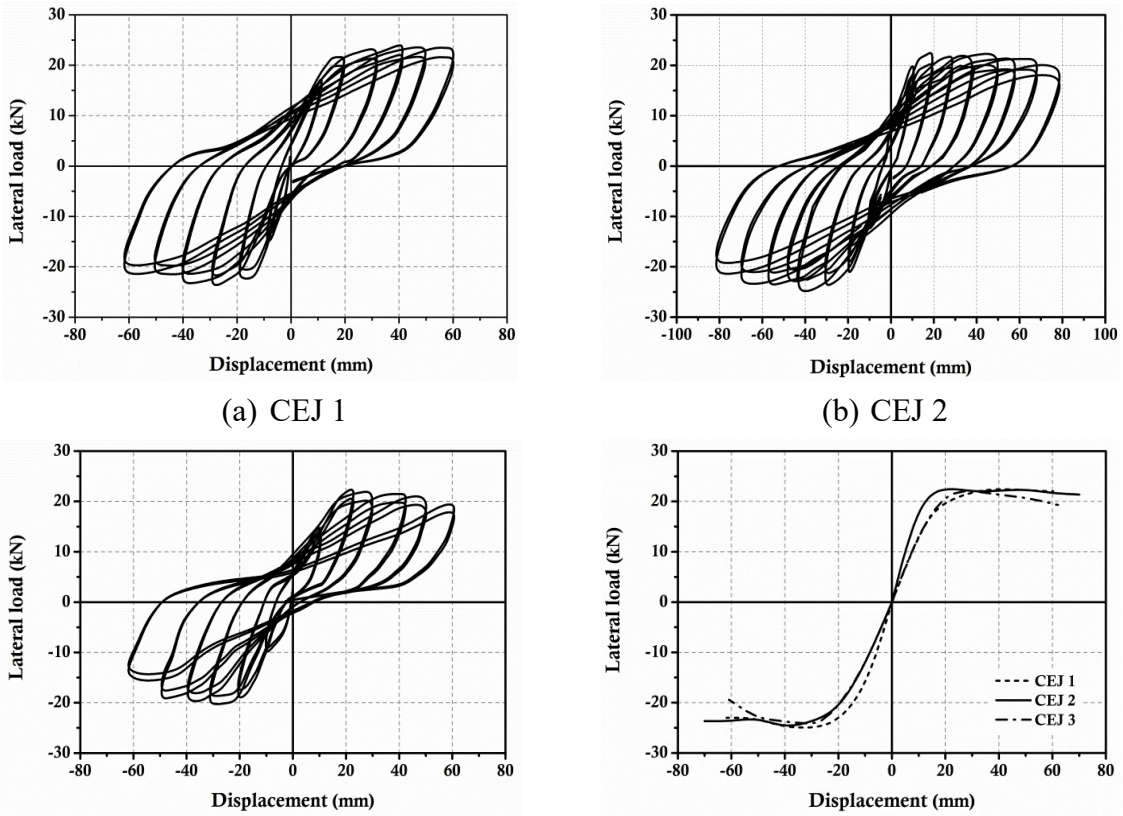

(a) CEJ 1 (b) CEJ 2

(c) CEJ 3 (d) Envelope curve

Figure 7.25: Hysteretic curve of all tested specimens

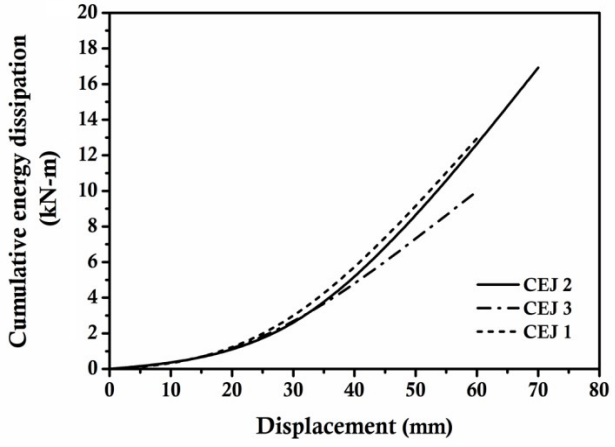

Figure 7.26: Cumulative energy dissipation

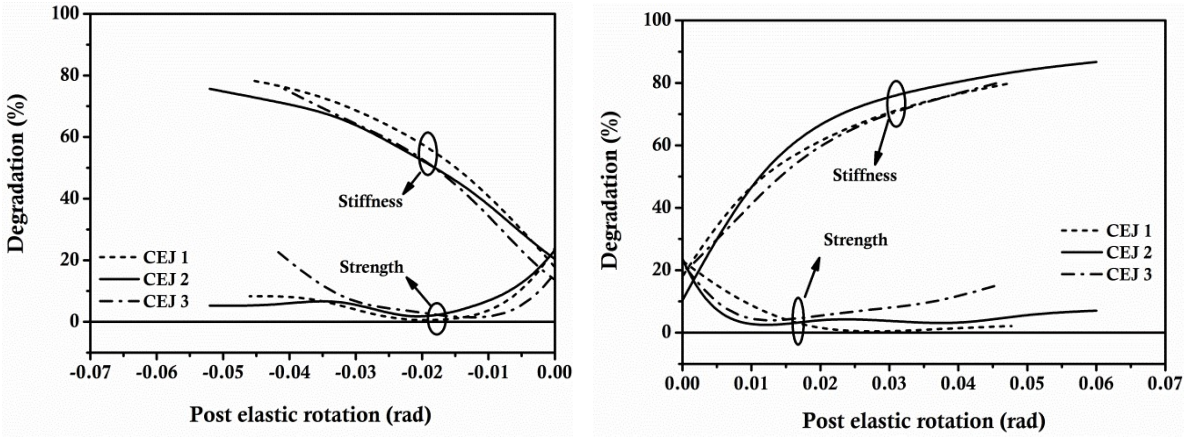

(a) Negative pull (b) Positive push

Figure 7.27: Stiffness degradation plot

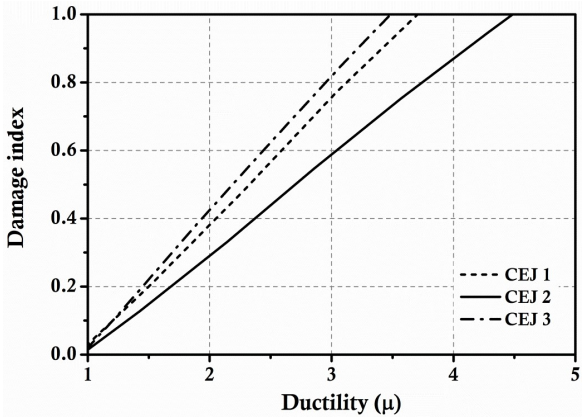

Figure 7.28: Damage index vs. ductility

7.6 Findings

The proposed study is focused on the behavior of coupler in rebar connection of flexural and beam-column joint members and compares the results with the conventional companion specimens. Four types of beam specimens and two types of beam-column joint specimens are prepared under different diameters of longitudinal tension bars. These specimens are tested under static and cyclic loading. Following are the main conclusions of the study;

1. The coupler may be a very practical and viable solution for the retrofitting of damaged structures under earthquake or other environmental reasons to restrain the load carrying capacity of structural member. The couplers are more effective in lower diameter of reinforcing bars and the efficacy of the coupler may be restricted up to a certain diameter of connecting two cut/broken longitudinal bars.

2. The proposed coupler configuration is more effective and practical as compared to conventional type of couplers being used in the field. The external threaded bolts are able to restrict the slippage as well as apply the confining pressure on existing reinforcing bar which is the partial substitution of bond length. The efficiency of the coupler is further improved by filling the space between the coupler and reinforcement with a high strength epoxy.
3. The tensile test of reinforcing bar upto 12 mm diameter with epoxy filled threaded bolts coupler is nearly the same as original reinforcement. However, reinforcement with 16 mm diameter with the same type of coupler performs identically upto the yield point as in case of original reinforcement. The post yield behaviour of proposed coupler is also reasonably satisfactory since limit state of reinforcement in structural member is 0.87 *fy*.
4. The load - deflection plot under flexure test of beam specimens with and without couplers and the subsequent interpretation of result are in the form of M-Ø analysis, strength and stiffness degradation plot, energy dissipation and finally damage index authenticates the effectiveness and efficacy of coupler in flexure.
5. The hysteresis behavior of beam-column joint specimens with and without coupler and the subsequent interpretation of results are hysteretic curve, strength and stiffness degradation plot, energy dissipation and damage index that authenticate the effectiveness and efficacy of coupler connection under cyclic loading
6. The practical application of the couplers in axial, flexure and joint members again requires a systematic experimental test programme. The coupler technology in the field of retrofitting of RC members is a mile stone in case of structural damage in earthquakes, particularly where buckling of longitudinal reinforcement occurs.

References

Ahmed, E., and Hatem, M. M., (2014), "Effect of tension lap splice on the behavior of high strength concrete (HSC) beams," *HBRC Journal*, 10,287–297.

Azizinamini , A., Stark, M., Roller, J., and Ghosh, S., (1993), "Bond performance of reinforcing bars embedded in high-strength concrete," *ACI Structural Journal*,90(5),554–561.

Bilal, S. H., Harajli, M. H., and Ghaida, J., (2001), "Effect of fiber reinforcement on bond strength of tension lap splices in high strength concrete," *ACI Structural Journal*, 98(5),638- 647.

Esfahani, R., and Rangan, V., (1998), "Bond between normal strength and high-strength concrete (HSC) and reinforcing bars in splices in beams," ACI *Structural Journal*, 95(3), 272- 280.

Ezeldin, A. S., and Balaguru, P. N., (1989), "Bond behavior of normal and high strength fiber concrete," *ACI Materials Journal*, 86(5),515-524.

Harajli, M. H., (2006), "Effect of confinement using steel, FRC, or FRP on the bond stress-slip response of steel bars under cyclic loading," *Materials and Structures*, 39,621-634.

Hosny, A., Hatem, M. S., Sami, H. R., and Paul, Z., (2012), "Development length of unconfined conventional and high-strength steel reinforcing bars," *ACI Structural Journal*,109(5), 655-664.

Roufaiel, M., and Meyer, C., (1987), "Analytical modelling of hysteretic behavior of R/C frames," *Journal of Structural Engineering*, 113(3), 429–444.

Tarabia, A. M., Shoukry, M. S., and Diab, M. A., (2010), "Improving the behavior of reinforced concrete beams with lap splice reinforcement," *Challenges, Opportunities and Solutions in Structural Engineering and Construction – Ghafoori (ed.),* Taylor & Francis Group, London, 81-86.

Zuo, J., and Darwin, D.,(2000), "Splice strength of conventional and high relative rib area bars and high strength concrete," *ACI Structural Journal*, 97(4),630–641.

Chapter 8

Cyclic Testing of Retrofitted Columns with Buckled Reinforcement - An Experimental Case Study

8.1 Introduction

Earthquake damage survey reports of the past reveal that the buckling of main longitudinal reinforcement of axial members in the plastic hinge region is the most common mode of failure. It is mainly due to inadequate shear reinforcement, improper confinement of core concrete and large tie spacing. The repair and retrofitting of buckled reinforcement at the plastic hinge region of a column/pier under the heavy axial load is a challenging and realistic task since a large number of buildings need to be demolished due to this kind of failure. The common retrofitting solution under this situation is to replace the buckled portion of reinforcement with new reinforcement through welding. The difficulty in welding is that it requires removal of large intact concrete at both the sides of the damaged portion of column in order to expose the required length of un-yielded existing reinforcement for welding of new reinforcement. The present research work investigates an alternative and innovative approach to retrofit the buckled longitudinal reinforcement by using an epoxy filled mechanical coupler. External FRP wrapping at the buckled regions may also be used to provide an external confinement. The effectiveness of epoxy filled coupler with and without FRP wrapping is evaluated by carrying out cyclic testing of four retrofitted columns and the results are compared with welded reinforcement.

8.2 Early studies

Many studies were focused on seismic retrofitting of RC columns using RC jacketing, FRP jacketing with splice and with confining reinforcement and steel caging (Sengupta et al. 2003, Nagaprasad et al. 2009). In these studies the buckled reinforcement was removed and replaced by additional reinforcement of splicing in the hinge region with additional external jacketing. Raj et al. (1993) studied the use of external reinforced concrete jacketing and steel plate bonding for retrofitting of column but it increased in

dimension of column section as well as increased dead load on the structure. Hamid et al. (1997) studied the effect of FRP wrapping in repair of earthquake-damaged RC circular and rectangular columns with lap splice in the hinge region. In this study the buckled reinforcement was replaced by lap splice in the hinge region with external FRP confinement and better stiffness retention and ductility over original specimens were observed. Frieder et al. (1997) investigated the continuous CFRP wrapping in seismically damaged column retrofitting work. The columns were retrofitted with CFRP jacketing at different levels with and without lap splice in the hinge region. The results demonstrated that the CFRP jacketing exhibited good results and could act as an effective alternative for the conventional RC jacketing.

Pantelides et al. (2002; 2008; 2009; 2010) has studied the effect of FRP strengthening on various structural elements such as bridge piers and beam-column joints and observed strength enhancement using FRP strengthening. Xiao et al. (2003) studied the effect of partially stiffened steel jacketing in RC column retrofitting and observed enhanced shear and hysteresis behavior on the retrofitted deficient column. Richard et al. (2003) examined the CFRP confinement on strengthening and retrofitting of shear deficient square columns with axial load. The test results showed that the external CFRP confinement improved the hysteresis behavior and ductility of the shear deficient columns. Richard et al. (2004) retrofitted the shear deficient square column with CFRP confinement without increasing the flexural strength and initial stiffness and tested under cyclic loading with axial load. The test results showed that the external CFRP confinement on the non-seismically designed column improved the deformation capacity without increasing the strength. Prota et al. (2005) carried out an experimental investigation on seismic upgrade of under-designed RC square columns by combining steel spikes and GFRP laminates and suggested that the proposed method for the seismic strengthening of under-designed columns as very effective when necessary to relocalize the potential plastic hinges of columns by increasing their flexural strength. Cem et al. (2006) examined the external FRP wrapping using various FRP sheets in the plastic hinge regions to strengthen the element by external confinement. Dandapat et al.(2013) and Rimen et al. (2013) conducted an experimental study on the localized failure in FRP wrapped cylindrical concrete columns and studied the effect of imperfections at the interface between concrete and FRP and observed the presence of imperfect localization of deformation, adverse effect on the confining capacity of FRP, and reduction of the failure load.

8.3 Cyclic Testing of Retrofitted Columns with Buckled Reinforcement

Four columns with a cross sectional size of 275mm x 275mm with an effective height of 1.94m were tested under cyclic loading (Surya, 2010) as shown in Figure 8.1. The damaged columns were retrofitted with different types of schemes as illustrated in Table 8.1. The methodology adopted for the retrofitting of columns consisted of the following steps (i) to provide an additional support with the help of hydraulic jack and bracing before removing the cracked concrete in the damaged portion of the column (ii) the cracked concrete was completely removed in the affected region (iii) the buckled reinforcement was cut and removed as shown in Figure 8.2a (iv) after the reinforcement curtailment, the remaining buckled reinforcement was straightened manually as shown in Figure 8.2c, (v) the loose concrete surface was chiseled out and removed from the bottom foundation surface.

Table 8.1: Detailed configuration of column specimens

S. ID	Column reinforcement& Cross sectional size	Transverse reinforcement	Description
CF1	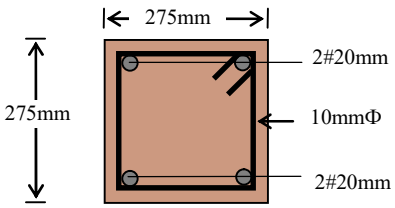	10mm Ø@300mm c/c	Control specimen
CF2		10mm Ø@300mm c/c + 6mm Ø in coupler region	Retrofitted by using coupler
CF3		10mm Ø@300mm c/c + 6mm Ø in welded region	Retrofitted by using welding
CF4		10mm Ø@300mm c/c + 6mm Ø in coupler region	Retrofitted using coupler +BFRP jacketing
CF5		10mm Ø@300mm c/c + 6mm Ø in coupler region	Retrofitted using coupler + CFRP jacketing

An eight bolt mechanical coupler with a length of 240mm with 4mm wall thickness was used to connect the two discontinuous ends of the reinforcing bar in the retrofitting work as shown in Figure 8.3a. In this coupler the inner surface was threaded to create friction resistance during loading, shown in Figure 8.3a. After connecting the broken reinforcement the vacuum space was filled with epoxy. This epoxy filler created better bond and increased the efficiency of frictional resistance.



(a) Impaired column members (b) Buckled reinforcement

Figure 8.1: Different failure pattern of conventional column members


(a) Foundation after removing the columns (b) Damaged concrete removed column


(c) Straightened buckled bar in column (d) Replacing the column again

Figure 8.2: Step-by-step retrofitting procedure for the buckling of reinforcing bar

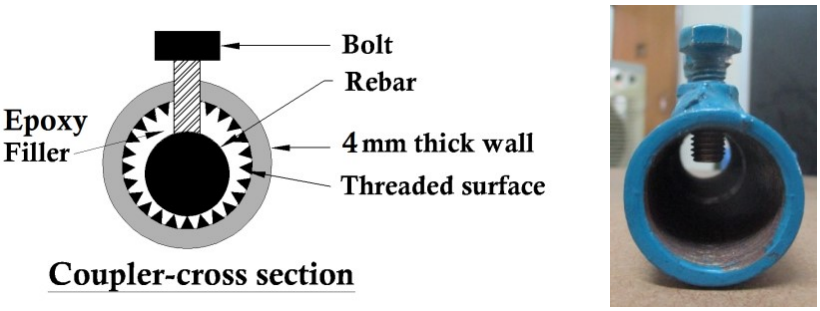

(a) Cross section of coupler (b) Typical coupler

Figure 8.3: Coupler configuration

The tensile behavior of the coupler connection is determined under uni-axial tensile test. Reinforcing bars of 200mm diameter were connected using a 120mm length coupler with four bolts (however in retrofitting of column, couplers of 240mm length with 8 bolts are used) and the vacuum space was filled with epoxy. The specimen resisted 350MPa before it starts to slip at the bottom portion as shown in Figure 8.4b. The average tensile strength and strain of the tested coupler specimen is shown in Figure 8.4a. This slipping behavior can be clearly understood from the stress vs. strain behavior of coupler.

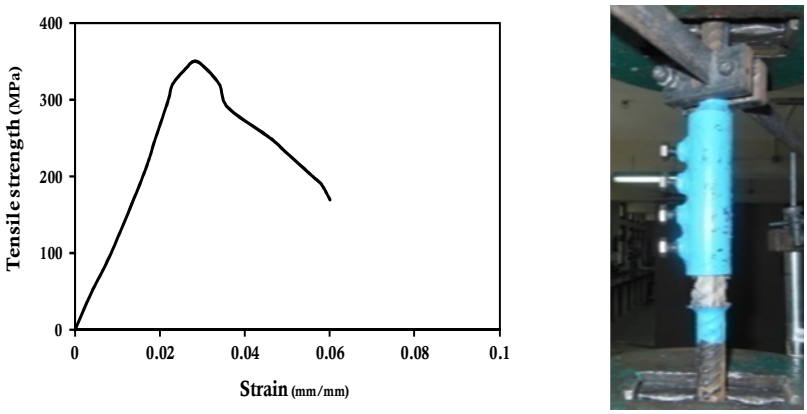

(a) (b)

Figure 8.4: (a) Stress strain graph of rebar with coupler (b) failure pattern

These couplers were inserted into the main bottom reinforcement and the other end of curtailed reinforcement of the column section was gradually inserted into the coupler, as shown in Figure 8.5. After insertion of both the curtailed ends of reinforcement into the coupler, the bolts were tightened properly. In order to increase stability of the connection, the vacuum space in the coupler was infiltrated by low viscosity epoxy binder as shown in Figure 8.5. Now the external support was released and the transverse reinforcement was inserted in the column member, Figure 8.5d.

One of the column members was retrofitted using welding technique. An additional 20mm diameter reinforcement bar with a length of 240 mm was used for welding to connect the curtailed rebar as shown in Figure 8.6. Welding was carried out from inside the column reinforcement; otherwise the concrete cover will get affected.

(a) Coupler connected in bottom portion (b) Column member connected (c) Epoxy infiltration (d) Extra confinement

Figure 8.5: Coupler connection procedure

(a) (b)

Figure 8.6: Retrofitted specimen using welding technique

After the reinforcement connection, the retrofitted region was filled with fresh concrete. To fill the concrete at the retrofitted portion, letter box type shuttering was used in order to avoid the contact problem between the existing concrete cut surfaces at both the ends with new concrete, as shown in Figure 8.7a-8.7b. Now, the specimens were properly cured for 28 days in laboratory. Among the four retrofitted columns two were additionally confined with external two layer of BFRP and CFRP sheet wrap in parallel and perpendicular direction, as shown in Figure 8.7d-8.7e. Before wrapping the FRP composites, the column concrete surface at the bottom region was thoroughly ground using grinding machine. After grinding, a primer coat was applied on the surface to fill the pores

and voids. After a day of curing, epoxy was applied on the primer surface to affix the FRP composites. Initially two layers of FRP in parallel as shown in Figure 8.7d to the column member were wrapped, afterwards FRP in perpendicular (Fig 8.7e) direction was wrapped on the existing parallel layer to increase the anchorage.

(a) Letter box form work | (b) Concerting | (c) Smoothened surface for FRP wrapping | (d) Epoxy application | (e) CFRP wrapping

Figure 8.7: Concreting and FRP wrapping procedure

8.3.1 Hysteretic Behavior of Column Specimens

Figure 8.8 shows the hysteresis behavior of retrofitted column specimens. The envelope curves of the five specimens are presented in Figure 8.9. In original specimen CF1, the yielding occurs at 35 mm deflection with the corresponding lateral load of 24 kN. The load remains constant in post-elastic range upto 115 mm deflections and afterwards it begins to degrade. The specimen fails at 140 mm deflection. The retrofitted column specimen CF2 with the mechanical coupler filled with epoxy shows entirely distinguished response over original specimen CF1. It shows higher yield load as compared to original specimen without manifesting of post- yield behavior. The mechanical anchorage connection through coupler does not behave perfectly as conventional reinforcing bar under tension since the reinforcing bars start slipping rather than elongated. The load-deformation behavior of specimen after the yielding entirely depends on the frictional force between the threaded surface and the reinforcing bar. Figure 8.8b shows a sudden drop in load at 85 mm deflection and a brittle failure is observed. It is also observed that loop area of specimen CF2 in each cycle is comparatively lesser than the original specimen CF1.

The column specimen CF3 is retrofitted with welding and it shows better pre and post yield deformation behavior rather than the original specimen CF. The connected region effectively transfers the applied load and allows the specimens to deform better than

conventional specimen CF1. At the deflection of 140 mm, the welded region breaks and the applied load drops suddenly. The column specimen CF 4, retrofitted by using coupler and wrapped with BFRP, behaves differently than the retrofitted specimen without FRP i.e. specimen CF 2. A sudden degradation in load is observed at 80 mm deflection and the specimen fails completely at 110 mm deformation as observed from the hysteresis loop. It shows the performance enhancement of rebar connector's activeness because of external confinement. Also the loop proves that the specimen encounters coupler failure but not so sudden as specimen CF2.

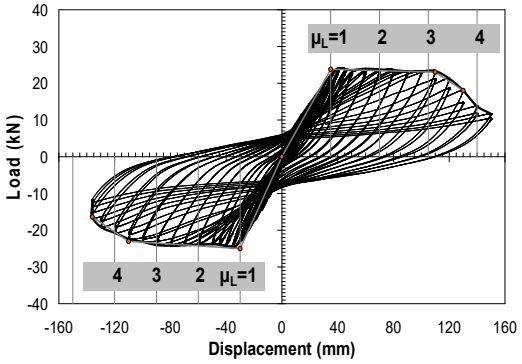

(a) CF1 - Conventional (Surya 2010)

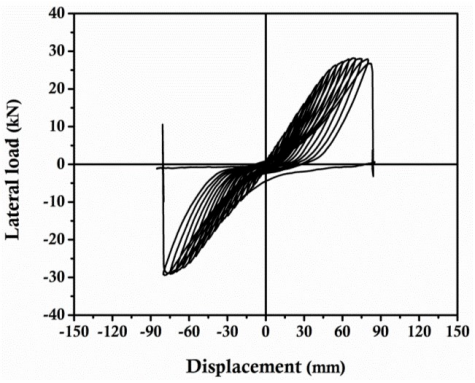

(b) CF2 – Retrofitted - coupler

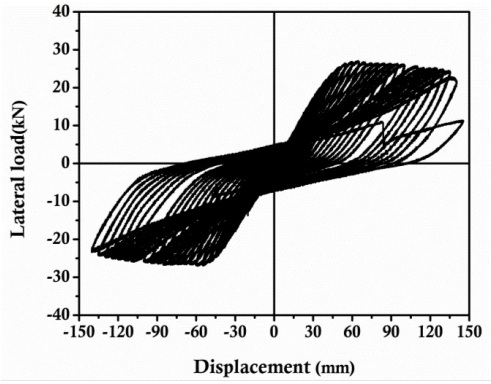

(c) CF3- Retrofitted - welded

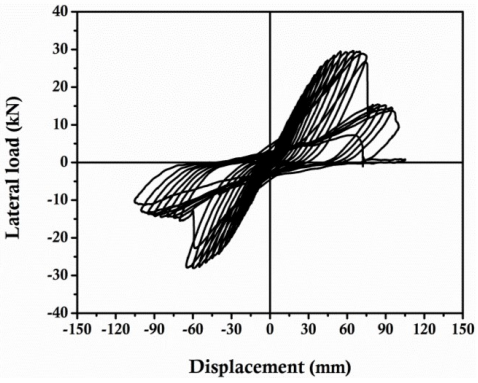

(d) CF4- Coupler - BFRP

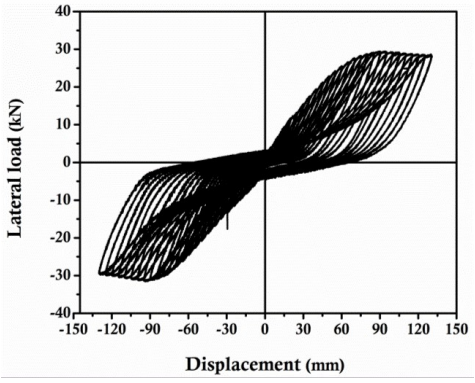

(e) CF5- Coupler - CFRP

Figure 8.8: Hysteresis curve of all tested specimens

The specimen CF 5, strengthened with CFRP wrapping shows enhanced post-yield performance over the other specimens. The higher tensile modulus of CFRP holds the column at top and bottom portions effectively and allows the coupler to transfer the load to the foundation. There is no sudden degradation in load or failure of reinforcing bar in specimen. The envelope curve of specimen CF5 is not only similar to the specimen CF1 but also manifests stable and enhanced deformation capacity even upto 140 mm. The additional CFRP confinement effectively confines the concrete and restricts the coupler failure. The effect of confinement holds the connected region actively to transfer the load and allows to rotate at foundation level.

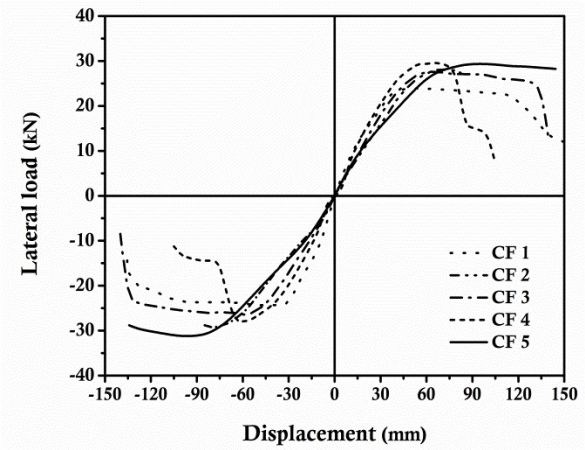

Figure 8.9: Envelope curve of all specimens

8.3.2 Stiffness and Strength Degradation

Figure 8.10 shows the strength and stiffness degradation over post elastic rotation of tested specimens. The retrofitted specimen CF2 manifests lesser post elastic rotation over the other specimen because of sudden failure of specimen after peak load. The rate of degradation is stable in welded specimen CF3 even at higher rotation. There is a loss of 70% stiffness over the post yield rotation of 0.045 radian. A low degradation in strength and stiffness is noticed from the plot of retrofitted specimen CF4 upto the rotation of 0.02 radian. Afterwards due to rupture of fiber and failure of coupler there is rapid increase in rate of degradation. The retrofitted specimen CF 5 with CFRP exhibits a stable behaviour as observed in original column CF 1 with very low rate of degradation. The external confinement enables to hold the coupler intact and allows the specimen to rotate at the bottom end. Coupler with CFRP wrapping is an effective and viable solution to the retrofitting of buckled reinforcing bar.

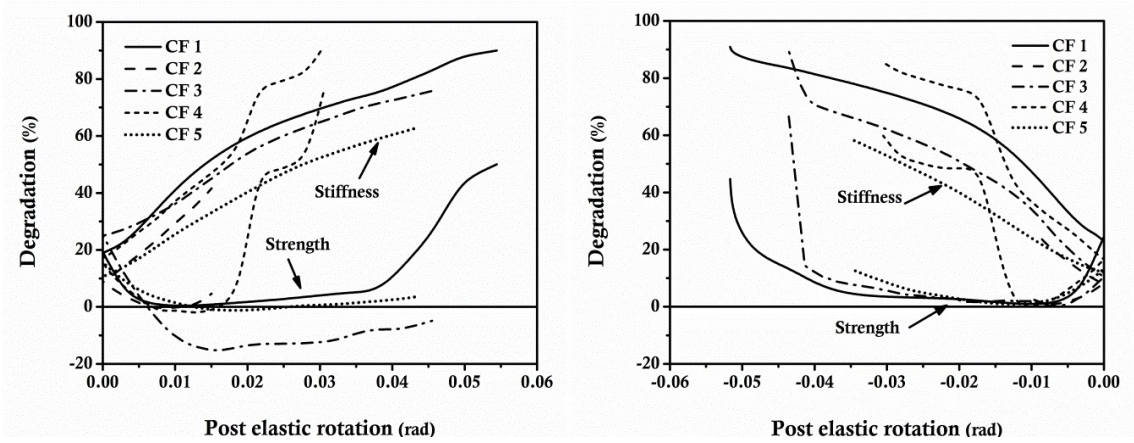

(a) Positive push (b) Negative pull

Figure 8.10: Stiffness and strength degradation of column specimens

8.3.3 Energy Dissipation

It can be understood that the dissipated energy level of specimens is nearly the same upto 80 mm deflections as shown in Figure 8.11.

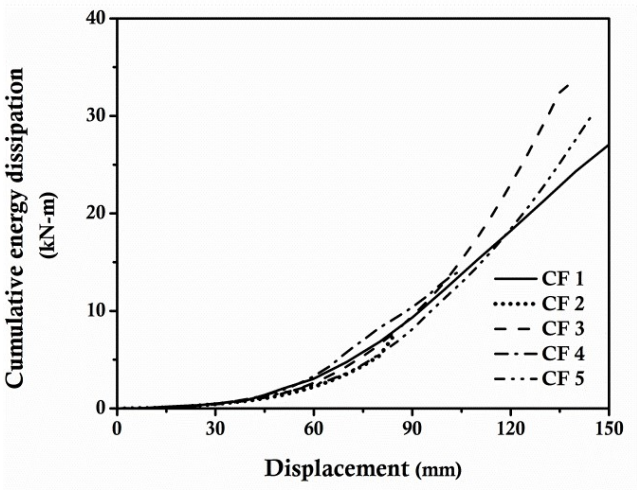

Figure 8.11: Energy dissipation curve

Beyond this point the activeness of employed connection plays vital role in enhancing the post yield response. The retrofitted specimen CF 1 exhibits least energy dissipation as compared to specimens retrofitted with either welding or FRP. The CFRP retrofitted specimen CF5 with coupler dissipates highest energy however welded specimen CF 3 exhibits relatively higher energy as compared to the specimen retrofitted only with coupler. The post elastic energy dissipation of retrofitted specimen CF5 authenticates the effectiveness of the adopted technique as compared to the conventional welding technique.

8.3.4 Failure Pattern

In original specimen CF1, flexural cracks are noticed during initial loading in the plastic hinge region as shown in Figure 8.12. Later the cracks in the column hinge region are too wide at the beginning due to lack of confinement in the plastic hinge region which leads the specimen to fail in shear. As the loading further increases, concrete begins to disintegrate and the load is carried by the concrete shifting to its longitudinal reinforcement. This additional load causes buckling of longitudinal reinforcement near foundation level as shown in Figure 8.12a.

In specimen CF2, flexural cracks are again noticed in the plastic hinge region of column upto 80 mm deflection under the cyclic testing of retrofitted column. As the deformation increases, couplers from both the sides of the reinforcement fail and specimens divide in two halves as shown in Figure 8.12b. The detached top portion of the column is lifted to examine the mode of failure of coupler as shown in Figure 8.12c. After the visual examination, it is observed that the location of failure of specimen is in coupler at the intersection point of top and bottom reinforcing bar.

In welded specimen flexural cracks are observed during initial stage of loading. As the displacement increases, the cracks in the hinge region begin to widen followed by spalling of concrete. As the deformation further increases, the welding fails, subsequently the load decreases and finally the concrete is crushed in the hinge region as shown in Figure 8.12d.

In BFRP retrofitted column specimen CF4 with couplers, rupture occurs in FRP resulting in crushing of concrete at the column foundation level as shown in Figure 8.12e. one by one failure of couplers takes place in the specimen as the displacement increases otherwise the type of failure is similar to specimen CF2. In CFRP retrofitted column specimen with coupler, significant improvement in load-deformation behavior is observed after yielding. The behavior of specimen CF5 in early stage of loading is similar to specimen CF1. The external CFRP confinement holds the connection region to remain active because of its higher modulus and finally the load shifts to foundation level. As the deformation increases the rotation at foundation increases but there is no de-bonding at the level of retrofitted portion as shown in Figure 8.12f.

(a) CF1 (b) CF2 (c) Broken coupler (d) CF 3 (e) CF4 (f) CF5

Figure 8.12: Failure pattern of column specimens

8.4 Findings

The objective of this experimental investigation is to examine influence of mechanical coupler in retrofitting of buckled longitudinal reinforcement of column under cyclic loading. The following conclusion may be drawn from this study;

1. The mechanical coupler with CFRP wrapping may be an effective solution for connection of two discontinuous reinforcements. This situation frequently arises in case of retrofitting of column under earthquake in which the plastic hinge forms at the top and bottom region of column and the main reinforcement buckles.

2. The mechanical coupler without CFRP may also be used for the gravity loads since there is no slippage in reinforcement at the connecting junction. The efficiency of the coupler may also be improved by increasing the wall thickness of coupler, threading with adequate bolts.

3. The external wrapping by CFRP confines the retrofitted portion and increases the strength of the section that not only allows the coupler to effectively transfer the load to the foundation but also completely eliminates the shear failure in the hinge region.

4. The load-deformation behavior of welded section is significantly improved and nearly exhibits the same pattern as in case of controlled specimen. The difficulty in welding at site and removal of large concrete at both the sides of damaged column to expose the reinforcement for suitable length restricts its practical application.

5. The stiffness degradation shows that the retrofitted specimen with coupler and CFRP confinement shows slower rate of degradation over the control and welded specimen. The stiffness retention in the post elastic rotation authenticates the effectiveness of employed retrofitting technique in RC column buckling reinforcement and retrofitting work under cyclic loading.

6. This study paves the way for bolted coupler in retrofitting of reinforced concrete structural components but for its versatility and reliability, more experiment tests are required using different wall thickness to length ratio under various types of load applications.

References

Cem, Y., Osman, K. and Mustafa, S., (2006), "Seismic retrofitting of R/C columns having plain rebars using CFRP sheets for improved strength and ductility," *Construction and Building Materials*, 22(3), 295–307.

Dandapat, R., Deb, A. and Bhattacharyya, S. K., (2012), "Localized failure in FRP wrapped cylindrical concrete columns," *ACI Structural Journal,* 109(4),445-456.

Frieder, S., Nigel,P. M. J., Gilbert, A., Hegemier., And Donato, I., (1997), "Seismic retrofit of RC columns with continuous carbon fiber jackets," *Journal of Composite and Constructtion*,1,52-62.

Hamid, S., Mohammad, R. E., and Limin, J., (1997), "Repair of Earthquake-damaged RC columns with FRP wraps," *ACI Structural Journal*, 94(2), 206-214.

Nagaprasad, P., Rai, D. C., and Sahoo, D. R., (2009), "Seismic strengthening of RC columns using external steel cage," *Journal of Earthquake Engineering & Structural Dynamics*,38(14),1563 – 1586.

Okahashi, Y., Pantelides, C. P., and Reaveley, L. D., (2010), "Selective seismic rehabilitation of RC interior beam-column joints with FRP composites." *9th US National and 10th Canadian Conference on Earthquake*

Pantelides, C. P., and Gergely, J., (2009), "Seismic retrofit of reinforced concrete beam-column T-joints in bridge piers with FRP composite jackets." *ACI Special Publication, SP-258*, 1-18.

Pantelides, C.P., Okahashi, Y. and Reaveley, L.D., (2008), "Seismic rehabilitation of reinforced concrete frame interior beam-column joints with FRP composites," *Journal of Composites for Construction*, 12(4), 435-445.

Pantelides, C. P., Hansen, J., Nadauld, J., and Reaveley, L. D., (2002), "Assessment of RC building exterior joints with substandard details," *PEER Report No. 2002/18*, College of Engineering, University of California, Berkely.

Prota, A., Manfredi, G., Balsamo, A., Nanni, A. and Cosenza, E., (2005), "Innovative technique for seismic upgrade of RC square columns," In *Proceedings of the 7th International Symposium on Fiber-Reinforced Polymer (FRP) Reinforcement for Concrete Structures*,1289-1304.

Raj, V., Michael, E. K., and James, O. J., (1993), "Strengthening of column splices for seismic retrofit of nonductile reinforced concrete frames," *ACI Structural Journal*, 90(4), 432-440.

Richard, D., Iacobucci, S. A., Sheikh, and Oguzhan, B., (2003) "Retrofit of square concrete columns with carbon fiber-reinforced polymer for seismic resistance," *ACI Structural Journal*, 100(6), 785-794.

Richard, S., Kent, A. H., Stephanie, L., Walkup, S. P., and James, M. R., (2004), "Flexural behavior of concrete columns retrofitted with carbon fiber-reinforced polymer jackets," *ACI Structural Journal*, 101(5), 708-716.

Rimen, J., Tabarak, H., Arghya, D., and Bhattacharyya, S.K., (2013), "Effect of imperfections in the bond on the strength of FRP wrapped cylindrical concrete columns," Composites: Part B, 53,297–307.

Sengupta, A. K., Badari, N. V. T., and Asokan, A., (2003), "Seismic retrofit of existing multi-storeyed buildings in India – an overview of the method and strategies", *Proceedings, Structural Engineering Convention*, Indian Institute of Technology, Kharagpur, India,181–190.

Sengupta, A. K., Chemuru, S. R., Badari, N. V. T., and Asokan A., (2004), "Seismic analysis and retrofit of existing multistoreyed buildings in India – an overview with a case study," *13th World Conference on Earthquake Engineering*, Canada,paper no.2571.

Xiao, Y. and Wu, H., (2003), "Retrofit of reinforced concrete columns using partially stiffened steel jackets," *Journal of Structural Engineering*, 129(6),725–732.

Chapter 9

Summary and Conclusions

This experimental research aims to investigate the influence of different high performance materials on the static and cyclic behavior of R.C structural components with and without confinement. The prime aim of this work is to examine the performance evaluation of high performance materials used in the joint core of exterior beam-column joint specimens to enhance the shear resistance and to predict the analytical shear strength model. A detailed experimental study is planned and carried out by testing the beam-column joints specimen and other companion specimens under monotonic and cyclic loading and results are interpreted in the form of hysteretic curve, load deflection behavior, stiffness degradation, energy dissipation, moment rotation behavior, crack pattern and damage tolerance behavior. The primary objective of this research is to investigate the inelastic behavior of exterior beam-column joints with different high performance materials. The following aspects are covered in the present study i.e. (i) investigation of inelastic behavior of geo-grid confinement with and without steel fiber as additional shear reinforcement to improve the shear performance of beams and beam-column joints component (ii) investigation on the possibility of using steel fibers and fiber hybridization with minimum shear reinforcement in beam-column joints (3) evaluation of the effectiveness of High Performance Fiber Reinforced Cementitious Composites (HPFRCC) using different fiber as a means to increase the inelastic response and damage tolerance capacity of beam-column joints (4) explore the possibility of use of SIFCON precast core in the beam-column joint region for improving the shear strength capacity and (5) development of analytical model to predict the shear strength of conventional, SIFCON precast core enabled and FRC beam-column joints based on regression study of experimental data. The proposed work also includes a detailed experimental investigation to examine the effectiveness of epoxy filled mechanical coupler with external bolt system to connect the two ends of main reinforcing bar in structural members. The outcome of different high performance materials on structural performance is as follows;

9.1 Effect of Geo-Grid Confinement

The feasibility of geo-grid as a partial confinement along-with conventional stirrups is examined by conducting the monotonic and cyclic tests on reinforced concrete beam specimens and beam-column joint specimens. The test results on geo-grid confinement at the plastic hinge regions of reinforced concrete components pave a new path in structural engineering as an alternative confining material. The test results are evaluated in the form of load - deflection curves, hysteretic behavior and stiffness retention behavior of geo-grid confined specimens. It shows that geo-grid confines the concrete and provides better post yield behavior and also significantly improves the shear capacity of beam and beam-column joints. The performance can be further improved by using steel fiber in concrete along with geo-grid confinement. The crack pattern and failure behavior unveil that the geo-grid confinement can sustain severe deformation and improves the core concrete strength. The presence of steel fiber in geo-grid confinement helps each other in improving the inelastic performance with better damage tolerance capacity.

9.2 Effect of Fiber Reinforced Concrete (FRC)

The mechanical properties of different fiber reinforced concrete (FRC) and hybrid fiber reinforced concrete (HyFRC) are determined under compression and flexure. The hysteresis behaviour of unconfined RC beam-column joint with FRC at the joint region is examined under cyclic loading. The axial stress-strain behaviour along-with failure pattern of different FRC composite manifests the softening behavior in contrast to conventional concrete. There is significant improvement in flexural behaviour of FRC concrete that underlines the use of FRC and HyFRC on ductility enhancement. The cyclic testing of beam-column joints with different FRC improves the shear resistance capacity and changes the failure mode from shear to ductile even without conventional confinement. The post peak strength and stiffness retention capacity of conventionally confined specimens is improved only upto a certain extent because of low tensile strength of concrete. The enlarged hysteretic loop of FRC composite specimens proves enhancement of shear strength and post yield stiffness retention of the joint even without confinement. It is mainly due to tensile nature of composite and stress transferring mechanism across the cracks. The failure mode of FRC and HyFRC specimens is mainly by yielding of reinforcement at the joint region that depicts that the specimens can sustain higher

deformation with better damage tolerance capacity over conventionally confined beam-column joint specimens.

9.3 Influence of High Performance Fiber Reinforced Cementitious Composites (HPFRCC)

The influence of HPFRCC with different fiber mix ratio in the hinge region with moderate confinement is studied by conducting the static and reverse cyclic tests on reinforced concrete beam specimens and exterior beam-column joint specimens. The experimental test outputs of HPFRCC reinforced concrete components authenticate the efficiency of HPFRCC in improving strength and inelastic behavior of RC components. The investigation results are assessed in the form of moment-curvature curve, hysteretic behavior, stiffness retention behavior and damage tolerance capacity of HPFRCC specimens. It shows that the presence of HPFRCC in the hinge region improves the post yield deflection and shear capacity of beam and beam-column joints without critical confinement. The presence of fibers and the absence of coarse aggregate in the composites restrict the early crack formation and by effective crack bridging action improves the damage tolerance capacity of structural components. The crack pattern and failure behavior of hybrid composites unveil that the hybrid composites can work effectively under severe deformation and improve the concrete tensile strength. It shows impressive energy dissipation and damping characteristic.

9.4 Influence of Precast SIFCON Core on Shear Behavior

The shear strength enhancement of beam-column joint specimens using precast SIFCON core element is evaluated under the cyclic testing. The compression and flexure behaviour of SIFCON is also studied after carrying out the standard tests. The test results indicate that there is a significant improvement in post yield behavior under compression with consistent increase and the observed flexural strength of SIFCON is nearly seven times higher than conventional concrete. The reverse cyclic testing of SIFCON enable beam-column joints specimens has larger shear strength with the change in failure mechanism. The specimens under cyclic testing have failed at the beam component of the joint and not at the joint region. There is a radical shift of failure mechanism from shear to flexure. The confining detailing at the joint region further improves the post yield behavior of SIFCON core enabled specimen. The inclusion of SIFCON core element in the joint

region improves the damage tolerance and stiffness retention capacity of joint over conventional joint.

9.5 Effectiveness of Proposed Shear Strength Model

An analytical model for predicting the shear strength of the beam-column joint is proposed under the unconfined and confined conditions based on existing experimental data base from past studies. A comparison is made for the predicted shear strength with the shear strength model proposed in ACI, NZ and ACI codes. The coefficient of variation (CoV) is 0.35, 0.26 and 0.33 respectively with average values 0f 0.99, 0.49 and 1.34 while the values for the proposed model are 0.13 and 0.91. The proposed equations are closer to experimental test results of the joint. The proposed model is further upgraded by adding the contribution of SIFCON Core and the modified equation is able to predict the shear strength of SIFCON core enabled specimen with an average of 0.99 and CoV is 6.5%.
The shear strength model of beam-column joint with confinement may also be applicable to predict the shear strength of beam-column joint with SFRC. The contribution of SFRC and its enhancement in strength is considered along with compressive strength of concrete, percentage of longitudinal reinforcement and stirrups in the joint. In addition, column axial load and joint index is also considered. The coefficient of variation (CoV) in the predicted model is nearly 14% with 98% average value. The maximum calculated shear strength values lie within 20% difference limit.

9.6 Influence of Mechanical Rebar Connection

The influence of mechanical rebar coupler in broken rebar connection in lieu of conventional methods in RC structural components using RC beams and beam-column joints with different reinforcement detailing is examined under static and cyclic loading. The axial tensile stress-strain behavior of rebar coupler under tension is also examined to investigate the effective connection under direct tension and the tensile test results show comparative response over conventional reinforcement. The couplers are used in different locations of beam and tested under static loading with different reinforcement diameter bars. The output of this experimental program authenticates the efficacy of rebar coupler in connecting the broken rebars in different location. Rebar couplers are used in different locations of rebars in beam-column joints within the plastic hinge region and tested under reverse cyclic loading. The hysteretic behaviour, energy dissipation and post failure analysis show the activeness of rebar couplers under cyclic loading within the plastic hinge

regions. This technique provides better damage tolerance capacity and has better stiffness retention. Also the failure behavior shows that the connection has no influence in failure mode.